frontiers | Research Topics

Neuromodulation using spatiotemporally complex patterns

Edited by
Hemant Bokil and Peter A. Tass

Published in
Frontiers in Neuroinformatics
Frontiers in Human Neuroscience

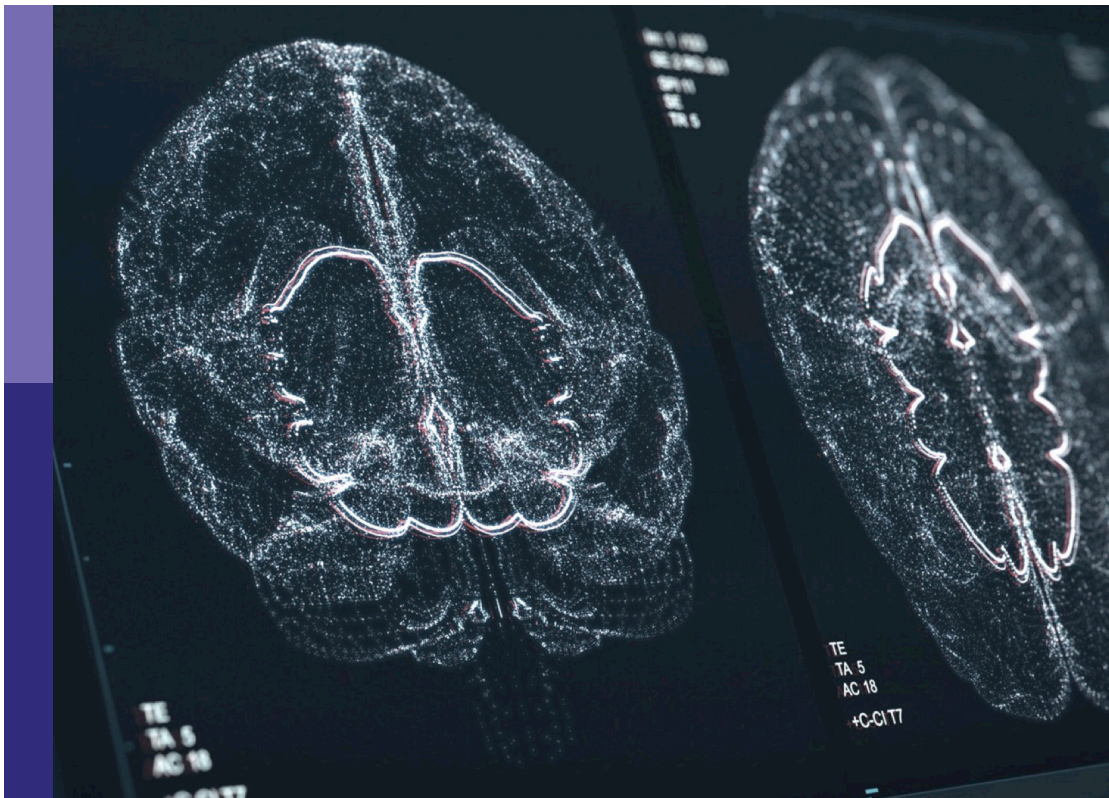

ISSN 1664-8714
ISBN 978-2-8325-5413-5
DOI 10.3389/978-2-8325-5413-5

About Frontiers

Frontiers is more than just an open access publisher of scholarly articles: it is a pioneering approach to the world of academia, radically improving the way scholarly research is managed. The grand vision of Frontiers is a world where all people have an equal opportunity to seek, share and generate knowledge. Frontiers provides immediate and permanent online open access to all its publications, but this alone is not enough to realize our grand goals.

Frontiers journal series

The Frontiers journal series is a multi-tier and interdisciplinary set of open-access, online journals, promising a paradigm shift from the current review, selection and dissemination processes in academic publishing. All Frontiers journals are driven by researchers for researchers; therefore, they constitute a service to the scholarly community. At the same time, the *Frontiers journal series* operates on a revolutionary invention, the tiered publishing system, initially addressing specific communities of scholars, and gradually climbing up to broader public understanding, thus serving the interests of the lay society, too.

Dedication to quality

Each Frontiers article is a landmark of the highest quality, thanks to genuinely collaborative interactions between authors and review editors, who include some of the world's best academicians. Research must be certified by peers before entering a stream of knowledge that may eventually reach the public - and shape society; therefore, Frontiers only applies the most rigorous and unbiased reviews. Frontiers revolutionizes research publishing by freely delivering the most outstanding research, evaluated with no bias from both the academic and social point of view. By applying the most advanced information technologies, Frontiers is catapulting scholarly publishing into a new generation.

What are Frontiers Research Topics?

Frontiers Research Topics are very popular trademarks of the *Frontiers journals series*: they are collections of at least ten articles, all centered on a particular subject. With their unique mix of varied contributions from Original Research to Review Articles, Frontiers Research Topics unify the most influential researchers, the latest key findings and historical advances in a hot research area.

Find out more on how to host your own Frontiers Research Topic or contribute to one as an author by contacting the Frontiers editorial office: frontiersin.org/about/contact

Neuromodulation using spatiotemporally complex patterns

Topic editors

Hemant Bokil — Neuromodulation Division, Boston Scientific, United States

Peter A. Tass — Stanford University, United States

Citation

Bokil, H., Tass, P. A., eds. (2024). *Neuromodulation using spatiotemporally complex patterns*. Lausanne: Frontiers Media SA. doi: 10.3389/978-2-8325-5413-5

Dr. Bokil is an employee of and owns stock in Boston Scientific. Dr. Tass is a consultant for and receives research funding from Boston Scientific. Both are involved in research on the research topic.

Table of contents

frontiers | Frontiers in Neuroinformatics

TYPE Editorial
PUBLISHED 05 August 2024
DOI 10.3389/fninf.2024.1454834

OPEN ACCESS

EDITED AND REVIEWED BY
Michael Denker,
Jülich Research Centre, Germany

*CORRESPONDENCE
Peter A. Tass
ptass@stanford.edu

RECEIVED 25 June 2024
ACCEPTED 25 July 2024
PUBLISHED 05 August 2024

CITATION
Tass PA and Bokil H (2024) Editorial: Neuromodulation using spatiotemporally complex patterns.
Front. Neuroinform. 18:1454834.
doi: 10.3389/fninf.2024.1454834

Editorial: Neuromodulation using spatiotemporally complex patterns

Peter A. Tass[1]* and Hemant Bokil[2]

[1]Department of Neurosurgery, Stanford University, Stanford, CA, United States,, [2]Boston Scientific Neuromodulation, Valencia, CA, United States

KEYWORDS

neuromodulation, deep brain stimulation, patterned stimulation, coordinated reset stimulation (CRS), plasticity, multi-channel stimulation

Editorial on the Research Topic
Neuromodulation using spatiotemporally complex patterns

Standard high-frequency deep brain stimulation (DBS) is an established therapy for the treatment of Parkinson's disease (PD) (Lozano et al., 2019). However, there is still a significant clinical need for further improvement, as DBS may cause side effects and its therapeutic effects may be limited, in particular, regarding axial symptoms (Baizabal-Carvallo and Jankovic, 2016; Lozano et al., 2019). The articles in this Research Topic highlight that stimulation with spatiotemporal patterns may engage the nervous system in fundamentally different ways than can be achieved with conventional single-frequency stimulation.

Theta burst stimulation (TBS) was initially developed for transcranial magnetic stimulation, especially to induce long-lasting modulation of motor networks (Huang et al., 2005). Later, this stimulus pattern was also applied to DBS. In a randomized, double-blind, clinical short-term trial, Horn et al. (2020) compared two types of TBS unilaterally delivered to the STN with standard unilateral DBS. Their results demonstrated safety and efficacy in this acute (20-30 min) setting, but no long-lasting aftereffects. Sáenz-Farret et al. (2021) studied safety and efficacy of chronically applied bilateral low intra-burst frequency TBS [as introduced by Horn et al. (2020)] in eight PD and one essential tremor patient. In seven patients TBS had to be discontinued due to side effects. Gülke et al. performed an analogous short-term study to test bilateral STN TBS under the same acute conditions and retrospectively combined their data with the data by Horn et al. (2020). Both unilateral and bilateral STN TBS reduced motor scores, where bilateral TBS did not lead to significant additive benefit. Note that the parameters for TBS used in these studies were not all the same which may explain the differences in results. In particular, Sáenz-Farret et al. (2021) utilized a lower intra-burst frequency and twice the inter-burst period as that used in Gülke et al..

Coordinated Reset (CR) stimulation is a patterned multi-site stimulation technique that was computationally developed to specifically counteract abnormal neuronal synchrony by demand-controlled delivery of stimuli that cause robust desynchronization, thereby overcoming limitations of phase-dependent stimulation (Tass, 2003). Using spike-timing dependent plasticity (STDP) (Markram et al., 1997)

in a variety of neuronal network models, CR stimulation turned out to induce cumulative and long-lasting desynchronizing effects, by inducing an unlearning of abnormal synaptic connectivity (Tass and Majtanik, 2006; Hauptmann and Tass, 2009). These computationally predicted, cumulative and weeks-long stimulus after-effects, very different compared to what was known from standard DBS, were verified in MPTP Parkinsonian monkeys (Tass et al., 2012; Wang et al., 2016, 2022; Bore et al., 2022) and human PD patients (Adamchic et al., 2014). Bosley et al. study the impact of CR-DBS delivered to the STN specifically on impaired gait in MPTP Parkinsonian monkeys. Their results show that CR-DBS can improve Parkinsonian gait. Kromer et al. present a computational model of the STN-GPe circuit and investigate how connectivity changes affect evoked responses and, hence, can be used to probe functional channels in the basal ganglia by means of a suggested two-site stimulation protocol. These results may lead to calibration techniques for CR-DBS enabled by implantable pulse generators that are able to sense.

In their review article, Najera et al. summarize alternative DBS stimulation approaches and their potential clinical applications. By the same token, in a review article, Cota et al. discuss standard and alternative brain stimulation techniques, including non-periodic stimulation. Different plasticity as well as compensatory mechanisms appear to play crucial roles in Parkinson's disease (Blandini et al., 2000; van Nuenen et al., 2012; Madadi Asl et al., 2022). Accordingly, in an opinion article, Asp et al. stress the importance of neuroplasticity as a key target for the development of novel stimulation techniques.

Adaptive deep brain stimulation (aDBS) has a long history, dating back to the 1980s (Krauss et al., 2021). One goal of aDBS is to reduce side effects by reducing stimulation current. In a computational study, Bahadori-Jahromi et al. compare standard DBS with aDBS with amplitude modulation in a cortico-BG-thalamic network. In their model, aDBS outperformed standard DBS with respect to reduction of beta band oscillations, restoring fidelity of thalamic throughput and overall stimulation current.

As shown computationally, properly timed multi-channel and multi-site stimulation can significantly reshape connectivity, thereby inducing long-lasting activity changes (Khaledi-Nasab et al., 2022; Kromer and Tass, 2022; Madadi Asl et al., 2023). Depending on the condition, restoring function may require to up- or down-regulate specific connections within and/or between brain areas and corresponding patterns of synchrony. In an N-of-1 case report study, Omae et al. use amplitude-modulated transcranial alternating current stimulation (AM-tACS) (Witkowski et al., 2016; Negahbani et al., 2018) to enhance low beta phase synchrony between Broca's area and the right homotopic area with the intend to improve language function in a patient with chronic post-stroke aphasia. Favorable electrophysiological outcomes and clinical benefits indicate that this approach deserves further clinical testing.

In mouse models of Alzheimer's disease, entrainment by gamma (40 Hz) rhythmic light flicker enabled to attenuate pathological processes associated with Alzheimer's disease (Iaccarino et al., 2016; Adaikkan et al., 2019). To computationally study the electrophysiology of gamma flicker entrainment, Wang et al. propose a neural network model for thalamocortical oscillations (TCOs) and computationally studied the impact of light flicker stimulation with different parameters in dependence on different thalamocortical oscillatory states. They revealed state-dependent stimulus responses that may inform future experiments.

EEG plays an important role in monitoring treatment effects and providing feedback for closed-loop stimulation techniques. Motivated by deep learning and stack generalization theory, Zhang et al. propose a novel method for the recognition of epileptic EEG signals: deep extreme learning machine (DELM) which consists of several independent, hierarchically aligned extreme learning machine (ELM) modules. They compared DELM with ELM alone, by applying it to the publicly available EEG data set from the Department of Epileptology at Bonn University, Germany (Andrzejak et al., 2001). In this comparison DELM outperformed ELM regarding accuracy and computing time.

Modern neuromodulation devices, increasingly capable of complex stimulation patterns, and modern tools for data analysis may pave the way for leveraging the potential of novel patterned and multichannel stimulation approaches for clinical use.

Author contributions

PT: Writing – original draft, Writing – review & editing. HB: Writing – review & editing.

Funding

The author(s) declare financial support was received for the research, authorship, and/or publication of this article. PT gratefully acknowledges support by the John A. Blum Foundation, the Alda Parkinson's Research Fund, the Ravi Neuro Research Fund, and the Vaughn Bryson Research Fund.

Conflict of interest

HB is an employee of and owns stock in Boston Scientific.

The remaining author declares that the research was conducted in the absence of any commercial or financial relationships that could be construed as a potential conflict of interest.

The author(s) declared that they were an editorial board member of Frontiers, at the time of submission. This had no impact on the peer review process and the final decision.

Publisher's note

References

Adaikkan, C., Middleton, S. J., Marco, A., Pao, P. C., Mathys, H., Kim, D. N., et al. (2019). Gamma entrainment binds higher-order brain regions and offers neuroprotection. *Neuron* 102, 929–943.e8. doi: 10.1016/j.neuron.2019.04.011

Adamchic, I., Hauptmann, C., Barnikol, U. B., Pawelcyk, N., Popovych, O. V., Barnikol, T., et al. (2014). Coordinated reset neuromodulation for Parkinson's disease: proof-of-concept study. *Mov. Disord.* 29, 1679–1684. doi: 10.1002/mds.25923

Andrzejak, R. G., Lehnertz, K., Mormann, F., Rieke, C., David, P., Elger, C. E., et al. (2001). Indications of non-linear deterministic and finite-dimensional structures in time series of brain electrical activity: dependence on recording region and brain state. *Phys. Rev. E Stat. Nonlin. Soft. Matter. Phys.* 64:e061907. doi: 10.1103/PhysRevE.64.061907

Baizabal-Carvallo, J. F., and Jankovic, J. (2016). Movement disorders induced by deep brain stimulation. *Parkinsonism Relat. Disord.* 25, 1–9. doi: 10.1016/j.parkreldis.2016.01.014

Blandini, F., Nappi, G., Tassorelli, C., and Martignoni, E. (2000). Functional changes of the basal ganglia circuitry in Parkinson's disease. *Progr. Neurobiol.* 62, 63–88. doi: 10.1016/S0301-0082(99)00067-2

Bore, J. C., Campbell, B. A., Cho, H., Pucci, F., Gopalakrishnan, R., Machado, A. G., et al. (2022). Long-lasting effects of subthalamic nucleus coordinated reset deep brain stimulation in the non-human primate model of parkinsonism: a case report. *Brain Stimul.* 15, 598–P600. doi: 10.1016/j.brs.2022.04.005

Hauptmann, C., and Tass, P. A. (2009). Cumulative and after-effects of short and weak coordinated reset stimulation - a modeling study. *J. Neural Eng.* 6:016004. doi: 10.1088/1741-2560/6/1/016004

Horn, M. A., Gulberti, A., Gülke, E., Buhmann, C., Gerloff, C., Moll, C. K. E., et al. (2020). A new stimulation mode for deep brain stimulation in Parkinson's disease: theta burst stimulation. *Mov. Disord.* 35, 1471–1475. doi: 10.1002/mds.28083

Huang, Y.-Z., Edwards, M. J., Rounis, E., Bhatia, K. P., and Rothwell, J. C. (2005) Theta burst stimulation of the human motor cortex. *Neuron* 45, 201–206. doi: 10.1016/j.neuron.2004.12.033

Iaccarino, H. F., Singer, A. C., Martorell, A. J., Rudenko, A., Gao, F., Gillingham, T. Z., et al. (2016). Gamma frequency entrainment attenuates amyloid load and modifies microglia. *Nature* 540, 230–251. doi: 10.1038/nature20587

Khaledi-Nasab, A., Kromer, J. A., and Tass, P.A. (2022) Long-lasting desynchronization of plastic neuronal networks by double-random coordinated reset stimulation. *Front. Netw. Physiol.* 2:864859. doi: 10.3389/fnetp.2022.864859

Krauss, J. K., Lipsman, N., Aziz, T., Boutet, A., Brown, P., Woo Chang, J., et al. (2021). Technology of deep brain stimulation: current state and future directions. *Nat. Rev. Neurol.* 17, 75–87. doi: 10.1038/s41582-020-00426-z

Kromer, J. A., and Tass, P. A. (2022). Synaptic reshaping of plastic neuronal networks by periodic multichannel stimulation with single-pulse and burst stimuli. *PLoS Comput. Biol.* 18:e1010568. doi: 10.1371/journal.pcbi.1010568

Lozano, A. M., Lipsman, N., Bergman, H., Brown, P., Chabardes, S., Chang, J. W., et al. (2019). Deep brain stimulation: current challenges and future directions. *Nat. Rev. Neurol.* 15, 148–160. doi: 10.1038/s41582-018-0128-2

Madadi Asl, M., Vahabie, A.-H., Valizadeh, A., and Tass, P. A. (2023). Decoupling of interacting neuronal populations by time-shifted stimulation through spike-timing-dependent plasticity. *PLoS Comput. Biol.* 19:e1010853. doi: 10.1371/journal.pcbi.1010853

Madadi Asl, M., Vahabie, A. H., Valizadeh, A., and Tass, P. A. (2022). Spike-timing-dependent plasticity mediated by dopamine and its role in Parkinson's disease pathophysiology. *Front. Netw. Physiol.* 2, 1–18. doi: 10.3389/fnetp.2022.817524

Markram, H., Lübke, J., Frotscher, M., and Sakmann, B. (1997). Regulation of synaptic efficacy by coincidence of postsynaptic aps and Epsps. *Science* 275, 213–215. doi: 10.1126/science.275.5297.213

Negahbani, E., Kasten, F. H., Herrmann, C. S., and Fröhlich, F. (2018). Targeting alpha-band oscillations in a cortical model with amplitude-modulated high-frequency transcranial electric stimulation. *Neuroimage* 173, 3–12. doi: 10.1016/j.neuroimage.2018.02.005

Sáenz-Farret, M., Loh, A., Boutet, A., Germann, J., Elias, G. J. B., Kalia, S. K., et al. (2021). Theta burst deep brain stimulation in movement disorders. *Mov. Disord. Clin. Pract.* 8, 282–285. doi: 10.1002/mdc3.13130

Tass, P. A. (2003). A model of desynchronizing deep brain stimulation with a demand-controlled coordinated reset of neural subpopulations. *Biol. Cybern.* 89, 81–88. doi: 10.1007/s00422-003-0425-7

Tass, P. A., and Majtanik, M. (2006). Long-term anti-kindling effects of desynchronizing brain stimulation: a theoretical study. *Biol. Cybern.* 94, 58–66. doi: 10.1007/s00422-005-0028-6

Tass, P. A., Qin, L., Hauptmann, C., Dovero, S., Bezard, E., Boraud, T., et al. (2012). Coordinated reset has sustained after-effects in Parkinsonian monkeys. *Ann. Neurol.* 72, 816–820. doi: 10.1002/ana.23663

van Nuenen, B. F. L., Helmich, R. C., Buenen, N., van de Warrenburg, B. P. C., Bloem, B. R., Toni, I., et al. (2012). Compensatory activity in the extrastriate body area of Parkinson's disease patients. *J. Neurosci.* 32, 9546–53. doi: 10.1523/JNEUROSCI.0335-12.2012

Wang, J., Fergus, S. P., Johnson, L. A., Nebeck, S. D., Zhang, J., Kulkarni, S., et al. (2022). Shuffling improves the acute and carryover effect of subthalamic coordinated reset deep brain stimulation. *Front. Neurol.* 13:716046. doi: 10.3389/fneur.2022.716046

Wang, J., Nebeck, S., Muralidharan, A., Johnson, M. D., Vitek, J. L., Baker, K. B., et al. (2016). Coordinated reset deep brain stimulation of subthalamic nucleus produces long-lasting, dose-dependent motor improvements in the 1- methyl-4-phenyl-1,2,3,6-tetrahydropyridine non-human primate model of parkinsonism. *Brain Stimul.* 9, 609–617. doi: 10.1016/j.brs.2016.03.014

Witkowski, M., Garcia-Cossio, E., Chander, B. S., Braun, C., Birbaumer, N., Robinson, S. E., et al. (2016). Mapping entrained brain oscillations during transcranial alternating current stimulation (tACS). *Neuroimage* 140, 89–98. doi: 10.1016/j.neuroimage.2015.10.024

frontiers | Frontiers in Neuroinformatics

TYPE Original Research
PUBLISHED 23 August 2022
DOI 10.3389/fninf.2022.968907

OPEN ACCESS

EDITED BY
Peter A. Tass,
Stanford University, United States

REVIEWED BY
Mojtaba Madadi Asl,
Institute for Research in Fundamental Sciences (IPM), Iran
Alexander Silchenko,
Forschungszentrum Jülich, Germany

*CORRESPONDENCE
Bo Cui
iamcuib@sina.com
Mengfu Zhu
zmf323@163.com

†These authors have contributed equally to this work

RECEIVED 14 June 2022
ACCEPTED 01 August 2022
PUBLISHED 23 August 2022

CITATION
Wang K, Wei A, Fu Y, Wang T, Gao X, Fu B, Zhu Y, Cui B and Zhu M (2022) State-dependent modulation of thalamocortical oscillations by gamma light flicker with different frequencies, intensities, and duty cycles.
Front. Neuroinform. 16:968907.
doi: 10.3389/fninf.2022.968907

State-dependent modulation of thalamocortical oscillations by gamma light flicker with different frequencies, intensities, and duty cycles

Kun Wang[1,2†], Aili Wei[2†], Yu Fu[2†], Tianhui Wang[2], Xiujie Gao[2], Bo Fu[2], Yingwen Zhu[2], Bo Cui[2*] and Mengfu Zhu[1*]

[1]Institute of Medical Support Technology, Academy of Military Science of Chinese PLA, Tianjin, China, [2]Department of Occupational Medicine, Tianjin Institute of Environmental and Operational Medicine, Tianjin, China

Rhythmic light flickers have emerged as useful tools to modulate cognition and rescue pathological oscillations related to neurological disorders by entrainment. However, a mechanistic understanding of the entrainment for different brain oscillatory states and light flicker parameters is lacking. To address this issue, we proposed a biophysical neural network model for thalamocortical oscillations (TCOs) and explored the stimulation effects depending on the thalamocortical oscillatory states and stimulation parameters (frequency, intensity, and duty cycle) using the proposed model and electrophysiology experiments. The proposed model generated alpha, beta, and gamma oscillatory states (with main oscillation frequences at 9, 25, and 35 Hz, respectively), which were successfully transmitted from the thalamus to the cortex. By applying light flicker stimulation, we found that the entrainment was state-dependent and it was more prone to induce entrainment if the flicker perturbation frequency was closer to the endogenous oscillatory frequency. In addition, endogenous oscillation would be accelerated, whereas low-frequency oscillatory power would be suppressed by gamma (30–50 Hz) flickers. Notably, the effects of intensity and duty cycle on entrainment were complex; a high intensity of light flicker did not mean high entrainment possibility, and duty cycles below 50% could induce entrainment easier than those above 50%. Further, we observed entrainment discontinuity during gamma flicker stimulations with different frequencies, attributable to the non-linear characteristics of the network oscillations. These results provide support for the experimental design and clinical applications of the modulation of TCOs by gamma (30–50 Hz) light flicker.

KEYWORDS

thalamocortical, oscillation, gamma light flicker, entrainment, biophysical model

Introduction

The thalamocortical (TC) loop plays a central role in cerebral rhythmogenesis (O'Reilly et al., 2021), and abnormal TC rhythms have been associated with disorders, such as depression, schizophrenia, Parkinson's disease and Alzheimer's disease (Niedermeyer, 1997; Llinás et al., 1999; Hughes and Crunelli, 2005; Madadi Asl et al., 2022). Gamma (40 Hz) rhythmic light flicker can entrain cortical gamma neural oscillations non-invasively and externally to restore cognitive dysfunctions or promote learning and memory (Adaikkan et al., 2019; Tian et al., 2021). Understanding the neurocircuit mechanisms of visually evoked entrainment of gamma can be useful when considering the possibility of the therapeutic and clinical adoption of visual gamma stimulation. However, how the stimulation paradigms interact with endogenous neural activity is currently unknown. It is also unclear how the stimulation effects depend on the TC state and stimulation doses, such as light flicker frequency and intensity. Addressing these issues requires a mechanistic understanding and systematic examination of the stimulation effects on TC network dynamics.

Neural oscillations are the rhythmic fluctuations of electrical activity in the central nervous system, which emerge due to the properties of different types of cells and interactions among them (Mathalon and Sohal, 2015). Many biophysical neural networks (NNs) based on mathematical models of different types of cells have been developed to study the characteristics of thalamus or cortex neural oscillations (Li and Cleland, 2013; Li et al., 2017; Chariker et al., 2018; Negahbani et al., 2018; Huang et al., 2021). For example, a unified biophysical thalamic NN model based on the Hodgkin–Huxley formalism was developed to explore the effect of deep brain stimulation (DBS) or repetitive transcranial magnetic stimulation (rTMS) on thalamic neural oscillations (Li et al., 2017). Similarly, a cortical NN model based on the Izhikevich formalism was developed to study the effect of transcranial alternating current stimulation (tACS) on cortical alpha-band (8–13 Hz) oscillations (Negahbani et al., 2018). Later, the abovementioned thalamic and cortical NN models were coupled to study how tACS entrains the endogenous alpha-band oscillations of TC NNs (Huang et al., 2021). These experiment-based models were employed to analyze the interaction mechanism of exogenous electromagnetic stimulation on internal neural oscillation, providing a good reference for this study.

For visually evoked gamma-band (30–100 Hz) oscillations, a neural synchronization may first be generated by retinal mechanisms (Adaikkan and Tsai, 2020). Next, a feedforward network carries the synchronization from the retina to the lateral geniculate nucleus (LGN) and then to the visual cortex (Adaikkan and Tsai, 2020). Thus, information about light flicker frequency is processed at multiple levels along the retinothalamocortical pathway. Early studies have shown the response of retinal ganglion (GC) cells to frequency global flicker stimulation (Schwartz et al., 2007; Schwartz and Berry, 2008) and how to simulate the transmission from the retina to thalamus (Casti et al., 2008; Werner et al., 2008). However, these studies on retinothalamocortical pathway simulation have focused on the transmission of visual information rather than the oscillation effect of networks; a TC oscillation (TCO) NN model in response to light flicker is lacking.

To gain an in-depth understanding of the entrainment mechanism of TCOs induced by gamma light flicker, we developed and investigated a biophysically detailed TCO NN model and explored the stimulation effects depending on the TC oscillatory states and stimulation parameters (frequency, intensity, and duty cycle).

Materials and methods

Thalamocortical network structure

We adopted a previously developed thalamic NN model (Li et al., 2017), which was used to study the effect of rhythmic stimulation on neural oscillations, and connected it to a simplified cortex NN model (Susin and Destexhe, 2021), which was used to study the mechanism of the gamma-band (30–100 Hz) oscillation generation.

The thalamic network included 144 relay-model thalamic cells (RTC), 100 reticular inhibitory neurons (RE), 49 high-threshold bursting thalamic cells (HTC), and 64 local interneurons (IN) based on cat physiological data (Hughes et al., 2004; Lörincz et al., 2008). All thalamic neurons were modeled using the Hodgkin–Huxley formalism of point neurons connected with glutamatergic (mediated by both AMPA and NMDA receptors) and GABAergic (mediated by GABAA receptors) synaptic currents (with implemented short-term synaptic depression) or via gap junctions, with the previously described parameter values (Li et al., 2017).

For the cortical part, we reduced the number of neural cells in the original cortex NN model (Susin and Destexhe, 2021) to match the thalamic NN and increased the possibility of a synaptic connection as another cortex NN model that has the same number of cells (Negahbani et al., 2018), including 80 pyramidal (PY) and 20 fast-spiking inhibitory (FS) neurons. All neurons were connected globally with a probability of 0.8, except for the connections within PY neurons, which was 0.5. Individual PY and FS cells were modeled using the Izhikevich formalism for point neurons with the previously described parameter values (Susin and Destexhe, 2021).

The thalamic and cortex NN models were connected in a biologically plausible manner (Izhikevich and Edelman, 2008) to form the TCO NN model (**Figure 1**); the essential features are highlighted in the following brief description of the model equations.

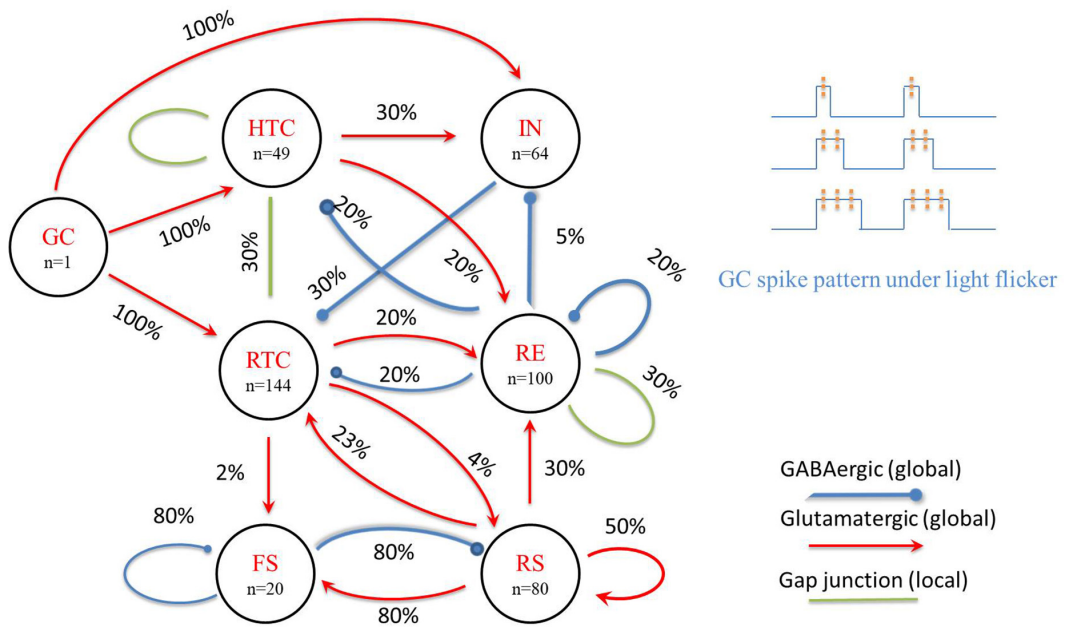

FIGURE 1
A schematic of the proposed TCO NN model (left) and GC spike pattern under light flicker (upper right). The percentage value represents the possibility of a connection between neuron groups.

Computational model of thalamocortical network

Thalamic model

The current balance is described by the Hodgkin–Huxley formalism:

$$Cm\frac{dv}{dt} = -g_L\left(V - E_L\right) - g_{KL}\left(V - E_{KL}\right) - \sum I^{int} - \sum I^{syn} \tag{1}$$

where Cm denotes the membrane capacitance, g_L denotes the leakage conductance, g_{KL} denotes the potassium leak conductance, E_L denotes the leakage reversal potential, E_{KL} denotes the reversal potential for the potassium leak current (see **Supplementary Table 1** for details), and I^{int} and I^{syn} denote the intrinsic ionic and synaptic currents, respectively. An ion current is described as follows:

$$Ii = g_i m^p h^q \left(V - E_i\right) \tag{2}$$

where g_i denotes its maximal conductance density (see **Supplementary Table 2** for details), m denotes its activation variable (with exponent p), h denotes its inactivation variable (with exponent q), and E_i denotes its reversal potential. The gating variable (m or h) kinetic equations satisfy the first-order kinetic model:

$$\frac{dx}{dt} = \phi_x \frac{x_\infty\left(V, [Ca]_i\right) - x}{\tau_X\left(V, [Ca]_i\right)} \tag{3}$$

where ϕ_x denotes a temperature-dependent factor, $x_\infty\left(V, [Ca]_i\right)$ represents the voltage– or Ca^{2+}-dependent steady-state, and τ_X denotes the voltage– or Ca^{2+}-dependent time constant (see **Supplementary Table 3** for details). Intracellular calcium is regulated by a simple first-order differential equation of the form:

$$\frac{d\left[Ca^{2+}\right]_i}{dt} = -\frac{I_{ca}}{zFw} + \frac{\left[Ca^{2+}\right]_{rest} - \left[Ca^{2+}\right]}{\tau_{Ca}} \tag{4}$$

where I_{ca} denotes the summation of all Ca^{2+} currents, w denotes the thickness of the perimembranous "shell" in which calcium can affect membrane properties, z denotes the valence of the Ca^{2+} ion, F represents the Faraday constant, and τ_{Ca} denotes the Ca^{2+} removal rate. $\left[Ca^{2+}\right]_{rest}$ is the resting Ca^{2+} concentration (see **Supplementary Table 1** for details).

For synaptic currents, the gap junction current is computed as follows:

$$Igap = \left(V_{pre} - V_{post}\right)/R_g \tag{5}$$

where V_{pre} and V_{post} denote the membrane potentials of the presynaptic and postsynaptic neurons, respectively. $R_g$is the gap junction resistance ($R_g = 100$ MΩ for the HTC-HTC synapses, $R_g = 300$ MΩ for the HTC-RTC and RE-RE synapses), Chemical synaptic currents are calculated as follows:

$$I_{syn} = sDg_{syn}B\left(V\right)\left(V - E_{syn}\right) \tag{6}$$

where g_{syn} denotes the maximal synaptic conductance, and E_{syn} denotes the synaptic reversal potential. The function $B(V)$

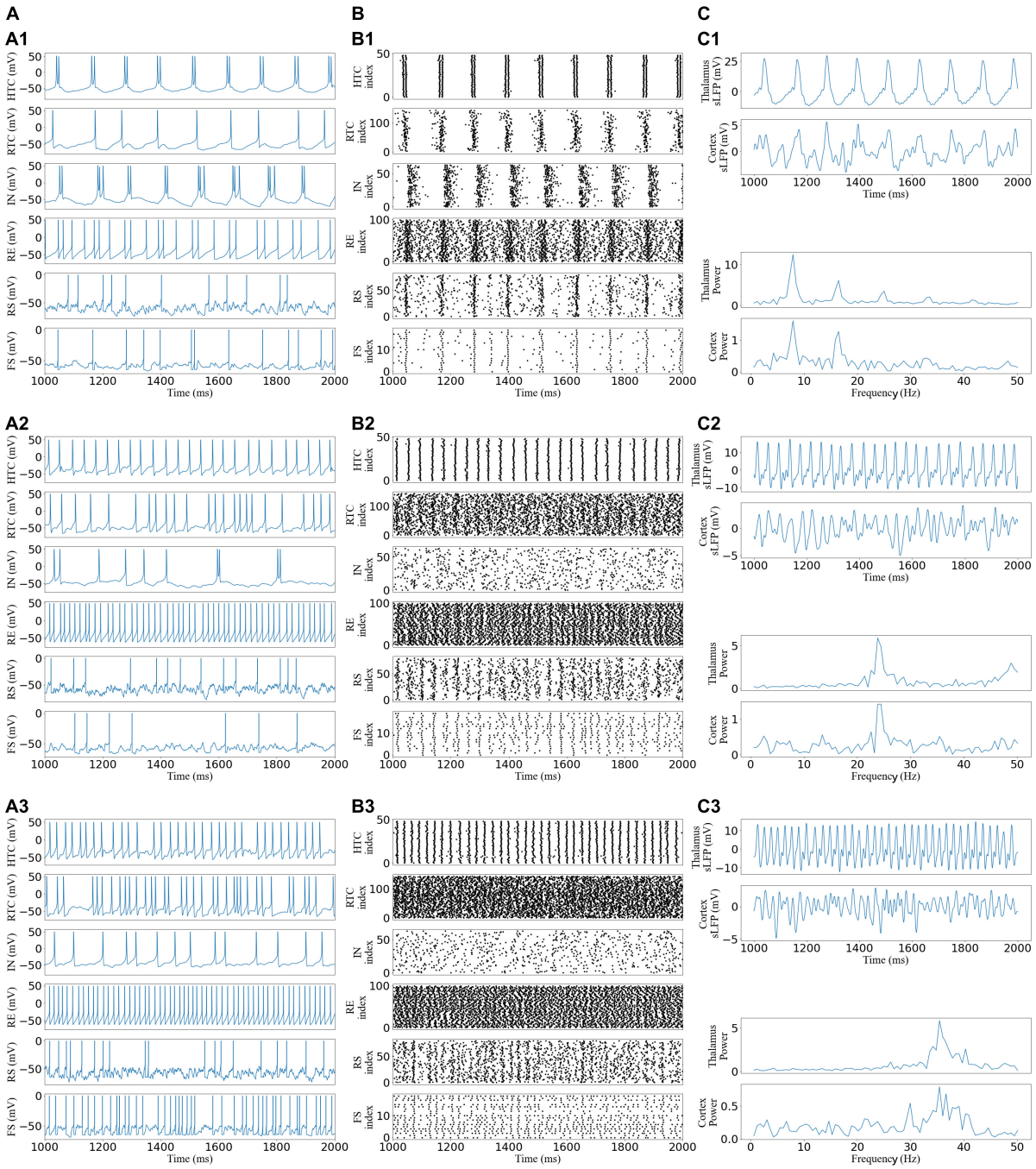

FIGURE 2
Generation of alpha, beta, and gamma oscillatory states in the TCO NN model under different afferent excitations. **(A)** Voltage traces of representative HTC, IN, RTC, RE, RS, and FS cells each: (A1,A2) alpha, beta, and gamma oscillatory states, respectively. **(B)** Spike rastergrams of HTC, IN, RTC, RE, RS, and FS cells. **(C)** Simulated LFP (top) of thalamus and cortex networks with associated frequency power spectrum (bottom).

implements the Mg^{2+} block for NMDA currents, the gating variable, s, represents the fraction of open synaptic ion channels and obeys the first-order kinetics:

$$\frac{ds}{dt} = \alpha\,[T]\,(1-s) - \beta s \tag{7}$$

where $[T]$ denotes the concentration of the neurotransmitter in the synapse which is assumed to be a brief pulse that has duration of 0.3 ms and amplitude of 0.5 mM following an action potential in the presynaptic neuron, and α and β denote forward- and backward-binding rates, respectively. Short-term

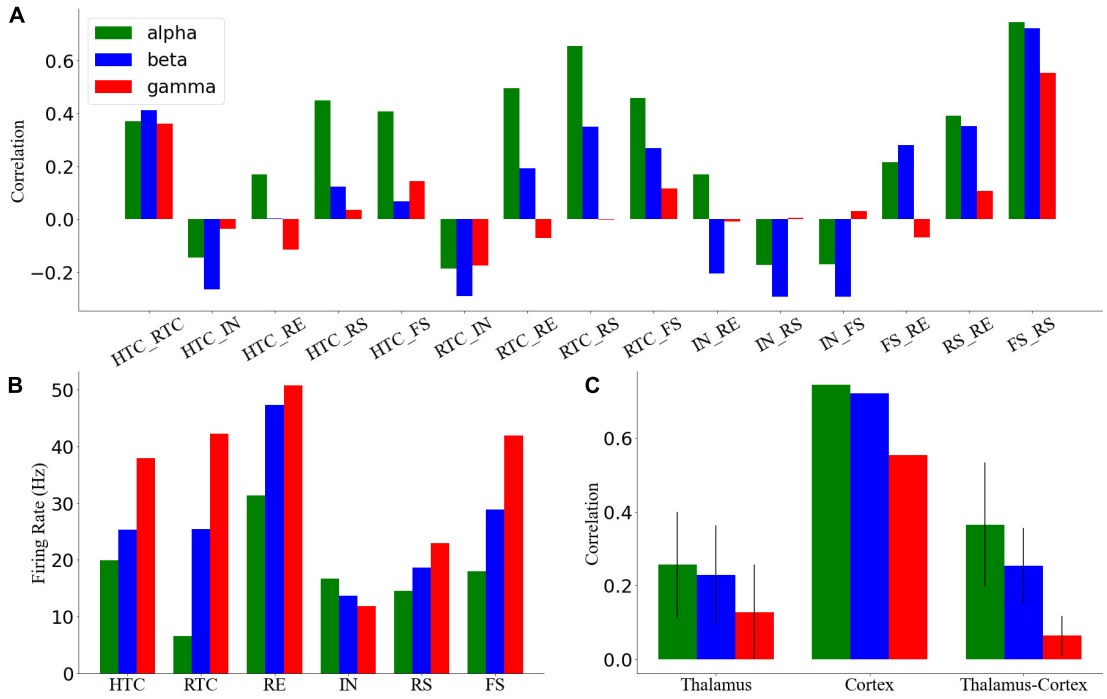

FIGURE 3
Quantification of network activity. **(A)** Cross-correlation between each pair of the neuronal group during three oscillatory states. **(B)** Average firing rates of all types of neurons across three oscillatory states. Cross-correlation between different groups of thalamic neurons during four oscillatory states. **(C)** Average cross-correlation of the thalamus, cortex, and thalamus to cortex of neuronal groups. Error bars indicate standard deviation.

synaptic depression is implemented in all chemical synapses and is modeled by scaling the maximal conductance of a given synaptic channel by a depression variable D, which is expressed as follows:

$$D = 1 - (1 - D_i(1 - U)) \exp\left(-\frac{t - t_i}{\tau}\right) \tag{8}$$

where U denotes the fraction of resources used per action potential, τ denotes the time constant of the synaptic vesicle recovery, D_i represents the value of D immediately before the ith presynaptic spike, and t_i represents the timing of the ith spike event. The numerical value of the above parameters are indicated in the **Supplementary materials** (**Supplementary Table 4**).

Cortical neural network model

In summary, the current balance equation is given by

$$Cm\frac{dv}{dt} = -g_L(v - E_L) + g_L\Delta \exp\left[\frac{(v - v_{th})}{\Delta}\right]\tau - w - I_{syn} \tag{9}$$

where Cm denotes the membrane capacitance, g_L denotes the leakage conductance, E_L denotes the leaky membrane potential, v_{th} denotes the effective threshold, and Δ denotes the threshold slope factor. w is the adaptation current, given by

$$\tau_w\frac{dw}{dt} = a(v - E_L) - w + b\sum_j \delta(t - t_j) \tag{10}$$

It increases by an amount b when the neuron emits a spike at t_j and decays exponentially with time scale τ_w. The parameter a indicates the subthreshold adaptation. The synaptic current I_{syn} is calculated as follows:

$$I_{syn} = g_E(v - E_E) + g_I(v - E_I) \tag{11}$$

where E_E and E_I denote the reversal potential of excitatory and inhibitory synapses, respectively; g_E and g_I denote the maximal synaptic conductances; they obey the first-order kinetics:

$$\tau_{E,I}\frac{dg_{E,I}}{dt} = -g_{E,I} + Q_{E,I}\sum_k \delta(t - t_k) \tag{12}$$

where $\tau_{E,I}$ denotes the decay time constant. Every time (t_k) the presynaptic neuron generates a spike, the excitatory (g_E) or inhibitory (g_I) synaptic conductance increases by a discrete amount $Q_{E,I}$ (excitatory or inhibitory synaptic strength, respectively). When $v = v_{th}$, the membrane potential is reset to v_{rest}, which is kept constant until the end of the refractory period. After the refractory period, the equations are being integrated again. The numerical value of the above

parameters are provided in the **Supplementary Materials** (**Supplementary Table 5**).

Formation of oscillations and neuronal heterogeneity

All neurons in the thalamic network received independent Poisson-distributed spike inputs at an average rate of 100 Hz. The random inputs represent both the extrinsic sources of background noise and asynchronous visual input and were exclusively mediated by AMPA receptors modeled as an instantaneous step followed by an exponential decay with a time constant of 5 ms. Alpha, beta, and gamma oscillatory states (with main oscillation frequencies at 9, 25, and 35 Hz, respectively) are formed by changing random input synaptic conductances (2.5, 15, and 25 nS, respectively). Each cortical neuron received an external drive (noise), which was implemented as 80 independent and identically distributed excitatory Poissonian spike trains with a spiking frequency of 2 Hz, as in a previous study (Susin and Destexhe, 2021). To introduce heterogeneity to model neurons, the leakage conductance (g_L) of thalamic network neurons is drawn from a uniform distribution within ± 25% of the default value (i.e., 0.0075–0.0125 ms/cm^2). The leakage conductance variation, random synaptic connectivity, and random external inputs constituted neuronal heterogeneity.

Input from ganglion cells

In this study, we focus on the intensity and frequency of global flicker stimulation and set the gamma stimulation frequency increased from 30 to 50 Hz with a 1-Hz step increment. As in a biophysical NN model of the dorsal LGN (dLGN) circuit (Heiberg et al., 2016), the input from GC cells to the TC network is spike trains, which are modeled as a firing-rate based model. Early experimental data showed that GC cells had harmonic firing patterns during flicker sequences, especially the ON-bipolar cells (a type of GC cells) that probably oscillate resonantly at the stimulus frequency (Schwartz et al., 2007; Schwartz and Berry, 2008). Thus, for the entire GC cell network, periodic global flicker stimulation can entrain the resonance response, and the input from GC cells can be modeled as a periodic firing model with a frequency consistent with the flicker stimulation. As the duration of each gamma flicker is very short [about 10 ms, which is close to a GC spike duration (Yan et al., 2016)] and the firing rate of GC cells is positively correlated with the intensity of light stimulation (Einevoll and Heggelund, 2000), the firing pattern of GC cells is simplified to one, two, or three spikes during a flicker to represent different light stimulation intensities. We also assume that the duty cycle is proportional to the number of spikes during each flicker and divide a 40-Hz flicker cycle into six equal parts, considering each flicker can emit up to three spikes of GC cells. Then, the 1/6 duty cycle flicker corresponds to GC cells giving one spike during the 1/6 duty cycle, and the 2/6 duty cycle flicker corresponds to GC cells giving two spikes during the 2/6 duty cycle, and so on (**Figure 1**, upper right). Instead of using a group of GC cells firing with the flicker frequency, we constructed one GC cell to generate spike trains considering that the flicker is global and connected it to all TC and IN cells consistent with physiological data of cat LGN (Van Horn et al., 2000). The properties of the GC-IN synapse are adapted to give responses in accordance with experimental data, where EPSPs are dependent on AMPA and NMDA activation, and typically, three to four simultaneous synapse activations are required to evoke action potentials in IN cells (Acuna-Goycolea et al., 2008). The response of TCs to GC spike is adapted to experimental data (Blitz and Regehr, 2005), i.e., monosynaptic excitation is assumed, mediated by AMPA receptors with a reversal potential of 10 mV. The synaptic conductance agreed with a retina-LGN transmission model (Casti et al., 2008), where the maximal synaptic conductance of AMPA and NMDA was 0.15 and 0.05 μS, respectively.

Stimulation protocol

The computational modeling was implemented using the Brian2 simulator in Python. All simulations were performed using the fourth-order Runge-Kutta [RK(4)] method with a fixed time step of 0.02 ms. After the initial parameters, including the network connection and leakage conductance (g_L) of thalamic NNs, were determined, the flicker stimulation of different frequencies (30–50 Hz), intensities (one, two, and three spikes), and duty cycles (1/6–5/6) was applied repeatedly to the same network. The simulation duration of each parameter was 10 s.

Oscillatory evaluation index

Simulated local field potential

Thalamic **S**imulated local field potential (sLFP) was constructed by filtering the mean membrane potentials across all TCs (Li et al., 2019). Similarly, the cortical sLFP was constructed by filtering the mean membrane potentials of all cortical cells as follows:

$$sLFP = \frac{1}{N}\sum_{i=1}^{N} V^i, \tag{13}$$

where N denotes the number of cells, and V denotes the membrane potential. The raw sLFP was filtered numerically using a bandpass filter (0.5–80 Hz). The frequency power spectrum of the signal was obtained using the Fast Fourier transform of the filtered sLFP with Python functions firwin. The network oscillation frequency was determined from the position of the spectral peak in the frequency spectrum, and the power spectrum heat map was generated using the Python function heatmap.

Synchronization index

The phase of each spike (φ) was computed as follows:

$$\phi = \frac{t_{spike} - t_{lastLFPpeak}}{t_{nextLFPpeak} - t_{lastLFPpeak}} \times 360, \quad (14)$$

where t_{spike} denotes the spike time, $t_{lastLFPpeak}$ denotes the time of the preceding positive sLFP peak, and $t_{nextLFPpeak}$ denotes the time of the following positive sLFP peak. Then, the SI was calculated as follows:

$$k = 1/N \sqrt{[\sum_{i=1}^{N} \sin(\phi i)]^2 + [\sum_{i=1}^{N} \cos(\phi i)]^2}, \quad (15)$$

where ϕi denotes the phase of each spike relative to the sLFP peaks and N denotes the total number of spikes for both HTC and RTC cells. The SI measures the degree of mutual synchronization between neurons; when all spikes have identical phases, the SI achieves its maximal value of unity.

Oscillation power

The oscillation power is calculated as the (maximal) spectral peak of sLFP. For comparison among different states, the oscillation power was normalized by the original spectral peak (without stimulation).

Correlation index

To compute the CI, the peri-event time histogram (PETH) for each of the cells (HTC, RTC, IN, RE, FS, and RS) was generated by dividing the simulation time interval into small bins (2 ms) and summing up the number of spikes in each bin. The CI between two cell groups was determined as the peak of the cross-correlation between the mean-removed PETH of the two cell groups. For the thalamus network, the CI was calculated as the mean of the respective index values for all six pairs of neuronal populations within the thalamic network. For the cortex network, the CI is the same as that of RS–FS. In addition, the CI between the thalamic and cortex networks was calculated as the mean of the respective indices for RS–RTC, RS–RE, and FS–RTC.

Entrainment judgment

The network is judged to be entrained, when the flicker stimulation frequency (f_s), dominant oscillation frequency (f_d), spectral peak power ($P_{\max}$), and average TC firing rates (FHTC and FRTC) satisfy the following criteria:

$$|f_s - f_d| < \in \quad (16)$$

$$\frac{P_{\max}}{P_0} > \sigma \quad (17)$$

where P_0 denotes the spectral peak without stimulation; $\in$ and σ denote the frequency and amplitude thresholds, respectively ($\in = 1$ Hz and $\sigma = 1$).

Electrophysiological recording and flicker stimulation

Four adult male Sprague-Dawley rats weighing about 250 g were used to implement electrophysiological recording. First, the rat was anesthetized by intraabdominal injection with 2% sodium pentobarbital (40 mg/kg), and pain sensitivity was tested by paw pinches. Then, the head of the rat was shaved and immobilized in a standard stereotaxic frame. After a midsagittal incision was made in the scalp, the craniotomy window was carefully made as a 3-mm square hole 4-mm anterior to the Bergman and 4 mm to the right of the midline. Four skull screws were placed in burr holes drilled with a microdrill. Phosphate-buffered saline was used to wash away the bone debris. After the endocranium was stripped, a microwire array (Plexon, 2 × 2, column and row spacing of 250 μm) was implanted in the thalamus. The reference and counter electrodes were connected to the ground bone screws in the skull by silver-coated copper wires. The electrode array was inserted using a micropositioner and advanced about every 40 s at an increment of 100 μm to a depth of 4,000 μm. After a week of recovery, the LFP data were taken by a 64-channel neural acquisition processor (Plexon, Dallas, TX, United States.) and its preamplifier (Plexon, Dallas, TX, United States.). Neural electrophysiological data were filtered by a 4–90-Hz bandpass and analyzed by Neuroexplorer. A 30-W LED light source (SENNO-HSL–39536, Shen Zhen, China) was placed above the rat and triggered by a function signal generator to emit light flicker with different parameters. Data were recorded for 10 min for each flicker stimulation parameter. The flicker was turned on at 5 min.

Results

Quantification of the thalamocortical network activity

From **Figure 2**, by varying the afferent excitation in the TC cells of the TC network, we generated alpha, beta, and gamma oscillatory states that appear under different behavioral and cognitive conditions in the awake state (Bouyer et al., 1981; Steriade et al., 1993; Brücke et al., 2013). The network reproduces the main features of neural oscillations (Li et al., 2017). For example, as the afferent excitation increased, HTC cells switched from two spike high-threshold bursts (HTBs) during the alpha oscillatory state to one spike tonic spiking during the beta and gamma oscillatory states while remaining well synchronized because of the gap junction connections (**Figure 2A1**), and the depolarization-induced transition from high-threshold bursting to high-frequency tonic spiking in HTC cells matches the experimental data [**Figure 2B**

in Steriade et al. (1991)]. The thalamus sLFP of the alpha oscillatory state had a strong rhythmic structure (**Figure 2B1**) and the spectrum revealed the peak power at 9 Hz (**Figure 2C1**), which was close to the alpha frequency (8.9 ± 1.2 Hz) recorded from freely moving cats during natural wakefulness (Lorincz et al., 2009). The neural oscillations of the thalamic network were transmitted to the cortex network during the three oscillatory states (**Figures 2B,C**), i.e., the spike rastergrams and simulated LFP of the cortex network had the same oscillatory frequency as those of the thalamus network.

To quantify the network activity, we calculated cross-CI between different neuronal populations. From **Figure 3A**, the cross-CI was related to the direct or indirect connection of synapses between two neuron groups, and when two groups of neurons were connected through inhibitory synapses, such as RTC–IN, the cross-CI was negative. When both inhibitory and excitatory synaptic connections existed, such as RTC–RE and HTC–RE, the CI between two groups of neurons gradually became negative with an increase in the oscillation frequency. Further, we calculated the average cross-CIs of the thalamus, cortex, and thalamus to cortex, which decreased with an increase in oscillation frequency (**Figures 3B,C**), attributable to the change in the RTC cells firing pattern among the three oscillations, which was well synchronized (**Figure 2B1**) with high CIs for RS and FS cells during the alpha oscillatory state (**Figure 3A**), but the synchrony fade away for the beta and gamma oscillatory states (**Figures 2B2,B3**) with low CIs for RS and FS cells (**Figure 3A**). From the average firing rates given in **Figure 3B**, we found that the average firing rates of HTC, RTC, FS, and RS cells, which formed the sLFP, increased substantially with an increase in oscillatory frequency; the sLFP power decreased more for the beta and gamma oscillatory states than the alpha oscillatory state (**Figure 2C**).

Overall, the above results suggest that the thalamic network could generate stable oscillatory states and transmit them to the cortex through RTC cells, so the synchronization of RTC cells would affect the cortex synchronization, which was highly synchronous under the alpha oscillatory state with high cross-CI but poorly synchronous under the beta and gamma oscillatory states.

Effect of 40-Hz light flicker on signal cells of the thalamocortical network

Before embarking on the TC network activity under gamma (30–50 Hz) flicker stimulation, we demonstrate the effect of light (take 40 Hz as an example) flicker on signal cells of the TC network (**Figure 4**). As shown in **Figure 4A**, the excitatory GC input to the HTC and RTC cells alone would evoke the action potential of the HTC and RTC cells immediately, whereas the IN cells need three GC spikes arriving in a short time to evoke an action potential, which agreed with the experimental data (Blitz and Regehr, 2005; Acuna-Goycolea et al., 2008). To observe the response of cells stimulated by light in the circuit, the response of the TC and IN cells under the alpha oscillation with a low cell firing rate is shown in **Figure 4B**; not every GC excitatory input could evoke a spike of TC cells in the network in accordance with previous studies (Casti et al., 2008; Heiberg et al., 2016). When the flicker was on, the firing rate of the HTC and IN cells decreased, whereas that of the other cells increased under the alpha oscillation (**Figure 4C**). Flicker stimulation changed the firing pattern of HTC cells from HTBs to tonic spiking, and the firing pattern of IN cells was a mix of HTBs and tonic spiking under the alpha oscillatory state (**Figure 4B**).

For the beta and gamma oscillatory states, the HTC cells fired in a tonic spiking pattern originally, and the light flicker increased the firing rate of the TC and IN cells, which further increased the firing rate of other cells in the network. We found that the firing rate of the IN cells decreased with an increase in the network oscillatory frequency ahead (**Figure 3B**); however, it increased under flicker stimulation, which increased the oscillatory frequency (**Figure 4C**). The IN cells received excitatory synapses from the GC and HTC cells, inhibitory synapses from the RE cells, and outputed inhibitory synapses to the RTC cells. The firing rate of the RE cells changed slightly (**Figures 4C2,C3**). Thus, flicker stimulation increased the firing rate of the IN cells by excitatory input from the GC and HTC cells and then enhanced its inhibition on the RTC cells, but this inhibition effect was less than that of light stimulation on the firing rate of the TC cells. Next, we further analyzeed the influence of flicker stimulation on the TC network oscillation.

Entrainment of 40-Hz light flicker depends on oscillatory states

A gamma frequency of 40 Hz, which is called the "cortical arousal" or working frequency of the brain, is considered an essential frequency for the interaction of various brain regions (Mcdermott et al., 2018). Experimental results showed that 40-Hz flicker stimulation induced the entrainment of the visual cortex, prefrontal cortex, and hippocampus (Herrmann, 2001; Adaikkan et al., 2019; Jones et al., 2019). Thus, we first explored the effect of the 40-Hz flicker stimulation on TCO (**Figure 5**). For the alpha oscillatory state, the 40-Hz flicker stimulation switched the firing pattern of the HTC cells and accelerated the oscillation frequency (**Figures 5A1,B1**), and the sLFP of both the thalamus and cortex revealed the occurrence of 40-Hz frequency oscillation with lower power than the endogenous oscillatory frequency (**Figure 5C1**). In addition, the 40-Hz flicker stimulation accelerated the endogenous oscillation frequency and induced a 40-Hz oscillation of the beta oscillation state (**Figure 5C2**). Meanwhile, for the gamma oscillation state, the 40-Hz flicker stimulation changed the endogenous oscillation frequency to 40 Hz and dramatically increased

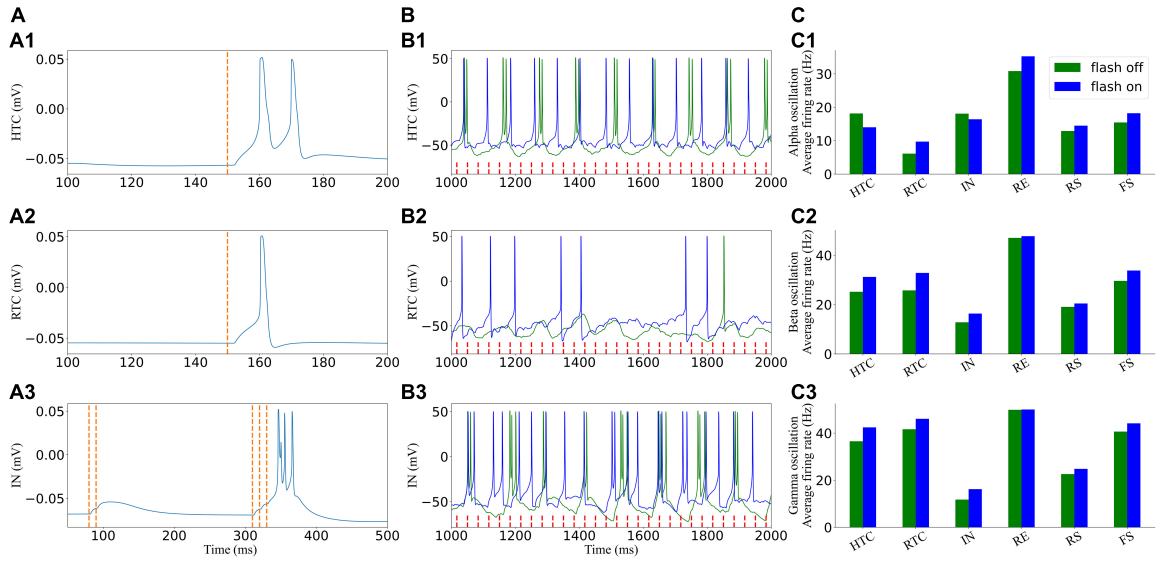

FIGURE 4
Effects of light (40 Hz) flicker on the TC network signal cells. **(A)** Single cells respond to incoming GC spikes: (A1–A3) HTC, RTC, and IN, respectively. **(B)** Voltage traces of two representative cells in the TC network before (green) and under (blue) light (40 Hz) flicker stimulation. **(C)** Average firing rate when the flicker was on and off: (C1–C3) alpha, beta, and gamma oscillatory states, respectively. The red dotted line represents incoming GC spikes.

the oscillation power (**Figure 5C3**), i.e., the 40-Hz flicker stimulation induced a resonant response (Herrmann et al., 2016). Because the cortex oscillation was mainly regulated by the RTC cells, these results suggest that the 40-Hz flicker induced a resonant response of the RTC cells, which made the cortex resonant at 40 Hz.

Effects of stimulation depend on gamma light frequency and intensity

To explore how different response patterns unfolded as a function of stimulation frequency and intensity, we generated a frequency spectrum heatmap of the sLFP in response to ascending gamma flicker stimulation (30–50 Hz) with three stimulation intensities for the three oscillatory states (**Figure 6**). In addition, to examine the oscillation dynamics and network synchronization modulated by gamma (30–50 Hz) flicker, we plot the peak network oscillation frequency, oscillation index (normalized spectral peak) along with the SI as a function of the stimulation frequency in response to the three stimulation intensities for the three oscillatory states in **Figure 7**.

There were some common effects of the dynamic interaction between stimulation and endogenous network oscillation across the three oscillatory states. First, the flicker stimulations accelerated all three oscillatory states (**Figure 6**). For the alpha oscillatory state, the endogenous oscillatory frequency changed from 9 to 12 Hz by flicker stimulation (**Figures 2C1**, **6A,D**). For the beta oscillatory state, the endogenous oscillatory frequency changed from 25 Hz to the gamma band (about 30 Hz) by flicker stimulation (**Figures 2C2**, **6B,E**). Meanwhile, for the gamma oscillatory state, the endogenous oscillatory frequency changed from about 35–40 Hz (**Figures 2C3**, **6C,F**). Second, different from the results of electrical or magnetic stimulation (Frohlich and McCormick, 2010; Li et al., 2019), the entrainment frequency range and oscillation power did not increase with the stimulation intensity, suggesting that more inputs at the same stimulation frequency could not yield more entrainment. For example, the entrainment frequency number decreased and the endogenous oscillatory frequency changed slightly with an increase in the stimulation intensity (**Figures 7B,C,E,F**). Finally, we found that the stimulation with one spike during each flicker induced the largest number of entrainment frequencies in the cortex under a gamma oscillation state (**Figure 7F1**) and the number of entrainment frequencies decreased non-linearly with an increase in the stimulation intensity (**Figure 7F**). For example, the entrainment phenomenon disappeared at 30, 32, 33, and 38 Hz of the cortex under the stimulation intensity of two spikes (**Figure 7F2**) compared with that of one spike (**Figure 7F1**), and 45-Hz stimulation induced the cortex entrainment for the stimulation intensity of two spikes, which was not entrainment under one spike stimulation intensity. This entrainment discontinuity phenomenon can also be observed in both the thalamus and cortex for the beta and gamma oscillatory states (**Figure 7**), suggesting that the network has the characteristics of a non-linear system, which agrees with previous studies (Popovych et al., 2005; Li et al., 2019).

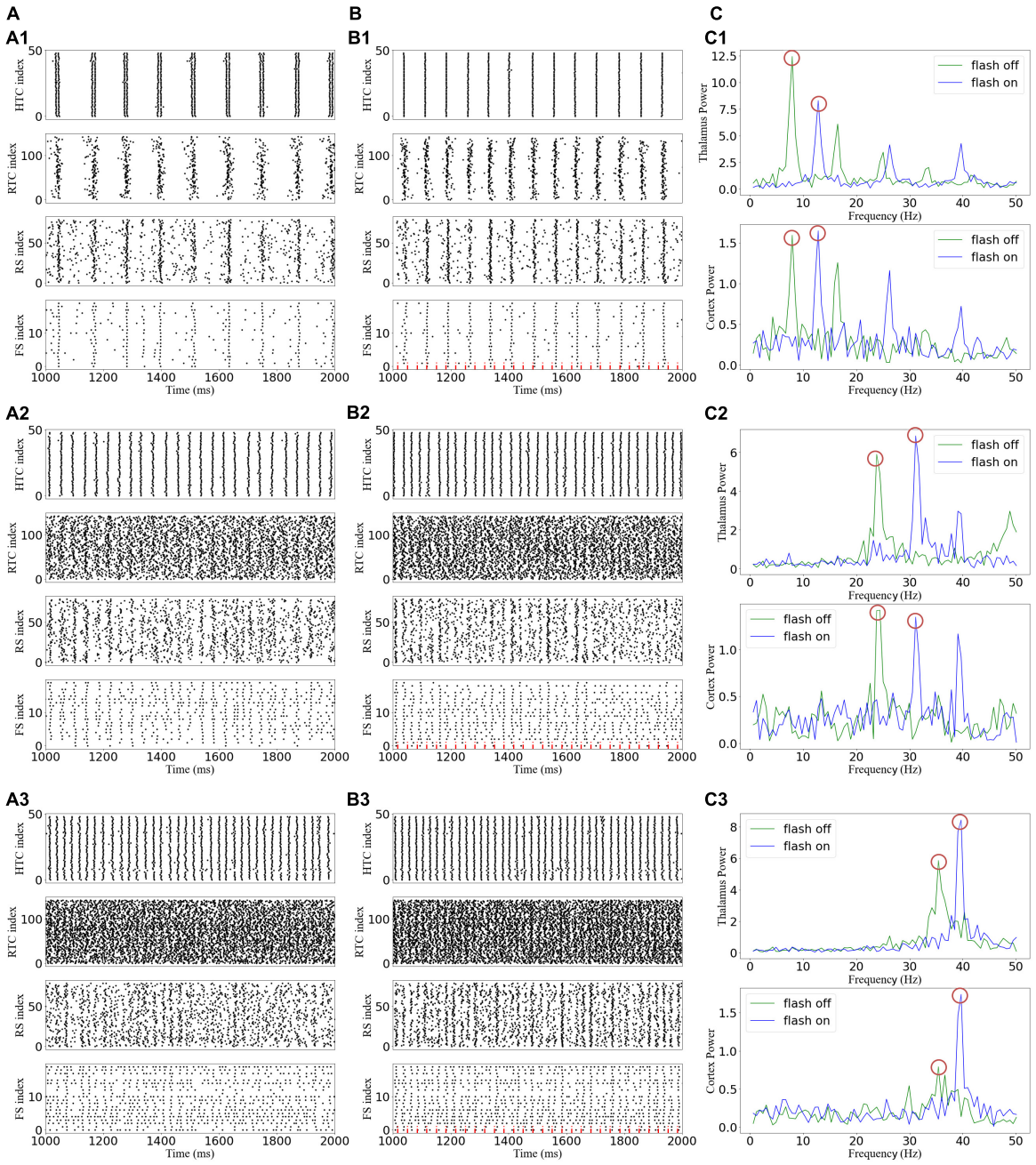

FIGURE 5
Effects of gamma (40 Hz) flicker on the TC network oscillatory state. **(A)** Spike rastergrams of HTC, RTC, RS, and FS cells before flicker stimulation: (A1–A3) alpha, beta, and gamma oscillatory states, respectively. **(B)** Spike rastergrams of HTC, RTC, RS, and FS cells under flicker stimulation. The red dotted line represents incoming GC spikes. **(C)** Frequency power spectrum of sLFP from the thalamus (top) and cortex (bottom). The red circles indicate the main oscillation frequencies.

Despite the similarities, stimulation also induced substantially different effects among the three oscillatory states. First, under the alpha oscillatory state, it did not evoke entrainment as the flicker frequency was far from the main endogenous oscillatory frequency. Similar to the non-linear characteristics of entrainment, the oscillation disappeared for the 36- and 39-Hz stimulation of one spike intensity and 48-Hz stimulation of two spike intensity (Figure 6A). There were multiple endogenous oscillations (about 14, 28, and 42 Hz) in the range of 0–50 Hz with weakened oscillatory power for high oscillatory frequency under the alpha oscillatory state, explaining the 40-Hz harmonic oscillation occurrence under

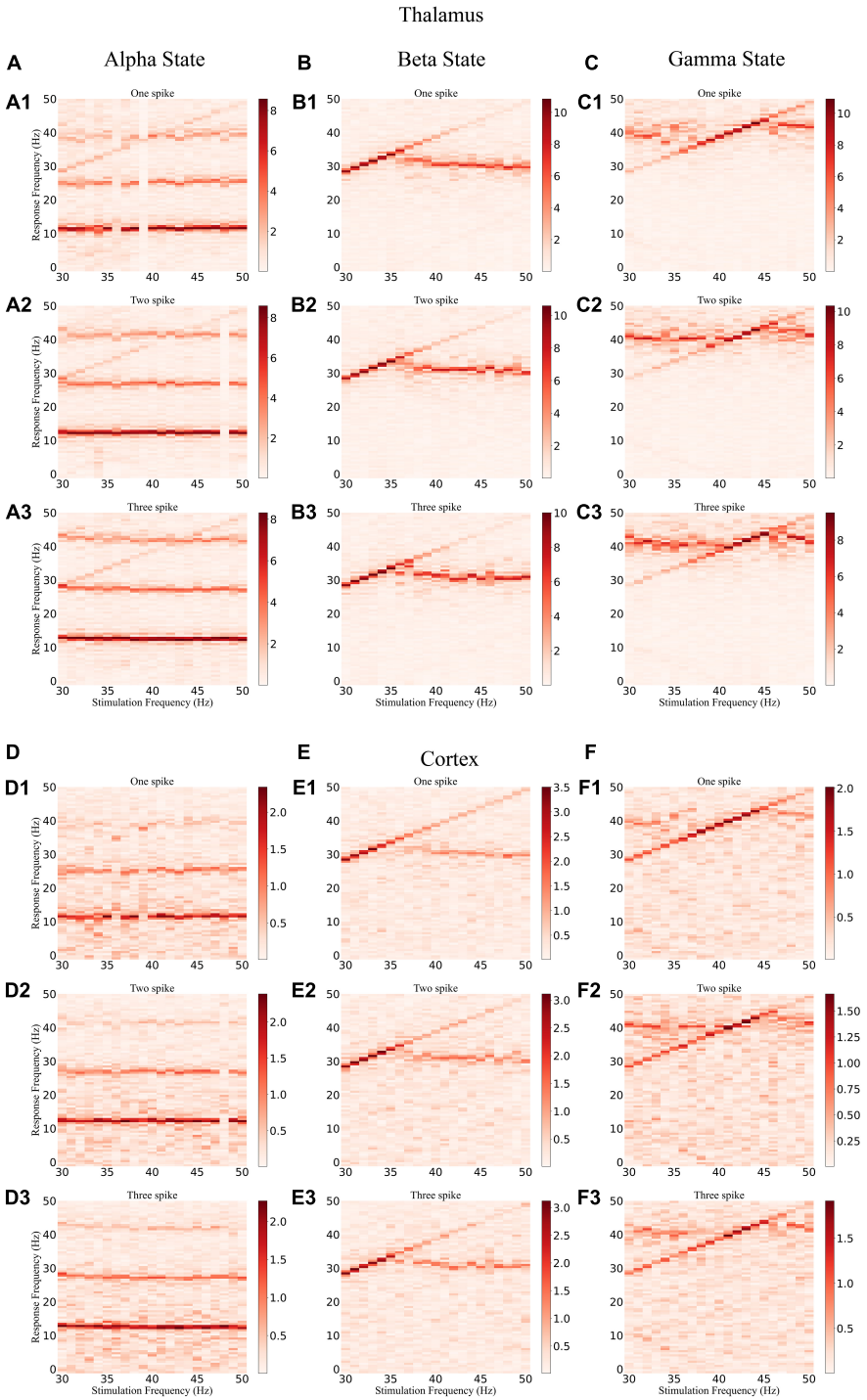

FIGURE 6
Frequency spectrum heatmap of the sLFP. **(A)** The alpha oscillatory state of the thalamus under light flickers: (A1–A3) intensity of one, two, and three spikes, respectively. **(B,C)** The beta and gamma oscillatory states of the thalamus under light flickers, respectively. **(D–F)** The alpha, beta, and gamma oscillatory states under light flickers of the cortex, respectively.

the 40-Hz flicker stimulation of the alpha oscillatory state (Figure 5C1). Meanwhile, for the beta and gamma oscillatory states, the network was prone to be entrained around the endogenous frequency, which was reflected by the highlighted spectral power along the diagonal in the frequency spectrum heatmap (Figures 6B,C,E,F), and the network synchrony

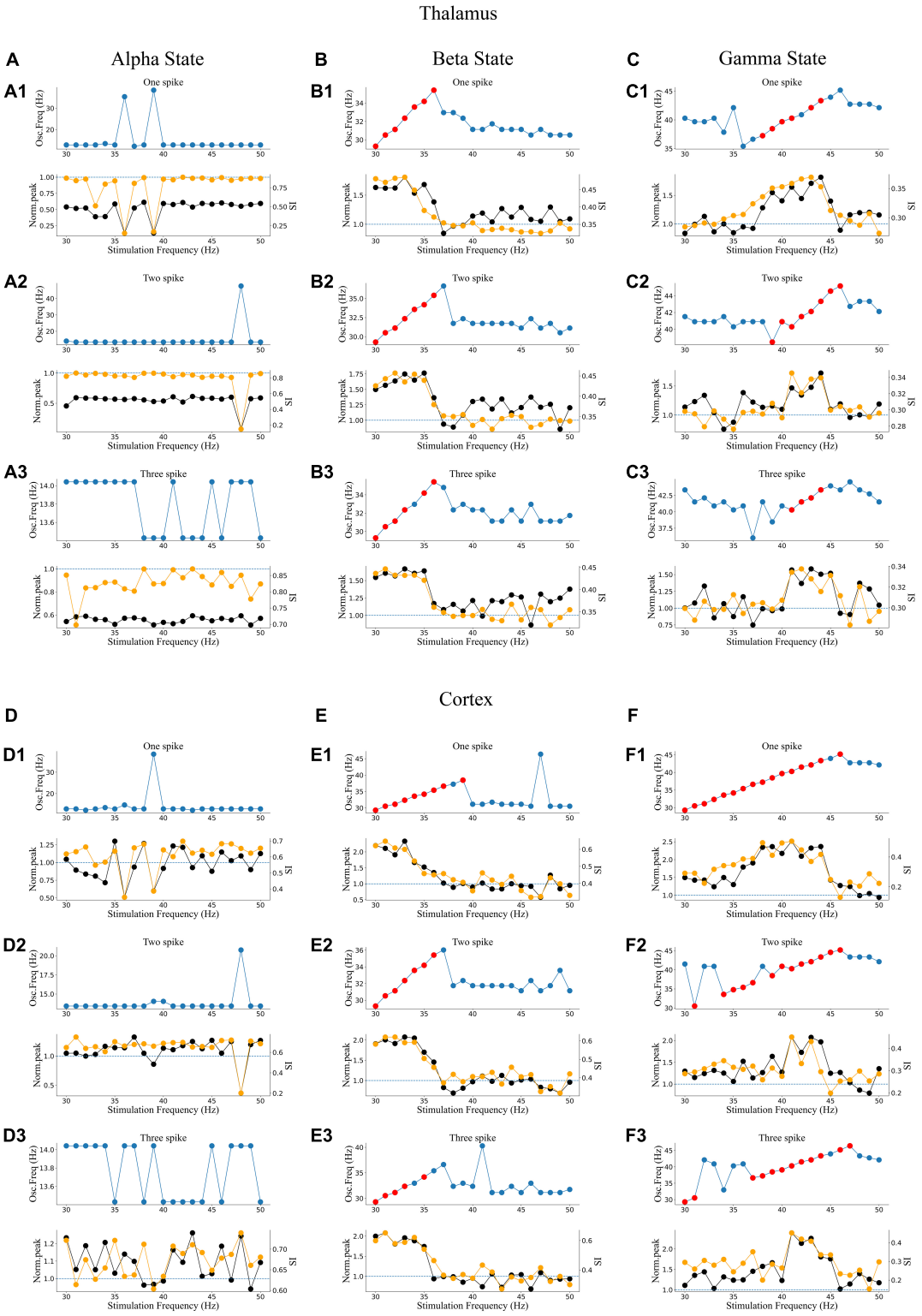

FIGURE 7
Oscillatory dynamics modulated by gamma flicker. **(A)** Effect of stimulation on the network dynamics of the alpha oscillatory state for the thalamus. Top: Dominant network oscillation frequency; Bottom: Normalized spectral peak (black) along with SI (orange) as a function of stimulation frequency (30–50 Hz) in the presence of three levels of stimulation intensity (A1–A3: one, two, and three spikes, respectively). **(B,C)** The beta and gamma oscillatory states of the thalamus, respectively. **(D–F)** The alpha, beta, and gamma oscillatory states of the cortex, respectively.

(SI) and oscillation power were enhanced by stimulation during entrainment (**Figures 7B,C,E,F**). These observations were consistent with previous findings that coupled oscillator systems failed to be entrained by a periodic drive if the stimulation frequency was far away from the average frequency of the system (Antonsen et al., 2008). Second, under the gamma oscillatory state, there were more entrainment frequencies in the cortex than in the thalamus (**Figures 7C,F**), attributable to the flicker stimulation inducing RTC cell entrainment more easily than both the HTC and RTC cells that made up the thalamus sLFP, and then the entrainment of RTC cells induced cortex entrainment. Finally, gamma (30–50 Hz) flicker stimulation suppressed alpha oscillation in the thalamus, as the normal peak power was always below 1 (**Figure 7A**), whereas the normal peak power is above 1 when entrainment for beta and gamma oscillations (**Figures 7B,C,E,F**). In addition, the highest oscillation power did not correspond to the highest SI; 43- or 44-Hz frequency flickers would evoke an entrainment response with the highest oscillation power under the gamma oscillatory state (**Figures 7C,F**).

Effects of stimulation depend on gamma (40 Hz) flicker duty cycle

A 50% duty cycle flicker stimulation is commonly used in experimental studies to realize gamma oscillation entrainment of the brain (Singer et al., 2018). The effects of light flicker duty cycles have been examined on electroencephalogram responses (Teng et al., 2011); it was found that for the flicker at 11–22 Hz, 50% duty cycles were more reliable than 25 or 10% duty cycles in inducing entrainment in the human occipital lobe. However, whether the duty cycle has similar effects for higher frequency flicker was not addressed. Considering the 40-Hz flicker stimulation as an example, the spectrum, peak power, and SI of the 40-Hz flicker stimulation with different duty cycles under the gamma oscillatory state are shown in **Figure 8**. Entrainment occurs when the duty cycle is less than or equal to 50%. For a duty cycle above 50%, the endogenous oscillatory frequency exceeds 40 Hz with a decrease in peak power and SI compared to that below 50%. For a duty cycle below or equal to 50%, one spike during each flicker could induce the entrainment with the highest peak power and SI. These results suggest that an effective method to enhance entrainment is ensuring each flicker makes the GC cells give only one spike within a 50% duty cycle instead of increasing the flicker intensity.

Experimental verification of the simulation entrainment

To verify the simulation results, we recorded the response of thalamic LFP under different light stimulation conditions. From **Figures 9A,B**, the entrainment could be observed when the flicker frequency was less than or equal to 40 Hz, and the entrainment of double stimulation frequency occurred at 30 and 32 Hz, attributable to the GC cells having both on and off cells that generated spikes when the light is on and off, respectively, and then formed an oscillation of double stimulation frequency. The spectral peak power was higher at 30, 32, and 34 Hz than at 36, 38, and 40 Hz (**Figure 9B**), attributable to the endogenous oscillatory power being higher at around 32 Hz than at around 38 Hz. These results suggest that the entrainment was affected by the endogenous oscillation, which corresponds to the oscillatory state. Compared with the frequency power spectrum without flicker stimulation, the low-frequency oscillation, such as the alpha oscillation, was suppressed (8–14 Hz), which agrees with the simulation results (**Figure 5C1**). For all flicker stimulations with different frequencies, the inhibitory effect is significant (**Figure 5B**). We also found that the oscillatory power was increased for beta oscillation (17–30 Hz). In addition, the flicker stimulation of different duty cycles was tested (**Figure 9C**); we found that the 10% duty cycle induced entrainment with the highest oscillatory power which agreed with the simulation results (**Figure 8**), and the oscillatory power was in descending order for duty cycles, 10, 30, 50, 70, and 90% (**Figure 9C**). Overall, part of the simulation results was verified by the experiments, i.e., the low-frequency suppression and oscillatory frequency acceleration effects were statistically significant, and the duty cycle below 50% was easier to induce entrainment.

Discussion

The TC pathway is the main route of communication between the eye and cerebral cortex (Kremkow and Alonso, 2018). Given how sensitive the human brain is to light, the use of light flickers to modulate the brain is commonly employed to improve cognition and restore cognitive dysfunctions (Martorell et al., 2019; Park et al., 2020; Zheng et al., 2020). In recent studies, visually evoked entrainment was evaluated in mice, revealing that 40-Hz visual stimuli induced 40-Hz entrainment in the visual, somatosensory, and prefrontal cortex, as well as in CA1 (Adaikkan et al., 2019). However, it remains unclear how the stimulation interacts with endogenous neural dynamics. Computational modeling offers a robust tool to examine the impact of rhythmic stimulation on oscillatory brain dynamics, but a brain oscillations network model in response to light flickers is lacking. To close this gap, we developed a TCO NN model and observed state-dependent entrainment of TCOs along with novel response mechanisms, such as entrainment discontinuity. Notably, we observed the modulation of TCOs by flickers from cell dynamics to network responses through a computational model and verified the low-frequency suppression and oscillatory frequency acceleration effects of gamma (30–50 Hz) flicker through experiments. The

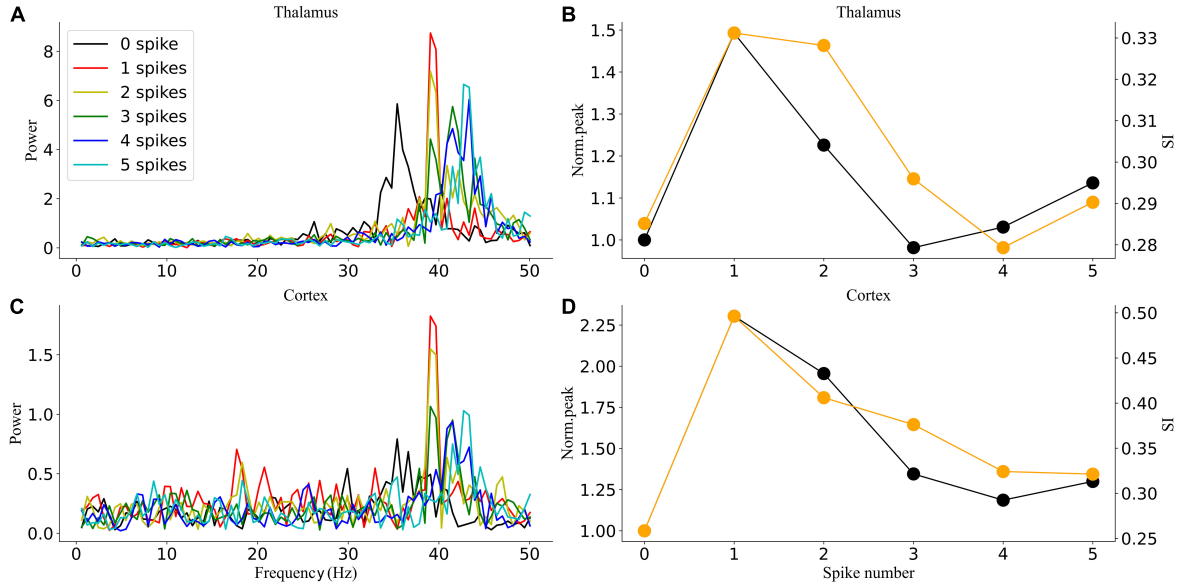

FIGURE 8
Oscillatory dynamics modulated by 40-Hz flicker with different duty cycles. **(A)** The sLFP spectrum of the thalamus. **(B)** The peak power and SI of the thalamus. **(C)** The sLFP spectrum of the cortex. **(D)** The peak power and SI of the cortex.

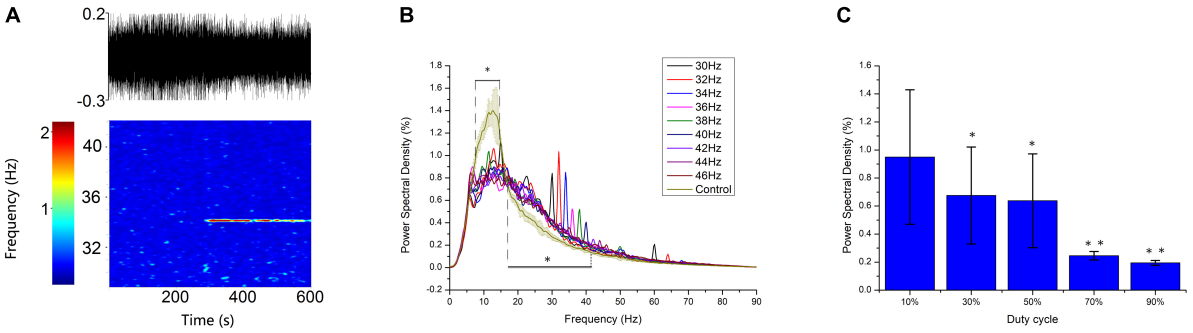

FIGURE 9
Experimental verification of the simulation entrainment. **(A)** Spectrogram analysis of 34-Hz flicker entrainment. Top: raw LFP of 10 min; Bottom: heatmap of the raw LFP. The flicker was turned on at 300 s. **(B)** A 5-min frequency power spectrum of flicker stimulation with different frequencies on a typic electrode. Error bars indicate s.e.m.; *indicate two-sample *t*-test between the oscillatory power with flicker stimulation and without flicker stimulation for all frequencies within the horizontal line, unequal variance statistical significance, $n = 9$, $p < 0.01$. **(C)** Power spectra density of flicker stimulation with different duty cycles at 40 Hz. Error bars indicate s.e.m.; *indicate two-sample *t*-test between 10% duty cycle and 30% or 50% duty cycle; **indicate two-sample *t*-test between 50% duty cycle and 70 or 90% duty cycle, unequal variance statistical significance, $n = 16$, $p < 0.01$.

simulation results offered crucial mechanistic insights into the modulation of TCOs in both dose- and state-dependent manner.

Entrainment mechanism of gamma (30–50 Hz) flicker

In this study, we investigated the entrainment mechanisms of gamma (30–50 Hz) flicker on TCOs; there were many interesting findings. First, we observed that the TC network carries oscillation information from the retina to the LGN and then to the cortex. Partial GC cells may generate resonant spike trains by light flicker, which agrees with a previous experimental study (Schwartz et al., 2007). In addition, the resonant spike trains induce TC cell entrainment when the stimulation frequency matches the intrinsic frequency of the NN (**Figures 6B,C**, **7B,C**). Then, the entrainment of TC cells further induces the cortex network resonant response (**Figures 6E,F**, **7E,F**). Second, the entrainment is state-dependent. With the HTC cells' firing pattern changed from a highly synchronous burst mode to a tonic spiking mode, gamma (30–50 Hz) flicker merely accelerated the network

oscillation and reduced the oscillation power for the alpha oscillatory state; moreover, all gamma (30–50 Hz) flickers fail to induce entrainment for the endogenous oscillatory frequency, which is almost unchanged by different gamma (30–50 Hz) flicker frequencies and intensities (**Figures 6A,D**, **7A,D**). Meanwhile, for the beta or gamma oscillatory state, entrainment occurs around the endogenous oscillatory frequency with high oscillation power and SI (**Figures 7B,C,E,F**). Finally, we found that a high firing rate of GC cells induced by high gamma (30–50 Hz) light intensity was not positively correlated with the enhancement of oscillation power or synchronization and the entrainment probability decreased on the contrary (**Figure 7**). As computational simulation and human EEG studies have shown a positive relationship between stimulus intensity and the level of entrainment (Herrmann et al., 2016; Jones et al., 2019), it may be that the high intensity flicker activated more GC cells to periodic firing which enhance the entrainment. Further investigating the effects of stimulation depending on the gamma (40 Hz) flicker duty cycle, we found that a single periodic input (GC cells give one spike during each flicker) could induce stronger entrainment than a periodic input with more than one spike during each flicker (**Figure 8**). In addition, part of the simulation results was verified by the experiments. These findings provide valuable insights into the application of gamma (30–50 Hz) flicker stimulation to treat neurological and psychiatric disorders.

Model limitations

Like any scientific study, there are some limitations to our study. First, the input from GC cells to LGN induced by gamma (30–50 Hz) flicker is simplified, as mentioned above. GC cells had complex harmonic patterns during the flicker sequence; we only simulated the resonant part, whereas some GC cells exhibited period-doubling, period-tripling, or other beat patterns (Schwartz et al., 2007), especially for flickers with frequencies below 34 Hz, as the experimental results show (**Figure 9B**). For the visual input of the non-resonant part, it may become the noise input and contribute to neuronal heterogeneity. More detailed experiment data are needed to construct realistic oscillation input from the GC cell network to LGN. Second, because the proposed model is a small-scale network focusing on neural oscillation generation and transition, it can only reproduce part of the NN characteristics. The simulation findings provide ideas for the experiments, but further experimental verification of the simulation is required. For example, the dependence of entrainment on the endogenous brain oscillatory states cannot be directly observed by animal experiments in this study. Third, the proposed model is based on data from several animal species, e.g., the GC cells' responses to flickers were from salamander and mouse, whereas the GC–TC and GC–IN synapse parameters were from cat dLGN. The main features of thalamic physiology seem to be well-conserved across species, but the comparison of model predictions with experimental data from the various species is required.

Conclusion

In conclusion, we demonstrated that the rhythmic modulation of TCOs by gamma (30–50 Hz) flicker is state-dependent. The endogenous oscillation state of the network determines whether gamma (30–50 Hz) stimulation can induce entrainment. In particular, the gamma (30–50 Hz) flicker induces entrainment under the beta and gamma oscillatory states but not for the alpha oscillatory state. Moreover, it is more prone to induce entrainment for gamma (30–50 Hz) flicker when GC cells give one spike during each flicker compared with multiple spikes. Overall, this study provides insights into how the biophysics of TCOs guides the emergence of complex, state-dependent mechanisms of target engagement, which can be leveraged for the future rational design of novel therapeutic stimulation modalities.

Data availability statement

The original contributions presented in this study are included in the article/**Supplementary material**, further inquiries can be directed to the corresponding authors.

Ethics statement

The animal study was reviewed and approved by Institutional Animal Care and Use Committee (IACUC) of the Chinese Academy of Military Medical Science.

Author contributions

BC and MZ contributed to the conception and design of the study. KW, AW, and YF contributed to the experiment of the study, analyzed the data, and wrote the first draft of the manuscript. All authors contributed to manuscript revision, read, and approved the submitted version.

Funding

This study was supported by the Tianjin Institute of Environmental and Operational Medicine.

Conflict of interest

The authors declare that the research was conducted in the absence of any commercial or financial relationships that could be construed as a potential conflict of interest.

Publisher's note

All claims expressed in this article are solely those of the authors and do not necessarily represent those of their affiliated organizations, or those of the publisher, the editors and the reviewers. Any product that may be evaluated in this article, or claim that may be made by its manufacturer, is not guaranteed or endorsed by the publisher.

Supplementary material

The Supplementary Material for this article can be found online at: https://www.frontiersin.org/articles/10.3389/fninf.2022.968907/full#supplementary-material

References

Acuna-Goycolea, C., Brenowitz, S. D., and Regehr, W. G. (2008). Active dendritic conductances dynamically regulate GABA release from thalamic interneurons. *Neuron* 57, 420–431. doi: 10.1016/j.neuron.2007.12.022

Adaikkan, C., Middleton, S. J., Marco, A., Pao, P. C., Mathys, H., Kim, D. N., et al. (2019). Gamma Entrainment Binds Higher-Order Brain Regions and Offers Neuroprotection. *Neuron* 102:929–943e8. doi: 10.1016/j.neuron.2019.04.011

Adaikkan, C., and Tsai, L. H. (2020). Gamma Entrainment: Impact on Neurocircuits, Glia, and Therapeutic Opportunities. *Trends Neurosci.* 43, 24–41. doi: 10.1016/j.tins.2019.11.001

Antonsen, T. M. Jr., Faghih, R. T., Girvan, M., Ott, E., and Platig, J. (2008). External periodic driving of large systems of globally coupled phase oscillators. *Chaos* 18:037112. doi: 10.1063/1.2952447

Blitz, D. M., and Regehr, W. G. (2005). Timing and specificity of feed-forward inhibition within the LGN. *Neuron* 45, 917–928. doi: 10.1016/j.neuron.2005.01.033

Bouyer, J. J., Montaron, M. F., and Rougeul, A. (1981). Fast fronto-parietal rhythms during combined focused attentive behaviour and immobility in cat: Cortical and thalamic localizations. *Electroencephalogr. Clin. Neurophysiol.* 51, 244–252. doi: 10.1016/0013-4694(81)90138-3

Brücke, C., Bock, A., Huebl, J., Krauss, J. K., Schönecker, T., Schneider, G. H., et al. (2013). Thalamic gamma oscillations correlate with reaction time in a Go/noGo task in patients with essential tremor. *Neuroimage* 75, 36–45. doi: 10.1016/j.neuroimage.2013.02.038

Casti, A., Hayot, F., Xiao, Y., and Kaplan, E. (2008). A simple model of retina-LGN transmission. *J. Comput. Neurosci.* 24, 235–252. doi: 10.1007/s10827-007-0053-7

Chariker, L., Shapley, R., and Young, L. S. (2018). Rhythm and Synchrony in a Cortical Network Model. *J. Neurosci.* 38, 8621–8634. doi: 10.1523/JNEUROSCI.0675-18.2018

Einevoll, G. T., and Heggelund, P. (2000). Mathematical models for the spatial receptive-field organization of nonlagged X-cells in dorsal lateral geniculate nucleus of cat. *Visual. Neurosci.* 17, 871–885. doi: 10.1017/s0952523800176060

Frohlich, F., and McCormick, D. A. (2010). Endogenous electric fields may guide neocortical network activity. *Neuron* 67, 129–143. doi: 10.1016/j.neuron.2010.06.005

Heiberg, T., Hagen, E., Halnes, G., and Einevoll, G. T. (2016). Biophysical Network Modelling of the dLGN Circuit: Different Effects of Triadic and Axonal Inhibition on Visual Responses of Relay Cells. *PLoS Comput. Biol.* 12:e1004929. doi: 10.1371/journal.pcbi.1004929

Herrmann, C. S. (2001). Human EEG responses to 1-100 Hz flicker: Resonance phenomena in visual cortex and their potential correlation to cognitive phenomena. *Exp. Brain Res.* 137, 346–353. doi: 10.1007/s002210100682

Herrmann, C. S., Murray, M. M., Ionta, S., Hutt, A., and Lefebvre, J. (2016). Shaping Intrinsic Neural Oscillations with Periodic Stimulation. *J. Neurosci.* 36, 5328–5337. doi: 10.1523/jneurosci.0236-16.2016

Huang, W. A. I, Stitt, M., Negahbani, E., Passey, D. J., Ahn, S., Davey, M., et al. (2021). Transcranial alternating current stimulation entrains alpha oscillations by preferential phase synchronization of fast-spiking cortical neurons to stimulation waveform. *Nat. Commun.* 12:3151. doi: 10.1038/s41467-021-23021-2

Hughes, S. W., and Crunelli, V. (2005). Thalamic mechanisms of EEG alpha rhythms and their pathological implications. *Neuroscientist* 11, 357–372. doi: 10.1177/1073858405277450

Hughes, S. W., Lörincz, M., Cope, D. W., Blethyn, K. L., Kékesi, K. A., Parri, H. R., et al. (2004). Synchronized oscillations at alpha and theta frequencies in the lateral geniculate nucleus. *Neuron* 42, 253–268. doi: 10.1016/s0896-6273(04)00191-6

Izhikevich, E. M., and Edelman, G. M. (2008). Large-scale model of mammalian thalamocortical systems. *Proc. Natl. Acad. Sci. U.S.A.* 105, 3593–3598. doi: 10.1073/pnas.0712231105

Jones, M., McDermott, B., Oliveira, B. L., O'Brien, A., Coogan, D., and Lang, M. (2019). Gamma Band Light Stimulation in Human Case Studies: Groundwork for Potential Alzheimer's Disease Treatment. *J. Alzheimer's Dis.* 70, 171–185. doi: 10.3233/jad-190299

Kremkow, J., and Alonso, J. M. (2018). Thalamocortical Circuits and Functional Architecture. *Annu. Rev. Vis. Sci.* 4, 263–285. doi: 10.1146/annurev-vision-091517-034122

Li, G., and Cleland, T. A. (2013). A two-layer biophysical model of cholinergic neuromodulation in olfactory bulb. *J. Neurosci.* 33, 3037–3058. doi: 10.1523/JNEUROSCI.2831-12.2013

Li, G., Henriquez, C. S., and Frohlich, F. (2017). Unified thalamic model generates multiple distinct oscillations with state-dependent entrainment by stimulation. *PLoS Comput. Biol.* 13:e1005797. doi: 10.1371/journal.pcbi.1005797

Li, G., Henriquez, C. S., and Frohlich, F. (2019). Rhythmic modulation of thalamic oscillations depends on intrinsic cellular dynamics. *J. Neural Eng.* 16:016013. doi: 10.1088/1741-2552/aaeb03

Llinás, R. R., Ribary, U., Jeanmonod, D., Kronberg, E., and Mitra, P. P. (1999). Thalamocortical dysrhythmia: A neurological and neuropsychiatric syndrome characterized by magnetoencephalography. *Proc. Natl. Acad. Sci. U.S.A.* 96, 15222–15227. doi: 10.1073/pnas.96.26.15222

Lörincz, M. L., Crunelli, V., and Hughes, S. W. (2008). Cellular dynamics of cholinergically induced alpha (8-13 Hz) rhythms in sensory thalamic nuclei in vitro. *J. Neurosci.* 28, 660–671. doi: 10.1523/jneurosci.4468-07.2008

Lorincz, M. L., Kékesi, K. A., Juhász, G., Crunelli, V., and Hughes, S. W. (2009). Temporal framing of thalamic relay-mode firing by phasic inhibition during the alpha rhythm. *Neuron* 63, 683–696. doi: 10.1016/j.neuron.2009.08.012

Madadi Asl, M., Vahabie, A.-H., Valizadeh, A., and Tass, P. A. (2022). Spike-Timing-Dependent Plasticity Mediated by Dopamine and its Role in Parkinson's Disease Pathophysiology. *Front. Netw.Physiol.* 2:817524. doi: 10.3389/fnetp.2022.817524

Martorell, A. J., Paulson, A. L., Suk, H. J., Abdurrob, F., Drummond, G. T., Guan, W., et al. (2019). Multi-sensory Gamma Stimulation Ameliorates Alzheimer's-Associated Pathology and Improves Cognition. *Cell* 177:256-271.e22. doi: 10.1016/j.cell.2019.02.014

Mathalon, D. H., and Sohal, V. S. (2015). Neural Oscillations and Synchrony in Brain Dysfunction and Neuropsychiatric Disorders: It's About Time. *JAMA psychiatry* 72, 840–844. doi: 10.1001/jamapsychiatry.2015.0483

Mcdermott, B., Porter, E., Hughes, D., Mcginley, B., Lang, M., Halloran, M. O., et al. (2018). Gamma Band Neural Stimulation in Humans and the Promise of

a New Modality to Prevent and Treat Alzheimer's Disease. *J. Alzheimers Dis.* 65, 1–30. doi: 10.3233/JAD-180391

Negahbani, E., Kasten, F. H., Herrmann, C. S., and Frohlich, F. (2018). Targeting alpha-band oscillations in a cortical model with amplitude-modulated high-frequency transcranial electric stimulation. *Neuroimage* 173, 3–12. doi: 10.1016/j.neuroimage.2018.02.005

Niedermeyer, E. (1997). Alpha rhythms as physiological and abnormal phenomena. *Int. J. Psychophysiol.* 26, 31–49. doi: 10.1016/s0167-8760(97)00754-x

O'Reilly, C., Iavarone, E., Yi, J., and Hill, S. L. (2021). Rodent somatosensory thalamocortical circuitry: Neurons, synapses, and connectivity. *Neurosci. Biobehav. Rev.* 126, 213–235. doi: 10.1016/j.neubiorev.2021.03.015

Park, S. S., Park, H. S., Kim, C. J., Kang, H. S., Kim, D. H., Baek, S. S., et al. (2020). Physical exercise during exposure to 40-Hz light flicker improves cognitive functions in the 3xTg mouse model of Alzheimer's disease. *Alzheimer's Res. Ther.* 12:62. doi: 10.1186/s13195-020-00631-4

Popovych, O. V., Hauptmann, C., and Tass, P. A. (2005). Effective desynchronization by nonlinear delayed feedback. *Physical. Rev. Lett.* 94:164102. doi: 10.1103/PhysRevLett.94.164102

Schwartz, G., and Berry, M. J. II (2008). Sophisticated temporal pattern recognition in retinal ganglion cells. *J. Neurophysiol.* 99, 1787–1798. doi: 10.1152/jn.01025.2007

Schwartz, G., Harris, R., Shrom, D., and Berry, M. J. II (2007). Detection and prediction of periodic patterns by the retina. *Nat. Neurosci.* 10, 552–554. doi: 10.1038/nn1887

Singer, A. C., Martorell, A. J., Douglas, J. M., Abdurrob, F., Attokaren, M. K., Tipton, J., et al. (2018). Noninvasive 40-Hz light flicker to recruit microglia and reduce amyloid beta load. *Nat. Protoc.* 13, 1850–1868. doi: 10.1038/s41596-018-0021-x

Steriade, M., Dossi, R. C., Paré, D., and Oakson, G. (1991). Fast oscillations (20-40 Hz) in thalamocortical systems and their potentiation by mesopontine cholinergic nuclei in the cat. *Proc. Natl. Acad. Sci. U.S. A.* 88, 4396–4400. doi: 10.1073/pnas.88.10.4396

Steriade, M., McCormick, D. A., and Sejnowski, T. J. (1993). Thalamocortical oscillations in the sleeping and aroused brain. *Science* 262, 679–685. doi: 10.1126/science.8235588

Susin, E., and Destexhe, A. (2021). Integration, coincidence detection and resonance in networks of spiking neurons expressing Gamma oscillations and asynchronous states. *PLoS Comput. Biol.* 17:e1009416. doi: 10.1371/journal.pcbi.1009416

Teng, F., Chen, Y., Choong, A. M., Gustafson, S., Reichley, C., Lawhead, P., et al. (2011). Square or sine: Finding a waveform with high success rate of eliciting SSVEP. *Comput. Intell. Neurosci.* 2011:364385. doi: 10.1155/2011/364385

Tian, T., Qin, X., Wang, Y., Shi, Y., and Yang, X. (2021). 40 Hz Light Flicker Promotes Learning and Memory via Long Term Depression in Wild-Type Mice. *J. Alzheimer's Dis.* 84, 983–993. doi: 10.3233/JAD-215212

Van Horn, S. C., Erişir, A., and Sherman, S. M. (2000). Relative distribution of synapses in the A-laminae of the lateral geniculate nucleus of the cat. *J. Comp. Neurol.* 416, 509–520.

Werner, B., Cook, P. B., and Passaglia, C. L. (2008). Complex temporal response patterns with a simple retinal circuit. *J. Neurophysiol.* 100, 1087–1097. doi: 10.1152/jn.90527.2008

Yan, R. J., Gong, H. Q., Zhang, P. M., and Liang, P. J. (2016). Coding Properties of Mouse Retinal Ganglion Cells with Dual-Peak Patterns with Respect to Stimulus Intervals. *Front. Comput. Neurosci.* 10:75. doi: 10.3389/fncom.2016.00075

Zheng, L., Yu, M., Lin, R., Wang, Y., Zhuo, Z., Cheng, N., et al. (2020). Rhythmic light flicker rescues hippocampal low gamma and protects ischemic neurons by enhancing presynaptic plasticity. *Nat. Commun.* 11:3012. doi: 10.1038/s41467-020-16826-0

frontiers | Frontiers in Human Neuroscience

TYPE Original Research
PUBLISHED 26 January 2023
DOI 10.3389/fnhum.2022.1013155

OPEN ACCESS

EDITED BY
Hemant Bokil,
Boston Scientific, United States

REVIEWED BY
Justus Alfred Kromer,
Stanford University, United States
Nada Yousif,
University of Hertfordshire, United Kingdom

*CORRESPONDENCE
Sina Salehi
✉ sina253@gmail.com
Mojtaba Madadi Asl
✉ m.madadi@ipm.ir

SPECIALTY SECTION
This article was submitted to Brain Imaging and Stimulation, a section of the journal Frontiers in Human Neuroscience

RECEIVED 06 August 2022
ACCEPTED 09 December 2022
PUBLISHED 26 January 2023

CITATION
Bahadori-Jahromi F, Salehi S, Madadi Asl M and Valizadeh A (2023) Efficient suppression of parkinsonian beta oscillations in a closed-loop model of deep brain stimulation with amplitude modulation. *Front. Hum. Neurosci.* 16:1013155. doi: 10.3389/fnhum.2022.1013155

Efficient suppression of parkinsonian beta oscillations in a closed-loop model of deep brain stimulation with amplitude modulation

Fatemeh Bahadori-Jahromi[1], Sina Salehi[2]*, Mojtaba Madadi Asl[3,4]* and Alireza Valizadeh[1,4]

[1]Department of Physics, Institute for Advanced Studies in Basic Sciences (IASBS), Zanjan, Iran, [2]Shiraz Neuroscience Research Center, Shiraz University of Medical Sciences, Shiraz, Iran, [3]School of Biological Sciences, Institute for Research in Fundamental Sciences (IPM), Tehran, Iran, [4]Pasargad Institute for Advanced Innovative Solutions (PIAIS), Tehran, Iran

Introduction: Parkinson's disease (PD) is a movement disorder characterized by the pathological beta band (15–30 Hz) neural oscillations within the basal ganglia (BG). It is shown that the suppression of abnormal beta oscillations is correlated with the improvement of PD motor symptoms, which is a goal of standard therapies including deep brain stimulation (DBS). To overcome the stimulation-induced side effects and inefficiencies of conventional DBS (cDBS) and to reduce the administered stimulation current, closed-loop adaptive DBS (aDBS) techniques were developed. In this method, the frequency and/or amplitude of stimulation are modulated based on various disease biomarkers.

Methods: Here, by computational modeling of a cortico-BG-thalamic network in normal and PD conditions, we show that closed-loop aDBS of the subthalamic nucleus (STN) with amplitude modulation leads to a more effective suppression of pathological beta oscillations within the parkinsonian BG.

Results: Our results show that beta band neural oscillations are restored to their normal range and the reliability of the response of the thalamic neurons to motor cortex commands is retained due to aDBS with amplitude modulation. Furthermore, notably less stimulation current is administered during aDBS compared with cDBS due to a closed-loop control of stimulation amplitude based on the STN local field potential (LFP) beta activity.

Discussion: Efficient models of closed-loop stimulation may contribute to the clinical development of optimized aDBS techniques designed to reduce potential stimulation-induced side effects of cDBS in PD patients while leading to a better therapeutic outcome.

KEYWORDS

beta oscillation, Parkinson's disease, closed-loop deep brain stimulation, amplitude modulation, synchronization

1. Introduction

Parkinson's disease (PD) is a neurodegenerative movement disorder characterized by abnormal neural oscillations in the beta band (15–30 Hz) frequency within the basal ganglia (BG) (Brown et al., 2001; Hammond et al., 2007; Mallet et al., 2008; Asadi et al., 2022). The BG circuitry is massively modulated by dopamine (DA) released from dopaminergic (DAergic) neurons in the substantia nigra pars compacta (SNc). Significant degeneration of DAergic neurons triggers a cascade of maladaptive or compensatory changes within the BG (Blandini et al., 2000; Madadi Asl et al., 2022b), ultimately resulting in the emergence of pathological patterns of activity and connectivity observed

in experimental PD models (Galvan et al., 2015; Madadi Asl et al., 2022b). Particularly, striatal inhibition in the direct pathway is suppressed following DA loss, whereas it is enhanced in the indirect pathway (Lemos et al., 2016). As a result, the inhibitory control of globus pallidus externus (GPe) over subthalamic nucleus (STN) reduced (Fan et al., 2012; Madadi Asl et al., 2022a) and excessive beta oscillations emerged (Brown et al., 2001; Hammond et al., 2007; Mallet et al., 2008; Asadi et al., 2022). Finally, globus pallidus internus (GPi) receives more excitatory drive leading to an enhanced inhibition of the thalamo-cortical circuits, which contributes to motor dysfunction in PD (DeLong, 1990; Graybiel et al., 1994).

It is shown that the reduction of pathological beta oscillations is correlated with improved motor performance in PD (Meissner et al., 2005; Kühn et al., 2006, 2008). High-frequency (>100 Hz) deep brain stimulation (HF-DBS) is the standard clinical therapy for medically refractory PD (Benabid, 2003; Benabid et al., 2009). In a conventional DBS (cDBS) protocol, a train of electrical pulses is continuously administered to the target structure, for example, the STN using chronically implanted depth electrodes (Benabid, 2003; Benabid et al., 2009). HF-DBS may cause side effects, such as dysarthria, dysesthesia, and cerebellar ataxia (Volkmann, 2004; Baizabal-Carvallo and Jankovic, 2016). On the other hand, some patients with PD may show unsatisfactory outcomes despite proper electrode placement (Limousin et al., 1999). This led to the pre-clinical and clinical testing of closed-loop and on-demand adaptive DBS (aDBS) (Little et al., 2013, 2016; Priori et al., 2013; Rosa et al., 2015, 2017; Johnson et al., 2016; Piña-Fuentes et al., 2017; Tinkhauser et al., 2017; Guidetti et al., 2021) for a more effective control of pathological beta band oscillatory activity.

In a closed-loop aDBS configuration, the patient's clinical state is assessed and utilized to adjust stimulation parameters, that is, to modify the frequency and/or amplitude of stimulation in a state-dependent manner (Daneshzand et al., 2018; Popovych and Tass, 2019; Fleming et al., 2020b). This can ultimately reduce possible side effects by reducing the amount of administered stimulation current (Pyragas et al., 2020). The modulation of stimulation parameters in closed-loop approaches is realized based on specific biomarkers that are used to estimate the symptom severity. One of the appealing biomarkers for closed-loop DBS in PD is the power of beta band oscillatory activity in the STN local field potential (LFP) that has been utilized in several variations of aDBS protocols addressed both in computational (Tukhlina et al., 2007; Popovych et al., 2017b; Popovych and Tass, 2019; Fleming et al., 2020a,b) and experimental (Little et al., 2013; Rosa et al., 2015; Arlotti et al., 2018; Velisar et al., 2019) studies.

One of the first closed-loop strategies tested in patients with PD was the on–off stimulation strategy where stimulation is turned on and off depending on whether the biomarker exceeded a predefined threshold (Little et al., 2013, 2016). More specifically, aDBS of the STN in patients with advanced PD improved motor symptoms by 66%, which were 29% better than cDBS, despite delivering $\lesssim$ 50% less current than cDBS. These improvements were achieved with a 56% reduction in stimulation time compared with cDBS (Little et al., 2013). In comparison with the open-loop stimulation, the on–off stimulation strategy can be more effective in suppressing abnormal oscillations in patients with PD; however, its effectiveness is limited by the fixed choice of stimulation parameters (Little et al., 2013, 2016), as in open-loop cDBS. Later, a dual threshold strategy was introduced that modifies the amplitude of stimulation to confine the biomarker within the desired range (Velisar et al., 2019). Alternatively, stimulation strategies employing proportional amplitude modulation, in which the DBS amplitude is proportional to the measured biomarker (e.g., LFP beta band activity), can be, in principle, more beneficiary as demonstrated both computationally (Tukhlina et al., 2007; Popovych and Tass, 2019) and clinically (Rosa et al., 2015; Arlotti et al., 2018). Indeed, the adjustment of stimulation amplitude based on slowly varying beta activity is not only well-tolerated by patients but also can effectively reduce pathological beta oscillations to improve PD symptoms (Rosa et al., 2015; Arlotti et al., 2018).

In the context of amplitude modulation stimulation strategies, control theory incorporates a variety of schemes that may be more efficient in suppressing PD symptoms, while reducing the amount of delivered current. Development and testing of effective control schemes for DBS in a clinical situation are challenging due to the invasive nature of DBS surgery. Alternatively, computational modeling offers a suitable framework for designing and testing different versions of closed-loop DBS control (Goldobin et al., 2003; Rosenblum and Pikovsky, 2004; Gorzelic et al., 2013; Popovych et al., 2017a; Popovych and Tass, 2019; Su et al., 2019; Fleming et al., 2020a,b). For example, adaptive pulsatile linear delayed feedback stimulation (apLDF) with on–off delivery can induce desynchronization in pathologically synchronized network models (Popovych and Tass, 2019). Interestingly, introducing interphase gap between the stimulation pulses can significantly improve the stimulation-induced desynchronization (Popovych et al., 2017b). Recent computational studies employed clinically viable control schemes for amplitude and frequency modulation, for example, proportional (P) and proportional–integral (PI) closed-loop controllers to suppress PD-related pathological beta activity with a reduced amount of delivered stimulation current in simple network models (Fleming et al., 2020a,b; Weerasinghe et al., 2021). Other closed-loop computational approaches such as phase-specific aDBS, whereby the stimulation is locked to a particular phase of tremor, have been shown to improve therapeutic efficacy (Toth and Wilson, 2022). Specifically, near-periodic phase-specific aDBS can effectively disrupt excessive synchronization in large populations of oscillatory neurons caused by strong coupling.

In this study, our aim was to present a simple, yet comprehensive bio-inspired model of the cortico-BG-thalamic network comprising cortex, striatal D1 and D2 medium spiny neurons (MSNs), GPe, globus pallidus internus (GPi), STN, and thalamus. A more complete set of the BG nuclei used here improves the model predictions and its accuracy. Specifically, we set the model parameters in a way that the dynamics of the network were similar to those reported experimentally for normal and PD states (Holgado et al., 2010; Pavlides et al., 2015). Then, we administered high-frequency stimulation to the parkinsonian STN in our model and investigated its effect on the pathological beta oscillations within the BG. First, we used a cDBS protocol where stimulation pulses were continuously delivered to the STN with a fixed frequency and amplitude. To improve the beta suppression efficiency while consuming less stimulation current, we then used an aDBS protocol that employed the same stimulation frequency but with a closed-loop feedback control of stimulation amplitude based on the STN beta activity.

Our results show that aDBS protocol can effectively suppress abnormal beta oscillations within the BG and preserve thalamus reliability while a notably low level of stimulation current is administered in comparison with the cDBS protocol. Particularly, the beta band peaks in the power spectrum density (PSD) of the parkinsonian STN, GPe, and GPi activities were robustly suppressed and shifted to their normal range by aDBS. Comparison between aDBS and cDBS shows that the aDBS protocol with amplitude modulation can be more efficient at different stimulation frequencies, that is, abnormal beta oscillations were effectively suppressed while the administered stimulation current was reduced. Developing such closed-loop models of aDBS may contribute to the pre-clinical testing and clinical optimization of more efficient aDBS techniques by reducing stimulation current to reduce potential side effects in patients with PD undergoing treatment.

2. Methods

2.1. Network model

We considered a bio-inspired and comprehensive cortico-BG-thalamic network model implemented in MATLAB comprising cortex (simulated as 500 external inputs), striatal D1 MSNs (85 neurons) and D2 MSNs (85 neurons), GPe (17 neurons), GPi (17 neurons), STN (137 neurons), and thalamus (140 neurons), as schematically shown in Figure 1A1. The ratio of cells was estimated based on the experimentally reported number of neurons per volume, that is, neuronal density in rats (Oorschot, 1996). Connection probability and the strength of synaptic connections between different pathways used in our simulations are shown in Table 1, which are chosen in accordance with experimental observations in rats (Kita and Kita, 1994; Mink, 1996; Baufreton et al., 2009). Specifically, in the PD state, D2 $\longrightarrow$ GPe synaptic strength was increased, whereas D1 $\longrightarrow$ GPi and GPe $\longrightarrow$ GPe synaptic strengths were decreased with respect to the normal state (see Figures 1A1, A2). Furthermore, an external current mimicking the input from other brain regions was applied to STN, GPe, and GPi, that is, $I_{app}(\text{STN}) = 18\,\text{pA}/\mu\text{m}^2$, $I_{app}(\text{GPe}) = 12\,\text{pA}/\mu\text{m}^2$, and $I_{app}(\text{GPi}) = 4.0\,\text{pA}/\mu\text{m}^2$ in normal condition, and $I_{app}(\text{STN}) = 15.5\,\text{pA}/\mu\text{m}^2$, $I_{app}(\text{GPe}) = 0.4\,\text{pA}/\mu\text{m}^2$, and $I_{app}(\text{GPi}) = 0.0\,\text{pA}/\mu\text{m}^2$ in the PD state. Other parameters in the PD state were similar to those used in the normal state.

In the cortico-BG-thalamic circuitry shown in Figure 1A1, the striatum receives excitatory inputs from the cortex and relays them toward GPi using two competing pathways: the direct pathway comprising striatal D1 receptor expressing MSNs and the indirect pathway governed by D2 receptor expressing MSNs. Cortical inputs in the indirect pathway are then mediated by the inhibitory GPe neurons, which are bidirectionally connected to STN neurons. The output of STN is then transmitted to the GPi, which inhibits the thalamus. The thalamus sends excitatory input to the cortex and receives excitatory feedback. The STN also receives direct excitatory input from the cortex using the hyperdirect pathway. Altered synaptic transmission in the PD condition with respect to normal condition is schematically presented in Figures 1A1, A2, by changing the relative thickness of arrows in different pathways.

2.2. Neuron model

2.2.1. STN neurons

The membrane potential dynamics of STN neurons are described by a single-compartment conductance-based model introduced by Terman et al. (2002), as follows:

$$C_m \frac{dV_i}{dt} = -I_L - I_K - I_{Na} - I_T - I_{Ca} - I_{AHP} - I_{GPe\to STN} + I_{SM} + I_{app} + I_{DBS}, \tag{1}$$

where $C_m = 1\,\text{pF}/\mu\text{m}^2$ is the membrane capacitance. $I_{GPe\to STN}$ is the synaptic current, I_{SM} is the cortical sensorimotor input to the thalamus, I_{app} is the external applied current, and I_{DBS} is the stimulation current (see below). The leak current (I_L), potassium current (I_K), sodium current (I_{Na}), high-threshold calcium current (I_{Ca}), and calcium-dependent afterhyperpolarization (AHP) (I_{AHP}) are described by Hodgkin–Huxley type equations as follows:

$$\begin{aligned}
&I_L(V) = g_L(V - V_L),\\
&I_K(V) = g_K n^4 (V - V_K),\\
&I_{Na}(V) = g_{Na} m_\infty^3(V) h (V - V_{Na}),\\
&I_{Ca}(V) = g_{Ca} s_\infty^2(V)(V - V_{Ca}),\\
&I_T(V) = g_T a_\infty^3(V) b_\infty^2(r)(V - V_{Ca}),\\
&I_{AHP}(V) = g_{AHP}(V - V_K)([Ca]/([Ca] + k_1)).
\end{aligned} \tag{2}$$

The slowly operating gating variables ($X = n, h, r$) are treated as functions of both time and voltage and have first-order kinetics governed by differential equations of the form:

$$\begin{aligned}
&dX/dt = \phi_X((X_\infty(V) - X)/\tau_X(V)),\\
&\tau_X(V) = \tau_X^0 + \tau_X^1/(1 + \exp(-(V - \theta_X^\tau)/\sigma_X^\tau)),
\end{aligned} \tag{3}$$

where activation (and inactivation) time constants have a sigmoidal dependence on voltage, such that the voltage at which the time constant is midway between its maximum and minimum values is θ^τ, and σ^τ is the slope factor for the voltage dependence of the time constant (see Table 3).

Activation gating for the rapidly activating channels (m, a, and s) was treated as instantaneous. For all gating variables ($X = n, m, h, a, r, s$), the steady-state voltage dependence was determined using:

$$\begin{aligned}
&X_\infty(V) = [1 + \exp(-\tfrac{V - V_X}{k_X})]^{-1},\\
&I_T : b_\infty(r) = [1 + \exp((r - \theta_b)/\sigma_b)]^{-1} - [1 + \exp(-\theta_b/\sigma_b)]^{-1}.
\end{aligned} \tag{4}$$

The intracellular concentration of Ca^{2+} ions ([Ca]) is governed by the differential equation $d[Ca]/dt = \varepsilon(-I_{Ca} - I_T - k_{Ca}[Ca])$. The constant ε combines the effects of buffers, cell volume, and the molar charge of calcium in units of mole-s/coulombs-liter. The constant k_1 is the dissociation constant of the calcium-dependent AHP current. The constant k_{Ca} is the calcium pump rate constant in units of coulombs-liter/mole-s. Relevant kinetic parameters used in simulations are presented in Tables 2, 3.

2.2.2. GPe/GPi neurons

The membrane potential dynamics of GPe neurons are described as follows Terman et al. (2002) and Rubin and Terman (2004):

$$\begin{aligned}
C_m \frac{dV_i}{dt} = &-I_L - I_K - I_{Na} - I_T - I_{Ca} - I_{AHP}\\
&- I_{STN\to GPe} - I_{GPe\to GPe} - I_{D2\to GPe} + I_{app}.
\end{aligned} \tag{5}$$

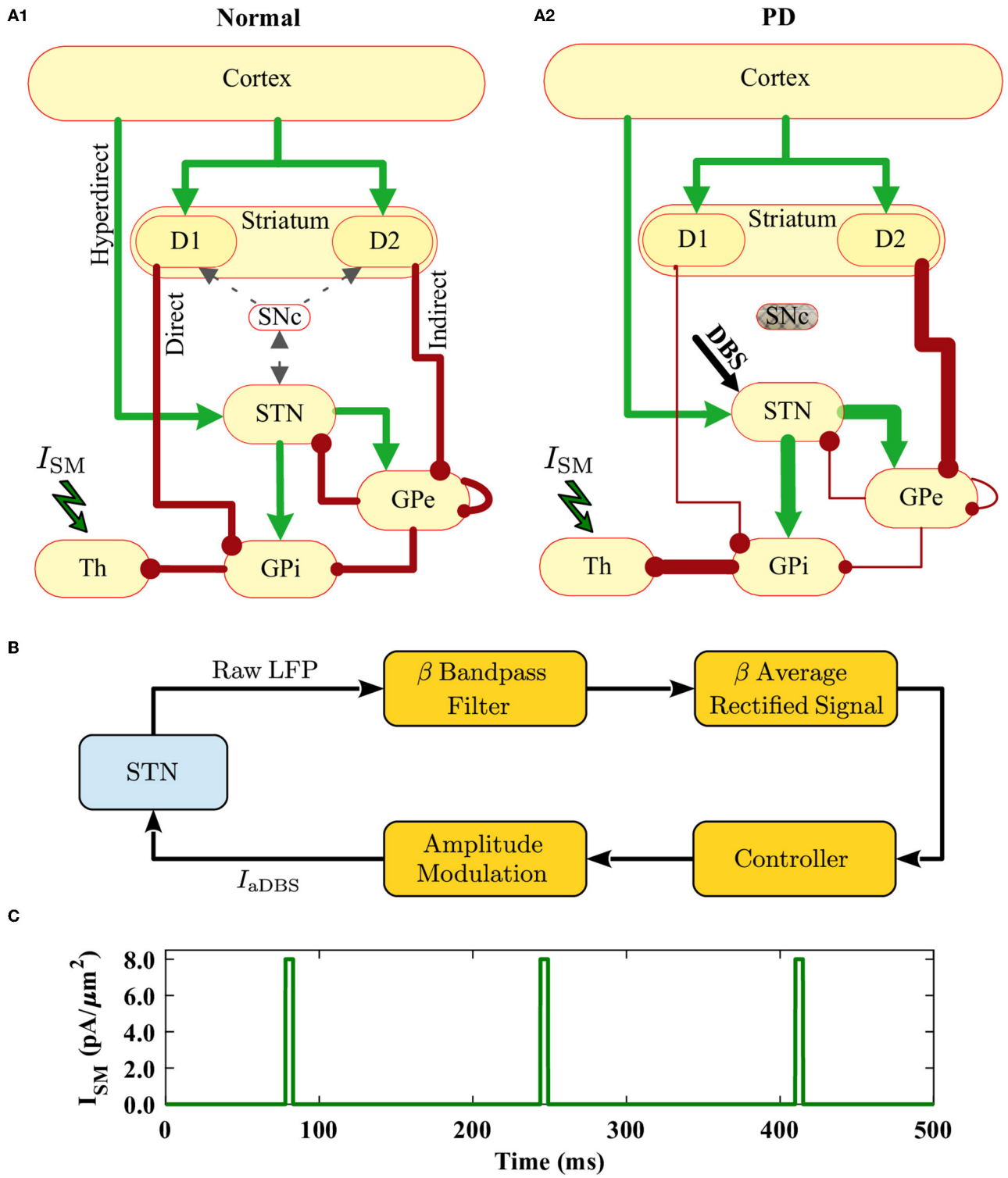

FIGURE 1
Schematic illustration of the cortico-BG-thalamic network model and closed-loop stimulator. **(A1, A2)** The cortico-BG-thalamic circuitry in the normal **(A1)** and PD **(A2)** conditions. Excitatory (green) and inhibitory (red) pathways are marked by arrows where their relative thickness indicates the strength of the input. STN was the target of DBS in the PD condition. **(B)** Schematic representation of the closed-loop stimulator utilizing STN beta band activity. The raw LFP recorded from STN is beta band (15–30 Hz) filtered, rectified, and averaged to calculate the average rectified value (ARV) of the LFP beta band activity. The beta ARV is then fed to the controller, which updates the amplitude of the stimulation current. **(C)** Time trace of the cortical sensorimotor input (I_{SM}) to the thalamus given by Equation (17) below.

The ionic currents are similar to STN neurons, as described in Equation (2) except for the low-threshold T-type calcium current (I_T) that is defined differently:

$$I_T(V) = g_T a_\infty^3(V) r(V - V_{Ca}), \tag{6}$$

TABLE 1 Connection probability and the strength of synaptic connections between different pathways used in our simulations in normal and PD conditions (Mink, 1996; Leblois et al., 2006; Corbit et al., 2016).

Pathway	Connection probability	g (nS/μm^2)	
		Normal	PD
STN ⟶ GPe	40%	0.82	0.82
STN ⟶ GPi	40%	0.15	0.15
GPe ⟶ STN	7%	0.14	0.14
GPe ⟶ GPi	6%	1.39	1.39
GPe ⟶ GPe	45%	0.61	0.25
D1 ⟶ GPi	37.5%	0.225	0.08
D2 ⟶ GPe	37.5%	0.221	0.66
GPi ⟶ Th	70%	0.03	0.03

where the dynamics of gating variable a are similar to Equation (4) and the dynamics of variable r are the same as Equation (3). GPe parameters used in simulations are presented in Tables 2, 3.

The dynamics of GPi neurons were modeled similar to the dynamics of GPe neurons. We used the following current balance equation to calculate the GPi membrane potential:

$$C_m \frac{dV_i}{dt} = -I_L - I_K - I_{Na} - I_T - I_{Ca} - I_{AHP} - I_{STN\to GPi} - I_{GPe\to GPi} - I_{D1\to GPi} + I_{app}. \tag{7}$$

The corresponding numerical values for parameters are shown in Tables 2, 3.

2.2.3. Thalamic neurons

The membrane potential dynamics of thalamic cells are modeled as follows Rubin and Terman (2004):

$$C_m \frac{dV_{Th}}{dt} = -I_L - I_K - I_{Na} - I_T - I_{GPi\to Th} + I_{SM}. \tag{8}$$

The ionic currents I_{Na} and I_L are similar to those defined for the STN neurons, as described in Equation (2), whereas I_T and I_K are

TABLE 2 Kinetic parameters for STN, GP (GPe/GPi), and thalamus.

Variable	Nucleus	θ_x	σ_x	τ_x^0	τ_x^1	θ_x^τ	σ_x^τ	Q_x
m	STN	−30	15	—	—	—	—	—
	GP	−37	10	—	—	—	—	—
	Th	−37	7	—	—	—	—	—
h	STN	−39	−3.1	1	500	−57	−3	0.75
	GP	−58	−12	0.05	0.27	−40	-12	0.05
	Th	−41	4	—	—	—	—	—
n	STN	−32	8	1	100	−80	−26	0.75
	GP	−50	14	0.05	0.27	-40	−12	0.1
r	STN	−67	−2	7.1	17.5	68	−2.2	0.5
	GP	−70	−2	30	0	—	—	1
	Th	−84	4	—	—	—	—	—
a	STN	−63	7.8	—	—	—	—	—
	GP	−57	2	—	—	—	—	—
s	STN	−39	8	—	—	—	—	—
	GP	−35	2	—	—	—	—	—
b	STN	0.4	−0.1	—	—	—	—	—
p	Th	−60	6.2	—	—	—	—	—

TABLE 3 Maximal conductances (g_x), calcium dynamic parameters, and reversal potentials (E_x) of the membrane currents for STN, GP (GPe/GPi), and thalamus.

	$\bar{g}$ (mS/cm^2)									E (mV)			
	L	K	Na	T	Ca	AHP	ε_{Ca}	k_{Ca}	k_1	L	K	Na	Ca
STN	2.25	45	37.5	0.5	0.5	9	3.75×10^{-5}	22.5	15	−60	−80	55	140
GP	0.1	30	120	0.5	0.1	30	1.00×10^{-4}	20	30	−55	−80	55	120
Th	0.05	5	3	5	—	—	—	—	—	−70	−90	50	0

defined as follows:

$$I_K(V) = g_K[0.75(1-h_{Th})]^4(V-V_K),$$
$$I_T(V) = g_T\, p_\infty^2(V) r(V-V_T). \quad (9)$$

The gating variables are of the form:

$$dh(t)/dt = (h_\infty(V_{Th}) - h_{Th})/\tau_h(V_{Th}),$$
$$dr(t)/dt = (r_\infty(V_{Th}) - r_{Th})/\tau_r(V_{Th}),$$
$$\tau_h(V) = 1/(a_h + b_h),$$
$$a_h = 0.128\exp(-(V+46)/18), \quad (10)$$
$$b_h(V) = 4/[1+\exp(-(V+23)/5)],$$
$$\tau_r(V) = 0.4[28+\exp(-(V+25)/10.5)].$$

Relevant kinetic parameters used in simulations are presented in Table 2.

2.2.4. Striatum: D1 and D2 MSNs

Two subpopulations of neurons representing D1 and D2 receptor-expressing MSNs were considered to model the striatum. The membrane potential dynamics for MSNs are of the form (Mahon et al., 2000):

$$C_m \frac{dV_i}{dt} = -I_L - I_K - I_{Na} - I_{Kir} - I_{Af} - I_{As} - I_{Krp} - I_{NaP} - I_{NaS}. \quad (11)$$

The ionic currents (I_{Na}, I_K, and I_L) are similar to those used for modeling the STN neurons, as described in Equation (2), but gating variables were taken from the study of Wang and Buzsáki (1996). The gating variable m was approximated by $m_\infty = \alpha_m/(\alpha_m + \beta_m)$, where $\alpha_m(V) = -0.1(V+35)/(\exp(-0.1(V+35)) - 1)$ and $\beta_m(V) = 4\exp(-(V+60)/18)$. Other gating variables ($X = h, n$) obey the following first-order kinetics:

$$dX/dt = \phi\,(\alpha_X(1-X) - \beta_X X) \quad (12)$$

where ϕ is constant, $\alpha_h(V) = 0.07\exp(-(V+58)/20)$, $\beta_h(V) = 1/(\exp(-0.1(V+28))+1)$, $\alpha_n(V) = -0.01(V+34)/(\exp(-0.1(V+34)) - 1)$, and $\beta_n(V) = 0.125\exp(-(V+44)/80)$.

Fast (I_{Af}) and slow (I_{As}) A-type potassium currents, inward rectifier potassium current (I_{Kir}), persistent potassium current (I_{Krp}), and persistent (I_{NaP}) and slowly inactivating (I_{NaS}) sodium currents are defined as follows (Wood et al., 2004):

$$I_X(V) = g_X m_\infty^k(V) h(V - E_X), \quad (13)$$

where $X \in \{Kir, Af, As, Krp, NaS, NaP\}$. Gating variables obey differential equations defined in Equations (3), (4). Other parameters are defined as follows:

$$\tau(V) = \tau_0[\exp(-\tfrac{V-V_\tau}{k_\tau}) + \exp(\tfrac{V-V_\tau}{k_\tau})]^{-1}, \quad (14)$$

except for the inactivation of slow A-type potassium current for which the kinetics were defined by $\tau_{hAs}(V) = 1790 + 2930 \cdot \exp(-(\tfrac{V+38.2}{28})^2) \cdot (\tfrac{V+38.2}{28})$. The numerical values of parameters used in our simulations are listed in Table 4.

2.2.5. Synaptic currents

The synaptic current $I_{\alpha\to\beta}$ from the presynaptic nucleus (α) to the postsynaptic nucleus (β), with $\alpha \in \{STN, GPe, GPi, D1, D2\}$, and $\beta \in \{STN, GPe, GPi, Th\}$, is given by (Rubin and Terman, 2004):

$$I_{\alpha\to\beta} = g_{\alpha\to\beta}(V_\alpha - E_{\alpha\to\beta}) \sum_\alpha s_\alpha(t), \quad (15)$$

where $g_{\alpha\to\beta}$ is the maximal synaptic conductance presented in Table 1, and $E_{\alpha\to\beta}$ is the synaptic reversal potential presented in Table 3. $s_\alpha(t)$ represents the synaptic gating variable that obeys the following differential Equation (Rubin and Terman, 2004):

$$\frac{ds_\alpha}{dt} = A_\alpha(1-s_\alpha)\cdot H_\infty(V_\alpha - \theta_\alpha) - B_\alpha s_\alpha, \quad (16)$$

where $H_\infty(V_\alpha) = 1/(1+\exp[-(V_\alpha - \theta_\alpha^H)/\sigma_\alpha^H])$ is a smooth approximation of the Heaviside step function (relevant parameters are given in Table 5), and A_α and B_α control the synaptic time courses.

2.2.6. Cortical current

The cortical sensorimotor input to the thalamus is approximated as a train of rectangular depolarizing current pulses (I_{SM}), which is shown in Figure 1C, based on Equation (17) (Rubin and Terman, 2004):

$$I_{SM} = i_{SM}\, H(\sin(2\pi t/\rho_{SM}))\cdot\left[1 - \sin\left(\frac{2\pi(t+\delta_{SM})}{\rho_{SM}}\right)\right], \quad (17)$$

Where $i_{SM} = 8\,pA/\mu m^2$ is the amplitude of the current, $\rho_{SM} = 166\,ms$ denotes the period of the current signal, and $\delta_{SM} = 5\,ms$ represents the duration of each individual pulse.

2.3. Stimulation protocol

The stimulation was administered to the STN as schematically shown in Figure 1A2. The stimulation current was modeled by the following protocol (Rubin and Terman, 2004):

$$I_{DBS} = i_{DBS}\, H(\sin(2\pi t/\rho_{DBS}))\cdot\left[1 - \sin\left(\frac{2\pi(t+\delta_{DBS})}{\rho_{DBS}}\right)\right], \quad (18)$$

Where $i_{DBS} = 2\,mA/\mu m^2$ is the amplitude of the stimulation signal, $\rho_{DBS} = 1/130\,ms$ denotes the stimulation period, and $\delta_{DBS} = 5\,ms$ is the duration of individual stimulation pulses (Fleming et al., 2020a). In the cDBS protocol, the model stimulation signal was continuously delivered to the STN with a 130-Hz frequency (Fleming et al., 2020a). The same frequency was used for the aDBS protocol; however, the amplitude of the signal was modulated based on a closed-loop control scheme described later.

2.4. Data analysis

The LFP of the oscillatory neural activity was defined as $LFP(t) = N^{-1}\sum_\alpha s_\alpha(t)$, where $s(t)$ is the synaptic variable introduced in Equation (16). Rigorous computational approximations showed that a simple weighted sum of the model synaptic currents excellently

TABLE 4 Model parameters for striatal MSNs.

Current	m^k, h	$\bar{g}$ (mS/cm^2)	X_∞(V)		E (mV)	τ(V)		
			V_x (mV)	k_x (mV)		τ_0 (ms)	V_τ (mV)	k_τ (mV)
Kir	m_{Kir}	0.15	−100	−10	−90	—	—	—
Af	m_{Af}	0.09	−33.1	7.5	−73	1	—	—
	h_{Af}		−70.4	−7.6		25	—	—
As	m_{As}	0.32	−25.6	13.3	−85	131.4	−37.4	27.3
	h_{As}		−78.8	—10.4		—	—	—
Krp	m_{Krp}	0.42	−13.4	12.1	−77.5	206	−53.9	26.5
	h_{Krp}		−55	−19		—	—	—
NaP	m_{NaP}	0.02	−47.8	3.1	45	1	—	—
NaS	m_{NaS}	0.11	−16	9.4	40	637.8	−33.5	26.3

TABLE 5 Model parameters of the smooth approximation of the Heaviside step function for STN, GP (GPe/GPi), and D1/D2 MSN.

	θ_α^H	σ_α^H	θ_α
STN	−39.0	8.0	30.0
GP	−57.0	2.0	20.0
MSN	−42.0	5.0	18.0

captures the time course of the LFP signal (Mazzoni et al., 2015). This provides a simple formula by which the LFP signal can be estimated directly from network activity, providing a missing quantitative link between simplified neuronal models and LFP measures *in vivo* (Mazzoni et al., 2015).

The beta band-filtered LFP of the STN was calculated by using the bandpass filter of the simulated raw STN LFP using the bandpass filter function implemented in MATLAB within the frequency range of 15–30 Hz.

The power spectrum of each calculated signal was computed by the fast Fourier transform (FFT) function implemented in MATLAB.

2.5. Closed-loop control scheme

In the closed-loop control of aDBS administered to the STN, the stimulation current is delivered in the form of high-frequency pulses with the same frequency used in the open-loop cDBS but with a modified amplitude. Amplitude modulation was implemented by the closed-loop feedback of the measured beta band LFP activity of the STN, which is schematically shown in Figure 1B. The average rectified value (ARV) of the STN beta band LFP was calculated by full-wave rectifying of the filtered LFP signal. The maximum value of beta ARV in the normal state was assumed as a target value for the beta ARV. During controller simulations, a beta ARV above the target value was considered as the pathological beta activity, while a beta ARV below the target value was assumed as the fluctuations of normal beta activity.

The controller input (e) at a given time was calculated as the normalized error between the measured beta ARV ($\beta_{measured}$) and the target beta ARV (β_{target}), which is as follows (Fleming et al., 2020a,b):

$$e(t) = \frac{\beta_{measured}(t) - \beta_{target}}{\beta_{target}} \quad (19)$$

The controller operated with a sampling interval $T_s = 50$ ms (Fleming et al., 2020a), updating the modulated aDBS parameter at each controller call. Other choices for the sampling time window resulted in the same observed beta power and stimulation performance (see Supplementary Figure S1). The P controller for closed-loop control of the aDBS amplitude can be defined as follows (Fleming et al., 2020a,b):

$$u(t) = K_p \cdot e(t). \quad (20)$$

where $u(t)$ is the modulated aDBS parameter value, that is, the stimulation amplitude at a given time, $K_p = 5$ (Fleming et al., 2020a) is the controller proportional gain of the aDBS parameter at each controller call, and $e(t)$ is the controller error input signal at a given time. The aDBS current is given as follows:

$$I_{aDBS}(t) = u(t) \cdot I_{DBS}(t). \quad (21)$$

2.6. Stimulation performance assessment

Computational results show that synchronized activity interrupts the thalamic reliability to transmit sensorimotor inputs, which may lead to akinesia and rigidity (Rubin and Terman, 2004). One way to assess and compare the efficiency of different DBS protocols in restoring sensorimotor functionality is their effectiveness in improving the response of the thalamus to sensorimotor stimuli. Thalamic reliability ($\mathcal{R}$) is a measure that quantifies the faithfulness of the thalamic relay defined in terms of the generation of thalamo-cortical activity patterns that match the inputs to thalamo-cortical cells. It is determined by the fraction of sensorimotor stimuli that elicit a single action potential in the thalamus so that a *missed* spike is recorded when no spikes are fired in response to a sensorimotor input, whereas a *bad* spike is recorded when multiple spikes are fired in response to a single sensorimotor input. The reliability of transmitting information of the thalamus can be regarded as an evaluation of the effectiveness of DBS. This is quantified by the error

index introduced by Rubin and Terman (2004) for the fidelity of thalamic throughput such that the minimal error is achieved when each sensorimotor input pulse results in a single action potential in a thalamic neuron (also see Supplementary Figure S2 and Section 4). The reliability of the thalamus is defined as follows (Gorzelic et al., 2013):

$$\mathcal{R} = 1 - \frac{b+m}{N_{SM}}. \tag{22}$$

where b is the number of bad spikes, m is the number of missed spikes, and N_{SM} is the total number of sensorimotor inputs in the simulation.

Another way to quantify the performance of stimulation is to calculate the energy (power) expenditure index ($\mathcal{E}$), which is a measure of the amount of administered stimulation current, defined as the root mean square (RMS) of the stimulation current signal (Su et al., 2018) as follows:

$$\mathcal{E} = \sqrt{\frac{1}{T}\int_T I_{DBS}^2 dt}. \tag{23}$$

where T is the total time of the simulation.

Ultimately, the beta suppression efficiency of cDBS and aDBS protocols was quantified as the percentage of beta suppression in the STN per unit of the consumed energy, defined as follows (Fleming et al., 2020a):

$$\eta = \frac{1}{\mathcal{E}} \times \left(1 - \frac{1}{T}\int_T \frac{\beta_{NoDBS}(t) - \beta_{DBS}(t)}{\beta_{NoDBS}(t)}\, dt\right) \times 100 \tag{24}$$

where $\mathcal{E}$ was introduced in Equation (23), T is the total time of simulation, $\beta_{NoDBS}(t)$ is the beta ARV signal measured when DBS is off, and $\beta_{DBS}(t)$ is the beta ARV signal measured when DBS was administered.

3. Results

3.1. Properties of normal and PD network model

First, we set the model parameters to mimic the normal and PD network dynamics. The raster plots shown in Figures 2A1–C1, top illustrate the dynamics of STN, GPe, and GPi neurons in normal condition, respectively. The synchronized neural activity led to pronounced rhythmic activity and large-amplitude oscillations in the LFP of different nuclei (shown in Figures 2A1–C1, bottom). The raster plots and LFP of STN, GPe, and GPi neurons in the PD condition are shown in Figures 2A2–C2.

Notably, in the normal condition, STN exhibited a relatively desynchronized neural activity (see Figure 2A1, top), characterized by small-amplitude oscillations in the STN LFP shown in Figure 2A1, bottom. In the PD state, however, the activity of STN neurons became strongly synchronized (Figure 2A2, top), characterized by large-amplitude rhythmic oscillations in the STN LFP (Figure 2A2, bottom). The mean firing rate of STN neurons in the normal state was 12 ± 0.6 Hz, which increased to 19 ± 0.8 Hz in the PD state. The PSD of STN activity in the PD state is characterized by a sharp peak in the beta band (approximately 20 Hz) as shown in Figure 3A (red), whereas the normal PSD hardly showed any pronounced peak (Figure 3A, blue).

In the normal condition, GPe neurons fired in a relatively irregular manner, as it is shown in the raster plot (Figure 2B1, top) and LFP activity (Figure 2B1, bottom), with a mean firing rate of 60 ± 2.4 Hz. In the PD state, the mean firing rate of GPe neurons decreased to 32 ± 1.3 Hz where the firing activity of neurons was more synchronized (Figure 2B2, top), characterized by rhythmic LFP oscillations shown in Figure 2B2, bottom. The firing activity of GPi neurons, however, was relatively sparse in the normal condition (Figure 2C1), with a mean firing rate of 20 ± 0.9 Hz. The activity of GPi neurons in the PD condition is shown in Figure 2C2, where the mean firing rate increased to 28 ± 1.3 Hz. The PSD of GPe and GPi activities in the PD state showed a sharp peak at approximately 20 Hz (Figures 3B, C, red), whereas their normal PSD did not show any pronounced peak in the beta band (Figures 3B, C, blue). For example, single-cell membrane voltage traces of randomly chosen STN, GPe, and GPi neurons in normal (top) and PD (bottom) conditions are presented in Figure 4.

3.2. Suppression of pathological oscillations by model DBS

To suppress parkinsonian beta oscillations within the BG nuclei (i.e., to suppress pronounced peaks in the PSD of STN, GPe, and GPi activities in Figure 3, red), the model stimulation was administered to the STN using two different stimulation protocols, that is, cDBS and aDBS. In the cDBS protocol, high-frequency (130 Hz) stimulation pulses are continuously delivered to STN with a fixed amplitude, as described in Equation (18). In the aDBS protocol, stimulation pulses were continuously delivered to STN with the same frequency that was used in cDBS; however, the stimulation amplitude is modulated by a control signal that sets the current amplitude based on the beta band activity of the STN, as described in Equation (21).

The closed-loop control stimulator of the model aDBS utilizing the STN beta band activity is schematically shown in Figure 1B. In the model, as presented in Figure 5A, the raw LFP recorded from the STN was first filtered in the beta band (15–30 Hz) frequency (Figure 5B, violet); also see Section 2. The beta band filtered output of the parkinsonian STN activity, when the DBS was off (NoDBS), is also depicted for better comparison (Figure 5B, gray). The beta bandpass filtered was then rectified and averaged to calculate the ARV of the LFP beta band activity (Figure 5C). The target level for the beta ARV (i.e., $\beta_{target} = 0.005$ mV) is denoted by a red dashed line in Figure 5C, which was estimated based on the STN beta band activity in the normal condition. To efficiently suppress the pathological beta activity within STN (i.e., beta ARV above the target value), the beta ARV is fed to the controller to update the amplitude of the aDBS current, as shown in Figure 5D.

The dynamics of STN, GPe, and GPi neurons are shown in Figure 6 when the STN was stimulated by both cDBS and aDBS protocols. Before the stimulation onset (i.e., $t < 0$ s in Figures 6A1, A2), the model parameters were set to mimic the PD state characterized by the overly synchronized neural activity in the STN raster plot (Figures 6A1, A2, top) and by large-amplitude oscillations in the beta band-filtered LFP (Figures 6A1, A2, bottom). The stimulation was then turned on at $t = 0$ s. When cDBS was turned on (i.e., $t > 0$ s in Figure 6A1, top), the activity of STN neurons was entrained to the stimulation frequency (i.e., 130 Hz) and

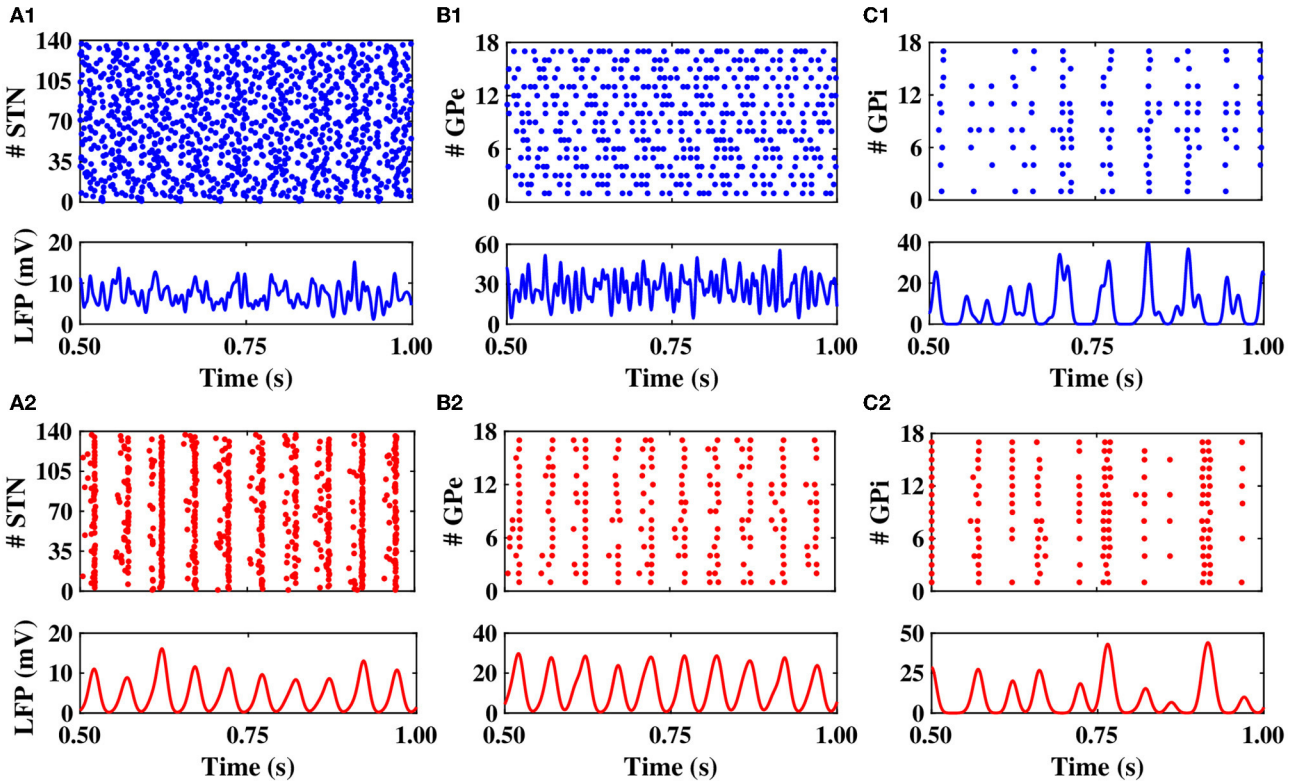

FIGURE 2
Population dynamics of the STN, GPe, and GPi in normal and PD conditions. Raster plots (top) and LFPs (bottom) of the STN, GPe, and GPi activities in normal **(A1–C1)** and PD **(A2–C2)** conditions.

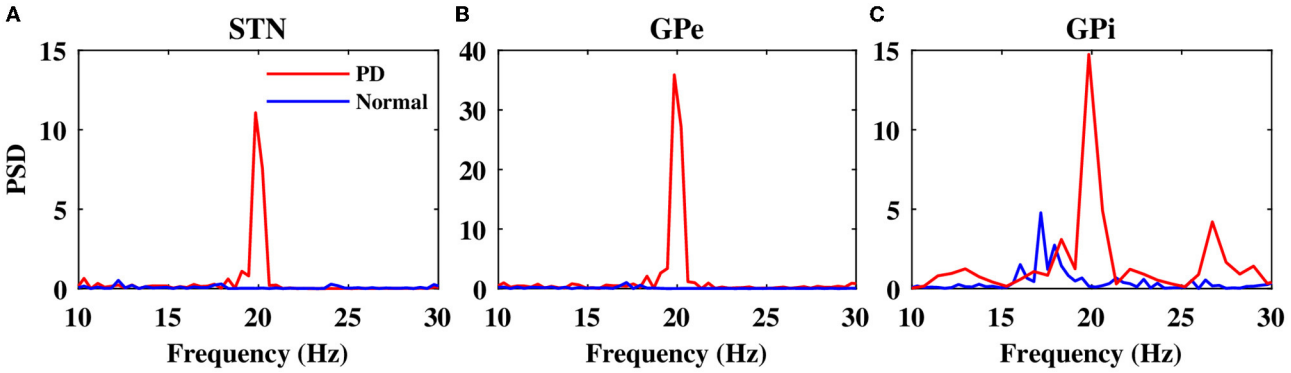

FIGURE 3
Power spectrum of the STN, GPe, and GPi LFP activities. Power spectrum density of the STN **(A)**, GPe **(B)**, and GPi **(C)** LFP activities in normal (blue) and PD (red) conditions.

the large-amplitude oscillations in the beta band-filtered LFP were considerably suppressed (Figure 6A1, bottom). When aDBS was used (i.e., $t > 0$ s in Figure 6A2, top), the stimulation pulse train was delivered to the STN with a variable amplitude (see Figure 5D). In this case, the suppression of parkinsonian beta oscillations in the STN was less than cDBS (cf. Figures 6A1, A2, bottom). However, as we will show later, overall less stimulation current was delivered in aDBS while resulting in a more suppression efficiency of the aDBS protocol.

The stimulation of the STN not only directly affected the firing activity of STN neurons but also indirectly mediated the firing activity of GPe and GPi neurons. Particularly, cDBS of STN led to the entrainment of GPe neurons to the stimulation frequency (i.e., $t > 0$ s in Figure 6B1), leading to the inhibition of the activity of GPi neurons (i.e., $t > 0$ s in Figure 6C1). On the other hand, aDBS of the STN just increased the firing activity of the GPe neurons and did not result in the entrainment of the GPe activity to the stimulation frequency (i.e., $t > 0$ s in Figure 6B2). Consequently, the activity of GPi neurons was relatively the same before and after stimulation (Figure 6C2). In addition, as it is shown in Figure 7, PSD of the activity of neurons in STN, GPe, and GPi shows that

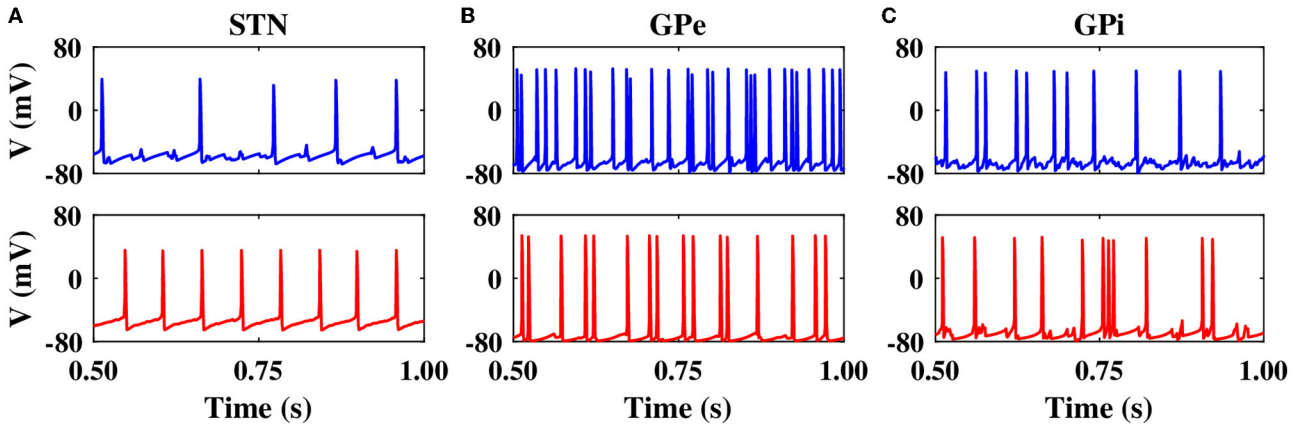

FIGURE 4
Single-cell membrane voltage traces of STN, GPe, and GPi neurons. Time course of membrane voltages of single STN **(A)**, GPe **(B)**, and GPi **(C)** neurons randomly chosen from the network in normal (top) and PD (bottom) conditions.

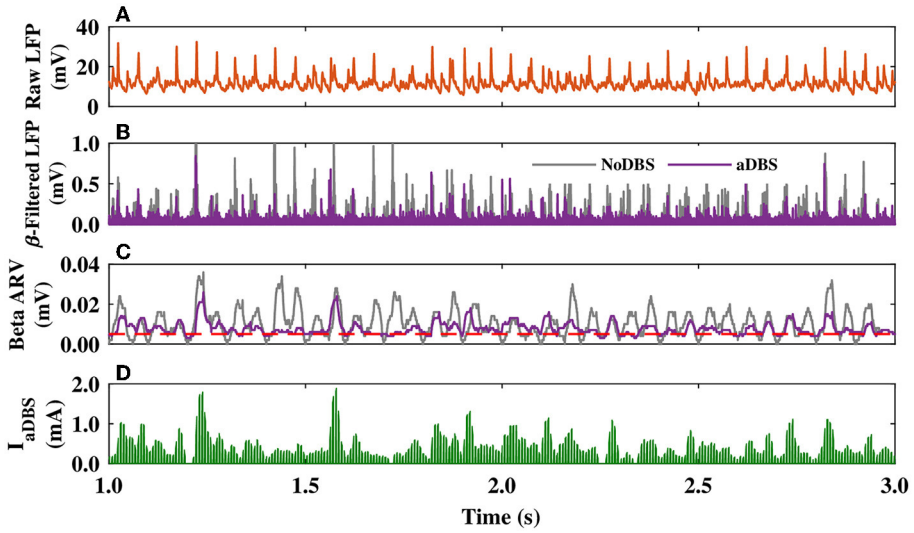

FIGURE 5
STN LFP and amplitude modulation of the aDBS current. **(A–C)** The simulated raw LFP of the STN **(A)**, beta band filtered LFP **(B)**, and beta ARV **(C)** for DBS off (NoDBS; gray) and aDBS (violet). The target level for the beta ARV ($\beta_{target} = 0.005$ mV) is denoted by the red dashed line in **(C)**. **(D)** Amplitude modulation of the aDBS current by the P controller. The aDBS amplitude was restricted between 0.0 and 2.0 mA.

both cDBS and aDBS effectively suppressed beta band oscillations (cf. Figures 3, 7). Interestingly, the suppression of parkinsonian beta oscillations was more pronounced in cDBS of STN (cf. Figure 7A, green and red) and in aDBS of GPe (cf. Figure 7B, green and red). The effects of cDBS and aDBS on the GPi PSD were roughly similar (Figure 7C).

Differential modulation of the STN, GPe, and GPi beta activities by stimulation was directly related to the model connectivity. While cDBS at 130 Hz effectively suppressed beta activity in the STN, aDBS at the same frequency was less effective in the suppression of STN beta activity, simply because less current was delivered to the STN (Figure 7A). However, we evaluated the stimulation performance based on the percentage of beta suppression in the STN per unit of the consumed energy (see Figure 8). Therefore, based on Figure 8, assuming that the energy consumption of cDBS at 130 Hz was 100%, aDBS at 130 Hz consumed approximately 50% less energy, leading to efficiency about two times as high as the one for cDBS. On the other hand, the STN was connected to the GPe (Table 1; connection strength $g = 0.82\,\mathrm{nS}/\mu\mathrm{m}^2$) more stronger than GPi (Table 1; connection strength $g = 0.15\,\mathrm{nS}/\mu\mathrm{m}^2$). Therefore, cDBS at 130 Hz entrained GPe neurons at the stimulation frequency, leading to an enhanced inhibition among GPe cells and the STN itself, which ultimately prevented effective beta suppression in the GPe. In contrast, adaptive delivery of the stimulation current in the aDBS protocol allowed stimulation to effectively suppress beta activity in the GPe. Finally, weak connections from the STN to GPi minimized the effect of stimulation on GPi, making no particular difference in either case.

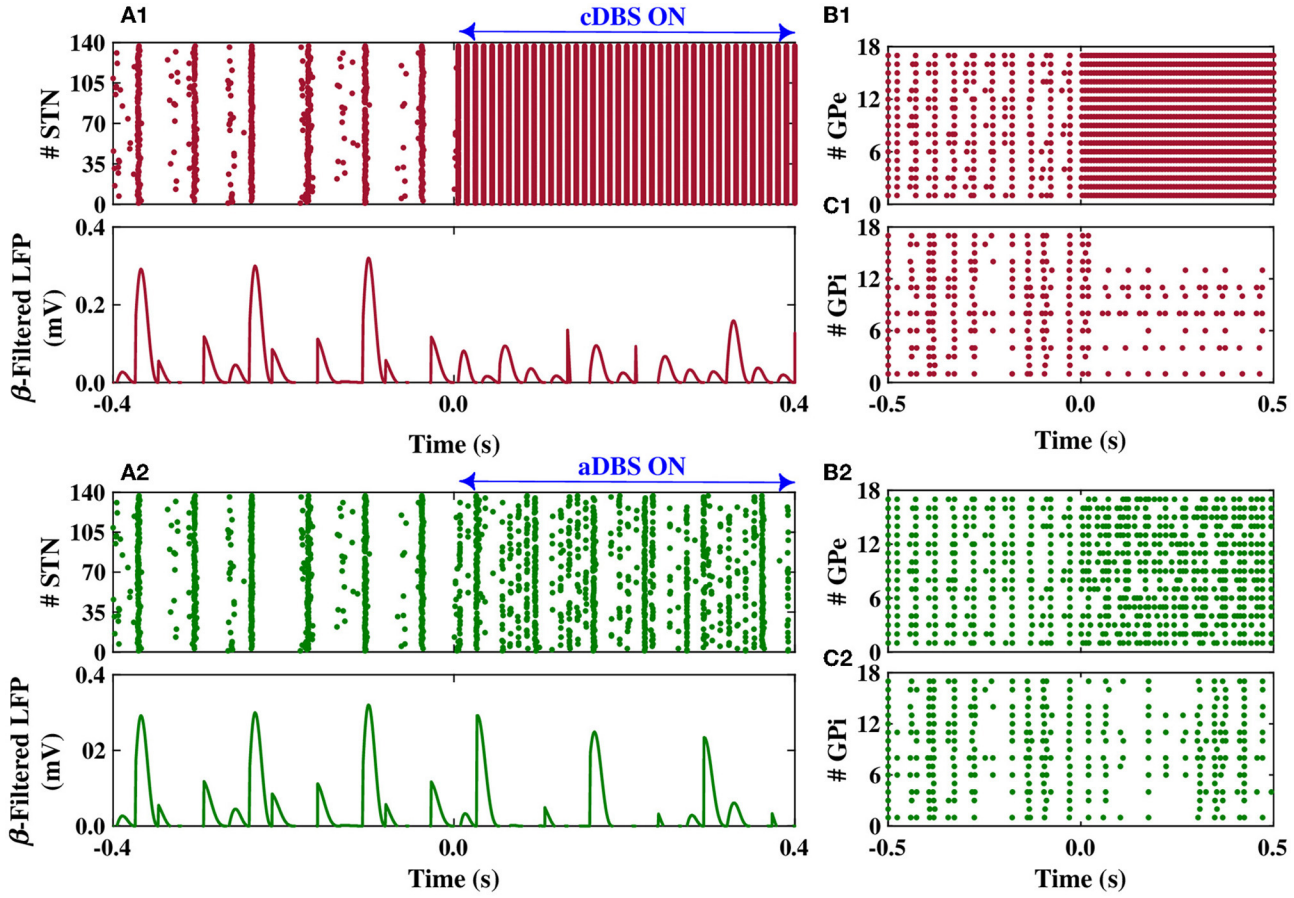

FIGURE 6
Population dynamics of the STN, GPe, and GPi when the STN was the target of stimulation. Raster plot (top) and beta band filtered LFP (bottom) of the STN, and raster plots of the GPe and GPi when cDBS **(A1–C1)** or aDBS **(A2–C2)** is administered to the STN. The model DBS was off before time $t = 0$ s and was switched on at $t = 0$ s.

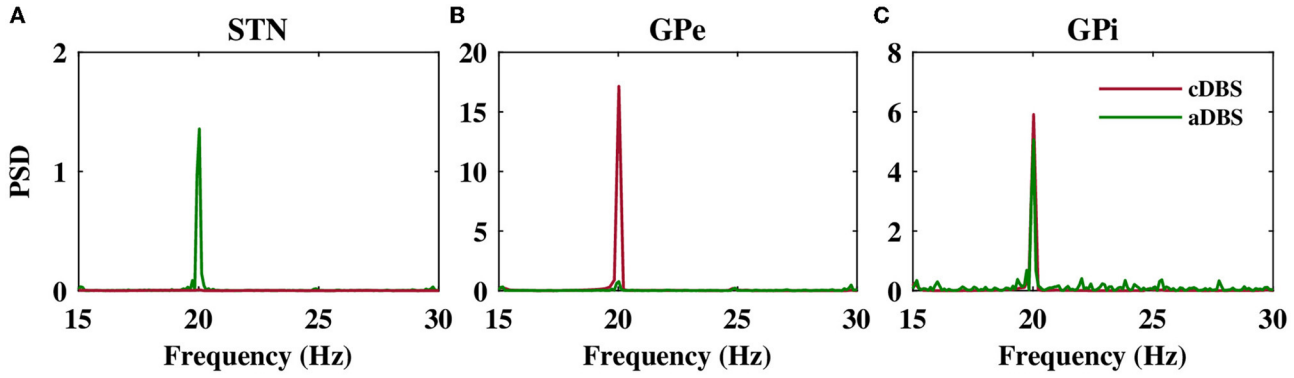

FIGURE 7
Power spectrum of the STN, GPe, and GPi LFP activities. Power spectrum density of the STN **(A)**, GPe **(B)**, and GPi **(C)** LFP activities when cDBS (maroon) or aDBS (green) is administered to the STN.

3.3. Stimulation performance

To evaluate the performance of cDBS vs. aDBS, we calculated thalamic reliability given by Equation (22), the energy expenditure index described in Equation (23) as a measure of the amount of delivered stimulation current, and the beta suppression efficiency of the stimulation protocol defined in Equation (24). The results are presented in Figure 8 where the performance of the cDBS protocol is compared with the aDBS protocol for a variety of stimulation frequencies. The PD condition (NoDBS) was used to

set a reference for the thalamic reliability (i.e., 0%). The reference value for the energy expenditure (i.e., delivered stimulation current) was set to 100%, measured when the cDBS protocol (with 130 Hz stimulation frequency) was used for the STN model stimulation. The administration of cDBS led to a 1.7% suppression efficiency and an acceptable value for the thalamic reliability (i.e., 52%).

Interestingly, STN aDBS with the same stimulation frequency as the cDBS protocol (i.e., 130 Hz) led to an increased beta suppression efficiency (i.e., 3.6%), while the energy expenditure was 41% less than cDBS, as shown in Figure 8. Notably, in this case, the value of thalamic reliability was relatively unchanged (i.e., aDBS: 53% vs. cDBS: 52%). Restoring the thalamic reliability and effective suppression of beta oscillations by cDBS comes at the cost of a higher administered stimulation current, resulting in a smaller suppression efficiency than aDBS. In this way, amplitude modulation by closed-loop aDBS (with the same stimulation frequency as the open-loop cDBS) led to more efficient suppression of pathological beta oscillations in the model while notably less stimulation current was used.

As one could expect, increasing the stimulation frequency of aDBS led to increased energy expenditure (Figure 8, gray bars) where the thalamic reliability and suppression efficiency reached their maximum values approximately at 130 Hz stimulation frequency. The overall performance of the stimulation is determined by the trade-off between the energy expenditure and beta suppression outcome of the stimulation protocol.

3.4. Monopolar vs. bipolar stimulation

Typically, charge-balanced stimuli are used in DBS to avoid tissue damage. We repeated our simulations to test whether the stimulation performance is affected by charge-balanced stimulation. The biphasic charge-balanced stimulation pulses were implemented similar to those used by Popovych and Tass (2019), which consist of a short cathodic pulse (first phase) followed by a longer charge-balancing second phase with opposite polarity. We used the frequency of 130 Hz for the aDBS pulse train and the width of the short pulse (first phase) $PW = 0.5$ ms (Popovych and Tass, 2019). The stimulation signal consisting of electrical biphasic charge-balanced pulses is shown in Figure 9A. The stimulation current can then be constructed as follows (Popovych and Tass, 2019):

$$I_{\mathrm{DBS}}(t) = \begin{cases} -10, & t_n \le t < t_n + PW, \\ 0, & t_n + PW \le t < t_n + PW + GW, \\ 1, & t_n + PW + GW \le t < t_n + 11PW + GW, \\ 0, & \text{otherwise}, \end{cases} \tag{25}$$

For $t \in (t_n, t_{n+1})$, where $t_n = 1,000n/f$ ms, $n = 0, 1, 2, \ldots$ are the times of the pulse onsets, as presented in Figure 9A, and $f = 130$ Hz is the frequency of the stimulation. We considered an interphase time gap of width $GW = 4.5$ ms between the cathodic and anodic phases of the biphasic pulses (Popovych and Tass, 2019). While consistent with previous computational studies (Popovych and Tass, 2019), the interphase gap utilized in our modeling of biphasic stimulation pulses is a fair bit larger than in current DBS systems, where the interphase gap is generally at the smaller time scale of several tens of microseconds (Boogers et al., 2022). This might critically affect the outcome of the biphasic stimulation, for example, shrink the corresponding therapeutic window (Boogers et al., 2022). The amplitude modulation of the bipolar aDBS current is shown in Figure 9B.

The power spectrum of the STN, GPe, and GPi LFP activities is shown in Figure 10 when monopolar (red) or bipolar (blue) aDBS is administered to the STN. In addition, the performances of monopolar and bipolar aDBS protocols are presented in Figure 11. Taken together, the results demonstrate that the performance of the model aDBS is roughly the same for monopolar aDBS and bipolar aDBS.

4. Discussion

Pre-clinical and clinical achievements of closed-loop DBS in the treatment of PD attracted a lot of attention during the past decade (Little et al., 2013, 2016; Priori et al., 2013; Rosa et al., 2015, 2017; Johnson et al., 2016; Piña-Fuentes et al., 2017; Tinkhauser et al., 2017). One way for closed-loop control of pathologically synchronized neural activity within the parkinsonian BG is to monitor the collective activity of neurons in the target network (e.g., the STN) and adapt the stimulation amplitude (strength) to the level of neural synchrony (Tass, 2003; Popovych et al., 2017b; Popovych and Tass, 2019; Fleming et al., 2020a,b). Neural synchrony can be, for example, estimated by the large-amplitude oscillations of collective activity in a population of interacting oscillatory neurons. This idea was taken into account to develop a closed-loop aDBS for the treatment of patients with PD where stimulation delivery was modulated according to the level of STN beta band activity (Little et al., 2013, 2016), leading to a better improvement in motor symptoms while reducing the delivered stimulation current compared with cDBS (Little et al., 2013, 2016).

Here, we developed a comprehensive cortico-BG-thalamic network model to investigate the efficiency of closed-loop control of the aDBS amplitude in comparison with the open-loop cDBS. The parkinsonian network model was characterized by excessive beta oscillations within STN, GPe, and GPi and reduced thalamic reliability. Subthalamic aDBS effectively suppressed parkinsonian beta oscillations and restored normal range of firing activity (in STN, GPe, and GPi) and preserved thalamic reliability. STN aDBS led to better suppression of pathological beta oscillations while notably less stimulation current was delivered compared with cDBS. Particularly, aDBS with the same stimulation frequency as cDBS led to a better beta suppression efficiency (i.e., aDBS: 3.6% vs. cDBS: 1.7%), while the energy expenditure was 41% less than cDBS (see Figure 8). Interestingly, the value of thalamic reliability was similar for both stimulation protocols (i.e., aDBS: 53% vs. cDBS: 52%).

In computational models of PD, response failures of thalamocortical cell populations tend to coincide temporally, whereas under DBS, these failures, when they occurr, are temporally dispersed (Guo et al., 2008). To explore the effect of DBS frequency on the thalamic reliability, we calculated the error index introduced by Rubin and Terman (2004), defined as the total number of errors divided by the total number of input stimuli (Rubin and Terman, 2004; So et al., 2012; Alavi et al., 2022). In this context, the optimal performance is achieved when each sensorimotor input pulse results in a single action potential in a thalamic neuron. As shown previously, in a model developed by Rubin and Terman (2004), DBS above 20 Hz

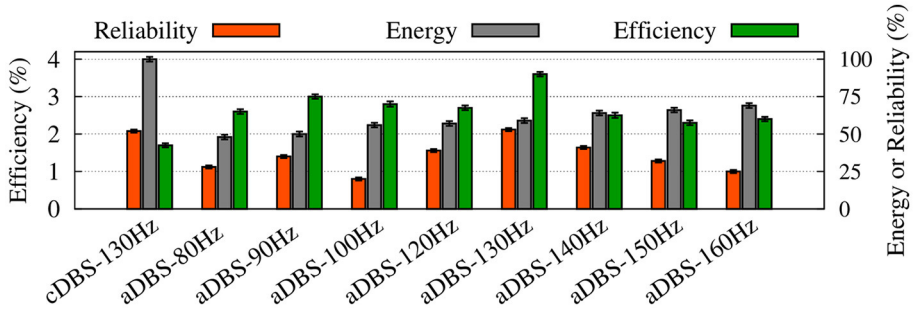

FIGURE 8
Summary of the performance of cDBS and aDBS protocols. The thalamic reliability (orange), the energy expenditure index as a measure of the amount of delivered stimulation current (gray), and the beta suppression efficiency for the STN (green) of each stimulation protocol at a given frequency were used to assess the performance of stimulation. Standard deviation bars are shown for 10 simulations under each condition.

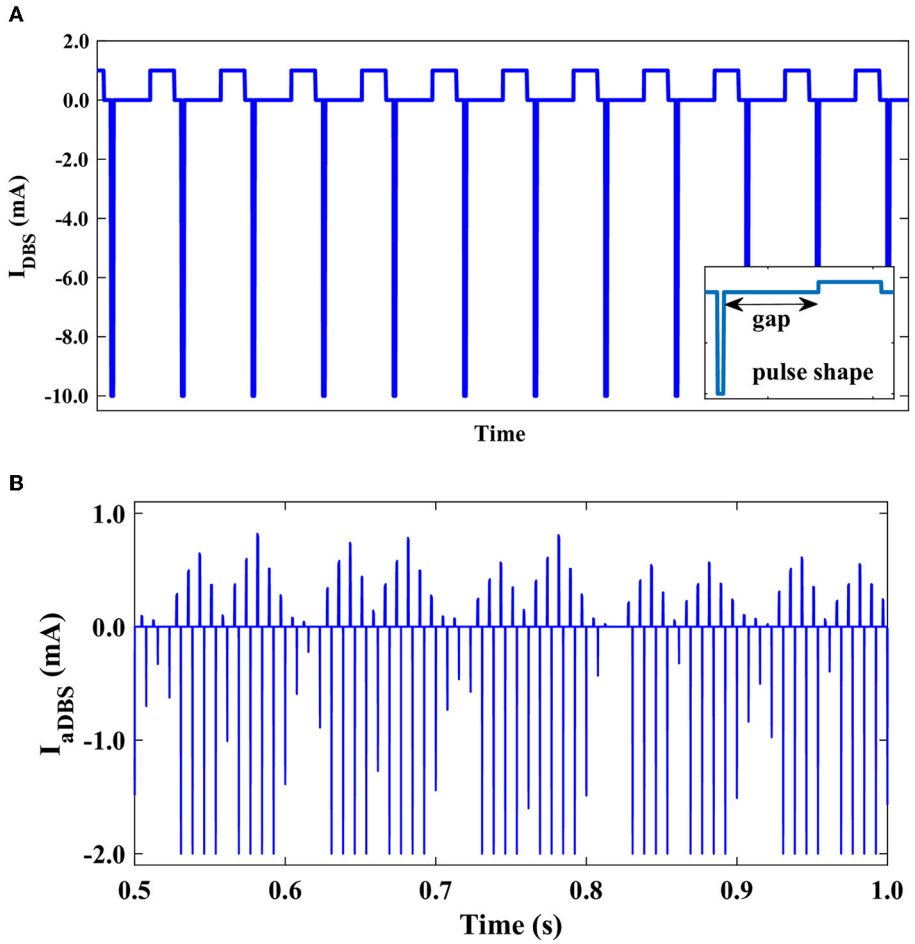

FIGURE 9
Stimulation signal of electrical biphasic charge-balanced pulses. **(A)** Schematically depicted biphasic charge-balanced pulses without amplitude modulation. Each pulse consists of an interphase gap between the cathodic and anodic phases of the pulse (inset). **(B)** The time course of the bipolar stimulation with amplitude modulation.

was effective at restoring the accuracy of thalamic transmission. Later, it was shown that stimulation below 40 Hz caused the rate of errors made by the thalamic cell to remain high, while stimulation above 100 Hz restored thalamic fidelity in a computational model of the BG (So et al., 2012). As shown in Supplementary Figure S2, our results show that aDBS above 100 Hz is effective at restoring the thalamic fidelity to its healthy level, with the best performance at 130 Hz.

In this study, the amplitude (strength) modulation in closed-loop control of the STN aDBS was performed by using the P controller scheme utilizing an LFP-derived measure of network beta band oscillatory activity (Fleming et al., 2020a,b), similar to that used during clinical closed-loop DBS protocols (Little et al., 2013, 2016). However, several studies employed alternative biomarkers for PD symptoms, such as entropy (Dorval et al.,

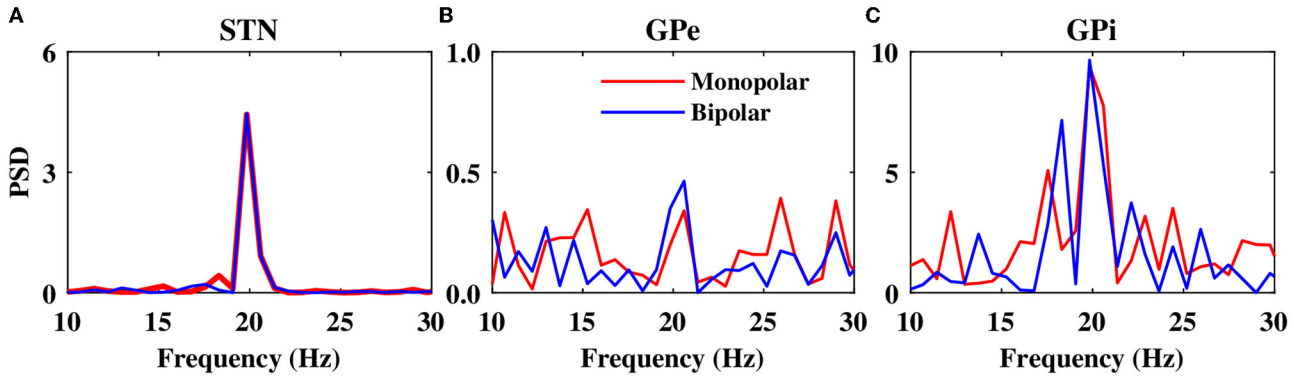

FIGURE 10
Power spectrum of the LFP activity. Power spectrum density of the STN **(A)**, GPe **(B)**, and GPi **(C)** LFP activities when monopolar aDBS (red) or bipolar aDBS (blue) is administered to the STN.

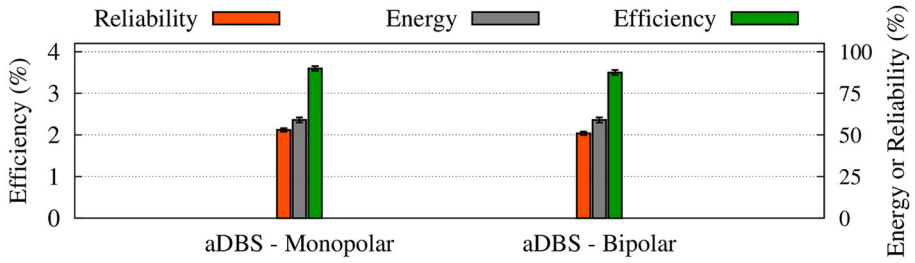

FIGURE 11
Performance of the monopolar and bipolar aDBS protocols. The thalamic reliability (orange), the energy expenditure index (green), and the beta suppression efficiency for the STN (gray) of each stimulation protocol at 130 Hz frequency were used to assess the performance of stimulation. Standard deviation bars are shown for 10 simulations under each condition.

2010; Dorval and Grill, 2014; Anderson et al., 2015; Syrkin-Nikolau et al., 2017), phase-amplitude coupling (De Hemptinne et al., 2013, 2015), coherence (Al-Fatly, 2019), and gamma band (30–80 Hz) activity-based measures (Swann et al., 2016, 2018). While amplitude modulation by the P controller utilizing LFP beta activity may not capture the neural mechanisms behind some of the parkinsonian symptoms and their specifically developed closed-loop DBS protocols, it may still be applicable to alternative stimulation methods, such as phase-based (Tass, 2003; Holt et al., 2016, 2019) linear delayed feedback (Popovych and Tass, 2019) and optogenetic (Detorakis et al., 2015) stimulation paradigms.

Taken together, closed-loop aDBS protocols with different stimulation frequencies led to better suppression of parkinsonian beta oscillations than open-loop cDBS while reducing the amount of delivered current and, thereby, may reduce potential stimulation-induced side effects (Baizabal-Carvallo and Jankovic, 2016; Pyragas et al., 2020). This suggests that closed-loop aDBS with amplitude modulation can efficiently maintain the beta band activity in the STN LFP below the target pathological level. As previously shown in several studies (Su et al., 2019; Fleming et al., 2020a,b), the suppression efficiency of closed-loop aDBS may depend on the stimulation frequency, controller type, and parameters. For instance, stimulation frequency modulation in closed-loop aDBS (instead of stimulation amplitude modulation) can effectively suppress abnormal beta oscillations, but it may also significantly increase the amount of administered stimulation current (Fleming et al., 2020a).

Moreover, another limitation of our model is that we tuned synaptic couplings and applied currents in the model to mimic parkinsonian beta band oscillatory activity within the cortico-BG-thalamic network, where cortical input was simplified as an external current. However, cortical input shapes rhythmic activity in the GPe-STN network in the PD state. Experimental findings suggest that the beta band oscillatory activity of the cortex and STN are significantly coherent and the beta band synchrony is notably increased between the GPe and STN as well as between the STN and the cortex following DA depletion (Sharott et al., 2005; Mallet et al., 2008). Computationally, excessive beta band oscillatory activity within the GPe-STN loop can be phase-locked to cortical beta inputs in PD models (Koelman and Lowery, 2019). Hence, our model may not be able to capture the complex network interactions leading to pathological beta oscillations in PD but still can reproduce suppression efficient characteristics of closed-loop aDBS compared with the open-loop cDBS.

Several experimental findings suggested that DA deficiency in PD can lead to exaggerated beta band (15–30 Hz) activity within the BG (Brown et al., 2001; Sharott et al., 2005; Mallet et al., 2008); however, the exact mechanisms underlying pathological beta oscillations remain poorly understood. Experimental and mathematical models have shown that beta oscillations can emerge from inhibitory interactions among striatal MSNs (McCarthy et al., 2011), increased levels of the striatal cholinergic drive (Kondabolu et al., 2016), or GPe-STN interactions (Brown et al., 2001; Holgado

et al., 2010; Tachibana et al., 2011). Yet, abnormal beta oscillations may not appear until the advanced stages of PD and are supposedly correlated with the extent of progressive degeneration of nigral DAergic neurons (Asadi et al., 2022). The degree of neural beta oscillatory activity is related to the magnitude of the response of the BG to DAergic neurons rather than directly to the severity of the patients' symptoms (Weinberger et al., 2006). Variability in the symptoms of patients with PD suggests that neural beta oscillatory activity, alone, may not reflect the clinical state of the patient, and other complex mechanisms must be involved in the disease pathophysiology (Weinberger et al., 2006). For instance, it has been shown that administration of some drugs increases STN beta oscillations while decreasing tremor and rigidity (Priori et al., 2004) and that clinical improvement after DBS is not associated with an expected decrease in beta LFP activity in the STN (Foffani et al., 2006). While our model did not take into account patient-specific variability of abnormal beta oscillations, the development of customized patient-specific models of DBS in future studies may promote clinical improvements (Hollunder et al., 2022).

Intriguingly, a number of experiments failed to establish a significant correlation among PD motor symptoms, such as bradykinesia, akinesia and rigidity, and excessive beta oscillations during parkinsonism (Weinberger et al., 2006; Stein and Bar-Gad, 2013). In fact, abnormal synchrony in patients with PD has been observed in different frequency bands that can be related to different disease symptoms (Kühn et al., 2006; Weinberger et al., 2006; Steigerwald et al., 2008; Contarino et al., 2012). For instance, the presence of tremor in patients with PD has been linked to beta band (3–8 Hz) neural oscillations in the dorsal STN (Contarino et al., 2012). While, in some studies, synchronized beta band (15–30 Hz) oscillations in the STN were specifically attributed to the presence of tremor (Levy et al., 2000), others did not find any difference between PD patients with or without resting tremor in the frequency distribution of oscillatory neural activity when considering the entire frequency range of 1–100 Hz (Steigerwald et al., 2008). In the context of the choice of frequency band used as a biomarker for closed-loop aDBS, beta frequency oscillations in the LFP may capture variation in bradykinesia and rigidity across patients (Little and Brown, 2012), but this should be confirmed in each patient since it may impact the set of symptoms that can be suppressed by the presented aDBS approach (Little and Brown, 2012; Johnson et al., 2016). More importantly, biomarkers that reliably reflect other impairments, such as tremor, also need to be tested. Of note, beta band power may not be the best biomarker for closed-loop aDBS. For instance, a recent longitudinal study showed that although DBS significantly suppressed beta band activity, the suppression effect appeared to attenuate gradually during a long-term 6-month follow-up period after surgery (Chen et al., 2020). While long-term attenuation of DBS effects may be due to the progression of the disease or the stimulation protocol itself (i.e., cDBS vs. aDBS), the sensitivity and reliability of other frequency bands as potential biomarkers that are selective to different PD symptoms need to be investigated.

The presence of beta oscillations (15–30 Hz) within the BG may not be always pathological, and transient beta oscillations can be related to the normal activity of the motor system, such as the intention and initiation of movement (Little and Brown, 2014; Khanna and Carmena, 2017). However, beta oscillations are significantly enhanced in PD, and there is strong correlative evidence linking beta activity at rest to the changes in beta power in response to treatment in patients with bradykinesia and rigidity (Sharott et al., 2005; Mallet et al., 2008; Little and Brown, 2014). In our model, the stimulation has only been delivered during periods of elevated beta activity through the closed-loop aDBS protocol. Our model, therefore, ignores the selectivity of the abnormal beta activity and always suppresses the beta activity regardless of its causal or quantitative origin. It remains to be studied in future how normal and pathological beta oscillations can be distinguished and how stimulation delivery protocol can be improved, accordingly.

Our aim was to present a simple, yet comprehensive model of the BG. Therefore, we ignored the role of fast-spiking interneurons (FSIs) in the BG circuitry since they supposedly constitute <5% of total striatal neurons (Koós and Tepper, 1999). However, as shown previously, the presence of FSIs may impact the emergence of strong synchronization and propagation of beta oscillations, which are a hallmark of parkinsonian circuit dysfunction (Corbit et al., 2016). Particularly, when GPe spikes are synchronous, the GPe-FSI pathway results in synchronous FSI activity pauses, allowing for a transient window of disinhibition for MSNs (Corbit et al., 2016). Accordingly, the inclusion of FSI into the BG circuitry in our model may affect the presented results by indirectly modulating the level of abnormal beta activity used as the biomarker of the disease.

In our study, the model parameters were extracted from the rodent models of PD. This might affect the impact of the aDBS protocol used in this study and need to be adopted for success in human clinical trials. Animal models may suffer from several limitations. For instance, in rodents, interventions may precede induction of the model and the outcomes may be less commonly assessed at multiple time points (Zeiss et al., 2017). Therefore, potential therapies for PD that are successful in animal studies may fail in human trials. The translational gap for potential therapeutic interventions in PD in part results from study designs that fail to model the progressive nature and relatively late intervention characteristic of PD (Zeiss et al., 2017). Yet, animal models enable the possibility to study the pathological mechanisms and the therapeutic principles of treating disease symptoms in humans. Once the causative mechanisms are clarified, animal models can be helpful in the development of therapeutic approaches and pave way for the transition from animal models to translational application in patients with PD.

Finally, abnormal synchronization is a hallmark of PD (Brown et al., 2001; Hammond et al., 2007). Such abnormal synchronization can be controlled by the administration of high-frequency desynchronizing brain stimulation to the diseased network (Popovych and Tass, 2014). However, the emergence of abnormal neural synchronization during parkinsonism cannot be solely ascribed to the pathological changes of neural dynamics following DA loss. Other complex mechanisms may be involved (Madadi Asl et al., 2018b, 2022b; Ziaeemehr et al., 2020). For instance, dysfunction of DA-mediated synaptic plasticity during parkinsonism shapes abnormal synaptic connectivity within the BG (Fan et al., 2012; Madadi Asl et al., 2019, 2022b). This further supports the emergence of pathological neural activity and synaptic connectivity patterns (Madadi Asl and Ramezani Akbarabadi, 2022) within the parkinsonian BG (Madadi Asl et al., 2022b). Thus,

an effective brain stimulation technique should in fact decouple neurons (Madadi Asl et al., 2023), that is, desynchronize overly synchronized neural activity and reduce pathological synaptic connectivity to ensure long-lasting therapeutic effects that persist after stimulation offset (Madadi Asl et al., 2023).

In this study, the synaptic connections among neurons in the network model were assumed to be static, that is, the synaptic strengths were fixed in time. However, beneficiary long-lasting stimulation effects can be, in principle, achieved in neural network models of PD with plastic synapses modified by spike-timing-dependent plasticity (STDP) (Gerstner et al., 1996; Markram et al., 1997; Bi and Poo, 1998), as shown by computational studies (Tass and Majtanik, 2006; Hauptmann and Tass, 2009; Popovych and Tass, 2012; Lourens et al., 2015; Kromer and Tass, 2020). STDP can mold multistable neural and synaptic network dynamics (Madadi Asl et al., 2017, 2018a,c; Ratas et al., 2021) that can be computationally attributed to physiological and pathological basins of attraction (Madadi Asl et al., 2022b). In this way, appropriately tuned, STDP-targeting stimulation protocols can shift patterns of neural activity and synaptic connectivity in plastic networks from pathological states (characterized by strong synchrony and strong connectivity) to more physiologically favored states (characterized by weak synchrony and weak connectivity) (Madadi Asl et al., 2022b, 2023).

Data availability statement

The original contributions presented in the study are included in the article/Supplementary material, further inquiries can be directed to the corresponding authors.

Author contributions

AV and SS conceived and designed the study. FB-J performed the material preparation and numerical simulations. FB-J, SS, MM, and AV analyzed the results. MM wrote the first draft of the manuscript. All authors contributed to manuscript revision, read, and approved the submitted version.

Conflict of interest

The authors declare that the research was conducted in the absence of any commercial or financial relationships that could be construed as a potential conflict of interest.

Publisher's note

All claims expressed in this article are solely those of the authors and do not necessarily represent those of their affiliated organizations, or those of the publisher, the editors and the reviewers. Any product that may be evaluated in this article, or claim that may be made by its manufacturer, is not guaranteed or endorsed by the publisher.

Supplementary material

The Supplementary Material for this article can be found online at: https://www.frontiersin.org/articles/10.3389/fnhum.2022.1013155/full#supplementary-material

References

Alavi, S. M., Mirzaei, A., Valizadeh, A., and Ebrahimpour, R. (2022). Excitatory deep brain stimulation quenches beta oscillations arising in a computational model of the subthalamo-pallidal loop. *Sci. Rep.* 12, 1–20. doi: 10.1038/s41598-022-10084-4

Al-Fatly, B. (2019). Coherence: a unifying mechanism of deep brain stimulation. *J. Neurophysiol.* 121, 1–3. doi: 10.1152/jn.00563.2018

Anderson, C. J., Sheppard, D. T., Huynh, R., Anderson, D. N., Polar, C. A., and Dorval, A. D. (2015). Subthalamic deep brain stimulation reduces pathological information transmission to the thalamus in a rat model of Parkinsonism. *Front. Neural Circ.* 9, 31. doi: 10.3389/fncir.2015.00031

Arlotti, M., Marceglia, S., Foffani, G., Volkmann, J., Lozano, A. M., Moro, E., et al. (2018). Eight-hours adaptive deep brain stimulation in patients with Parkinson disease. *Neurology* 90, e971-e976. doi: 10.1212/WNL.0000000000005121

Asadi, A., Madadi Asl, M., Vahabie, A. H., and Valizadeh, A. (2022). The origin of abnormal beta oscillations in the Parkinsonian corticobasal ganglia circuits. *Parkinsons Dis.* 2022, 1–13. doi: 10.1155/2022/7524066

Baizabal-Carvallo, J. F., and Jankovic, J. (2016). Movement disorders induced by deep brain stimulation. *Parkinsonism Related Disord.* 25, 1–9. doi: 10.1016/j.parkreldis.2016.01.014

Baufreton, J., Kirkham, E., Atherton, J. F., Menard, A., Magill, P. J., Bolam, J. P., et al. (2009). Sparse but selective and potent synaptic transmission from the globus pallidus to the subthalamic nucleus. *J. Neurophysiol.* 102, 532–545. doi: 10.1152/jn.00305.2009

Benabid, A. L. (2003). Deep brain stimulation for Parkinson's disease. *Curr. Opin. Neurobiol.* 13, 696–706. doi: 10.1016/j.conb.2003.11.001

Benabid, A. L., Chabardes, S., Mitrofanis, J., and Pollak, P. (2009). Deep brain stimulation of the subthalamic nucleus for the treatment of Parkinson's disease. *Lancet Neurol.* 8, 67–81. doi: 10.1016/S1474-4422(08)70291-6

Bi, G. Q., and Poo, M. M. (1998). Synaptic modifications in cultured hippocampal neurons: dependence on spike timing, synaptic strength, and postsynaptic cell type. *J. Neurosci.* 18, 10464–10472. doi: 10.1523/JNEUROSCI.18-24-10464.1998

Blandini, F., Nappi, G., Tassorelli, C., and Martignoni, E. (2000). Functional changes of the basal ganglia circuitry in Parkinson's disease. *Progr. Neurobiol.* 62, 63–88. doi: 10.1016/S0301-0082(99)00067-2

Boogers, A., Peeters, J., Van Bogaert, T., De Vloo, P., Vandenberghe, W., Nuttin, B., et al. (2022). Interphase gaps in symmetric biphasic pulses reduce the therapeutic window in ventral intermediate nucleus of the thalamus-deep brain stimulation for essential tremor. *Neuromodulation* 2022, 12. doi: 10.1016/j.neurom.2022.09.012

Brown, P., Oliviero, A., Mazzone, P., Insola, A., Tonali, P., and Di Lazzaro, V. (2001). Dopamine dependency of oscillations between subthalamic nucleus and pallidum in Parkinson's disease. *J. Neurosci.* 21, 1033–1038. doi: 10.1523/JNEUROSCI.21-03-01033.2001

Chen, Y., Gong, C., Tian, Y., Orlov, N., Zhang, J., Guo, Y., et al. (2020). Neuromodulation effects of deep brain stimulation on beta rhythm: a longitudinal local field potential study. *Brain Stimulat.* 13, 1784–1792. doi: 10.1016/j.brs.2020.09.027

Contarino, M. F., Bour, L. J., Bot, M., Van Den Munckhof, P., Speelman, J. D., Schuurman, P. R., et al. (2012). Tremor-specific neuronal oscillation pattern in dorsal subthalamic nucleus of Parkinsonian patients. *Brain Stimulat.* 5, 305–314. doi: 10.1016/j.brs.2011.03.011

Corbit, V. L., Whalen, T. C., Zitelli, K. T., Crilly, S. Y., Rubin, J. E., and Gittis, A. H. (2016). Pallidostriatal projections promote β oscillations in a dopamine-depleted biophysical network model. *J. Neurosci.* 36, 5556–5571. doi: 10.1523/JNEUROSCI.0339-16.2016

Daneshzand, M., Faezipour, M., and Barkana, B. D. (2018). Robust desynchronization of Parkinson's disease pathological oscillations by frequency

modulation of delayed feedback deep brain stimulation. *PLoS ONE* 13, e0207761. doi: 10.1371/journal.pone.0207761

De Hemptinne, C., Ryapolova-Webb, E. S., Air, E. L., Garcia, P. A., Miller, K. J., Ojemann, J. G., et al. (2013). Exaggerated phase-amplitude coupling in the primary motor cortex in Parkinson disease. *Proc. Natl. Acad. Sci. U.S.A.* 110, 4780–4785. doi: 10.1073/pnas.1214546110

De Hemptinne, C., Swann, N. C., Ostrem, J. L., Ryapolova-Webb, E. S., San Luciano, M., Galifianakis, N. B., et al. (2015). Therapeutic deep brain stimulation reduces cortical phase-amplitude coupling in Parkinson's disease. *Nat. Neurosci.* 18, 779–786. doi: 10.1038/nn.3997

DeLong, M. R. (1990). Primate models of movement disorders of basal ganglia origin. *Trends Neurosci.* 13, 281–285. doi: 10.1016/0166-2236(90)90110-V

Detorakis, G. I., Chaillet, A., Palfi, S., and Senova, S. (2015). Closed-loop stimulation of a delayed neural fields model of Parkinsonian STN-GPE network: a theoretical and computational study. *Front. Neurosci.* 9, 237. doi: 10.3389/fnins.2015.00237

Dorval, A. D., and Grill, W. M. (2014). Deep brain stimulation of the subthalamic nucleus reestablishes neuronal information transmission in the 6-ohda rat model of Parkinsonism. *J. Neurophysiol.* 111, 1949–1959. doi: 10.1152/jn.00713.2013

Dorval, A. D., Kuncel, A. M., Birdno, M. J., Turner, D. A., and Grill, W. M. (2010). Deep brain stimulation alleviates Parkinsonian bradykinesia by regularizing pallidal activity. *J. Neurophysiol.* 104, 911–921. doi: 10.1152/jn.00103.2010

Fan, K. Y., Baufreton, J., Surmeier, D. J., Chan, C. S., and Bevan, M. D. (2012). Proliferation of external globus pallidus-subthalamic nucleus synapses following degeneration of midbrain dopamine neurons. *J. Neurosci.* 32, 13718–13728. doi: 10.1523/JNEUROSCI.5750-11.2012

Fleming, J. E., Dunn, E., and Lowery, M. M. (2020a). Simulation of closed-loop deep brain stimulation control schemes for suppression of pathological beta oscillations in Parkinson's disease. *Front. Neurosci.* 14, 166. doi: 10.3389/fnins.2020.00166

Fleming, J. E., Orłowski, J., Lowery, M. M., and Chaillet, A. (2020b). Self-tuning deep brain stimulation controller for suppression of beta oscillations: analytical derivation and numerical validation. *Front. Neurosci.* 14, 639. doi: 10.3389/fnins.2020.00639

Foffani, G., Ardolino, G., Egidi, M., Caputo, E., Bossi, B., and Priori, A. (2006). Subthalamic oscillatory activities at beta or higher frequency do not change after high-frequency dbs in Parkinson's disease. *Brain Res. Bull.* 69, 123–130. doi: 10.1016/j.brainresbull.2005.11.012

Galvan, A., Devergnas, A., and Wichmann, T. (2015). Alterations in neuronal activity in basal ganglia-thalamocortical circuits in the Parkinsonian state. *Front. Neuroanat.* 9, 5. doi: 10.3389/fnana.2015.00005

Gerstner, W., Kempter, R., van Hemmen, J. L., and Wagner, H. (1996). A neuronal learning rule for sub-millisecond temporal coding. *Nature* 383, 76. doi: 10.1038/383076a0

Goldobin, D., Rosenblum, M., and Pikovsky, A. (2003). Controlling oscillator coherence by delayed feedback. *Phys. Rev. E* 67, 061119. doi: 10.1103/PhysRevE.67.061119

Gorzelic, P., Schiff, S., and Sinha, A. (2013). Model-based rational feedback controller design for closed-loop deep brain stimulation of Parkinson's disease. *J. Neural Eng.* 10, 026016. doi: 10.1088/1741-2560/10/2/026016

Graybiel, A. M., Aosaki, T., Flaherty, A. W., and Kimura, M. (1994). The basal ganglia and adaptive motor control. *Science* 265, 1826–1831. doi: 10.1126/science.8091209

Guidetti, M., Marceglia, S., Loh, A., Harmsen, I. E., Meoni, S., Foffani, G., et al. (2021). Clinical perspectives of adaptive deep brain stimulation. *Brain Stimulat.* 14, 1238–1247. doi: 10.1016/j.brs.2021.07.063

Guo, Y., Rubin, J. E., McIntyre, C. C., Vitek, J. L., and Terman, D. (2008). Thalamocortical relay fidelity varies across subthalamic nucleus deep brain stimulation protocols in a data-driven computational model. *J. Neurophysiol.* 99, 1477–1492. doi: 10.1152/jn.01080.2007

Hammond, C., Bergman, H., and Brown, P. (2007). Pathological synchronization in Parkinson's disease: networks, models and treatments. *Trends Neurosci.* 30, 357–364. doi: 10.1016/j.tins.2007.05.004

Hauptmann, C., and Tass, P. (2009). Cumulative and after-effects of short and weak coordinated reset stimulation: a modeling study. *J. Neural Eng.* 6, 016004. doi: 10.1088/1741-2560/6/1/016004

Holgado, A. J. N., Terry, J. R., and Bogacz, R. (2010). Conditions for the generation of beta oscillations in the subthalamic nucleus-globus pallidus network. *J. Neurosci.* 30, 12340–12352. doi: 10.1523/JNEUROSCI.0817-10.2010

Hollunder, B., Rajamani, N., Siddiqi, S. H., Finke, C., Kühn, A. A., Mayberg, H. S., et al. (2022). Toward personalized medicine in connectomic deep brain stimulation. *Progr. Neurobiol.* 210, 102211. doi: 10.1016/j.pneurobio.2021.102211

Holt, A. B., Kormann, E., Gulberti, A., Pötter-Nerger, M., McNamara, C. G., Cagnan, H., et al. (2019). Phase-dependent suppression of beta oscillations in Parkinson's disease patients. *J. Neurosci.* 39, 1119–1134. doi: 10.1523/JNEUROSCI.1913-18.2018

Holt, A. B., Wilson, D., Shinn, M., Moehlis, J., and Netoff, T. I. (2016). Phasic burst stimulation: a closed-loop approach to tuning deep brain stimulation parameters for parkin|SonŠs disease. *PLoS Comput. Biol.* 12, e1005011. doi: 10.1371/journal.pcbi.1005011

Johnson, L. A., Nebeck, S. D., Muralidharan, A., Johnson, M. D., Baker, K. B., and Vitek, J. L. (2016). Closed-loop deep brain stimulation effects on Parkinsonian motor symptoms in a non-human primate-is beta enough? *Brain Stimulat.* 9, 892–896. doi: 10.1016/j.brs.2016.06.051

Khanna, P., and Carmena, J. M. (2017). Beta band oscillations in motor cortex reflect neural population signals that delay movement onset. *eLife* 6, e24573. doi: 10.7554/eLife.24573

Kita, H., and Kita, S. (1994). The morphology of globus pallidus projection neurons in the rat: an intracellular staining study. *Brain Res.* 636, 308–319. doi: 10.1016/0006-8993(94)91030-8

Koelman, L. A., and Lowery, M. M. (2019). Beta-band resonance and intrinsic oscillations in a biophysically detailed model of the subthalamic nucleus-globus pallidus network. *Front. Comput. Neurosci.* 13, 77. doi: 10.3389/fncom.2019.00077

Kondabolu, K., Roberts, E. A., Bucklin, M., McCarthy, M. M., Kopell, N., and Han, X. (2016). Striatal cholinergic interneurons generate beta and gamma oscillations in the corticostriatal circuit and produce motor deficits. *Proc. Natl. Acad. Sci. U.S.A.* 113, E3159-E3168. doi: 10.1073/pnas.1605658113

Koós, T., and Tepper, J. M. (1999). Inhibitory control of neostriatal projection neurons by gabaergic interneurons. *Nat. Neurosci.* 2, 467–472. doi: 10.1038/8138

Kromer, J. A., and Tass, P. A. (2020). Long-lasting desynchronization by decoupling stimulation. *Phys. Rev. Res.* 2, 033101. doi: 10.1103/PhysRevResearch.2.033101

Kühn, A. A., Kempf, F., Brücke, C., Doyle, L. G., Martinez-Torres, I., Pogosyan, A., et al. (2008). High-frequency stimulation of the subthalamic nucleus suppresses oscillatory β activity in patients with Parkinson's disease in parallel with improvement in motor performance. *J. Neurosci.* 28, 6165–6173. doi: 10.1523/JNEUROSCI.0282-08.2008

Kühn, A. A., Kupsch, A., Schneider, G.-H., and Brown, P. (2006). Reduction in subthalamic 8-35 hz oscillatory activity correlates with clinical improvement in Parkinson's disease. *Eur. J. Neurosci.* 23, 1956–1960. doi: 10.1111/j.1460-9568.2006.04717.x

Leblois, A., Boraud, T., Meissner, W., Bergman, H., and Hansel, D. (2006). Competition between feedback loops underlies normal and pathological dynamics in the basal ganglia. *J. Neurosci.* 26, 3567–3583. doi: 10.1523/JNEUROSCI.5050-05.2006

Lemos, J. C., Friend, D. M., Kaplan, A. R., Shin, J. H., Rubinstein, M., Kravitz, A. V., et al. (2016). Enhanced gaba transmission drives bradykinesia following loss of dopamine d2 receptor signaling. *Neuron* 90, 824–838. doi: 10.1016/j.neuron.2016.04.040

Levy, R., Hutchison, W. D., Lozano, A. M., and Dostrovsky, J. O. (2000). High-frequency synchronization of neuronal activity in the subthalamic nucleus of Parkinsonian patients with limb tremor. *J. Neurosci.* 20, 7766–7775. doi: 10.1523/JNEUROSCI.20-20-07766.2000

Limousin, P., Speelman, J., Gielen, F., Janssens, M., et al. (1999). Multicentre european study of thalamic stimulation in Parkinsonian and essential tremor. *J. Neurol. Neurosurg. Psychiatry* 66, 289–296. doi: 10.1136/jnnp.66.3.289

Little, S., Beudel, M., Zrinzo, L., Foltynie, T., Limousin, P., Hariz, M., et al. (2016). Bilateral adaptive deep brain stimulation is effective in Parkinson's disease. *J. Neurol. Neurosurg. Psychiatry* 87, 717–721. doi: 10.1136/jnnp-2015-310972

Little, S., and Brown, P. (2012). What brain signals are suitable for feedback control of deep brain stimulation in Parkinson's disease? *Ann. N. Y. Acad. Sci.* 1265, 9–24. doi: 10.1111/j.1749-6632.2012.06650.x

Little, S., and Brown, P. (2014). The functional role of beta oscillations in Parkinson's disease. *Parkinsonism Related Disord.* 20:S44-S48. doi: 10.1016/S1353-8020(13)70013-0

Little, S., Pogosyan, A., Neal, S., Zavala, B., Zrinzo, L., Hariz, M., et al. (2013). Adaptive deep brain stimulation in advanced Parkinson disease. *Ann. Neurol.* 74, 449–457. doi: 10.1002/ana.23951

Lourens, M. A., Schwab, B. C., Nirody, J. A., Meijer, H. G., and van Gils, S. A. (2015). Exploiting pallidal plasticity for stimulation in ParkinsonŠs disease. *J. Neural Eng.* 12, 026005. doi: 10.1088/1741-2560/12/2/026005

Madadi Asl, M., Asadi, A., Enayati, J., and Valizadeh, A. (2022a). Inhibitory spike-timing-dependent plasticity can account for pathological strengthening of pallido-subthalamic synapses in Parkinson's disease. *Front. Physiol.* 13, 1–13. doi: 10.3389/fphys.2022.915626

Madadi Asl, M., and Ramezani Akbarabadi, S. (2022). Delay-dependent transitions of phase synchronization and coupling symmetry between neurons shaped by spike-timing-dependent plasticity. *Cogn. Neurodyn.* 2022, 1–14. doi: 10.1007/s11571-022-09850-x

Madadi Asl, M., Vahabie, A. H., and Valizadeh, A. (2019). Dopaminergic modulation of synaptic plasticity, its role in neuropsychiatric disorders, and its computational modeling. *Basic Clin. Neurosci.* 10, 1. doi: 10.32598/bcn.9.10.125

Madadi Asl, M., Vahabie, A. H., Valizadeh, A., and Tass, P. A. (2022b). Spike-timing-dependent plasticity mediated by dopamine and its role in Parkinson's disease pathophysiology. *Front. Netw. Physiol.* 2, 1–18. doi: 10.3389/fnetp.2022.817524

Madadi Asl, M., Valizadeh, A., and Tass, P. A. (2017). Dendritic and axonal propagation delays determine emergent structures of neuronal networks with plastic synapses. *Sci. Rep.* 7, 39682. doi: 10.1038/srep39682

Madadi Asl, M., Valizadeh, A., and Tass, P. A. (2018a). Delay-induced multistability and loop formation in neuronal networks with spike-timing-dependent plasticity. *Sci. Rep.* 8, 12068. doi: 10.1038/s41598-018-30565-9

Madadi Asl, M., Valizadeh, A., and Tass, P. A. (2018b). Dendritic and axonal propagation delays may shape neuronal networks with plastic synapses. *Front. Physiol.* 9, 1849. doi: 10.3389/fphys.2018.01849

Madadi Asl, M., Valizadeh, A., and Tass, P. A. (2018c). Propagation delays determine neuronal activity and synaptic connectivity patterns emerging in plastic neuronal networks. *Chaos* 28, 106308. doi: 10.1063/1.5037309

Madadi Asl, M., Valizadeh, A., and Tass, P. A. (2023). Decoupling of interacting neuronal populations by time-shifted stimulation through spike-timing-dependent plasticity. *PLoS Comput. Biol.* doi: 10.1371/journal.pcbi.1010853

Mahon, S., Deniau, J.-M., Charpier, S., and Delord, B. (2000). Role of a striatal slowly inactivating potassium current in short-term facilitation of corticostriatal inputs: a computer simulation study. *Learn. Mem.* 7, 357–362. doi: 10.1101/lm.34800

Mallet, N., Pogosyan, A., Sharott, A., Csicsvari, J., Bolam, J. P., Brown, P., et al. (2008). Disrupted dopamine transmission and the emergence of exaggerated beta oscillations in subthalamic nucleus and cerebral cortex. *J. Neurosci.* 28, 4795–4806. doi: 10.1523/JNEUROSCI.0123-08.2008

Markram, H., Lübke, J., Frotscher, M., and Sakmann, B. (1997). Regulation of synaptic efficacy by coincidence of postsynaptic aps and epsps. *Science* 275, 213–215. doi: 10.1126/science.275.5297.213

Mazzoni, A., Lindén, H., Cuntz, H., Lansner, A., Panzeri, S., and Einevoll, G. T. (2015). Computing the local field potential (lfp) from integrate-and-fire network models. *PLoS Comput. Biol.* 11, e1004584. doi: 10.1371/journal.pcbi.1004584

McCarthy, M., Moore-Kochlacs, C., Gu, X., Boyden, E., Han, X., and Kopell, N. (2011). Striatal origin of the pathologic beta oscillations in Parkinson's disease. *Proc. Natl. Acad. Sci. U.S.A.* 108, 11620–11625. doi: 10.1073/pnas.1107748108

Meissner, W., Leblois, A., Hansel, D., Bioulac, B., Gross, C. E., Benazzouz, A., et al. (2005). Subthalamic high frequency stimulation resets subthalamic firing and reduces abnormal oscillations. *Brain* 128, 2372–2382. doi: 10.1093/brain/awh616

Mink, J. W. (1996). The basal ganglia: focused selection and inhibition of competing motor programs. *Progr. Neurobiol.* 50, 381–425. doi: 10.1016/S0301-0082(96)00042-1

Oorschot, D. E. (1996). Total number of neurons in the neostriatal, pallidal, subthalamic, and substantia nigral nuclei of the rat basal ganglia: a stereological study using the cavalieri and optical disector methods. *J. Compar. Neurol.* 366, 580–599. doi: 10.1002/(SICI)1096-9861(19960318)366:4<580::AID-CNE3>3.0.CO;2-0

Pavlides, A., Hogan, S. J., and Bogacz, R. (2015). Computational models describing possible mechanisms for generation of excessive beta oscillations in Parkinson's disease. *PLoS Comput. Biol.* 11, e1004609. doi: 10.1371/journal.pcbi.1004609

Pi na-Fuentes, D., Little, S., Oterdoom, M., Neal, S., Pogosyan, A., Tijssen, M. A., et al. (2017). Adaptive dbs in a Parkinson's patient with chronically implanted DBS: a proof of principle. *Mov. Disord.* 32, 1253–1254. doi: 10.1002/mds.26959

Popovych, O. V., Lysyansky, B., Rosenblum, M., Pikovsky, A., and Tass, P. A. (2017a). Pulsatile desynchronizing delayed feedback for closed-loop deep brain stimulation. *PLoS ONE* 12, e0173363. doi: 10.1371/journal.pone.0173363

Popovych, O. V., Lysyansky, B., and Tass, P. A. (2017b). Closed-loop deep brain stimulation by pulsatile delayed feedback with increased gap between pulse phases. *Sci. Rep.* 7, 1–14. doi: 10.1038/s41598-017-01067-x

Popovych, O. V., and Tass, P. A. (2012). Desynchronizing electrical and sensory coordinated reset neuromodulation. *Front. Hum. Neurosci.* 6, 58. doi: 10.3389/fnhum.2012.00058

Popovych, O. V., and Tass, P. A. (2014). Control of abnormal synchronization in neurological disorders. *Front. Neurol.* 5, 268. doi: 10.3389/fneur.2014.00268

Popovych, O. V., and Tass, P. A. (2019). Adaptive delivery of continuous and delayed feedback deep brain stimulation-a computational study. *Sci. Rep.* 9, 1–17. doi: 10.1038/s41598-019-47036-4

Priori, A., Foffani, G., Pesenti, A., Tamma, F., Bianchi, A., Pellegrini, M., et al. (2004). Rhythm-specific pharmacological modulation of subthalamic activity in Parkinson's disease. *Exp. Neurol.* 189, 369–379. doi: 10.1016/j.expneurol.2004.06.001

Priori, A., Foffani, G., Rossi, L., and Marceglia, S. (2013). Adaptive deep brain stimulation (adbs) controlled by local field potential oscillations. *Exp. Neurol.* 245, 77–86. doi: 10.1016/j.expneurol.2012.09.013

Pyragas, K., Fedaravičius, A. P., Pyragienė, T., and Tass, P. A. (2020). Entrainment of a network of interacting neurons with minimum stimulating charge. *Phys. Rev. E* 102, 012221. doi: 10.1103/PhysRevE.102.012221

Ratas, I., Pyragas, K., and Tass, P. A. (2021). Multistability in a star network of kuramoto-type oscillators with synaptic plasticity. *Sci. Rep.* 11, 1–15. doi: 10.1038/s41598-021-89198-0

Rosa, M., Arlotti, M., Ardolino, G., Cogiamanian, F., Marceglia, S., Di Fonzo, A., et al. (2015). Adaptive deep brain stimulation in a freely moving Parkinsonian patient. *Mov. Disord.* 30, 1003–1005. doi: 10.1002/mds.26241

Rosa, M., Arlotti, M., Marceglia, S., Cogiamanian, F., Ardolino, G., Fonzo, A. D., et al. (2017). A daptive deep brain stimulation controls levodopa-induced side effects in p arkinsonian patients. *Mov. Disord.* 32, 628–629. doi: 10.1002/mds.26953

Rosenblum, M., and Pikovsky, A. (2004). Delayed feedback control of collective synchrony: an approach to suppression of pathological brain rhythms. *Phys. Rev. E* 70, 041904. doi: 10.1103/PhysRevE.70.041904

Rubin, J. E., and Terman, D. (2004). High frequency stimulation of the subthalamic nucleus eliminates pathological thalamic rhythmicity in a computational model. *J. Comput. Neurosci.* 16, 211–235. doi: 10.1023/B:JCNS.0000025686.47117.67

Sharott, A., Magill, P. J., Harnack, D., Kupsch, A., Meissner, W., and Brown, P. (2005). Dopamine depletion increases the power and coherence of β-oscillations in the cerebral cortex and subthalamic nucleus of the awake rat. *Eur. J. Neurosci.* 21, 1413–1422. doi: 10.1111/j.1460-9568.2005.03973.x

So, R. Q., Kent, A. R., and Grill, W. M. (2012). Relative contributions of local cell and passing fiber activation and silencing to changes in thalamic fidelity during deep brain stimulation and lesioning: a computational modeling study. *J. Comput. Neurosci.* 32, 499–519. doi: 10.1007/s10827-011-0366-4

Steigerwald, F., Potter, M., Herzog, J., Pinsker, M., Kopper, F., Mehdorn, H., et al. (2008). Neuronal activity of the human subthalamic nucleus in the Parkinsonian and nonparkinsonian state. *J. Neurophysiol.* 100, 2515–2524. doi: 10.1152/jn.90574.2008

Stein, E., and Bar-Gad, I. (2013). Beta oscillations in the cortico-basal ganglia loop during Parkinsonism. *Exp. Neurol.* 245, 52–59. doi: 10.1016/j.expneurol.2012.07.023

Su, F., Kumaravelu, K., Wang, J., and Grill, W. M. (2019). Model-based evaluation of closed-loop deep brain stimulation controller to adapt to dynamic changes in reference signal. *Front. Neurosci.* 13, 956. doi: 10.3389/fnins.2019.00956

Su, F., Wang, J., Niu, S., Li, H., Deng, B., Liu, C., et al. (2018). Nonlinear predictive control for adaptive adjustments of deep brain stimulation parameters in basal ganglia-thalamic network. *Neural Netw.* 98, 283–295. doi: 10.1016/j.neunet.2017.12.001

Swann, N. C., de Hemptinne, C., Miocinovic, S., Qasim, S., Wang, S. S., Ziman, N., et al. (2016). Gamma oscillations in the hyperkinetic state detected with chronic human brain recordings in Parkinson's disease. *J. Neurosci.* 36, 6445–6458. doi: 10.1523/JNEUROSCI.1128-16.2016

Swann, N. C., de Hemptinne, C., Thompson, M. C., Miocinovic, S., Miller, A. M., Ostrem, J. L., et al. (2018). Adaptive deep brain stimulation for ParkinsonŠs disease using motor cortex sensing. *J. Neural Eng.* 15, 046006. doi: 10.1088/1741-2552/aabc9b

Syrkin-Nikolau, J., Koop, M. M., Prieto, T., Anidi, C., Afzal, M. F., Velisar, A., et al. (2017). Subthalamic neural entropy is a feature of freezing of gait in freely moving people with Parkinson's disease. *Neurobiol. Dis.* 108, 288–297. doi: 10.1016/j.nbd.2017.09.002

Tachibana, Y., Iwamuro, H., Kita, H., Takada, M., and Nambu, A. (2011). Subthalamo-pallidal interactions underlying Parkinsonian neuronal oscillations in the primate basal ganglia. *Eur. J. Neurosci.* 34, 1470–1484. doi: 10.1111/j.1460-9568.2011.07865.x

Tass, P. A. (2003). A model of desynchronizing deep brain stimulation with a demand-controlled coordinated reset of neural subpopulations. *Biol. Cybern.* 89, 81–88. doi: 10.1007/s00422-003-0425-7

Tass, P. A., and Majtanik, M. (2006). Long-term anti-kindling effects of desynchronizing brain stimulation: a theoretical study. *Biol. Cybern.* 94, 58–66. doi: 10.1007/s00422-005-0028-6

Terman, D., Rubin, J. E., Yew, A., and Wilson, C. (2002). Activity patterns in a model for the subthalamopallidal network of the basal ganglia. *J. Neurosci.* 22, 2963–2976. doi: 10.1523/JNEUROSCI.22-07-02963.2002

Tinkhauser, G., Pogosyan, A., Little, S., Beudel, M., Herz, D. M., Tan, H., et al. (2017). The modulatory effect of adaptive deep brain stimulation on beta bursts in Parkinson's disease. *Brain* 140, 1053–1067. doi: 10.1093/brain/awx010

Toth, K., and Wilson, D. (2022). Control of coupled neural oscillations using near-periodic inputs. *Chaos* 32, 033130. doi: 10.1063/5.0076508

Tukhlina, N., Rosenblum, M., Pikovsky, A., and Kurths, J. (2007). Feedback suppression of neural synchrony by vanishing stimulation. *Phys. Rev. E* 75, 011918. doi: 10.1103/PhysRevE.75.011918

Velisar, A., Syrkin-Nikolau, J., Blumenfeld, Z., Trager, M., Afzal, M., Prabhakar, V., et al. (2019). Dual threshold neural closed loop deep brain stimulation in Parkinson disease patients. *Brain Stimulat.* 12, 868–876. doi: 10.1016/j.brs.2019.02.020

Volkmann, J. (2004). Deep brain stimulation for the treatment of ParkinsonŠs disease. *J. Clin. Neurophysiol.* 21, 6–17. doi: 10.1097/00004691-200401000-00003

Wang, X. J., and Buzsáki, G. (1996). Gamma oscillation by synaptic inhibition in a hippocampal interneuronal network model. *J. Neurosci.* 16, 6402–6413. doi: 10.1523/JNEUROSCI.16-20-06402.1996

Weerasinghe, G., Duchet, B., Bick, C., and Bogacz, R. (2021). Optimal closed-loop deep brain stimulation using multiple independently controlled contacts. *PLoS Comput. Biol.* 17, e1009281. doi: 10.1371/journal.pcbi.1009281

Weinberger, M., Mahant, N., Hutchison, W. D., Lozano, A. M., Moro, E., Hodaie, M., et al. (2006). Beta oscillatory activity in the subthalamic nucleus and its relation to dopaminergic response in Parkinson's disease. *J. Neurophysiol.* 96, 3248–3256. doi: 10.1152/jn.00697.2006

Wood, R., Gurney, K. N., and Wilson, C. (2004). A novel parameter optimisation technique for compartmental models applied to a model of a striatal medium spiny neuron. *Neurocomputing* 58, 1109–1116. doi: 10.1016/j.neucom.2004.01.174

Zeiss, C. J., Allore, H. G., and Beck, A. P. (2017). Established patterns of animal study design undermine translation of disease-modifying therapies for Parkinson's disease. *PLoS ONE* 12, e0171790. doi: 10.1371/journal.pone.0171790

Ziaeemehr, A., Zarei, M., Valizadeh, A., and Mirasso, C. R. (2020). Frequency-dependent organization of the brainŠs functional network through delayed-interactions. *Neural Netw.* 132, 155–165. doi: 10.1016/j.neunet.2020.08.003

frontiers | Frontiers in Neuroinformatics

TYPE Opinion
PUBLISHED 24 March 2023
DOI 10.3389/fninf.2023.1150157

OPEN ACCESS

EDITED BY
Peter A. Tass,
Stanford University, United States

REVIEWED BY
Mojtaba Madadi Asl,
Institute for Research in Fundamental Sciences (IPM), Iran
Justus Alfred Kromer,
Stanford University, United States

*CORRESPONDENCE
J. Luis Lujan
✉ lujan.luis@mayo.edu

RECEIVED 23 January 2023
ACCEPTED 06 March 2023
PUBLISHED 24 March 2023

CITATION
Asp AJ, Chintaluru Y, Hillan S and Lujan JL (2023) Targeted neuroplasticity in spatiotemporally patterned invasive neuromodulation therapies for improving clinical outcomes.
Front. Neuroinform. 17:1150157.
doi: 10.3389/fninf.2023.1150157

Targeted neuroplasticity in spatiotemporally patterned invasive neuromodulation therapies for improving clinical outcomes

Anders J. Asp[1], Yaswanth Chintaluru[2,3], Sydney Hillan[1] and J. Luis Lujan[2,4]*

[1]Mayo Clinic Graduate School of Biomedical Sciences, Mayo Clinic, Rochester, MN, United States, [2]Department of Neurologic Surgery, Mayo Clinic, Rochester, MN, United States, [3]Department of Neurology and Neurosurgery, University of Colorado Anschutz School of Medicine, Aurora, CO, United States, [4]Department of Physiology and Biomedical Engineering, Mayo Clinic, Rochester, MN, United States

KEYWORDS

neuroplasticity, spike timing dependant plasticity, deep brain stimulation (DBS), biofeedback, network control, transcranial magnetic stimulation (TMS), neuromodulation, neurosurgery

Introduction

Invasive neuromodulation is routinely used to effectively treat the symptoms of movement (Dallapiazza et al., 2019; Limousin and Foltynie, 2019) and psychiatric (Visser-Vandewalle et al., 2022) disorders with high success despite a limited understanding of their mechanisms of action. While the distinct neuroanatomical targets that are stimulated vary depending on the condition being treated and any existing comorbidities, the predominant neuromodulation strategy is to apply a fixed-frequency electrical current to the corresponding neural targets for symptom relief. In the case of movement disorders such as Parkinson's disease (PD), symptom reduction manifests within seconds or minutes following stimulation onset and disappears within a similar time course following the cessation of stimulation (Hristova et al., 2000; Temperli et al., 2003; Ducharme et al., 2011; Pugh, 2019). Maladaptive neuroplasticity, defined as plasticity underlying a disruption in normal neural network function, contributes to numerous neurologic and psychiatric conditions such as chronic pain (Kuner and Flor, 2017), mood disorders (Duman, 2002), movement disorders (McPherson et al., 2015; Li, 2017; Seeman et al., 2017; Peng et al., 2018; Versace et al., 2018; Madadi Asl et al., 2022), tinnitus (Engineer et al., 2011), addiction (Kauer and Malenka, 2007; Kalivas and O'Brien, 2008; Famitafreshi and Karimian, 2019), and depression (Duman et al., 2016). While some invasive neuromodulation approaches treat this underlying neuroplasticity (Creed et al., 2015; McPherson et al., 2015; Seeman et al., 2017; Peng et al., 2018; Versace et al., 2018; Asl et al., 2023), most do not. Thus, the neuromodulation community must consider well-characterized biophysical phenomena such as synaptic plasticity as inspiration when developing next-generation neuromodulation therapies rather than re-applying stimulation paradigms designed for movement disorders

to improve treatment outcomes in all conditions, such as psychiatric disorders.

Targeted neuroplasticity as a tool to treat neurologic and psychiatric indications

Targeted neuroplasticity encompasses neuromodulation approaches designed to induce and maintain a long-term influence over nervous system function through long-term potentiation (LTP) or long-term depression (LTD) such that symptom improvement persists after stimulation cessation. Examples of non-invasive neuromodulation approaches that maintain targeted neuroplasticity include transcranial magnetic stimulation (TMS) (Horvath et al., 2010; Valero-Cabré et al., 2017) and vibrotactile coordinated reset (CR) (Syrkin-Nikolau et al., 2018; Pfeifer et al., 2021). These approaches contrast with some conventional invasive neuromodulation approaches such as fixed-frequency deep brain stimulation (DBS), in which acute symptoms are managed only during stimulation (Herrington et al., 2015; Ashkan et al., 2017; Pugh, 2019).

Here, we postulate that targeted neuroplasticity through spatiotemporally patterned stimulation may improve clinical outcomes and enhance invasive therapies such as DBS by reversing maladaptive plasticity rather than treating symptoms. To this end, we propose four considerations for incorporating targeted neuroplasticity into invasive neuromodulation therapies (Figure 1).

Control of complex networks requires spatiotemporally precise stimulation at multiple network locations to improve clinically significant long-term symptom reduction

Neurologic conditions are often associated with neural network dysfunction (Spencer, 2002; Palop et al., 2006; Rosin et al., 2007), and as such, clinically-effective outcomes require timely interventions at multiple network locations (Tu et al., 2018). While initial studies suggested neural activity could be altered from a single node (Gu et al., 2015), the interconnected topology of neural networks complicates selection of a single control node from which to apply stimulation. Furthermore, multiple studies using functional magnetic resonance imaging (fMRI) and other techniques have demonstrated that stimulation at multiple nodes enhances network control (Capotosto et al., 2014; Fox et al., 2014; Pasqualetti et al., 2014; Tu et al., 2018). More importantly, studies have shown that enhanced multi-node network controllability can be achieved *via* paired stimulation of multiple connected brain regions such as inter-hemispheric dPM-M1 cortex (Lafleur et al., 2016). A clear example of this concept is the use of dual-site DBS placed in the centromedian-parafascicular complex and ventral capsule/ventral striatum to effectively treat motor and non-motor symptoms of severe, medication-resistant Tourette syndrome (Kakusa et al., 2019). Studies thus suggest that multi-location stimulation may improve control of pathological network function underlying symptoms.

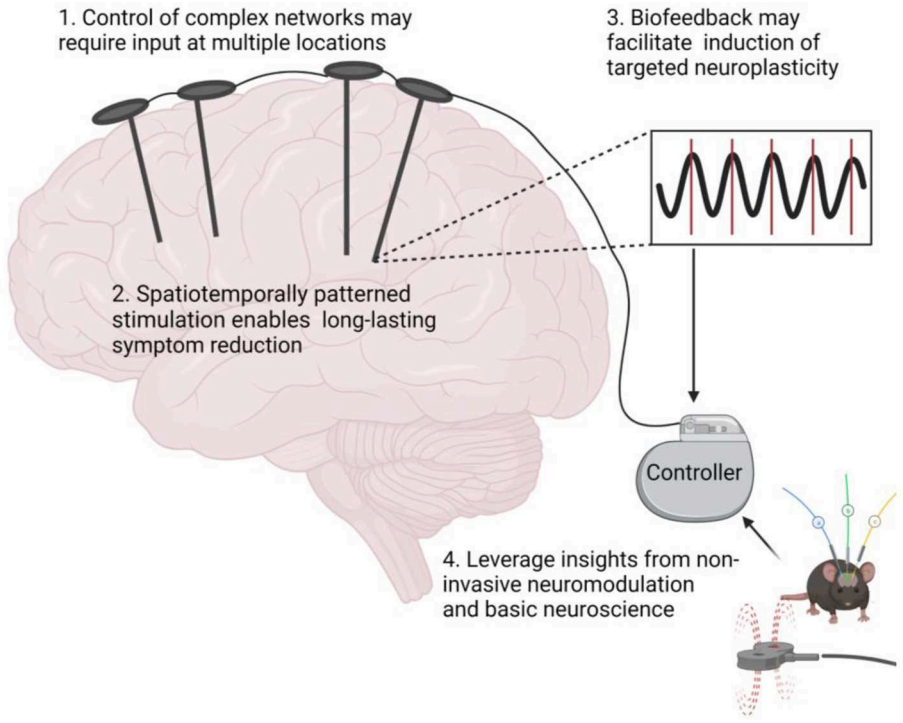

FIGURE 1
Targeted neuroplasticity approaches for invasive neuromodulation therapies. Figure created with Biorender.com.

Spatiotemporally patterned stimulation enables long-lasting desynchronization of pathological network activity and sustained symptom reduction

Spatiotemporally patterned stimulation has distinct advantages over traditional high-frequency (>100 Hz) stimulation such as facilitation of long-lasting targeted neuroplasticity and desynchronization of pathological network activity leading to symptom reduction. The relative timing between presynaptic and postsynaptic activation influences synaptic strength through a mechanism known as spike-timing dependent plasticity (STDP), is known to profoundly influence brain network function through changes in the direction and magnitude of synaptic strength (Markram et al., 1997; Bi and Poo, 1998; Dan and Poo, 2004; Caporale and Dan, 2008; Brzosko et al., 2019). STDP mechanisms are leveraged by emerging spatiotemporally patterned neuromodulation approaches such as decoupling time-shifted stimulation (Kromer and Tass, 2020; Asl et al., 2023) periodic multichannel stimulation (Kromer and Tass, 2022), and CR (Pfister et al., 2010). These therapies facilitate long-lasting desynchronization of pathologically coherent network activity underlying conditions like Parkinson's Disease (PD) by applying spatiotemporally patterned electric stimulation across subcortical targets such as the STN (Tass, 2003; Tass and Majtanik, 2006; Pfister et al., 2010; Adamchic et al., 2014; Ebert et al., 2014; Wang et al., 2016; Madadi Asl et al., 2018). From a therapeutic standpoint, a major benefit of spatiotemporally patterned therapies is that discontinuous and lower frequency stimulation may reduce the risk of side effects attributable to chronic continuous stimulation (Ferraye et al., 2008; Xie et al., 2012). Furthermore, therapies such as CR demonstrate sustained symptom reduction after stimulation cessation (Tass et al., 2012; Adamchic et al., 2017; Syrkin-Nikolau et al., 2018; Ho et al., 2021; Pfeifer et al., 2021; Wang et al., 2022). Similarly, paired phase-locked stimulation of the infralimbic cortex and basolateral amygdala alters synaptic strength and theta band coherence in a manner that that persists after stimulation cessation (Lo et al., 2020).

Numerous studies achieve targeted neuroplasticity with spatiotemporally patterned stimulation delivered across multiple stimulation modalities. For example, repeated pairing of low frequency (0.1 Hz) DBS with TMS of M1-cortex alters corticostriatal plasticity in humans (Udupa et al., 2016). Similarly, the application of transcranial direct or alternating current stimulation prior to TMS has been shown to alter the effectiveness of the TMS-based plasticity induction protocol (Cosentino et al., 2012; Guerra et al., 2018; Nakazono et al., 2021). Additionally, pairing DBS of midbrain locomotor regions with epidural stimulation of the lumbar spinal cord improves motor function in a rat model of spinal cord injury (Bonizzato et al., 2021). One clinical case report found improved motor function in a patient with multiple system atrophy and predominant parkinsonism when bilateral subthalamic nucleus (STN) DBS and spinal cord stimulation were combined (Li et al., 2022). Taken together, these examples demonstrate that spatiotemporally patterned simulation may enable long-lasting reductions in symptoms and side effects and expand invasive neuromodulation indications while improving power consumption efficiency.

Biofeedback may facilitate induction of targeted neuroplasticity

Closed-loop neuromodulation approaches leverage biofeedback to guide stimulation parameter selection in a wide range of circuitopathies underlying conditions such as epilepsy (Seitz, 2013), PD (Kühn et al., 2009; Weinberger et al., 2012), essential tremor (Thompson et al., 2014), and dystonia (Barow et al., 2014), in which oscillation frequency abnormalities serve as biomarkers that can inform stimulation parameter selection to improve symptom reduction (Thompson et al., 2014). For example, electrophysiological activity recorded during electrographic seizures can trigger DBS to interrupt seizure progression (Thomas and Jobst, 2015; Razavi et al., 2020). Furthermore, studies indicate that phase-aligned stimulation triggered by local field potentials can alter pathological cortical-striatal-pallidal activity and cortico-amygdalar coherence, reducing symptoms of obsessive-compulsive disorder (OCD) (Olsen et al., 2020) and anxiety (Lo et al., 2020), respectively. Stimulation of the ventrolateral (VL) thalamus aligned to patients' limb tremor reduces tremor severity in essential tremor patients through a mechanism involving STDP (Cagnan et al., 2017). Thus, initial exploration of closed-loop stimulation as a mechanism to achieve targeted neuroplasticity promises to be a versatile tool in the treatment of neurologic disease and injury. As such, an expanded investigation of targeted neuroplasticity that incorporates biofeedback measurements may expand this powerful technique into a readily translatable clinical treatment.

Insights from non-invasive neuromodulation and basic neuroscience may inform novel invasive targeted neuroplasticity approaches

Non-invasive neuromodulation therapies such as TMS or focused ultrasound have embraced the targeted neuroplasticity philosophy out of necessity. The immobile nature of non-invasive systems, frequently due to large size and cost of the necessary hardware (Horvath et al., 2010; Anderson et al., 2012; Santarnecchi et al., 2018; Carmi et al., 2019; Mehta et al., 2019; Sabbagh et al., 2020), has necessitated the development of stimulation protocols designed to induce long-term plastic changes in brain function. Consequently, numerous non-invasive stimulation protocols have been designed to facilitate long-term changes in neuroplasticity (Todd et al., 2010; Bunday and Perez, 2012; Jacobs et al., 2012; Urbin et al., 2017; Aftanas et al., 2018; Kozyrev et al., 2018). Despite being limited to engaging cortical targets at a poor spatial specificity on the order of 1,000 mm^2 (van de Ruit and Grey, 2016), TMS has succeeded where more precise invasive approaches such as DBS have failed (e.g., treatment-resistant major depressive disorder). It is thus surprising that few studies are seeking to translate FDA-approved non-invasive plasticity-inducing stimulation protocols to invasive techniques such as DBS, which offer a more selective target engagement and, therefore, fewer side effects (Ni et al., 2019).

Adapting classical neuroplasticity induction protocols rooted in basic neuroscience may form the foundation for novel therapies for treatment-resistant clinical indications. An example where DBS has produced less-than-satisfactory results is in the treatment of Alzheimer's disease. A randomized, sham-controlled, double-blinded clinical trial of patients with Alzheimer's disease found

continuous high frequency (130 Hz) DBS of the fornix, a brain region implicated in learning and memory (Douet and Chang, 2015), does not improve cognitive function (Lozano et al., 2016). Theta burst microstimulation (5 pulses separated by 200 ms, 100 Hz) is a well-described plasticity induction protocol established *ex vivo* to cause LTP in neural circuits (Abrahamsson et al., 2016). Theta burst stimulation of the right entorhinal cortex significantly increased performance on pattern separation and memory recall, suggesting utility for the treatment of Alzheimer's disease (Titiz et al., 2017). Moreover, intermittent theta-burst stimulation results in safe and reliable changes in dorsolateral prefrontal cortex electrophysiology (Bentley et al., 2020) and may improve treatment of neurological conditions with historically poor success rates. Emerging optogenetics-inspired DBS protocols consisting of 1 Hz electrical stimulation of the Nucleus Accumbens paired with a D1-Dopamine receptor antagonist reverse behavioral adaptations in a rodent model of addiction (Creed et al., 2015). Similarly, brief bursts of electrical stimulation in the external Globus Pallidus enables control of distinct neuronal subpopulations and produces long-lasting therapeutic benefits in dopamine depleted mice (Spix et al., 2021). Taken together, targeted neuroplasticity induction protocols should be considered as an alternative to high-frequency stimulation to treat neurological conditions in which disease symptomology is predicated on maladaptive neuroplasticity.

Discussion

A strong feature of traditional DBS is its reversibility, which led it to become a favorable alternative to lesioning procedures for treatment of neurologic and psychiatric disorders (Pugh, 2019). While targeted plasticity can be viewed as a shift away from a reversible surgical procedure, it must be noted that traditional DBS, such as STN DBS also causes changes in plasticity (Herrington et al., 2015; Melon et al., 2015; Chassain et al., 2016). However, high-frequency STN DBS does not create long-lasting neuroplastic changes that may support symptom reduction after cessation of stimulation, supporting the reversibility of DBS therapies (Pugh, 2019).

Interventions that provide long-term changes in targeted neuroplasticity through spatiotemporally patterned stimulation offer distinct advantages over traditional high-frequency invasive neuromodulation, chiefly the ability to manipulate underlying disease pathophysiology, persistent symptom improvement after stimulation cessation, reduced power consumption from lower stimulation frequencies, amplitudes, and duty cycles, and improved circuit specificity that minimizes off-target effects. Thus, targeted neuroplasticity approaches may enable expanded avenues for treatment of disorders associated with maladaptive plasticity, such as Tourette's syndrome (Nespoli et al., 2018), OCD (Kreitzer and Malenka, 2008; Maia et al., 2008), Schizophrenia (McCutcheon et al., 2019), PD (Shen et al., 2008; Kravitz et al., 2010; Parker et al., 2018), and Manic Depression (Lee et al., 2018).

Despite the advantages of leveraging targeted neuroplasticity in spatiotemporally patterned invasive neuromodulation therapies, there remain numerous barriers to clinical implementation. When considering the need for multi-nodal circuit control, it is paramount to consider that additional hardware may incur additional surgical risks (Chiong et al., 2018). However, multi-lead DBS procedures are safe and routinely performed (Dallapiazza et al., 2019). Non-invasive options such as TMS can be paired with invasive stimulation to decrease surgical risk of additional implants while enabling additional therapeutic approaches.

There remains a real risk that preclinical findings do not translate between species, particularly to humans (de Oliveira et al., 2021). Consequently, caution must be taken when applying plasticity induction protocols clinically. While application of any novel stimulation paradigm comes with risk, a reasonable starting point for translating a novel neuroplasticity induction protocol to humans is to test plasticity induction protocols in individuals with existing implanted pulse generators, particularly if the system is capable of electrophysiological monitoring. An example of this strategy is evident in the previously mentioned multi-modal approach, where TMS pulses were paired with electrical stimulation of previously indwelling STN DBS electrodes (Udupa et al., 2016). Testing plasticity protocols in such a manner enables feasibility testing in humans without risks inherent in *de novo* surgical procedures.

Considering the advantages of invasive over non-invasive neuromodulation approaches, we must ask the question, "Why is it that targeted neuroplasticity-inducing protocols such as those used by non-invasive therapies are not widely used invasive neuromodulation therapies?" Perhaps the immediately effective therapeutic benefits of invasive neuromodulation approaches unnecessarily constrain parameter selection. Rather than treat stimulation-induced synaptic plasticity as an obstacle that interferes with long-term efficacy of traditional high-frequency stimulation, stimulation-induced neuroplasticity should be considered as a therapeutic mechanism. This mechanism may be sensitive to numerous parameters, including the type of underlying synaptic plasticity, synaptic transmission delays, the spatiotemporal stimulation pattern, the stimuli shape, and stimulation context. Borrowing inspiration from the protocols of non-invasive neuromodulation like TMS, vibrotactile CR, and basic neuroscience may help improve the clinical outcomes of DBS by creating lasting symptom benefit while broadening the clinical indications that can be treated with invasive therapies.

Clinical invasive neuromodulation approaches have remained largely unchanged since their inception. For example, high-frequency DBS is still the gold standard for treating medically refractory movement disorders. However, neuromodulation is limited in its ability to relieve disease symptoms after stimulation cessation. Re-designing stimulation protocols to address the underlying pathophysiology of disease circuitopathies may improve the current treatment of disorders and expand clinical applications. Integrating this approach into stimulation protocols may require control of complex networks through input at multiple nodes, long-lasting desynchronization of pathologically coherent network activity for long-lasting symptom reduction, and insight from non-invasive neuromodulation and basic neuroscience. Thus, targeted neuroplasticity may pave new paths

in neuromodulation, expanding indications and improving disease pathophysiology.

Author contributions

AA and JL conceived of the idea. YC and AA wrote the manuscript. AA, YC, and SH prepared figures. All authors discussed the results and contributed to the final manuscript.

Acknowledgments

We would like to thank Megan L. Gill, P.T., D.P.T. for reviewing and providing feedback on the manuscript.

Conflict of interest

The authors declare that the research was conducted in the absence of any commercial or financial relationships that could be construed as a potential conflict of interest.

Publisher's note

All claims expressed in this article are solely those of the authors and do not necessarily represent those of their affiliated organizations, or those of the publisher, the editors and the reviewers. Any product that may be evaluated in this article, or claim that may be made by its manufacturer, is not guaranteed or endorsed by the publisher.

References

Abrahamsson, T., Lalanne, T., Watt, A. J., and Sjöström, P. J. (2016). Long-term potentiation by theta-burst stimulation using extracellular field potential recordings in acute hippocampal slices. *Cold Spring Harb. Protoc.* 2016, pdb.prot091298. doi: 10.1101/pdb.prot091298

Adamchic, I., Hauptmann, C., Barnikol, U. B., Pawelczyk, N., Popovych, O., Barnikol, T. T., et al. (2014). Coordinated reset neuromodulation for Parkinson's disease: proof-of-concept study. *Mov. Disord. Off. J. Mov. Disord. Soc.* 29, 1679–1684. doi: 10.1002/mds.25923

Adamchic, I., Toth, T., Hauptmann, C., Walger, M., Langguth, B., Klingmann, I., et al. (2017). Acute effects and after-effects of acoustic coordinated reset neuromodulation in patients with chronic subjective tinnitus. *NeuroImage Clin.* 15, 541–558. doi: 10.1016/j.nicl.2017.05.017

Aftanas, L. I., Gevorgyan, M. M., Zhanaeva, S. Y., Dzemidovich, S. S., Kulikova, K. I., and Al'perina, E. L., et al. (2018). Therapeutic effects of repetitive transcranial magnetic stimulation (rTMS) on neuroinflammation and neuroplasticity in patients with parkinson's disease: a placebo-controlled study. *Bull. Exp. Biol. Med.* 165, 195–199. doi: 10.1007/s10517-018-4128-4

Anderson, R. J., Frye, M. A., Abulseoud, O. A., Lee, K. H., McGillivray, J. A., Berk, M., et al. (2012). Deep brain stimulation for treatment-resistant depression: efficacy, safety and mechanisms of action. *Neurosci. Biobehav. Rev.* 36, 1920–1933. doi: 10.1016/j.neubiorev.2012.06.001

Ashkan, K., Rogers, P., Bergman, H., and Ughratdar, I. (2017). Insights into the mechanisms of deep brain stimulation. *Nat. Rev. Neurol.* 13, 548–554. doi: 10.1038/nrneurol.2017.105

Asl, M. M., Valizadeh, A., and Tass, P. A. (2023). Decoupling of interacting neuronal populations by time-shifted stimulation through spike-timing-dependent plasticity. *PLoS Comput. Biol.* 19, e1010853. doi: 10.1371/journal.pcbi.1010853

Barow, E., Neumann, W.-., J., Brücke, C., Huebl, J., Horn, A., et al. (2014). Deep brain stimulation suppresses pallidal low frequency activity in patients with phasic dystonic movements. *Brain J. Neurol.* 137, 3012–3024. doi: 10.1093/brain/awu258

Bentley, J. N., Irwin, Z. T., Black, S. D., Roach, M. L., Vaden, R. J., Gonzalez, C. L., et al. (2020). Subcortical intermittent theta-burst stimulation (iTBS) increases theta-power in dorsolateral prefrontal cortex (DLPFC). *Front. Neurosci.* 14, 1–10. doi: 10.3389/fnins.2020.00041

Bi, G., and Poo, M. (1998). Synaptic modifications in cultured hippocampal neurons: dependence on spike timing, synaptic strength, and postsynaptic cell type. *J. Neurosci.* 18, 10464–10472. doi: 10.1523/JNEUROSCI.18-24-10464.1998

Bonizzato, M., James, N. D., Pidpruzhnykova, G., Pavlova, N., Shkorbatova, P., Baud, L., et al. (2021). Multi-pronged neuromodulation intervention engages the residual motor circuitry to facilitate walking in a rat model of spinal cord injury. *Nat. Commun.* 12, 1925. doi: 10.1038/s41467-021-22137-9

Brzosko, Z., Mierau, S. B., and Paulsen, O. (2019). Neuromodulation of spike-timing-dependent plasticity: past, present, and future. *Neuron.* 103, 563–581. doi: 10.1016/j.neuron.2019.05.041

Bunday, K. L., and Perez, M. A. (2012). Motor recovery after spinal cord injury enhanced by strengthening corticospinal synaptic transmission. *Curr. Biol.* 22, 2355–2361. doi: 10.1016/j.cub.2012.10.046

Cagnan, H., Pedrosa, D., Little, S., Pogosyan, A., Cheeran, B., Aziz, T., et al. (2017). Stimulating at the right time: phase-specific deep brain stimulation. *Brain.* 140, 132–145. doi: 10.1093/brain/aww286

Caporale, N., and Dan, Y. (2008). Spike timing-dependent plasticity: a Hebbian learning rule. *Annu. Rev. Neurosci.* 31, 25–46. doi: 10.1146/annurev.neuro.31.060407.125639

Capotosto, P., Babiloni, C., Romani, G. L., and Corbetta, M. (2014). Resting-state modulation of α rhythms by interference with angular gyrus activity. *J. Cogn. Neurosci.* 26, 107–119. doi: 10.1162/jocn_a_00460

Carmi, L., Tendler, A., Bystritsky, A., Hollander, E., Blumberger, D. M., Daskalakis, J., et al. (2019). Efficacy and safety of deep transcranial magnetic stimulation for obsessive-compulsive disorder: a prospective multicenter randomized double-blind placebo-controlled trial. *Am. J. Psychiatry.* 176, 931–938. doi: 10.1176/appi.ajp.2019.18101180

Chassain, C., Melon, C., Salin, P., Vitale, F., Couraud, S., Durif, F., et al. (2016). Metabolic, synaptic and behavioral impact of 5-week chronic deep brain stimulation in hemiparkinsonian rats. *J. Neurochem.* 136, 1004–1016. doi: 10.1111/jnc.13438

Chiong, W., Leonard, M. K., and Chang, E. F. (2018). Neurosurgical patients as human research subjects: ethical considerations in intracranial electrophysiology research. *Neurosurgery.* 83, 29–37. doi: 10.1093/neuros/nyx361

Cosentino, G., Fierro, B., Paladino, P., Talamanca, S., Vigneri, S., Palermo, A., et al. (2012). Transcranial direct current stimulation preconditioning modulates the effect of high-frequency repetitive transcranial magnetic stimulation in the human motor cortex. *Eur. J. Neurosci.* 35, 119–124. doi: 10.1111/j.1460-9568.2011.07939.x

Creed, M., Pascoli, V. J., and Lüscher, C. (2015). Refining deep brain stimulation to emulate optogenetic treatment of synaptic pathology. *Science.* 347, 659–664. doi: 10.1126/science.1260776

Dallapiazza, R. F., Lee, D. J., De Vloo, P., Fomenko, A., Hamani, C., Hodaie, M., et al. (2019). Outcomes from stereotactic surgery for essential tremor. *J. Neurol. Neurosurg. Psychiatry.* 90, 474–482. doi: 10.1136/jnnp-2018-318240

Dan, Y., and Poo, M. (2004). Spike timing-dependent plasticity of neural circuits. *Neuron.* 44, 23–30. doi: 10.1016/j.neuron.2004.09.007

de Oliveira, A. R., Reimer, A. E., Simandl, G. J., Nagrale, S. S., and Widge, A. S. (2021). Lost in translation: no effect of repeated optogenetic cortico-striatal stimulation on compulsivity in rats. *Transl. Psychiatry.* 11, 315. doi: 10.1038/s41398-021-01448-x

Douet, V., and Chang, L. (2015). Fornix as an imaging marker for episodic memory deficits in healthy aging and in various neurological disorders. *Front. Aging Neurosci.* 6, 1–19. doi: 10.3389/fnagi.2014.00343

Ducharme, S., Flaherty, A. W., Seiner, S. J., Dougherty, D. D., and Morales, O. G. (2011). Temporary interruption of deep brain stimulation for parkinson's disease during outpatient electroconvulsive therapy for major depression: a novel treatment strategy. *J. Neuropsychiatry Clin. Neurosci.* 23, 194–197. doi: 10.1176/jnp.23.2.jnp194

Duman, R. S. (2002). Synaptic plasticity and mood disorders. *Mol. Psychiatry.* 7, S29–S34. doi: 10.1038/sj.mp.4001016

Duman, R. S., Aghajanian, G. K., Sanacora, G., and Krystal, J. H. (2016). Synaptic plasticity and depression: new insights from stress and rapid-acting antidepressants. *Nat. Med.* 22, 238–249. doi: 10.1038/nm.4050

Ebert, M., Hauptmann, C., and Tass, P. A. (2014). Coordinated reset stimulation in a large-scale model of the STN-GPe circuit. *Front. Comput. Neurosci.* 8, 154. doi: 10.3389/fncom.2014.00154

Engineer, N. D., Riley, J. R., Seale, J. D., Vrana, W. A., Shetake, J. A., Sudanagunta, S. P., et al. (2011). Reversing pathological neural activity using targeted plasticity. *Nature.* 470, 101–104. doi: 10.1038/nature09656

Famitafreshi, H., and Karimian, M. (2019). Neuroplasticity-targeted therapy alleviates severe addiction. 9, 2436–2443. Available online at: https://www.jneuropsychiatry.org/peer-review/neuroplasticitytargeted-therapy-alleviates-severe-addiction-13112.html

Ferraye, M. U., Debû, B., Fraix, V., Xie-Brustolin, J., Chabardès, S., Krack, P., et al. (2008). Effects of subthalamic nucleus stimulation and levodopa on freezing of gait in Parkinson disease. *Neurology.* 70, 1431–1437. doi: 10.1212/01.wnl.0000310416.90757.85

Fox, M. D., Buckner, R. L., Liu, H., Chakravarty, M. M., Lozano, A. M., Pascual-Leone, A., et al. (2014). Resting-state networks link invasive and noninvasive brain stimulation across diverse psychiatric and neurological diseases. *Proc. Natl. Acad. Sci. U S A.* 111, E4367–4375. doi: 10.1073/pnas.1405003111

Gu, S., Pasqualetti, F., Cieslak, M., Telesford, Q. K., Yu, A. B., Kahn, A. E., et al. (2015). Controllability of structural brain networks. *Nat. Commun.* 6, 8414. doi: 10.1038/ncomms9414

Guerra, A., Suppa, A., Bologna, M., D'Onofrio, V., Bianchini, E., Brown, P., et al. (2018). Boosting the LTP-like plasticity effect of intermittent theta-burst stimulation using gamma transcranial alternating current stimulation. *Brain Stimulat.* 11, 734–742. doi: 10.1016/j.brs.2018.03.015

Herrington, T. M., Cheng, J. J., and Eskandar, E. N. (2015). Mechanisms of deep brain stimulation. *J. Neurophysiol.* 115, 19–38. doi: 10.1152/jn.00281.2015

Ho, A. L., Feng, A. Y., Barbosa, D. A., Wu, H., Smith, M. L., Malenka, R. C., et al. (2021). Accumbens coordinated reset stimulation in mice exhibits ameliorating aftereffects on binge alcohol drinking. *Brain Stimulat.* 14, 330–334. doi: 10.1016/j.brs.2021.01.015

Horvath, J., Mathews, J., Demitrack, M., and Pascual-Leone, A. (2010). The neurostar TMS device: conducting the FDA approved protocol for treatment of depression. *J. Vis. Exp. JoVE.* 54, e2354. doi: 10.3791/2345

Hristova, A., Lyons, K., Tröster, A. I., Pahwa, R., Wilkinson, S. B., Koller, W. C., et al. (2000). Effect and time course of deep brain stimulation of the globus pallidus and subthalamus on motor features of parkinson's disease. *Clin. Neuropharmacol.* 23, 208–211. doi: 10.1097/00002826-200007000-00007

Jacobs, M., Premji, A., and Nelson, A. J. (2012). Plasticity-inducing TMS protocols to investigate somatosensory control of hand function. *Neural Plast.* 2012, 350574. doi: 10.1155/2012/350574

Kakusa, B., Saluja, S., Tate, W. J., Espil, F. M., Halpern, C. H., Williams, N. R., et al. (2019). Robust clinical benefit of multi-target deep brain stimulation for treatment of Gilles de la Tourette syndrome and its comorbidities. *Brain Stimul. Basic Transl. Clin. Res. Neuromodulation.* 12, 816–818. doi: 10.1016/j.brs.2019.02.026

Kalivas, P. W., and O'Brien, C. (2008). Drug addiction as a pathology of staged neuroplasticity. *Neuropsychopharmacology.* 33, 166–180. doi: 10.1038/sj.npp.1301564

Kauer, J. A., and Malenka, R. C. (2007). Synaptic plasticity and addiction. *Nat. Rev. Neurosci.* 8, 844–858. doi: 10.1038/nrn2234

Kozyrev, V., Staadt, R., Eysel, U. T., and Jancke, D. (2018). TMS-induced neuronal plasticity enables targeted remodeling of visual cortical maps. *Proc. Natl. Acad. Sci. U S A.* 115, 6476–6481. doi: 10.1073/pnas.1802798115

Kravitz, A. V., Freeze, B. S., Parker, P. R. L., Kay, K., Thwin, M. T., Deisseroth, K., et al. (2010). Regulation of parkinsonian motor behaviours by optogenetic control of basal ganglia circuitry. *Nature.* 466, 622–626. doi: 10.1038/nature09159

Kreitzer, A. C., and Malenka, R. C. (2008). Striatal plasticity and basal ganglia circuit function. *Neuron.* 60, 543–554. doi: 10.1016/j.neuron.2008.11.005

Kromer, J. A., and Tass, P. A. (2020). Long-lasting desynchronization by decoupling stimulation. *Phys. Rev. Res.* 2, 033101. doi: 10.1103/PhysRevResearch.2.033101

Kromer, J. A., and Tass, P. A. (2022). Synaptic reshaping of plastic neuronal networks by periodic multichannel stimulation with single-pulse and burst stimuli. *PLoS Comput. Biol.* 18, e1010568. doi: 10.1371/journal.pcbi.1010568

Kühn, A. A., Tsui, A., Aziz, T., Ray, N., Brücke, C., Kupsch, A., et al. (2009). Pathological synchronisation in the subthalamic nucleus of patients with Parkinson's disease relates to both bradykinesia and rigidity. *Exp. Neurol.* 215, 380–387. doi: 10.1016/j.expneurol.2008.11.008

Kuner, R., and Flor, H. (2017). Structural plasticity and reorganisation in chronic pain. *Nat. Rev. Neurosci.* 18, 20–30. doi: 10.1038/nrn.2016.162

Lafleur, L-., P., Tremblay, S., Whittingstall, K., and Lepage, J-., F. (2016). Assessment of effective connectivity and plasticity with dual-coil transcranial magnetic stimulation. *Brain Stimulat.* 9, 347–355. doi: 10.1016/j.brs.2016.02.010

Lee, Y., Zhang, Y., Kim, S., and Han, K. (2018). Excitatory and inhibitory synaptic dysfunction in mania: an emerging hypothesis from animal model studies. *Exp. Mol. Med.* 50, 1–11. doi: 10.1038/s12276-018-0187-x

Li, J., Mei, S., Zhang, X., Wang, Y., Jia, X., Liu, J., et al. (2022). Case report: combined therapy of bilateral subthalamic nucleus deep brain stimulation and spinal cord stimulation significantly improves motor function in a patient with multiple system atrophy with predominant parkinsonism. *Front. Neurosci.* 16, 929273. doi: 10.3389/fnins.2022.929273

Li, S. (2017). Spasticity motor recovery, and neural plasticity after stroke. *Front. Neurol.* 8, 120. doi: 10.3389/fneur.2017.00120

Limousin, P., and Foltynie, T. (2019). Long-term outcomes of deep brain stimulation in Parkinson disease. *Nat. Rev. Neurol.* 15, 234–242. doi: 10.1038/s41582-019-0145-9

Lo, M-., C., Younk, R., and Widge, A. S. (2020). Paired electrical pulse trains for controlling connectivity in emotion-related brain circuitry. *IEEE Trans. Neural. Syst. Rehabil. Eng.* 28, 2721–2730. doi: 10.1109/TNSRE.2020.3030714

Lozano, A. M., Fosdick, L., Chakravarty, M. M., Leoutsakos, J. M., Munro, C., Oh, E., et al. (2016). A phase II study of fornix deep brain stimulation in mild Alzheimer's disease. *J. Alzheimers Dis.* 54, 777–787. doi: 10.3233/JAD-160017

Madadi Asl, M., Vahabie, A-., H., Valizadeh, A., and Tass, P. A. (2022). Spike-timing-dependent plasticity mediated by dopamine and its role in parkinson's disease pathophysiology. *Front. Netw. Physiol.* 2, 1–18. doi: 10.3389/fnetp.2022.817524

Madadi Asl, M., Valizadeh, A., and Tass, P. A. (2018). Dendritic and axonal propagation delays may shape neuronal networks with plastic synapses. *Front. Physiol.* 9, 1849. doi: 10.3389/fphys.2018.01849

Maia, T. V., Cooney, R. E., and Peterson, B. S. (2008). The neural bases of obsessive-compulsive disorder in children and adults. *Dev. Psychopathol.* 20, 1251–1283. doi: 10.1017/S0954579408000606

Markram, H., Lübke, J., Frotscher, M., and Sakmann, B. (1997). Regulation of synaptic efficacy by coincidence of postsynaptic APs and EPSPs. *Science.* 275, 213–215. doi: 10.1126/science.275.5297.213

McCutcheon, R. A., Abi-Dargham, A., and Howes, O. D. (2019). Schizophrenia, dopamine and the striatum: from biology to symptoms. *Trends Neurosci.* 42, 205–220. doi: 10.1016/j.tins.2018.12.004

McPherson, J. G., Miller, R. R., and Perlmutter, S. I. (2015). Targeted, activity-dependent spinal stimulation produces long-lasting motor recovery in chronic cervical spinal cord injury. *Proc. Natl. Acad. Sci. U S A.* 112, 12193–12198. doi: 10.1073/pnas.1505383112

Mehta, U. M., Thanki, M. V., Padmanabhan, J., Pascual-Leone, A., and Keshavan, M. S. (2019). Motor cortical plasticity in schizophrenia: a meta-analysis of transcranial magnetic stimulation-electromyography studies. *Schizophr. Res.* 207, 37–47. doi: 10.1016/j.schres.2018.10.027

Melon, C., Chassain, C., Bielicki, G., Renou, J.-., P., Goff, L., et al. (2015). Progressive brain metabolic changes under deep brain stimulation of subthalamic nucleus in parkinsonian rats. *J. Neurochem.* 132, 703–712. doi: 10.1111/jnc.13015

Nakazono, H., Ogata, K., Takeda, A., Yamada, E., Oka, S., Tobimatsu, S., et al. (2021). A specific phase of transcranial alternating current stimulation at the β frequency boosts repetitive paired-pulse TMS-induced plasticity. *Sci. Rep.* 11, 13179. doi: 10.1038/s41598-021-92768-x

Nespoli, E., Rizzo, F., Boeckers, T., Schulze, U., and Hengerer, B. (2018). Altered dopaminergic regulation of the dorsal striatum is able to induce tic-like movements in juvenile rats. *PLoS ONE.* 13, e0196515. doi: 10.1371/journal.pone.0196515

Ni, Z., Udupa, K., Hallett, M., and Chen, R. (2019). Effects of deep brain stimulation on the primary motor cortex: insights from transcranial magnetic stimulation studies. *Clin. Neurophysiol. Off. J. Int Fed. Clin. Neurophysiol.* 130, 558–567. doi: 10.1016/j.clinph.2018.10.020

Olsen, S. T., Basu, I., Bilge, M. T., Kanabar, A., Boggess, M. J., Rockhill, A. P., et al. (2020). Case report of dual-site neurostimulation and chronic recording of cortico-striatal circuitry in a patient with treatment refractory obsessive compulsive disorder. *Front. Hum. Neurosci.* 14, 1–22. doi: 10.3389/fnhum.2020.569973

Palop, J., Chin, J., and Mucke, L. A. (2006). Network dysfunction perspective on neurodegenerative diseases. *Nature.* 443, 768–773. doi: 10.1038/nature05289

Parker, J. G., Marshall, J. D., Ahanonu, B., Wu, Y.-., W., Kim, T. H., et al. (2018). Diametric neural ensemble dynamics in parkinsonian and dyskinetic states. *Nature.* 557, 177–182. doi: 10.1038/s41586-018-0090-6

Pasqualetti, F., Zampieri, S., and Bullo, F. (2014). "Controllability metrics, limitations and algorithms for complex networks." In: *2014 American Control Conference,* 3287–3292. doi: 10.1109/ACC.2014.6858621

Peng, X., Hickman, J. L., Bowles, S. G., Donegan, D. C., and Welle, C. G. (2018). Innovations in electrical stimulation harness neural plasticity to restore motor function. *Bioelectron. Med.* 1, 251–263. doi: 10.2217/bem-2019-0002

Pfeifer, K. J., Kromer, J. A., Cook, A. J., Hornbeck, T., Lim, E. A., Mortimer, B. J. P., et al. (2021). Coordinated reset vibrotactile stimulation induces sustained cumulative benefits in parkinson's disease. *Front. Physiol.* 12, 624317. doi: 10.3389/fphys.2021.624317

Pfister, J.-., P., and Tass, P. A. (2010). STDP in oscillatory recurrent networks: theoretical conditions for desynchronization and applications to deep brain stimulation. *Front. Comput. Neurosci.* 4, 1–10. doi: 10.3389/fncom.2010.00022

Pugh, J. (2019). No going back? reversibility and why it matters for deep brain stimulation. *J. Med. Ethics.* 45, 225. doi: 10.1136/medethics-2018-105139

Razavi, B., Rao, V. R., Lin, C., Bujarski, K. A., Patra, S. E., Burdette, D. E., et al. (2020). Real-world experience with direct brain-responsive neurostimulation for focal onset seizures. *Epilepsia.* 61, 1749–1757. doi: 10.1111/epi.16593

Rosin, B., Nevet, A., Elias, S., Rivlin-Etzion, M., Israel, Z., Bergman, H., et al. (2007). Physiology and pathophysiology of the basal ganglia-thalamo-cortical networks. *Parkinsonism Relat. Disord.* 13(Suppl 3), S437–439. doi: 10.1016/S1353-8020(08)70045-2

Sabbagh, M., Sadowsky, C., Tousi, B., Agronin, M. E., Alva, G., Armon, C., et al. (2020). Effects of a combined transcranial magnetic stimulation (TMS) and cognitive training intervention in patients with Alzheimer's disease. *Alzheimers Dement.* 16, 641–650. doi: 10.1016/j.jalz.2019.08.197

Santarnecchi, E., Momi, D., Sprugnoli, G., Neri, F., Pascual-Leone, A., Rossi, A., et al. (2018). Modulation of network-to-network connectivity *via* spike-timing-dependent noninvasive brain stimulation. *Hum. Brain. Mapp.* 39, 4870–4883. doi: 10.1002/hbm.24329

Seeman, S. C., Mogen, B. J., Fetz, E. E., and Perlmutter, S. I. (2017). Paired stimulation for spike-timing-dependent plasticity in primate sensorimotor cortex. *J. Neurosci.* 37, 1935–1949. doi: 10.1523/JNEUROSCI.2046-16.2017

Seitz, A. R. (2013). Cognitive neuroscience: targeting neuroplasticity with neural decoding and biofeedback. *Curr. Biol.* 23, R210–R212. doi: 10.1016/j.cub.2013.01.015

Shen, W., Flajolet, M., Greengard, P., and Surmeier, D. J. (2008). Dichotomous dopaminergic control of striatal synaptic plasticity. *Science.* 321, 848–851. doi: 10.1126/science.1160575

Spencer, S. S. (2002). Neural networks in human epilepsy: evidence of and implications for treatment. *Epilepsia.* 43, 219–227. doi: 10.1046/j.1528-1157.2002.26901.x

Spix, T. A., Nanivadekar, S., Toong, N., Kaplow, I. M., Isett, B. R., Goksen, Y., et al. (2021). Population-specific neuromodulation prolongs therapeutic benefits of deep brain stimulation. *Science.* 374, 201–206. doi: 10.1126/science.abi7852

Syrkin-Nikolau, J., Neuville, R., O'Day, J., Anidi, C., Koop, M. M., Martin, T., et al. (2018). Coordinated reset vibrotactile stimulation shows prolonged improvement in Parkinson's disease. *Mov. Disord. Off. J. Mov. Disord. Soc.* 33, 179–180. doi: 10.1002/mds.27223

Tass, P. A. (2003). A model of desynchronizing deep brain stimulation with a demand-controlled coordinated reset of neural subpopulations. *Biol. Cybern.* 89, 81–88. doi: 10.1007/s00422-003-0425-7

Tass, P. A., and Majtanik, M. (2006). Long-term anti-kindling effects of desynchronizing brain stimulation: a theoretical study. *Biol. Cybern.* 94, 58–66. doi: 10.1007/s00422-005-0028-6

Tass, P. A., Qin, L., Hauptmann, C., Dovero, S., Bezard, E., Boraud, T., et al. (2012). Coordinated reset has sustained aftereffects in Parkinsonian monkeys. *Ann. Neurol.* 72, 816–820. doi: 10.1002/ana.23663

Temperli, P., Ghika, J., Villemure, J-., G., Burkhard, P. R., Bogousslavsky, J., et al. (2003). How do parkinsonian signs return after discontinuation of subthalamic DBS? *Neurology.* 60, 78–81. doi: 10.1212/WNL.60.1.78

Thomas, G. P., and Jobst, B. C. (2015). Critical review of the responsive neurostimulator system for epilepsy. *Med. Devices Auckl. NZ.* 8, 405–411. doi: 10.2147/MDER.S62853

Thompson, J. A., Lanctin, D., Ince, N. F., and Abosch, A. (2014). Clinical implications of local field potentials for understanding and treating movement disorders. *Stereotact. Funct. Neurosurg.* 92, 251–263. doi: 10.1159/000364913

Titiz, A. S., Hill, M. R. H., Mankin, E. A., Aghajan, Z. M., Tchemodanov, N., Maoz, U., et al. (2017). Theta-burst microstimulation in the human entorhinal area improves memory specificity. *eLife.* 6, 1–18. doi: 10.7554/eLife.29515

Todd, G., Kimber, T. E., Ridding, M. C., and Semmler, J. G. (2010). Reduced motor cortex plasticity following inhibitory rTMS in older adults. *Clin. Neurophysiol. Off. J. Int. Fed. Clin. Neurophysiol.* 121, 441–447. doi: 10.1016/j.clinph.2009.11.089

Tu, C., Rocha, R. P., Corbetta, M., Zampieri, S., Zorzi, M., Suweis, S., et al. (2018). Warnings and caveats in brain controllability. *NeuroImage.* 176, 83–91. doi: 10.1016/j.neuroimage.2018.04.010

Udupa, K., Bahl, N., Ni, Z., Gunraj, C., Mazzella, F., Moro, E., et al. (2016). Cortical plasticity induction by pairing subthalamic nucleus deep-brain stimulation and primary motor cortical transcranial magnetic stimulation in parkinson's disease. *J. Neurosci.* 36, 396–404. doi: 10.1523/JNEUROSCI.2499-15.2016

Urbin, M. A., Ozdemir, R. A., Tazoe, T., and Perez, M. A. (2017). Spike-timing-dependent plasticity in lower-limb motoneurons after human spinal cord injury. *J. Neurophysiol.* 118, 2171–2180. doi: 10.1152/jn.00111.2017

Valero-Cabré, A., Amengual, J. L., Stengel, C., Pascual-Leone, A., and Coubard, O. A. (2017). Transcranial magnetic stimulation in basic and clinical neuroscience: a comprehensive review of fundamental principles and novel insights. *Neurosci. Biobehav. Rev.* 83, 381–404. doi: 10.1016/j.neubiorev.2017.10.006

van de Ruit, M., and Grey, M. J. (2016). The TMS map scales with increased stimulation intensity and muscle activation. *Brain Topogr.* 29, 56–66. doi: 10.1007/s10548-015-0447-1

Versace, V., Langthaler, P. B., Höller, Y., Frey, V. N., Brigo, F., Sebastianelli, L., et al. (2018). Abnormal cortical neuroplasticity induced by paired associative stimulation after traumatic spinal cord injury: a preliminary study. *Neurosci. Lett.* 664, 167–171. doi: 10.1016/j.neulet.2017.11.003

Visser-Vandewalle, V., Andrade, P., Mosley, P. E., Greenberg, B. D., Schuurman, R., McLaughlin, N. C., et al. (2022). Deep brain stimulation for obsessive–compulsive disorder: a crisis of access. *Nat. Med.* 28, 1529–1532. doi: 10.1038/s41591-022-01879-z

Wang, J., Fergus, S. P., Johnson, L. A., Nebeck, S. D., Zhang, J., Kulkarni, S., et al. Shuffling improves the acute and carryover effect of subthalamic coordinated reset deep brain stimulation. *Front. Neurol.* (2022) 13, 716046. doi: 10.3389/fneur.2022.716046

Wang, J., Nebeck, S., Muralidharan, A., Johnson, M. D., Vitek, J. L., Baker, K. B., et al. (2016). Coordinated reset deep brain stimulation of subthalamic nucleus produces long-lasting, dose-dependent motor improvements in the 1-Methyl-4-phenyl-1,2,3,6-tetrahydropyridine non-human primate model of parkinsonism. *Brain Stimulat.* 9, 609–617. doi: 10.1016/j.brs.2016.03.014

Weinberger, M., Hutchison, W. D., Alavi, M., Hodaie, M., Lozano, A. M., Moro, E., et al. (2012). Oscillatory activity in the globus pallidus internus: comparison between Parkinson's disease and dystonia. *Clin. Neurophysiol.* 123, 358–368. doi: 10.1016/j.clinph.2011.07.029

Xie, T., Kang, U. J., and Warnke, P. (2012). Effect of stimulation frequency on immediate freezing of gait in newly activated STN DBS in Parkinson's disease. *J. Neurol. Neurosurg. Psychiatry.* 83, 1015–1017. doi: 10.1136/jnnp-2011-302091

frontiers | Frontiers in Neuroinformatics

TYPE Review
PUBLISHED 24 May 2023
DOI 10.3389/fninf.2023.1173597

OPEN ACCESS

EDITED BY
Peter A. Tass,
Stanford University, United States

REVIEWED BY
Justus Alfred Kromer,
Stanford University, United States
Sonya Bahar,
University of Missouri–St. Louis, United States

*CORRESPONDENCE
Vinícius Rosa Cota
✉ vinicius.rosacota@iit.it
Márcio Flávio Dutra Moraes
✉ mfdm@icb.ufmg.br

†These authors have contributed equally to this work

RECEIVED 24 February 2023
ACCEPTED 02 May 2023
PUBLISHED 24 May 2023

CITATION
Cota VR, Cançado SAV and Moraes MFD (2023) On temporal scale-free non-periodic stimulation and its mechanisms as an infinite improbability drive of the brain's functional connectogram.
Front. Neuroinform. 17:1173597.
doi: 10.3389/fninf.2023.1173597

On temporal scale-free non-periodic stimulation and its mechanisms as an infinite improbability drive of the brain's functional connectogram

Vinícius Rosa Cota[1,2*†], Sérgio Augusto Vieira Cançado[3] and Márcio Flávio Dutra Moraes[4*†]

[1]Rehab Technologies - INAIL Lab, Istituto Italiano di Tecnologia, Genoa, Italy, [2]Laboratory of Neuroengineering and Neuroscience, Department of Electrical Engineering, Federal University of São João del-Rei, São João del Rei, Brazil, [3]Núcleo Avançado de Tratamento das Epilepsias (NATE), Felício Rocho Hospital, Fundação Felice Rosso, Belo Horizonte, Brazil, [4]Department of Physiology and Biophysics, Núcleo de Neurociências, Federal University of Minas Gerais, Belo Horizonte, Brazil

Rationalized development of electrical stimulation (ES) therapy is of paramount importance. Not only it will foster new techniques and technologies with increased levels of safety, efficacy, and efficiency, but it will also facilitate the translation from basic research to clinical practice. For such endeavor, design of new technologies must dialogue with state-of-the-art neuroscientific knowledge. By its turn, neuroscience is transitioning—a movement started a couple of decades earlier—into adopting a new conceptual framework for brain architecture, in which time and thus temporal patterns plays a central role in the neuronal representation of sampled data from the world. This article discusses how neuroscience has evolved to understand the importance of brain rhythms in the overall functional architecture of the nervous system and, consequently, that neuromodulation research should embrace this new conceptual framework. Based on such support, we revisit the literature on standard (fixed-frequency pulsatile stimuli) and mostly non-standard patterns of ES to put forward our own rationale on how temporally complex stimulation schemes may impact neuromodulation strategies. We then proceed to present a low frequency, on average (thus low energy), scale-free temporally randomized ES pattern for the treatment of experimental epilepsy, devised by our group and termed NPS (Non-periodic Stimulation). The approach has been shown to have robust anticonvulsant effects in different animal models of acute and chronic seizures (displaying dysfunctional hyperexcitable tissue), while also preserving neural function. In our understanding, accumulated mechanistic evidence suggests such a beneficial mechanism of action may be due to the natural-like characteristic of a scale-free temporal pattern that may robustly compete with aberrant epileptiform activity for the recruitment of neural circuits. Delivering temporally patterned or random stimuli within specific phases of the underlying oscillations (i.e., those involved in the communication within and across brain regions) could both potentiate and disrupt the formation of neuronal assemblies with random probability. The usage of infinite improbability drive here is obviously a reference to the "The Hitchhiker's Guide to the Galaxy" comedy science fiction classic, written by Douglas Adams. The parallel is that dynamically driving brain functional

connectogram, through neuromodulation, in a manner that would not favor any specific neuronal assembly and/or circuit, could re-stabilize a system that is transitioning to fall under the control of a single attractor. We conclude by discussing future avenues of investigation and their potentially disruptive impact on neurotechnology, with a particular interest in NPS implications in neural plasticity, motor rehabilitation, and its potential for clinical translation.

KEYWORDS

electrical stimulation, neuromodulation, coincidence-detection, temporal pattern, power-law, phase coupling, synchronization, neural circuits

1. Introduction

The powerful intuition that electricity applied to the body may bear therapeutic effects in many different ailments is much older than the knowledge of moving electrical charges itself, the potentials created by their separation, and all the related electromagnetic phenomena. Roman physicians prescribed Torpedo Ray Fishes to treat chronic pain and, before them, ancient Greeks used electrically charged amber collars with therapeutic intentions toward all natural and even unnatural afflictions (Gildenberg, 2006). Therefore, as it happens to therapeutic approaches with ancient roots, there was little to no theoretical basis to explain, or even to hypothesize on possible reasons, as to why it actually worked.

Following original insights of early investigators of bioelectrical phenomenal, such as Luigi Galvani and Alessandro Volta, and the development of rudimentary electrical devices (e.g., Leyden Jar and Van de Graaf's generator), an era of wide application of electricity as therapy quickly ensued. At this point, controlled demonstrations of the effects of electricity on biological tissue, both dead or alive (as in Giovanni Aldini's and Guillaume Duchenne's demonstrations), evoked at the will of the experimenter/therapist and observable to the naked eye, left no doubt that it could be used to elicit involuntary and targeted responses in an organism. Here, the early reasoning would state that if in fact, the human body could respond to electricity through some sort of electricity "receptor", there should also be an endogenous electricity generator to account for its existence, a process later termed bioelectrogenesis.

As often occurs after a scientific breakthrough, the rapid changes in paradigm not only spurred charlatanism—particularly during the 19th century—but also inspired notable sound technological and scientific progress. This story was extensively shared with the fields of neurology and neurosurgery, even before they were organized as areas of specific medical activity. Based on animal models and experimentation guided by cases, or even without so much scientific rigor, several physicians acted as electrotherapists. Among them, Jean-Martin Charcot laid the foundations of what many consider modern clinical neurology at the Salpêtrière Hospital, while Guillaume Duchenne consolidated electrotherapy as a treatment for diseases of the nervous system (Hagner, 2012). In fact, studies with electrostimulation of the brain were essential for supporting the localizationist theory, in which each brain function can be bi-univocally correlated to a brain area. In addition, the sometimes-conflicting interactions between physiologists and physicians led to the introduction of ES as a basic neurophysiology technique in clinical practice for questioning and confirming preclinical models. An obvious example of the great impact of this interdisciplinarity is Wilder Penfield's studies on adapting and applying electrical stimulation techniques to patients submitted to neurosurgical procedures, which lead to the human sensory-motor cortex topographical mapping [i.e., the sensory and motor homunculus (Penfield and Boldrey, 1937; Penfield and Jasper, 1954)].

The therapeutic application of electrical (and magnetic) fields to the brain is today a very well-established medical and scientific practice, known as neuromodulation or neurostimulation (Bao et al., 2020; Krauss et al., 2021; Foutz and Wong, 2022). In fact, the field bears testimony to its historical roots, displaying sometimes the content of trial-and-error practice, but also solid principles and protocols based on an ever-evolving conceptual framework in neurosciences (Hopkins et al., 1992; von der Malsburgl, 1994; Bennett, 1999; Varela et al., 2001). This conceptual framework is in the kernel for our understanding of the very nature of information processing within the nervous system, how the brain works, and the physiopathology of its dysfunctions. As reminded by one of the greatest geniuses of humanity's past, Leonardo da Vinci, "He who loves practice without theory is like the sailor who boards ship without a rudder and compass and never knows where he may cast.".

In Section "2. The ever-evolving neuroscientific framework" of this review, we revisit the evolution of such a conceptual framework which establishes, in our understanding, the guiding principles that pave the way for ever-more efficacious neurostimulation methods based on evidence and sitting on a solid theoretical foundation. Along with the advised practice of full disclosure, the authors have a particular interest in the aspect of temporal patterning, a considerably more recent strategy used in stimulation protocols. Its use derives from the knowledge scaffold supporting modern neurosciences, and how it relates to a more recently proposed coincidence-detection cerebral architecture (Hopkins et al., 1992; Abeles et al., 2004) rather than the more conventional integrate and fire model of neuronal processing (not to confound with IaF computational model) (McCulloch and Pitts, 1943; Rosenblatt, 1958). Therefore, it is not surprising that the review ends with the authors putting forward their own contributions to the field stemming from the proposition of a temporally complex pattern of ES to suppress seizures and treat epilepsy, termed

Non-periodic Stimulation (or NPS); as well as using ES for probing neuronal circuitry for diagnostic purposes. NPS is a non-standard form of ES in which the interpulse intervals (IPI) are randomized in a unitary exponent power-law fashion with a low average frequency (4 pulses per second). It has been shown to have robust anticonvulsant properties in animal models of acute seizure and also in animal models of epilepsy, in which permanent changes to neural tissue is induced so that seizures spontaneously occur in a chronic fashion. Mechanistic studies suggests NPS has a synchronization buffer effect (i.e., it maintains homeostatic levels, protecting against hypersynchronization), while also preserving neural function (de Oliveira et al., 2019). It is important to highlight here that research data from experiments designed to explain how such neuromodulation protocols worked only found a solid theoretical background under the coincidence detection perspective. These findings will be reviewed and discussed in Sections "3. Novel conceptions of the time dimension in the design of neuromodulation approaches" and "4. NPS meets the coincidence-detection framework: driving the infinite improbability of the brain's functional connectogram" of this text.

The lessons we learned from applying such temporally complex stimulation protocol for treating epilepsy in experimental animal models have fostered a diversity of investigational and developmental venues, some of which are purely physiological and have no association with brain dysfunctions. These include memory engrams; a further in-depth investigation of the mechanisms of NPS itself under the light of a coincidence detection conceptual framework; the implications of the effects of the therapy in the current neuroscientific understanding of the brain functioning and disorders; novel therapeutic applications toward distinct neurological disorders including pathological anxiety, Parkinson's, and motor deficits following stroke, and; translational research in human patients. The group is currently carrying out all these endeavors and such perspectives will be presented as a final discussion in Section "5. Discussion" of this article.

2. The ever-evolving neuroscientific framework

2.1. Beginning with the integrate and fire architecture

Even rudimentary electricity devices such as Leyden Jar and Van de Graaf's Generator, although quite popular as a handful of parlor tricks and quackery, are methods and tools that had noteworthy importance for evolving a conceptual framework to explain functions and diseases of the brain. To highlight just a few breakthroughs: the understanding that isolated nerves (Jan Swammerdam; 1637-80) and muscles (Albrecht von Haller; 1734) were electrically "irritable"—see Pearce's Historical Notes (Pearce, 1997), that the spinal cord was an important pathway for activating "body-motion", and the important role cortical electrostimulation played in establishing the idea—championed by Santiago Ramon y Cajal—of brain architecture based on functional neuroanatomy (Fritsch and Hitzig, 1870; Ferrier, 1890; Jackson, 1898; Brodmann, 1909; see for historical review Finger, 1994; Levine, 2007; Molnár and Brown, 2010). All these contributions lead to the seminal work of Sir Charles Sherrington (e.g., "The integrative action of the nervous system", with notable contributions of outstanding scientists such as Marshall Hall, Edgar Adrian, and Yngve Zotterman) which helped shape a hierarchical functional organization of the brain as layers upon layers of sensory-motor circuits, with respective modulatory inputs from several multimodal brain areas, coordinating an increasingly complex network of reflex-actions (Levine, 2007). Sherrington's proposal for the brain architecture had its foundations on neuronal communication, strongly based on four principles: (a) neurons would transmit information "digitally" across long distances[1] (i.e., action potentials) coding intensity as inter-pulse intervals—Adrian and Zotterman's work (Adrian, 1926; Adrian and Zotterman, 1926); (b) the synapse would integrate the arriving "pulses" as postsynaptic "analog" potentials—decoding the frequency of the all-or-nothing "digital" input signals into signal intensity levels; (c) neurons could receive inputs from several synapses, coming from different sources, each either exciting or inhibiting postsynaptic potential formation, and; (d) depending on the level of excitation of the postsynaptic neuron, it could fire and propagate information. This whole rational scheme is named integrate and fire.

The foundational work of Sherrington—and his predecessors—was complemented by the important contribution, a couple of decades later, of the theoretical framework of Frank Rosenblatt and the McCulloch-Pitts neuron. In fact, while those previous conceptions were mostly based on inductive thinking proposed in order to develop a comprehensive theory of brain function, Rosenblatt's implemented the McCulloch-Pitts "perceptron" as a means to test such a groundbreaking theory under a more deductive thought process made possible by mathematical models (McCulloch and Pitts, 1943; Rosenblatt, 1958). His attempt, named connectionism, was significantly different from the pure symbolic approach to "mimic" brain function without any concern for its biological substrate, defended by none other than Alan Turing (Daylight, 2015). On the contrary, the incorporation of neuroscientific ideas, such as Hebbian rules for learning and memory, largely contributed to the impact of such views in neuroscience in general, creating back-propagation models with a great impact on machine-learning systems (Lillicrap et al., 2020). Of particular importance here, it was also instrumental in laying down the later basis for ideas on how electrical stimulation could relay its effects, for example: (a) the higher the intensity of the current flowing through the stimulating electrodes, the higher the number of neurons recruited; (b) the higher the frequency of pulse stimulation, the higher the activation of each neuronal unit; (c) the pulse should obey the time-constraints known to the interpulse-interval associated to the "digital" propagation, i.e., the refractory period intrinsic to action potentials; (d) the target of the electrical stimulation should be chosen based on how its intrinsic functionality (localization v.s. function) could serve to alleviate symptoms, "remove" irritable areas (by either lesion or driving

1 Although the electric-field propagation within a conducting volume does allow for synaptic communication if the distances are sufficiently small (i.e., electrotonic conduction, electrical synapses, ephaptic transmission etc.), in order to overcome the constraints imposed by physics on electric field decay, a biological solution based on voltage-gated channels, working roughly as "repeater stations", allow for signal transmission over meter-long axonal processes.

them into refractory periods), and potentiate endogenous feedback mechanisms to restore homeostasis (Beenhakker and Huguenard, 2009; Kalitzin et al., 2010).

Serrington's work, although of undeniable genius and importance, was criticized and deemed incomplete especially due to its inability to properly address "the binding problem" and the temporal constrains that a cascade of integrator circuits would have on neuronal computation (Paz and Huguenard, 2015; Isbister et al., 2018). In short, not only the proposed conceptual framework struggled to explain how a "sensory-multimodal" object or process would be represented by the underlying neuronal network, but also that the neuronal computation of integrating neuronal frequency of discharge to an analog transmembrane potential in every synaptic relay would render complex sensory-motor integration (or decision making in voluntary movements) way too long a process to be useful in triggering behavior with an adaptive value. Therefore, adjustments should be made to the proposed framework regarding what kind of neuronal computational processes actually takes place within the brain. Nowadays we are on the verge of consolidating a new conceptual framework emerge: *time*. Time is the key element missing from the former early 20th-century debate.

2.2. Incorporating the coincidence detection architecture

The idea of a temporal structured organization, with neuronal circuitry designed to detect specific temporal discharge patterns, based on coincidence detector motifs rather than integrate and fire relays, has more recently (in the time frame of neuroscientific reasoning) been proposed as a conceptual framework alternative in neurosciences. Not that the current view completely erases previous conceptions, but rather that it complements ideas on brain physiology, in which an architecture based in space (i.e., anatomical-localizationism) on input areas (i.e., sensory systems) yields to a structure in time on more rostral substrates, allowing fast and reliable neuronal representation of the external world. Furthermore, at the output (i.e., rostral motor areas), the time-structured neuronal representations would gradually yield back to a framework based on a spatial organization, thus more akin to the integrate and fire paradigm. This central concept has received many different names/views and branched into many different ideas, all converging on the importance of time determining neuronal network organization and function: temporal-coding, phase-coding (Varela et al., 2001; Petersen and Buzsáki, 2020), phase-synchronization (Singer and Gray, 1995), time-synchronization (Grossberg and Schmajuk, 1989; Price and Gavornik, 2022), phase-coherence (Fries, 2005), amplitude-phase coupling (Aru et al., 2015), the neural syntax of brain rhythms (Buzsáki and Watson, 2012), spectral-signatures (Spadone et al., 2021), small-world network scheme (Liao et al., 2017), etc.

The very idea of a synchronous or coincident activity implies establishing the time-scale resolution deemed sufficiently small to be considered simultaneous, i.e., if it falls within the same time bin then it is synchronous. In fact, since multimodal information processing time-lags can vary throughout primary sensory pathways, due to the summation of sequential synaptic delays, a form of sustained activation state must exist in order to identify a "temporal pattern" of coincidental activity within increasingly larger time scales. That is the precise role fast brain oscillations are proposed to play within distributed local networks (i.e., neuronal assemblies) and the gradually decreasing frequency oscillations play on large-scale neuronal assembly integration (Varela et al., 2001). Consequently, the transient link that is established within local network assemblies (i.e., organized as small-world networks; Liao et al., 2017) and the dynamical large-scale transfer of information between such networks far apart in the brain have been referred to as a functional connectome (or connectogram)—in contrast with the quasi-static anatomical definition of a connectome (Contreras et al., 2015). One major corroboration of such perspective is the work done on selective attention and feature-binding neuronal visual processing, which has shown that phase-locking among neuronal groups ("temporal" coherence) plays an important role in efficacious communication between assemblies (Fries, 2005). In short, the same visual stimuli, applied during different attentional conditions, generate different temporal organizations amongst neuronal groups (not necessarily affecting "who" is being recruited—or "how much" that particular group is being recruited, but impacting "when" or in which sequence the neuronal groups are activated). The "binding-tag" could form transitory temporally coherent neuronal ensembles, creating a much more flexible and effective neuronal representation of a specific situation that could optimally trigger an appropriate sensory-motor response (Isbister et al., 2018).

Advances have also been made in proposing alternate mathematical models that are better suited to the idea of representation and communication by temporal organization of neuronal groups (i.e., binding-by-synchronization (BBS) hypothesis, communication-through-coherence, engram formation by temporal patterns). As an example, after observing precise firing sequences on task-triggered cortical activity, Abeles (Abeles, 1982; Abeles et al., 2004) coined the term "synfire-chain" to represent his idea of neuronal network organization based on "temporal patterns" of representation. Abeles "resurrected" previous models proposed by Griffith (1963) and Grossberg (Grossberg, 1969; Grossberg and Schmajuk, 1989) in which a version of Rosenblatt's perceptron was reorganized into sequentially connected layers of pools of neurons, i.e., a "complete transmission lines", each representing neurons that "synchronously" fired within a "hypothetical" time-bin. The "cortical songs", represented by such a model, would have complex space-time patterns associated with "specific" network states (Louie and Wilson, 2001). The model received several modifications and suggestions along the years, such as no need for the time bins (or synaptic delays) to be constant—Bienenstock's synfire braids (Bienenstock, 1995), and that synchronicity could be reinterpreted as a time-locked activity between neurons [not necessarily simultaneous firing (Izhikevich, 2006)]. These suggestions brought the proposed initial model much closer to current biological findings while also addressing criticisms against the model being able to provide an efficient, reliable, adaptive, and flexible representation of how the "real" world is represented by neuronal networks.

The aforementioned change in the conceptual framework of brain function and dysfunction has had a profound impact on conventional neuromodulation as a therapeutic and/or diagnostic tool. Patients with Schizophrenia have impaired performance on

Gestalt-related tests (e.g., Mooney Face Test) that nicely correlates with large-scale neuronal synchronization deficits (Uhlhaas et al., 2006). On the other hand, forcing network coupling between two separate small-world networks, through electrotherapy-induced neuromodulation, has been shown to significantly improve impaired cognitive processes in patients (Reinhart and Nguyen, 2019; Reinhart, 2022). In short, in situations where physiological function and brain disorders just would not correlate with the changes in discharge frequency or metabolism of any one specific area, the overall temporal patterns between areas became a much more reliable diagnostic and therapeutic alternative. Furthermore, it has been shown that targeting a specific brain nucleus for ES, while using a pattern having the overall same frequency (i.e., 6 pulses within 100 ms), may activate different functional connectome pathways depending on the specific combination of IPI values used (Mourão et al., 2016). This particular result comes very close to demonstrating that the integrate and fire paradigm is not as well suited as the coincident detector one regarding higher-level neuronal processing.

All this theoretical framework substantially changed the way we looked at neurophysiology and, consequently, how the brain functions. There is an obvious two-way relation between how we perceive function and the strategy we design to fix things when they become dysfunctional; neuromodulation is no exception to that rule.

3. Novel conceptions of the time dimension in the design of neuromodulation approaches

A brief discussion on the use of neuromodulation for the diagnosis and treatment of patients with epilepsy is in order before we start suggesting paradigm shifts on the matter. Roughly, neuromodulation of targeted excitable nervous tissue has focused on varying parameters such as polarity, waveform, amplitude, frequency, electrode material, dipole distance among others in search of an optimal therapy (Medeiros and Moraes, 2014). The goal is often to cause disturbances on the underlying neural network in effect to its ongoing intrinsic state (McIntyre et al., 2004). Perhaps the most distinguished breakthrough in seizure control using neuromodulation happened during the 80s: vagus nerve stimulation (VNS) (Binnie, 2000). The VNS treatment was proposed as an effective method for treating patients with refractory epilepsy, found unfit for ablation surgery. The success of VNS prompted other more invasive neuromodulation approaches such as cortical stimulation and deep brain stimulation (DBS) (Kinoshita et al., 2004; Vonck et al., 2005). These alternatives were reserved for more extreme cases (i.e., patients with spasticity, severe psychiatric disorders, etc.). Tackling the problem through the development of new pharmacological agents had not significantly improved seizure control on pharmaco-resistant patients. Thus, the use of neuromodulation has regained the interest of both basic science epileptologists and clinicians. The new interest spurred a myriad of methods. Seizure suppressing neuromodulation has been applied, with different levels of success, to the anterior nucleus of thalamus (Mirski et al., 1997; Hamani et al., 2004), the subthalamic nuclei (Benabid et al., 2002; Chabardès et al., 2002), and even the epileptogenic focus itself (Vonck et al., 2002), including large clinical trials (SANTE) and with state-of-the art closed-loop systems (e.g., NeuroPace® use in the treatment of refractory epilepsy, United States Food and Drug Administration) (Fisher et al., 2010; Morrell and RNS System in Epilepsy Study Group, 2011; Fridley et al., 2012).

It is not trivial to pinpoint the exact study or paper in which the time dimension for neuromodulation was first broadened into aspects beyond the integrate and fire framework and started affecting the design of the temporal structure of ES patterns. Although electrical stimulation has been used for rigorous scientific investigation of brain function for more than a century (Ferrier, 1887; Sherrington, 1906; Penfield and Boldrey, 1937)—see for review (Guenther, 2016), it was only after the birth of the modern era of neuromodulation in the '60s, with DBS and Spinal Cord Stimulation (SCS) for the treatment of motor disorders and chronic pain (Buyten et al., 2013; Tiede et al., 2013; Chakravarthy et al., 2018), that its therapeutic usage started to share the same rigorous scientific foundations. Only then, the bidirectional knowledge transfer between basic neurosciences and neuromodulation truly deepened. Thus, it is natural that the first publications that more comprehensively reviewed the neurophysics of ES, such as the works of Ranck (1975) and Tehovnik (1996), were naturally committed to the integrate and fire framework. In these reviews, which are nonetheless bibliographic cornerstones to the field, the contribution of the temporal dimension for recruitment and control of behavior is described in terms of pulse frequency and duration, naturally conditioned to the target area. Even later work and theories aimed at understanding the mechanisms underlying therapeutic effects of DBS—such as depolarization blockade, synaptic inhibition, synaptic depression, and network modulation—were, to a large extent, linked to such framework as illustrated, for instance, to the prominent importance given to stimulation frequency (Breit et al., 2004; McIntyre et al., 2004; Theodore and Fisher, 2004; Vonck et al., 2004). In the same vein, much of contemporary work aimed at finding optimal parameters for DBS was focused on pulse morphology parameters, pulse frequency, and anatomical target (Kuncel et al., 2006; Cymerblit-Sabba et al., 2013), not on the temporal structure of stimuli.

Possibly, a major pioneering contribution toward better incorporating the time dimension into the design of neuromodulation strategies can be found in a series of *in silico* studies by Peter Tass and collaborators who, inspired by the phase resetting of circadian rhythms phenomena, set out to investigate analogous processes related to brain oscillations and stimulation (Tass, 1996, 2001a,b, 2002a,b). By using different mathematical-computational models of neural oscillators, that author and his group studied effects, mechanisms, and applications of pulsatile stimuli which are time-locked to ongoing synchronized oscillations in order to obtain phase resetting of the rhythm and thus desynchronization. Based on these findings, that same author later proposed the Coordinated Reset (CR) approach, which was a novel DBS variation to be applied in the treatment of neurological diseases such as Parkinson's, motor disorders, and even epilepsy. Investigation of CR was first carried out *in silico* (Tass, 2003; Tass and Majtanik, 2006), and later in pre-clinical (Tass et al., 2012; Wang et al., 2016) and clinical settings (Adamchic et al., 2014) with considerable success.

In a parallel line of development, another important contribution stemmed from the efforts to better understand the mechanisms by which DBS is capable of suppressing motor symptoms of essential tremor. In 2004, Grill and colleagues put forward the informational lesion hypothesis to explain the therapeutic effects of high-frequency neurostimulation, stating that pathological activity would be masked by the input stimulus in a frequency-dependent fashion (Grill et al., 2004). In this *in silico* study, authors observed that the regularity of the firing of neurons increased (and thus the information content decreased) when increasing the stimulation frequency, which would corroborate two important DBS hallmarks: its efficacy in higher frequencies and its similarity to electrolytic lesions. This led the authors to postulate that application of irregular temporal patterns would be less efficacious in reducing essential tremor symptoms. This was, in fact, observed in a few following studies carried out *in silico* and also with human patients, by applying DBS in which IPI were drawn from Gaussian distributions with different coefficients of variation or in paired pulses (Birdno and Grill, 2008; Birdno et al., 2008, 2012). On the other hand, irregular temporal patterns—but of distinct features—of ES (uniform and unipeak distributions) were later demonstrated to improve the performance of Parkinsonian individuals in a finger-tapping task, while also suppressed aberrant electrophysiological spectral content in the beta band (Brocker et al., 2013). This set of results was of central importance in establishing the fact that temporal pattern is a determinant (a "new dimension") in the efficacy of an ES method, even though effects may vary according to several other factors such as the disorder being treated, target area, and general parameters (Grill, 2018). In any case, Grill and colleagues have recently proposed new approaches (e.g., Temporally optimized patterned stimulation or TOPS®) in which parameters—including temporal—have been carefully engineered using, among others, machine learning tools (Brocker et al., 2017; Okun et al., 2022).

Considering the well-known aberrations of electrophysiological neural activity underlying epileptic phenomena in general and hyper-synchronism of seizures in particular (Avoli et al., 2002, 2004; Benini et al., 2003; Garcia et al., 2005; Nariai et al., 2011; Medeiros et al., 2014; Edakawa et al., 2016; Li et al., 2016; Abreu et al., 2018; Yu et al., 2018; Batista Tsukahara et al., 2022), epilepsy was also a natural application field for temporally complex ES. At the beginning of 2000's, our group devised, patented, and tested—possibly the first therapeutically successful *in vivo* application of temporally structured ES—a novel temporally irregular pattern of ES later termed non-periodic stimulation (or NPS), in which the IPI were randomized in real-time, with the important advantage of being low frequency on average (mean of 4 pulses per second) (Cota et al., 2009, 2021; de Oliveira et al., 2019). Considering that therapeutic efficacy was obtained with pulse parameters compatible with other high-frequency methods, the low frequency directly implied low energy transfer from the stimulator to the neural tissue. This is highly advantageous for perspectives in engineering (greater autonomy of IPG batteries, less degradation of electrodes), medical practice (less interventions for battery substitution), and safety (lower risk of lesions and habituation) (Cota et al., 2016). In the first report on NPS anticonvulsant effects, seizures were induced in rats by the controlled intravenous infusion of pentylenetrazole (PTZ), a chemoconvulsant of broad action, while the occurrence of and latency to stereotypical convulsive behaviors were measured (Cota et al., 2009). Animals submitted to NPS applied to the right basolateral amygdala needed almost double the amount of PTZ to display generalized tonic-clonic seizures and displayed lower mortality levels when compared to fixed-frequency, burst, and quasi-uniformly distributed IPI patterns, as well as unstimulated controls. In an fMRI study using the same "ramp"-like infusion of PTZ, Mesquita and collaborators showed that the ipsilateral site of stimulation significantly increased activity during fixed frequency (also termed periodic) stimulation, while showing significant dampening of hyperactivity during NPS. These results confirmed the original 2009 data from Cota et al. (2009) and showed that the temporal dynamics of brain site activation during PTZ seizure onset was dependent on the temporal organization (inter-pulse-interval) of the same 4 pulses per second stimulation applied to the amygdala. In a way, NPS seemed to have a disruptive effect on the binding-by-synchronization dynamics of circuitry involved in the PTZ seizure model while the periodic stimulation facilitated and/or potentiated communication to the stimulated hemisphere.

The anticonvulsant effects of NPS were also demonstrated later in spontaneous seizures displayed by animals submitted to the temporal lobe epilepsy/chronic seizure experimental model of pilocarpine. After administering a bolus injection of the drug, animals develop status epilepticus which induces maladaptive plastic changes that will culminate in seizure susceptibility after a latent phase of 15 to 45 days (Turski et al., 1983; Clifford et al., 1987; Persinger et al., 1988). NPS-treated animals displayed fewer seizures, which were shorter and possibly less severe (Medeiros et al., 2014). Additional investigation also showed that the method is more efficacious if applied bilaterally and in an asynchronous fashion (Oliveira et al., 2018). While the anticonvulsant effects were confirmed by several mechanistic studies of our group (see next section) and other authors (see below), we also found preliminary evidence of beneficial effects in suppressing epileptogenesis and in the application towards pathological anxiety, which is mostly mediated by the amygdala (Cota et al., 2021). Finally, we recently demonstrated that neural function, including the sleep-wake cycle architecture, is preserved in animals undergoing NPS intervention (Réboli et al., 2022).

Among other groups that contributed to the investigation of non-standard temporal patterns of ES applied to the treatment of epilepsy, Wyckhuys and colleagues reported in 2010 the successful suppression of seizures in rats induced by kainate using ES with Poisson-distributed IPI at high frequency (130 Hz mean) (Wyckhuys et al., 2010). Quinkert and colleagues created non-standard temporal patterns of electrical stimulation with a mean frequency of 50 Hz by using a logistic equation and applied them to the hippocampus and medial thalamus of mice. They assessed behavioral and electrophysiologic biomarkers of arousal which may be related, by their turn, to disorders such as epilepsy or Parkinson's disease. The authors found pattern-dependent behavioral alterations of increased arousal with concomitant increases in delta-range power of local field potentials. The effects were particularly strong with the non-linear patterns and depended on the applied substrate (Quinkert et al., 2010). Furthermore, following a sequence of studies aimed at developing closed-loop neurotechnology for the treatment of epilepsy, Nelson and colleagues also used ES with Poisson-distributed pulses to investigate the tolerability of different spatial and temporal regimes in multisite application to the cortex of rats with

electrically-induced seizures. Authors found that synchronicity (temporal regime across areas) was more determinant in the suppression of seizures than the periodicity; fixed-frequency versus Poisson distributed IPI (Nelson et al., 2011). More recently, a temporal pattern similar to NPS was demonstrated to have, beyond anticonvulsant effects, anti-epileptogenic action in the amygdala kindling model in rats (Santos-Valencia et al., 2019).

All the studies discussed here show that the precise temporal structure of stimuli, beyond the fundamental concepts of frequency (or mean frequency) and pulse duration, is central in determining the effects, including therapeutic efficacy and collaterals, of a given neuromodulation approach. In our understanding, this should be considered a fact of past debate by now, even though several nuances remain to be elucidated. On the other hand, finding the precise common conceptual thread that binds all of them together into a unified scientific theory capable of explaining both brain function and the therapeutic efficacy of temporally structured ES, is challenging. In any case, we can benefit from some shared aspects of the neurological disorders and their neurostimulation methods discussed so far that, in our understanding, support the coincidence detection framework. In the next section of this manuscript, we will adopt this strategy, taking advantage of these ideas and also of the lessons learned from our own investigation of the mechanisms behind NPS, to put forward our attempt at a novel understanding of the mechanisms of temporally complex electrical stimulation. Naturally, this conceptual framework is largely based on coincidence-detection neuroscience introduced in earlier sections of this manuscript.

4. NPS meets the coincidence-detection framework: driving the infinite improbability of the brain's functional connectogram

The choice of how to frame any problem, including brain function and dysfunction, has an obvious impact on how one attempts to solve it. Thus, the first step to designing efficacious and safe ES and understanding the mechanisms behind its therapeutic effects is to reinterpret the pathophysiology of brain disorders in a shared perspective of the coincidence-detection framework. In this sense, while normal levels of coupling within neural circuits and between areas of the brain are central for proper brain function (Womelsdorf et al., 2007), deviations from the natural setpoint may cause dysfunction (Uhlhaas and Singer, 2006). Some disorders, such as epilepsy, can be seen as abnormal coupling and indiscriminate propagation of information along neuronal pathways, without the apparent proper homeostatic modulation of inhibitory feedback mechanisms, thus compromising overall network stability (Moraes et al., 2000; Medeiros et al., 2014; Cota et al., 2021). Conversely, there are other cases, in which the core of the disorder seems to be related to the compromise of information transfer from one processing relay to the next (i.e., either by lesion or interference from other abnormally activated brain areas). An illustrative result, in this case, is the significant cognitive improvement found in age-related working memory deficits after "forcing" the coupling between brain regions using high-density transcranial alternating current stimulation (HD-tACS) ES. The dual-site HD-tACS was effective not only in reversing age-related cognitive deficits but also improved spatial task performance in adult human subjects (Zhang et al., 2022). In other words, by "grossly" stimulating two different brain areas using a non-invasive procedure, Reinhart and Nguyen were able to frequency tune theta wave synchronization along the frontoparietal cortex (Reinhart and Nguyen, 2019; Reinhart, 2022). If one considers gamma oscillation as the electrophysiological counterpart of local circuitry motifs (Hasenstaub et al., 2005; Vida et al., 2006; Bartos et al., 2007), then theta-gamma phase-amplitude codes would represent a long-range sender-receiver flow of information throughout the neural network; which was enhanced after the synchronized stimulation.

The model of temporally structured information being transferred from one area to the next, as we saw in the BBS hypothesis or the communication-through-coherence, also requires a modulating oscillatory process phase-locking both regions. By creating "time-pockets" that favor activation of distinct and specific groups of neurons in the target network (i.e., in terms of propensity/probability to fire), in a selective fashion linked to the phase of the slow modulatory oscillation, distinct temporal patterns of discharge could be channeled through a particular node-hub from the origin—i.e., high degree participation coefficient nodes (Liao et al., 2017)—and thus would elicit an equally complex temporal and spatial activation pattern on the target network (**Figure 1**). Of particular importance here, this phase-locking scheme of neuronal communication between assemblies is only possible by looking through the coincidence-detection network framework. Following this logic, one could ask, what would happen, according to this scheme, if a random (or pseudo-random) distribution of discharge patterns is applied within a period of a coherent oscillation waveform between areas A and B? According to what was explained, a different and complex spatial and temporal pattern of activation on the target region would emerge every single time (**Figure 1C**). However, if a fixed pattern within an oscillation period were to be applied, then the same spatiotemporal pattern would be recruited over and over again in a reverberatory fashion (**Figure 1D**). Furthermore, this could result in its increasing control of the overall network activity due to Spike-Timing Dependent Plasticity—STDP (Feldman, 2012), eventually rendering the entrained circuit a self-sustained oscillator (**Figure 1E**).

The results we have been finding so far are evidence that this is precisely what happened when NPS produced anti-convulsant effects on animal models of epilepsy and periodic ES produced a proconvulsant effect (Cota et al., 2009; **Figure 2**). In other words, the therapeutic pattern resulted in a complex spatial and temporal activation of neuronal groups in the target and its afferent projections, thus preventing aberrantly synchronous recruitment of any specific neural circuitry into ictogenesis (**Figure 2B**). Conversely, using the same principles, simple low-frequency periodic activation resulted in the entrainment of the same network into pathological oscillation (**Figure 2A**). The imaging results using fMRI carried out by our group and discussed here (Mesquita et al., 2011) can be understood as first more direct evidence of that. Furthermore, functional characteristics of the stimulated neural substrate are naturally a major factor in these effects, as it happens with any other therapeutic application of ES, temporally complex or not. As mentioned, most of the findings are the result of the

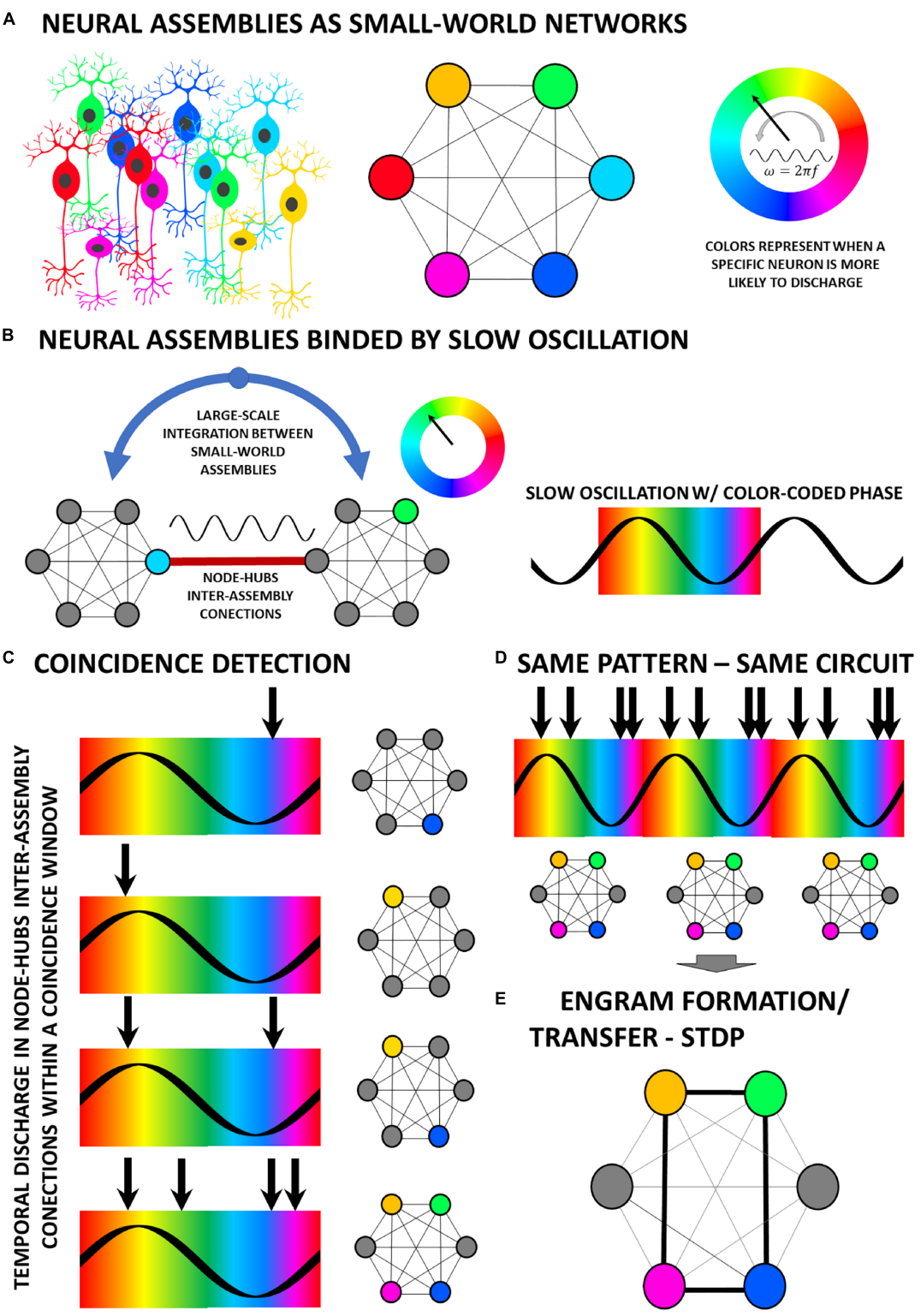

FIGURE 1
The time dimension in the processing of information across neural circuitry underlies the bidirectional interplay between temporal patterns of activity and the dynamic connectivity of neural circuits. **(A)** Neuronal motifs of multiple cells, codified by distinct colors, are organized as a highly interconnected network of nodes which are recruited in a time-basis locked to the oscillation phase, color-coded to match the motif which has a greater probability of recruitment. **(B)** Oscillations, which can be generated externally, synchronously entrain neural assemblies in a small-world network fashion for the transfer of information across long ranges (Varela et al., 2001). **(C)** By this coincidence detection scheme, the moment of occurrence of a given neuronal activity (e.g., firing of an action potential) in relation to the phase of the binding oscillation will determine which node will be activated in the afferent local network. **(D)** A specific temporal pattern coherently (to the phase of the slow oscillation) repeated over multiple cycles of reverberation will always recruit the same nodes in the local network. **(E)** Finally, the consistent spatiotemporal pattern of recruitment will induce, by means of mechanisms such as STDP, the creation of new engrams in the network.

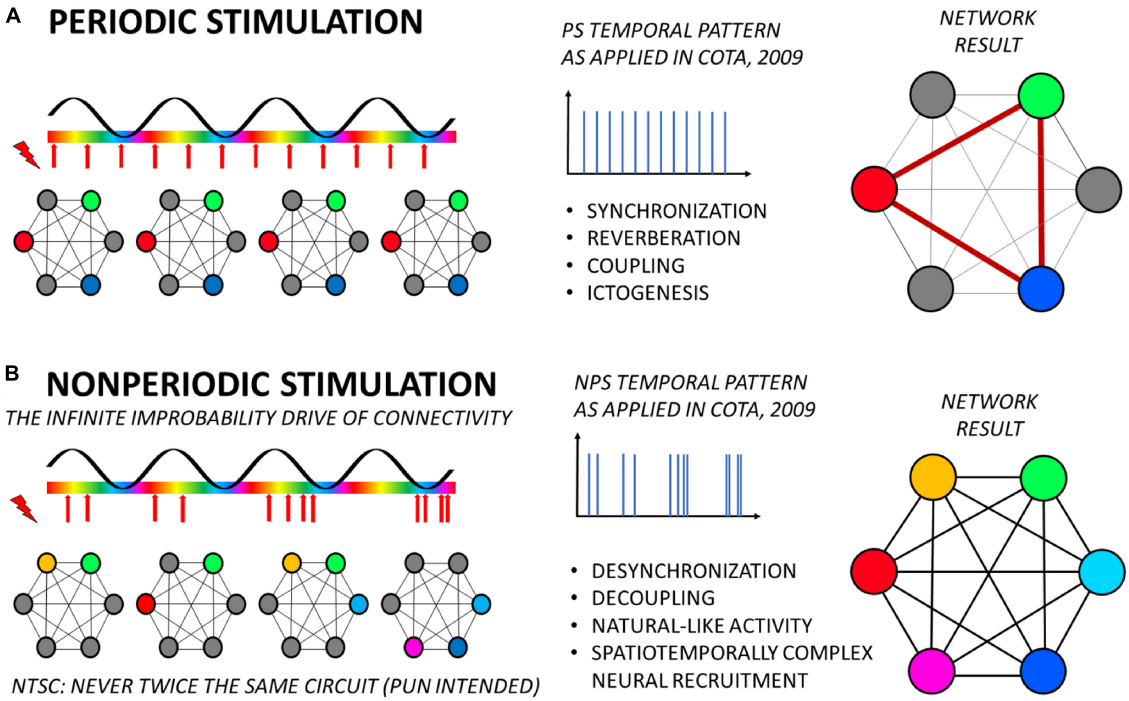

FIGURE 2
Temporally complex electrical stimulation applied to a hub-node (such as NPS target at the basolateral amygdala) benefits from the coincidence detection mechanism to deliver treatment by means of driving the functional connectivity of the brain with "infinite improbability". **(A)** Periodic stimulation, with a fixed frequency (as seen in the center panel), always recruits the same nodes in the network and in the the same temporal order. This consistent spatiotemporal recruitment will thus induce a set of brain phenomena, such as synchronization (as observed by electrophysiology or fMRI), reverberation and creation of stereotypical electrographic signatures, increases in synaptic weights (coupling of nodes), and even ictogenesis in susceptible tissue. **(B)** Conversely, temporally complex stimulation, with continuously randomized IPI, induces an equally complex spatial (and temporal) recruitment of nodes in the network, never repeating the same circuit or the same order. By its turn, the lack of repetition will induce desynchronization, decrease of synaptic weights (decoupling), and thus robust anticonvulsant effects. If stimuli are organized as a natural-like activity, network response may be putatively tuned to homeostasis levels, rectifying synchronization to baseline, while being innocuous to neural function and acting in a demand-only fashion. It is important to highlight that the relationship between frequencies of stimuli and of the slow oscillation are not depicted to scale. Yet, the same effects on the consistency of the resulting recruitment of nodes in the network will probably remain unaltered given only that fixed frequencies can entrain the slow oscillation (e.g., by means of phase resetting) and temporally complex patterns can not. Naturally, investigation of these specific aspects is of paramount importance to better understand the validity of this framework.

application of NPS to the basolateral amygdala, which is known to be a major node-hub connecting many territories in the forebrain, midbrain, and even hindbrain for the support of multiple neural functions (Antoniadis et al., 2009; Freese and Amaral, 2009), while also playing a major role in epileptic phenomena (Hirsch et al., 1997; Cota et al., 2016), directly or indirectly (de Oliveira et al., 2019). In the same vein, it is important to notice that more caudal structures in the primary-sensory relays may not be sensitive to such temporal organization of stimuli (Medeiros et al., 2012), while multiple site stimulation may contribute itself to uncoupling the coherence between large-scale information transfer (Oliveira et al., 2018).

Another important aspect that must be observed when considering the effects of NPS or other temporally complex approaches in the coincidence-detection perspective is that, in order to fit the idea of communication-through-coherence or BBS, the entire code generated by the ES pattern (i.e., the whole temporospatial representation within the network) must fit within a period of the oscillation in which communication is effective, whatever IPI distribution is chosen (**Figures 1**, **2**). Not forgetting, as said before, e.g., the synfire chains, that layers upon layers of such time-coded representations could be combined into one single temporally structured sequence (i.e., "a cortical song") representing a complex experience, object, qualia, or event. Nevertheless, the smallest unit of representation would still be organized within one oscillatory period of the "coupling" portion of the synchronization wave between two connected small-world- networks, thus allowing complex spatiotemporal representations to be channeled through node-hubs (i.e., optimizing neuronal processing and white matter taking up too much space). Importantly, in the end, this leads also to the understanding that frequency (in this case mean frequency) has also an important influence on the outcome of the pattern.

At this point, it is also important to recall that several of the proposed temporally complex ES protocols seem to have taken inspiration from the intuitive notion that temporal complex patterns of ES (random, non-linear, Poisson, and power-law distribution of IPI, etc.) mimicking physiological firing patterns of neurons would be able to resonate with neural circuitry and induce homeostatic physiological brain activity, suppressing aberrant sustained and/or high-intensity oscillations and promoting treatment. Such a concept has, in fact, inspired distinct studies non-related to therapeutic neurostimulation in the past. For instance, Gal and Marom used input-output joint statistics in order to assess the level of fidelity that a single

synaptically-isolated neuron would respond to temporally complex stimuli (Gal and Marom, 2013). They have found that neuronal firing better reproduces input stimulation (optimal fidelity) when it is structured with natural-like, scale-free statistics, in which IPIs are distributed following a power-law of unitary exponent. These observations were later reproduced and extended to small neuronal networks *in vitro* (Scarsi et al., 2017).

Moreover, these aspects also served as a basis for speculating on the nature of many of our own results, particularly in the perspective of why just a specific form of temporal distribution is therapeutic (power law), while others are not (quasi-uniform) (Cota et al., 2021). A recent *in silico* study of our group using an amygdala-like network of Izhikevich neurons showed that power-law distributed stimulation more effectively recruited the local network into synchronized activity when compared to quasi-uniform (Oliveira et al., 2022). Particularly, in our proposed therapeutic temporal distribution, we were careful, as were other stimuli (Brocker et al., 2013), to limit the minimum IPIs to a value large enough to overcome integration time determined by membrane potential decay; i.e., not falling within a time-bin short enough for being considered coincident. Nevertheless, by choosing also an upper limit to the IPI distribution, Brocker and colleagues had much better results treating Parkinson's; arguably making their distribution more alike a power-law distribution. On the other hand, it is also of paramount importance to recognize that different IPI distributions directly affect, as already mentioned, the mean frequency of stimuli or, when this parameter is controlled, its frequency content in distinct ranges of low versus high frequencies. Furthermore, other patterns very distinct from power-law or Poisson distributions (which are closely related to each other) have been shown to be efficacious in recruiting distributed local networks (Mourão et al., 2016). In fact, these data would corroborate the idea that normal base-line brain functioning would not favor one specific temporal arrangement over another; however, it would still depend on synchronizing such arrangements into timeframes established by oscillations (i.e., phase-coded processes) involved in the process, but not the pattern itself, of information transfer between nuclei. Finally, one has to consider the many differences across all these studies, such as the overall condition (homeostasis versus dysfunction) and the differences in experimental approaches (*in vivo* versus *in vitro* versus *in silico*). In the opinion of the authors, such a discussion is certainly related to a major knowledge gap in temporally complex ES. Hence, a thorough and careful investigation of the precise temporal structure of the ES must be carried out, with experiments specifically tailored to study the effects of all these aspects (IPI distribution, mean frequency, anatomical target) separately.

Looking at the problem from another angle, if the system has intrinsic transient "brain states" that favor abnormal coupling between brain areas, ES could be also used to probe how easily a signal from A would reach area B; thus, working quite effectively as a predictor of such brain-states. Medeiros et al. (2014) showed that a single pulse of ES applied every 2 s would be enough to synchronize spontaneous pre-ictal spikes long before any changes in parameters associated with passively recording EEG activity would be significantly different. Kalitzin et al. (2005) used probing ES to evaluate a measure (relative phase clustering index) of how much "synchronicity-prone" evoked activity existed between different regions of the brain as a form of predicting the emergence of seizures. Actually, probing ES as a surrogate marker of seizure onset was not only more effective than passively observing the electrographic activity of brain structures, but was also shown to be "plastically enhanced" if pre-conditioned to previous seizure episodes themselves (Medeiros et al., 2018)—i.e., the circuit learns to be a better biomarker if properly taught. These results not only show that the therapeutic, diagnostic, or predictive use of ES has very much shifted from the initial dogma that synchronicity is a consequence of excitability (Kudela et al., 2003), but rather that a myriad of new applications for ES arise if these two concepts (i.e., excitation/synchronicity) are untwined under the new proposed conceptual framework (Moraes et al., 2021). In fact, even the rationale for how some pharmacological targets are effective in treating epilepsy has been revisited under the coincidence-detector framework (Medeiros et al., 2020).

The intrinsic "brain states" mentioned at the beginning of the last paragraph, in some cases, could reflect structural abnormalities in the underlying neural network, with much more constant and permanent aftermath to the patients' health (Uhlhaas and Singer, 2006). Uhlhass and collaborators showed that patients with schizophrenia not only did not perform well in the Mooney Face Test (i.e., Gestalt perception), but that the "communication-through-coherence" long-scale information transfer between brain structures was also compromised during the test. Several neuropsychiatric disorders (i.e., anxiety, depression, bipolar disorder, ADHD, sleep disorder/apnea, movement disorder/tremor), pain disorders (i.e., migraine, chronic pain, fibromyalgia, neuropathic pain), and other conditions could share a "gradual" commitment of neuronal network stability and inter-assembly communication deficits, within an intensity spectrum, with common physiopathological origins. It is not surprising that all these conditions are comorbid with what would be the extreme expression of abnormal coupling, network instability, and mass neuronal recruitment: epilepsy. Genetic animal models of epilepsy, possessing an innate propensity to seize, even if naive to having had a seizure, still display abnormal behavioral traits associated with the aforementioned comorbidities (Jobe et al., 1999; Jobe, 2003; Castro et al., 2017). And not only can brain-states compromise proper large-scale interactions, information transfer between small-world networks and modulate overall neural network processing, but specific temporal patterns of stimulation are required to induce brain-states [e.g., arousal (Quinkert et al., 2010)].

5. Discussion

Development and assessment of novel neurotechnologies in which the practice of experiments are tightly conditioned to the best of our knowledge of the underlying mechanisms is a major contributing factor for the fostering of impactful findings and disruptive technology (Sunderam et al., 2010; Cota and Moraes, 2022). We can envisage several perspectives for temporally patterned ES in general and also NPS in particular.

A major interest of our research has been epilepsy, due not only to its high morbidity and prevalence, but also because it can serve as an optimal platform for neuroscientific investigation and neurotechnolgical development. Although up to 70% of patients

have seizure control with pharmacological treatment, a substantial number of individuals depend on surgical modalities for treatment (Sander, 1997; Brown, 2016; Johannessen Landmark et al., 2020). When it is not possible to identify the epileptogenic zone, or it is unresectable, the use of neuromodulation with electrical stimulation is an alternative for the reduction in the frequency and severity of seizures (George et al., 1994; Fisher et al., 2010; Heck et al., 2014; Velasco et al., 2022). Three modalities currently have devices commercially available for clinical use: VNS (George et al., 1994), DBS (Fisher et al., 2010), and RNS closed-loop responsive brain stimulation (Heck et al., 2014). Despite significant differences in the site and periodicity of stimulus administration, all use fixed frequency ES and show similar results with an approximate 50% reduction in seizure frequency in patients with focal refractory epilepsy (Ryvlin et al., 2021). They also use high-frequency fixed patterns with the main effect of putative direct target inhibition (functional injury) or activation interrupting pathological activity (jamming effect) of neural circuits (Carlson et al., 2010). On the other hand, robust evidence of therapeutic effects of using non-standard temporal patterns, from computational, animal, and human studies, has been accumulating over the years, as reviewed here. Together with the contribution of our own group, this support that NPS could also be an interesting alternative to increase the effectiveness of neuromodulation in the treatment of epileptic seizures, with a reduction in dysfunctions related to the effect of functional injury. Despite requiring hardware modifications, the adoption of this approach can be incorporated into clinical practice, as it does not increase the energy administered to the neural tissue, is reversible and can be applied to the same targets already used. As mentioned previously, NPS has been shown to be effective in dysfunctional tissue in animal models of the disease (de Oliveira et al., 2014), while also preserving neural function and the architecture of the sleep-wake cycle (Réboli et al., 2022). Both studies corroborate the translational potential of the method.

Despite the high morbidity of seizures, they represent only a small percentage of brain activity time. In this scenario, adoption of on-demand treatment measures is a logical path to pursue. Seizure prediction is pivotal to achieve this goal, but despite all the effort in trying to optimize such functionality using the recording of spontaneous brain activity, the time scale for anticipation is very small. Even with non-linear analyses, the prediction capacity usually does not exceed minutes, being debatable whether it is really a prediction or just early detection (Mormann et al., 2007; Andrzejak et al., 2009). The epileptic brain behaves as a complex system that, upon undergoing a critical transition, changes from a system resilient to hypersynchronism to a hypersynchronous and hyperexcitable system (Da Silva et al., 2003; Uhlhaas and Singer, 2006; Truccolo et al., 2011; Jiruska et al., 2013). More recently, algorithms that combine linear and non-linear analysis approaches have shown improvement in detection performance, although they still show large variability between individuals (Freestone et al., 2017; Karoly et al., 2017; Kuhlmann et al., 2018a,b). Thus, active probing of neural circuits, assessing the degree of resilience through stereotyped and predictable responses generated by external stimuli, can help detect critical transitions and favor better seizure detection (Moraes et al., 2021). With less effect of functional deficit associated with stimulation, NPS is also a promising technique in active probing, with the potential for more frequent circuit checks, using less energy. The lower functional deficit by suppression of local synaptic activity would cause fewer side effects in patients with non-ideally positioned electrodes. Targets where the functional deficit is unacceptable, could also be used.

If, in fact, temporally complex ES works by taking advantage of coincidence detection within the brain to recruit multiple microcircuits in the afferences of the node-hub target, a myriad of therapeutic possibilities ensues. The group is currently pursuing some of them by using the devised method NPS. Based on the rationale that the hyperfunction of the amygdala is directly related to pathological anxiety and/or chronic stress (Prager et al., 2014, 2016), we have been investigating therapeutic effects of NPS in animals submitted to stress model induced by chronic short-time confinement (Cota et al., 2021). We have also proposed its application to Parkinson's disease (PD) and it is envisaged for the application in the suppression of aberrant activity displayed by animals submitted to a stroke model, this last in the realm of the EU-funded project MoRPHEUS. Understanding time-dependent events in the target neural circuit is critical to optimize parameters for activity disruption. Therefore, computational modeling and case analysis, fundamental in translating the method to greater applicability in clinical practice, is currently being carried out (Carvalho et al., 2021; Batista Tsukahara et al., 2022; Oliveira et al., 2022; Terra et al., 2022). Finally, spatiotemporally complex ES (NPS included) is a major plus if one considers the application of neuromodulation in a personalized or individualized fashion. Such approach is in line with the concept of electroceuticals in which neuromodulation therapy should be delivered in a manner that is finely tuned to the dysfunction, including individual patient particularities (Famm et al., 2013). In fact, several groups have been pioneering the application of stimulation in which the temporal pattern is optimized for therapeutic efficacy (Okun et al., 2022) and/or when the stimulation pattern resembles that of spontaneous neural activity (Cottone et al., 2018; Persichilli et al., 2022). Thus, besides anatomical target, frequency, pulse duration, phase, and amplitude, physicians will be able to choose different temporal patterns that may be better suited to different scenarios, encompassing the variability seen in distinct patients suffering from the same neurological disorder.

Overall, like in the Douglas Adams' fiction—mentioned here simply to create a captivating analogy—in which zero-time space travel has been made possible due to an infinite improbability drive (a generator of randomness with infinite capacity), NPS applied to an important neural hub such as the amygdala creates ever changing temporal patterns of stimuli that would translate to ever changing recruitment of neural circuits or motifs and thus impair hypersynchronization; which, by its turn is characterized by excessive regularity. Differently from science fiction, the interchangeability between space and time in brain phenomena is a known and well-stablished scientific fact, with a powerful capability of explaining neural function and dysfunction, as we believe we made clear in this manuscript. We particularly envisage a future in which neurostimulation technology, enabled by closed-loop design and advanced-computing capability (e.g., neuromorphism; Chiappalone et al., 2022), will automatically choose among myriad parameters and also distinct temporal patterns (from fixed low frequency probing stimuli to high frequency random pulses) to

deliver efficacious, efficient, and safe therapy. Further investigation of this promising strategy should be encouraged.

Author contributions

VC and MM conceived the work and contributed the same to the writing of the manuscript. SC wrote smaller portions of the manuscript. All authors contributed to the article and approved the submitted version.

Funding

This work was supported by the Marie Skłodowska-Curie Individual Fellowship MoRPHEUS granted to VC, Grant Agreement no. 101032054, funded by the European Union under the framework programme H2020-EU.1.3. – EXCELLENT SCIENCE and by grant APQ 03295-18 from FAPEMIG (Fundação de Amparo à Pesquisa do Estado de Minas Gerais). MM is recipient of a productivity fellowship from CNPq (Conselho Nacional de Desenvolvimento Científico e Tecnológico), Brazil.

Acknowledgments

We thank all contributors of past works of the group that substantiated this review, especially Drs. Jasiara Carla de Oliveira and Daniel de Castro Medeiros.

Conflict of interest

The authors declare that the research was conducted in the absence of any commercial or financial relationships that could be construed as a potential conflict of interest.

Publisher's note

References

Abeles, M. (1982). *Local Cortical Circuits*, Vol. 6. Berlin: Springer. doi: 10.1007/978-3-642-81708-3

Abeles, M., Hayon, G., and Lehmann, D. (2004). Modeling compositionality by dynamic binding of synfire chains. *J. Comput. Sci.* 17, 179–201. doi: 10.1023/B:JCNS.0000037682.18051.5f

Abreu, R., Leal, A., Lopes da Silva, F., and Figueiredo, P. (2018). EEG synchronization measures predict epilepsy-related BOLD-fMRI fluctuations better than commonly used univariate metrics. *Clin. Neurophysiol.* 129, 618–635. doi: 10.1016/j.clinph.2017.12.038

Adamchic, I., Hauptmann, C., Barnikol, U. B., Pawelczyk, N., Popovych, O., Barnikol, T. T., et al. (2014). Coordinated reset neuromodulation for Parkinson's disease: proof-of-concept study. *Mov. Disord.* 29, 1679–1684. doi: 10.1002/mds.25923

Adrian, E. D. (1926). The impulses produced by sensory nerve endings: part I. *J. Physiol.* 61, 49–72. doi: 10.1113/jphysiol.1926.sp002273

Adrian, E. D., and Zotterman, Y. (1926). The impulses produced by sensory nerve-endings: part II. the response of a single end-organ. *J. Physiol.* 61, 151–171. doi: 10.1113/jphysiol.1926.sp002281

Andrzejak, R. G., Chicharro, D., Elger, C. E., and Mormann, F. (2009). Seizure prediction: any better than chance? *Clin. Neurophysiol.* 120, 1465–1478. doi: 10.1016/j.clinph.2009.05.019

Antoniadis, E. A., Winslow, J. T., Davis, M., and Amaral, D. G. (2009). The nonhuman primate amygdala is necessary for the acquisition but not the retention of fear-potentiated startle. *Biol. Psychiatry* 65, 241–248. doi: 10.1016/j.biopsych.2008.07.007

Aru, J., Aru, J., Priesemann, V., Wibral, M., Lana, L., Pipa, G., et al. (2015). Untangling cross-frequency coupling in neuroscience. *Curr. Opin. Neurobiol.* 31, 51–61. doi: 10.1016/j.conb.2014.08.002

Avoli, M., Benini, R., de Guzman, P., and Omar, A. (2004). GABAB receptor activation and limbic network ictogenesis. *Neuropharmacology* 46, 43–51. doi: 10.1016/S0028-3908(03)00307-1

Avoli, M., D'Antuono, M., Louvel, J., Köhling, R., Biagini, G., Pumain, R., et al. (2002). Network and pharmacological mechanisms leading to epileptiform synchronization in the limbic system in vitro. *Prog. Neurobiol.* 68, 167–207. doi: 10.1016/S0301-0082(02)00077-1

Bao, S., Khan, A., Song, R., and Kai-yu Tong, R. (2020). Rewiring the lesioned brain: electrical stimulation for post-stroke motor restoration. *J. Stroke* 22, 47–63. doi: 10.5853/jos.2019.03027

Bartos, M., Vida, I., and Jonas, P. (2007). Synaptic mechanisms of synchronized gamma oscillations in inhibitory interneuron networks. *Nat. Rev. Neurosci.* 8, 45–56. doi: 10.1038/nrn2044

Batista Tsukahara, V. H., de Oliveira Júnior, J. N., de Oliveira Barth, V. B., de Oliveira, J. C., Rosa Cota, V., and Maciel, C. D. (2022). Data-driven network dynamical model of rat brains during acute ictogenesis. *Front. Neural Circuits* 16:747910. doi: 10.3389/fncir.2022.747910

Beenhakker, M. P., and Huguenard, J. R. (2009). Neurons that fire together also conspire together: is normal sleep circuitry hijacked to generate epilepsy? *Neuron* 62, 612–632. doi: 10.1016/j.neuron.2009.05.015

Benabid, A. L., Minotti, L., Koudsié, A., de Saint Martin, A., and Hirsch, E. (2002). Antiepileptic effect of high-frequency stimulation of the subthalamic nucleus (corpus luysi) in a case of medically intractable epilepsy caused by focal dysplasia: a 30-month follow-up: technical case report. *Neurosurgery* 50, 1385–1391. doi: 10.1227/00006123-200206000-00037

Benini, R., D'Antuono, M., Pralong, E., and Avoli, M. (2003). Involvement of amygdala networks in epileptiform synchronization in vitro. *Neuroscience* 120, 75–84. doi: 10.1016/S0306-4522(03)00262-8

Bennett, M. R. (1999). The early history of the synapse: from plato to sherrington. *Brain Res. Bull.* 50, 95–118. doi: 10.1016/S0361-9230(99)00094-5

Bienenstock, E. (1995). A model of neocortex. *Netw. Comput. Neural Syst.* 6, 179–224. doi: 10.1088/0954-898X_6_2_004

Binnie, C. D. (2000). Vagus nerve stimulation for epilepsy: a review. *Seizure* 9, 161–169. doi: 10.1053/seiz.1999.0354

Birdno, M. J., and Grill, W. M. (2008). Mechanisms of deep brain stimulation in movement disorders as revealed by changes in stimulus frequency. *Neurotherapeutics* 5, 14–25. doi: 10.1016/j.nurt.2007.10.067

Birdno, M. J., Kuncel, A. M., Dorval, A. D., Turner, D. A., and Grill, W. M. (2008). Tremor varies as a function of the temporal regularity of deep brain stimulation. *Neuroreport* 19, 599–602. doi: 10.1097/WNR.0b013e3282f9e45e

Birdno, M. J., Kuncel, A. M., Dorval, A. D., Turner, D. A., Gross, R. E., and Grill, W. M. (2012). Stimulus features underlying reduced tremor suppression with temporally patterned deep brain stimulation. *J. Neurophysiol.* 107, 364–383. doi: 10.1152/jn.00906.2010

Breit, S., Schulz, J. B., and Benabid, A.-L. (2004). Deep brain stimulation. *Cell Tissue Res.* 318, 275–288. doi: 10.1007/s00441-004-0936-0

Brocker, D. T., Swan, B. D., So, R. Q., Turner, D. A., Gross, R. E., and Grill, W. M. (2017). Optimized temporal pattern of brain stimulation designed by computational evolution. *Sci. Transl. Med.* 9:eaah3532. doi: 10.1126/scitranslmed.aah3532

Brocker, D. T., Swan, B. D., Turner, D. A., Gross, R. E., Tatter, S. B., Koop, M. M., et al. (2013). Improved efficacy of temporally non-regular deep brain stimulation in Parkinson's disease. *Exp. Neurol.* 239, 60–67. doi: 10.1016/j.expneurol.2012.09.008

Brown, C. (2016). Pharmacological management of epilepsy. *Prog. Neurol. Psychiatry* 20, 27–34c. doi: 10.1002/pnp.422

Brodmann, K. (1909). *Vergleichende Lokalisationslehre der Grosshirnrinde in ihren Prinzipien dargestellt auf Grund des Zellenbaues von Dr. K. Brodmann*. Leipzig: Barth J. A. Barth.

Buyten, J. P. V., Al-Kaisy, A., Smet, I., Palmisani, S., and Smith, T. (2013). High-frequency spinal cord stimulation for the treatment of chronic back pain patients: results of a prospective multicenter European clinical study. *Neuromodulation J. Int. Neuromodulation Soc.* 16, 59–66. doi: 10.1111/ner.12006

Buzsáki, G., and Watson, B. O. (2012). Brain rhythms and neural syntax: implications for efficient coding of cognitive content and neuropsychiatric disease. *Dialogues Clin. Neurosci.* 14, 345–367. doi: 10.31887/DCNS.2012.14.4/gbuzsaki

Carlson, J. D., Cleary, D. R., Cetas, J. S., Heinricher, M. M., and Burchiel, K. J. (2010). Deep brain stimulation does not silence neurons in subthalamic nucleus in Parkinson's patients. *J. Neurophysiol.* 103, 962–967. doi: 10.1152/jn.00363.2009

Carvalho, V. R., Moraes, M. F. D., Cash, S. S., and Mendes, E. M. A. M. (2021). Active probing to highlight approaching transitions to ictal states in coupled neural mass models. *PLoS Comput. Biol.* 17:e1008377. doi: 10.1371/journal.pcbi.1008377

Castro, G. P., Medeiros, D. C., Guarnieri, L. O., Mourão, F. A. G., Pinto, H. P. P., Pereira, G. S., et al. (2017). Wistar audiogenic rats display abnormal behavioral traits associated with artificial selection for seizure susceptibility. *Epilepsy Behav.* 71, 243–249. doi: 10.1016/j.yebeh.2015.08.039

Chabardès, S., Kahane, P., Minotti, L., Koudsie, A., Hirsch, E., and Benabid, A.-L. (2002). Deep brain stimulation in epilepsy with particular reference to the subthalamic nucleus. *Epileptic Disord.* 4(Suppl. 3), S83–S93.

Chakravarthy, K., Richter, H., Christo, P. J., Williams, K., and Guan, Y. (2018). Spinal cord stimulation for treating chronic pain: reviewing preclinical and clinical data on paresthesia-free high-frequency therapy. *Neuromodulation Technol. Neural Interface* 21, 10–18. doi: 10.1111/ner.12721

Chiappalone, M., Cota, V. R., Carè, M., Di Florio, M., Beaubois, R., Buccelli, S., et al. (2022). Neuromorphic-based neuroprostheses for brain rewiring: state-of-the-art and perspectives in neuroengineering. *Brain Sci.* 12:1578. doi: 10.3390/brainsci12111578

Clifford, D. B., Olney, J. W., Maniotis, A., Collins, R. C., and Zorumski, C. F. (1987). The functional anatomy and pathology of lithium-pilocarpine and high-dose pilocarpine seizures. *Neuroscience* 23, 953–968. doi: 10.1016/0306-4522(87)90171-0

Contreras, J. A., Goñi, J., Risacher, S. L., Sporns, O., and Saykin, A. J. (2015). The structural and functional connectome and prediction of risk for cognitive impairment in older adults. *Curr. Behav. Neurosci. Rep.* 2, 234–245. doi: 10.1007/s40473-015-0056-z

Cota, V. R., and Moraes, M. F. D. (2022). Editorial: engineered neuromodulation approaches to treat neurological disorders. *Front. Neurosci.* 16:1038215. doi: 10.3389/fnins.2022.1038215

Cota, V. R., de Oliveira, J. C., Damázio, L. C. M., and Moraes, M. F. D. (2021). Nonperiodic stimulation for the treatment of refractory epilepsy: applications, mechanisms, and novel insights. *Epilepsy Behav.* 121:106609. doi: 10.1016/j.yebeh.2019.106609

Cota, V. R., Drabowski, B. M. B., de Oliveira, J. C., and Moraes, M. F. D. (2016). The epileptic amygdala: toward the development of a neural prosthesis by temporally coded electrical stimulation. *J. Neurosci. Res.* 94, 463–485. doi: 10.1002/jnr.23741

Cota, V. R., Medeiros, D. C., Vilela, M. R. S. P., Doretto, M. C., and Moraes, M. F. D. (2009). Distinct patterns of electrical stimulation of the basolateral amygdala influence pentylenetetrazole seizure outcome. *Epilepsy Behav.* 14, 26–31. doi: 10.1016/j.yebeh.2008.09.006

Cottone, C., Cancelli, A., Pasqualetti, P., Porcaro, C., Salustri, C., and Tecchio, F. (2018). A new, high-efficacy, noninvasive transcranial electric stimulation tuned to local neurodynamics. *J. Neurosci.* 38, 586–594. doi: 10.1523/JNEUROSCI.2521-16.2017

Cymerblit-Sabba, A., Schiller, M., and Schiller, Y. (2013). Termination of chemoconvulsant-induced seizures by synchronous and asynchronous electrical stimulation of the hippocampus in-vivo. *Brain Stimulat.* 6, 727–736. doi: 10.1016/j.brs.2013.03.006

Da Silva, F. L., Blanes, W., Kalitzin, S. N., Parra, J., Suffczynski, P., and Velis, D. N. (2003). Epilepsies as dynamical diseases of brain systems: basic models of the transition between normal and epileptic activity. *Epilepsia* 44, 72–83. doi: 10.1111/j.0013-9580.2003.12005.x

Daylight, E. G. (2015). Towards a historical notion of 'turing—the father of computer science.'. *Hist. Philos. Log.* 36, 205–228. doi: 10.1080/01445340.2015.1082050

de Oliveira, J. C., Drabowski, B. M. B., Rodrigues, S. M. A. F., Maciel, R. M., Moraes, M. F. D., and Cota, V. R. (2019). Seizure suppression by asynchronous non-periodic electrical stimulation of the amygdala is partially mediated by indirect desynchronization from nucleus accumbens. *Epilepsy Res.* 154, 107–115. doi: 10.1016/j.eplepsyres.2019.05.009

de Oliveira, J. C., Medeiros, D. C., de Souza E Rezende, G. H., Moraes, M. F. D., and Cota, V. R. (2014). Temporally unstructured electrical stimulation to the amygdala suppresses behavioral chronic seizures of the pilocarpine animal model. *Epilepsy Behav.* 36, 159–164. doi: 10.1016/j.yebeh.2014.05.005

Edakawa, K., Yanagisawa, T., Kishima, H., Fukuma, R., Oshino, S., Khoo, H. M., et al. (2016). Detection of epileptic seizures using phase-amplitude coupling in intracranial electroencephalography. *Sci. Rep.* 6:25422. doi: 10.1038/srep25422

Famm, K., Litt, B., Tracey, K. J., Boyden, E. S., and Slaoui, M. (2013). Drug discovery: A jump-start for electroceuticals. *Nature* 496, 159–161. doi: 10.1038/496159a

Feldman, D. E. (2012). The spike-timing dependence of plasticity. *Neuron* 75, 556–571. doi: 10.1016/j.neuron.2012.08.001

Ferrier, D. (1887). The functions of the brain. *J. Ment. Sci.* 32, 580–582. doi: 10.1192/bjp.32.140.580-a

Ferrier, D. (1890). The croonian lectures on cerebral localisation. *Br. Med. J.* 1, 1473–1479. doi: 10.1136/bmj.1.1537.1349

Finger, S. (1994). *Origins of Neuroscience: a History of Explorations into Brain Function*. New York, NY: Oxford University Press.

Fisher, R., Salanova, V., Witt, T., Worth, R., Henry, T., Gross, R., et al. (2010). Electrical stimulation of the anterior nucleus of thalamus for treatment of refractory epilepsy. *Epilepsia* 51, 899–908. doi: 10.1111/j.1528-1167.2010.02536.x

Foutz, T. J., and Wong, M. (2022). Brain stimulation treatments in epilepsy: Basic mechanisms and clinical advances. *Biomed. J.* 45, 27–37. doi: 10.1016/j.bj.2021.08.010

Freese, J. L., and Amaral, D. G. (2009). "Neuroanatomy of the primate amygdala," in *The Human Amygdala*, eds P. J. Whalen and E. A. Phelps (New York, NY: The Guilford Press), 3–42.

Freestone, D. R., Karoly, P. J., and Cook, M. J. (2017). A forward-looking review of seizure prediction. *Curr. Opin. Neurol.* 30, 167–173. doi: 10.1097/WCO.0000000000000429

Fridley, J., Thomas, J. G., Navarro, J. C., and Yoshor, D. (2012). Brain stimulation for the treatment of epilepsy. *Neurosurgical Focus* 32:E13. doi: 10.3171/2012.1.FOCUS11334

Fries, P. (2005). A mechanism for cognitive dynamics: neuronal communication through neuronal coherence. *Trends Cogn. Sci.* 9, 474–480. doi: 10.1016/j.tics.2005.08.011

Fritsch, G., and Hitzig, E. (1870). "über die elektrische Erregbarkeit des Grosshirns," *The cerebral cortex*, ed. trans. G. von Bonin (Springfield, IL: Thomas), 73–96.

Gal, A., and Marom, S. (2013). Entrainment of the intrinsic dynamics of single isolated neurons by natural-like input. *J. Neurosci.* 33, 7912–7918. doi: 10.1523/JNEUROSCI.3763-12.2013

Garcia, D. L., Wennberg, R. A., Gaetz, W., Cheyne, D., Snead, O. C., and Velazquez, J. L. P. (2005). Enhanced synchrony in epileptiform activity? local versus distant phase synchronization in generalized seizures. *J. Neurosci.* 25, 8077–8084. doi: 10.1523/JNEUROSCI.1046-05.2005

George, R., Salinsky, M., Kuzniecky, R., Rosenfeld, W., Bergen, D., Tarver, W. B., et al. (1994). Vagus nerve stimulation for treatment of partial seizures: 3. Long-term follow-up on first 67 patients exiting a controlled study. first international vagus nerve stimulation study group. *Epilepsia* 35, 637–643. doi: 10.1111/j.1528-1157.1994.tb02484.x

Gildenberg, P. L. (2006). History of electrical neuromodulation for chronic pain. *Pain Med.* 7, S7–S13. doi: 10.1111/j.1526-4637.2006.00118.x

Griffith, J. S. (1963). On the stability of brain-like structures. *Biophys. J.* 3, 299–308. doi: 10.1016/S0006-3495(63)86822-8

Grill, W. M. (2018). Temporal pattern of electrical stimulation is a new dimension of therapeutic innovation. *Curr. Opin. Biomed. Eng.* 8, 1–6. doi: 10.1016/j.cobme.2018.08.007

Grill, W. M., Snyder, A. N., and Miocinovic, S. (2004). Deep brain stimulation creates an informational lesion of the stimulated nucleus. *Neuroreport* 15, 1137–1140. doi: 10.1097/00001756-200405190-00011

Grossberg, S. (1969). Some networks that can learn, remember, and reproduce any number of complicated space-time patterns, I. *J. Math. Mech.* 19, 53–91. doi: 10.1512/iumj.1970.19.19007

Grossberg, S., and Schmajuk, N. A. (1989). Neural dynamics of adaptive timing and temporal discrimination during associative learning. *Neural Netw.* 2, 79–102. doi: 10.1016/0893-6080(89)90026-9

Guenther, K. (2016). Between clinic and experiment: wilder penfield's stimulation reports and the search for mind, 1929–55. *Can. Bull. Med. Hist.* 281–320. doi: 10.3138/cbmh.33.2.148-27012015

Hagner, M. (2012). The electrical excitability of the brain: toward the emergence of an experiment. *J. Hist. Neurosci.* 21, 237–249. doi: 10.1080/0964704X.2011.595634

Hamani, C., Ewerton, F. I. S., Bonilha, S. M., Ballester, G., Mello, L. E. A. M., and Lozano, A. M. (2004). Bilateral anterior thalamic nucleus lesions and high-frequency stimulation are protective against pilocarpine-induced seizures and status epilepticus. *Neurosurgery* 54, 191–195. doi: 10.1227/01.NEU.0000097552.31763.AE

Hasenstaub, A., Shu, Y., Haider, B., Kraushaar, U., Duque, A., and McCormick, D. A. (2005). Inhibitory postsynaptic potentials carry synchronized frequency information in active cortical networks. *Neuron* 47, 423–435. doi: 10.1016/j.neuron.2005.06.016

Heck, C. N., King-Stephens, D., Massey, A. D., Nair, D. R., Jobst, B. C., Barkley, G. L., et al. (2014). Two-year seizure reduction in adults with medically intractable partial onset epilepsy treated with responsive neurostimulation: final results of the RNS system pivotal trial. *Epilepsia* 55, 432–441. doi: 10.1111/epi.12534

Hirsch, E., Danober, L., Simler, S., Vasconcelos, A. P. D., Maton, B., Nehlig, A., et al. (1997). The amygdala is critical for seizure propagation from brainstem to forebrain. *Neuroscience* 77, 975–984. doi: 10.1016/S0306-4522(96)00503-9

Hopkins, J. L., Engel, A. K., Kiinig, P., and Singer, W. (1992). Integrator or coincidence detector? the role of the cortical neuron revisited. *Trends Neurosci.* 19, 130–137. doi: 10.1016/S0166-2236(96)80019-1

Isbister, J. B., Eguchi, A., Ahmad, N., Galeazzi, J. M., Buckley, M. J., and Stringer, S. (2018). A new approach to solving the feature-binding problem in primate vision. *Interface Focus* 8:20180021. doi: 10.1098/rsfs.2018.0021

Izhikevich, E. M. (2006). Polychronization: computation with spikes. *Neural Comput.* 18, 245–282. doi: 10.1162/089976606775093882

Jackson, J. H. (1898). "Relations of different divisions of the central neurons system to one another and to parts of the body," in *Selected writings of John Hughlings Jackson*, ed. J. Tailor (London: Hodder & Stoughton), 422–443.

Jiruska, P., Curtis, M., Jefferys, J. G., Schevon, C. A., Schiff, S. J., and Schindler, K. (2013). Synchronization and desynchronization in epilepsy: controversies and hypotheses. *J. Physiol.* 591, 787–797. doi: 10.1113/jphysiol.2012.239590

Jobe, P. C. (2003). Common pathogenic mechanisms between depression and epilepsy: an experimental perspective. *Epilepsy Behav.* 4, 14–24. doi: 10.1016/j.yebeh.2003.08.020

Jobe, P. C., Dailey, J. W., and Wernicke, J. F. (1999). A noradrenergic and serotonergic hypothesis of the linkage between epilepsy and affective disorders. *Crit. Rev. Neurobiol.* 13, 317–356. doi: 10.1615/CritRevNeurobiol.v13.i4.10

Johannessen Landmark, C., Johannessen, S. I., and Patsalos, P. N. (2020). Therapeutic drug monitoring of antiepileptic drugs: current status and future prospects. *Expert Opin. Drug Metab. Toxicol.* 16, 227–238. doi: 10.1080/17425255.2020.1724956

Kalitzin, S. N., Velis, D. N., and Silva, F. H. L. (2010). Stimulation-based anticipation and control of state transitions in the epileptic brain. *Epilepsy Behav.* 17, 310–323. doi: 10.1016/j.yebeh.2009.12.023

Kalitzin, S., Velis, D., Suffczynski, P., Parra, J., and Silva, F. L. (2005). Electrical brain-stimulation paradigm for estimating the seizure onset site and the time to ictal transition in temporal lobe epilepsy. *Clin. Neurophysiol.* 116, 718–728. doi: 10.1016/j.clinph.2004.08.021

Karoly, P. J., Ung, H., Grayden, D. B., Kuhlmann, L., Leyde, K., Cook, M. J., et al. (2017). The circadian profile of epilepsy improves seizure forecasting. *Brain* 140, 2169–2182. doi: 10.1093/brain/awx173

Kinoshita, M., Ikeda, A., Matsumoto, R., Begum, T., Usui, K., Yamamoto, J., et al. (2004). Electric stimulation on human cortex suppresses fast cortical activity and epileptic spikes. *Epilepsia* 45, 787–791. doi: 10.1111/j.0013-9580.2004.60203.x

Krauss, J. K., Lipsman, N., Aziz, T., Boutet, A., Brown, P., Chang, J. W., et al. (2021). Technology of deep brain stimulation: current status and future directions. *Nat. Rev. Neurol.* 17, 75–87. doi: 10.1038/s41582-020-00426-z

Kudela, P., Franaszczuk, P. J., and Bergey, G. K. (2003). Changing excitation and inhibition in simulated neural networks: effects on induced bursting behavior. *Biol. Cybern.* 88, 276–285. doi: 10.1007/s00422-002-0381-7

Kuhlmann, L., Karoly, P., Freestone, D. R., Brinkmann, B. H., Temko, A., Barachant, A., et al. (2018a). Epilepsyecosystem.org: crowd-sourcing reproducible seizure prediction with long-term human intracranial EEG. *Brain* 141, 2619–2630. doi: 10.1093/brain/awy210

Kuhlmann, L., Lehnertz, K., Richardson, M. P., Schelter, B., and Zaveri, H. P. (2018b). Seizure prediction — ready for a new era. *Nat. Rev. Neurol.* 14, 618–630. doi: 10.1038/s41582-018-0055-2

Kuncel, A. M., Cooper, S. E., Wolgamuth, B. R., Clyde, M. A., Snyder, S. A., Montgomery, E. B., et al. (2006). Clinical response to varying the stimulus parameters in deep brain stimulation for essential tremor. *Mov. Disord.* 21, 1920–1928. doi: 10.1002/mds.21087

Levine, D. N. (2007). Sherrington's "the integrative action of the nervous system": a centennial appraisal. *J. Neurol. Sci.* 253, 1–6. doi: 10.1016/j.jns.2006.12.002

Li, J.-J., Li, Y.-H., Gong, H.-Q., Liang, P.-J., Zhang, P.-M., and Lu, Q.-C. (2016). The spatiotemporal dynamics of phase synchronization during epileptogenesis in amygdala-kindling mice. *PLoS One* 11:e0153897. doi: 10.1371/journal.pone.0153897

Liao, X., Vasilakos, A. V., and He, Y. (2017). Small-world human brain networks: perspectives and challenges. *Neurosci. Biobehav. Rev.* 77, 286–300. doi: 10.1016/j.neubiorev.2017.03.018

Lillicrap, T. P., Santoro, A., Marris, L., Akerman, C. J., and Hinton, G. (2020). Backpropagation and the brain. *Nat. Rev. Neurosci.* 21, 335–346. doi: 10.1038/s41583-020-0277-3

Louie, K., and Wilson, M. A. (2001). Temporally structured replay of awake hippocampal ensemble activity during rapid eye movement sleep. *Neuron* 29, 145–156. doi: 10.1016/S0896-6273(01)00186-6

McCulloch, W. S., and Pitts, W. (1943). A logical calculus of the ideas immanent in nervous activity. *Bull. Math. Biophys.* 5, 115–133. doi: 10.1007/BF02478259

McIntyre, C. C., Savasta, M., Kerkerian-Le Goff, L., and Vitek, J. L. (2004). Uncovering the mechanism(s) of action of deep brain stimulation: activation, inhibition, or both. *Clin. Neurophysiol.* 115, 1239–1248. doi: 10.1016/j.clinph.2003.12.024

Medeiros, D. C., and Moraes, M. F. D. (2014). Focus on desynchronization rather than excitability: a new strategy for intraencephalic electrical stimulation. *Epilepsy Behav.* 38, 32–36. doi: 10.1016/j.yebeh.2013.12.034

Medeiros, D. C., Cota, V. R., Oliveira, A. C. P., Moreira, F. A., and Moraes, M. F. D. (2020). The endocannabinoid system activation as a neural network desynchronizing mediator for seizure suppression. *Front. Behav. Neurosci.* 14:603245. doi: 10.3389/fnbeh.2020.603245

Medeiros, D. C., Cota, V. R., Vilela, M. R. S. P., Mourão, F. A. G., Massensini, A. R., and Moraes, M. F. D. (2012). Anatomically dependent anticonvulsant properties of temporally-coded electrical stimulation. *Epilepsy Behav.* 23, 294–297. doi: 10.1016/j.yebeh.2012.01.004

Medeiros, D. C., Oliveira, L. B., Mourão, F. A. G., Bastos, C. P., Cairasco, N. G., Pereira, G. S., et al. (2014). Temporal rearrangement of pre-ictal PTZ induced spike discharges by low frequency electrical stimulation to the amygdaloid complex. *Brain Stimulat.* 7, 170–178. doi: 10.1016/j.brs.2013.11.005

Medeiros, D. C., Raspante, L. B. P., Mourão, F. A. G., Carvalho, V. R., Mendes, E. M. A. M., and Moraes, M. F. D. (2018). Deep brain stimulation probing performance is enhanced by pairing stimulus with epileptic seizure. *Epilepsy Ampmathsemicolon Behav.* 88, 380–387. doi: 10.1016/j.yebeh.2018.09.048

Mesquita, M. B. S., Medeiros, D. C., Cota, V. R., Richardson, M. P., Williams, S., and Moraes, M. F. D. (2011). Distinct temporal patterns of electrical stimulation influence neural recruitment during PTZ infusion: an fMRI study. *Prog. Biophys. Mol. Biol.* 105, 109–118. doi: 10.1016/j.pbiomolbio.2010.10.005

Mirski, M. A., Rossell, L. A., Terry, J. B., and Fisher, R. S. (1997). Anticonvulsant effect of anterior thalamic high frequency electrical stimulation in the rat. *Epilepsy Res.* 28, 89–100. doi: 10.1016/S0920-1211(97)00034-X

Molnár, Z., and Brown, R. E. (2010). Insights into the life and work of sir Charles Sherrington. *Nat. Rev. Neurosci.* 11, 429–436. doi: 10.1038/nrn2835

Moraes, M. F. D., de Castro Medeiros, D., Mourao, F. A. G., Cancado, S. A. V., and Cota, V. R. (2021). Epilepsy as a dynamical system, a most needed paradigm shift in epileptology. *Epilepsy Behav.* 121:106838. doi: 10.1016/j.yebeh.2019.106838

Moraes, M., Galvis-Alonso, O., and Garcia-Cairasco, N. (2000). Audiogenic kindling in the Wistar rat: a potential model for recruitment of limbic structures. *Epilepsy Res.* 39, 251–259. doi: 10.1016/S0920-1211(00)00107-8

Mormann, F., Andrzejak, R. G., Elger, C. E., and Lehnertz, K. (2007). Seizure prediction: the long and winding road. *Brain J. Neurol.* 130, 314–333. doi: 10.1093/brain/awl241

Morrell, M. J., and RNS System in Epilepsy Study Group (2011). Responsive cortical stimulation for the treatment of medically intractable partial epilepsy. *Neurology* 77, 1295–1304. doi: 10.1212/WNL.0b013e3182302056

Mourão, F. A. G., Lockmann, A. L. V., Castro, G. P., Medeiros, D. D. C., Reis, M. P., Pereira, G. S., et al. (2016). Triggering different brain states using asynchronous serial communication to the rat amygdala. *Cereb. Cortex* 26, 1866–1877. doi: 10.1093/cercor/bhu313

Nariai, H., Matsuzaki, N., Juhász, C., Nagasawa, T., Sood, S., Chugani, H. T., et al. (2011). Ictal high-frequency oscillations at 80-200 Hz coupled with delta phase in epileptic spasms. *Epilepsia* 52:e130-34. doi: 10.1111/j.1528-1167.2011.03263.x

Nelson, T. S., Suhr, C. L., Freestone, D. R., Lai, A., Halliday, A. J., Mclean, K. J., et al. (2011). Closed-loop seizure control with very high frequency electrical stimulation at seizure onset in the gaers model of absence epilepsy. *Int. J. Neural Syst.* 21, 163–173. doi: 10.1142/S0129065711002717

Okun, M. S., Hickey, P. T., Machado, A. G., Kuncel, A. M., and Grill, W. M. (2022). Temporally optimized patterned stimulation (TOPS§) as a therapy to personalize deep brain stimulation treatment of Parkinson's disease. *Front. Hum. Neurosci.* 16:929509. doi: 10.3389/fnhum.2022.929509

Oliveira, J. C., Maciel, R. M., Moraes, M. F. D., and Cota, V. R. (2018). Asynchronous, bilateral, and biphasic temporally unstructured electrical stimulation of amygdalae enhances the suppression of pentylenetetrazole-induced seizures in rats. *Epilepsy Res.* 146, 1–8. doi: 10.1016/j.eplepsyres.2018.07.009

Oliveira, J. P. S. E., Discacciati, V. R. P., Medeiros, D. C., Moraes, M. F. D., Pereira, G. S., França, K. L. A., et al. (2022). "In silico investigation of the effects of distinct temporal patterns of electrical stimulation to the amygdala using a network of izhikevich neurons," in *Computational Neuroscience Communications in Computer and Information Science*, eds P. R. de, A. Ribeiro, V. R. Cota, D. A. C. Barone, and A. C. M. de Oliveira (Cham: Springer International Publishing) doi: 10.1007/978-3-031-08443-0_9

Paz, J. T., and Huguenard, J. R. (2015). Microcircuits and their interactions in epilepsy: is the focus out of focus? *Nat. Neurosci.* 18, 351–359. doi: 10.1038/nn.3950

Pearce, J. M. S. (1997). Marshall hall and the concepts of reflex action. *J. Neurol. Neurosurg. Psychiatry* 62, 228–228. doi: 10.1136/jnnp.62.3.228

Penfield, W., and Boldrey, E. (1937). Somatic motor and sensory representation in the cerebral cortex of man as studied by electrical stimulation. *Brain* 60, 389–443. doi: 10.1093/brain/60.4.389

Penfield, W., and Jasper, H. (1954). *Epilepsy and the Functional Anatomy of the Human Brain*. Oxford: England: Little, Brown & Co. doi: 10.1097/00007611-195407000-00024

Persichilli, G., Grifoni, J., Pagani, M., Bertoli, M., Gianni, E., L'Abbate, T., et al. (2022). Sensorimotor interaction against trauma. *Front. Neurosci.* 16:913410. doi: 10.3389/fnins.2022.913410

Persinger, M. A., Makarec, K., and Bradley, J. C. (1988). Characteristics of limbic seizures evoked by peripheral injections of lithium and pilocarpine. *Physiol. Behav.* 44, 27–37. doi: 10.1016/0031-9384(88)90342-3

Petersen, P. C., and Buzsáki, G. (2020). Cooling of medial septum reveals theta phase lag coordination of hippocampal cell assemblies. *Neuron* 107, 731-744.e3. doi: 10.1016/j.neuron.2020.05.023

Prager, E. M., Aroniadou-Anderjaska, V., Almeida-Suhett, C. P., Figueiredo, T. H., Apland, J. P., Rossetti, F., et al. (2014). The recovery of acetylcholinesterase activity and the progression of neuropathological and pathophysiological alterations in the rat basolateral amygdala after soman-induced status epilepticus: relation to anxiety-like behavior. *Neuropharmacology* 81:64. doi: 10.1016/j.neuropharm.2014.01.035

Prager, E. M., Bergstrom, H. C., Wynn, G. H., and Braga, M. F. M. (2016). The basolateral amygdala γ-aminobutyric acidergic system in health and disease. *J. Neurosci. Res.* 94, 548–567. doi: 10.1002/jnr.23690

Price, B. H., and Gavornik, J. P. (2022). Efficient temporal coding in the early visual system: existing evidence and future directions. *Front. Comput. Neurosci.* 16:929348. doi: 10.3389/fncom.2022.929348

Quinkert, A. W., Schiff, N. D., and Pfaff, D. W. (2010). Temporal patterning of pulses during deep brain stimulation affects central nervous system arousal. *Behav. Brain Res.* 214, 377–385. doi: 10.1016/j.bbr.2010.06.009

Ranck, J. B. J. (1975). Which elements are excited in electrical stimulation of mammalian central nervous system: a review. *Brain Res.* 98, 417–440. doi: 10.1016/0006-8993(75)90364-9

Réboli, L. A., Maciel, R. M., de Oliveira, J. C., Moraes, M. F. D., Tilelli, C. Q., and Cota, V. R. (2022). Persistence of neural function in animals submitted to seizure-suppressing scale-free nonperiodic electrical stimulation applied to the amygdala. *Behav. Brain Res.* 426:113843. doi: 10.1016/j.bbr.2022.113843

Reinhart, R. M. G. (2022). Synchronizing neural rhythms. *Science* 377, 588–589. doi: 10.1126/science.add4834

Reinhart, R. M. G., and Nguyen, J. A. (2019). Working memory revived in older adults by synchronizing rhythmic brain circuits. *Nat. Neurosci.* 22, 820–827. doi: 10.1038/s41593-019-0371-x

Rosenblatt, F. (1958). The perceptron: a probabilistic model for information storage and organization in the brain. *Psychol. Rev.* 65, 386–408. doi: 10.1037/h0042519

Ryvlin, P., Rheims, S., Hirsch, L. J., Sokolov, A., and Jehi, L. (2021). Neuromodulation in epilepsy: state-of-the-art approved therapies. *Lancet Neurol.* 20, 1038–1047. doi: 10.1016/S1474-4422(21)00300-8

Sander, J. W. A. S. (1997). The epidemiology of the epilepsies: future directions. *Epilepsia* 38, 614–618. doi: 10.1111/j.1528-1157.1997.tb01148.x

Santos-Valencia, F., Almazán-Alvarado, S., Rubio-Luviano, A., Valdés-Cruz, A., Magdaleno-Madrigal, V. M., and Martínez-Vargas, D. (2019). Temporally irregular electrical stimulation to the epileptogenic focus delays epileptogenesis in rats. *Brain Stimulat.* 12, 1429–1438. doi: 10.1016/j.brs.2019.07.016

Scarsi, F., Tessadori, J., Chiappalone, M., and Pasquale, V. (2017). Investigating the impact of electrical stimulation temporal distribution on cortical network responses. *BMC Neurosci.* 18:49. doi: 10.1186/s12868-017-0366-z

Sherrington, C. S. (1906). *The Integrative Action of the Nervous System*. New Haven, CT: Yale University Press.

Singer, W., and Gray, C. M. (1995). Visual feature integration and the temporal correlation hypothesis. *Ann. Rev. Neurosci.* 18, 555–586. doi: 10.1146/annurev.ne.18.030195.003011

Spadone, S., Betti, V., Sestieri, C., Pizzella, V., Corbetta, M., and Penna, S. D. (2021). Spectral signature of attentional reorienting in the human brain. *NeuroImage* 244:118616. doi: 10.1016/j.neuroimage.2021.118616

Sunderam, S., Gluckman, B., Reato, D., and Bikson, M. (2010). Toward rational design of electrical stimulation strategies for epilepsy control. *Epilepsy Behav.* 17, 6–22. doi: 10.1016/j.yebeh.2009.10.017

Tass, P. (1996). Resetting biological oscillators—a stochastic approach. *J. Biol. Phys.* 22, 27–64. doi: 10.1007/BF00383820

Tass, P. A. (2001a). Desynchronizing double-pulse phase resetting and application to deep brain stimulation. *Biol. Cybern.* 85, 343–354. doi: 10.1007/s004220100268

Tass, P. A. (2001b). Effective desynchronization by means of double-pulse phase resetting. *Europhys. Lett.* 53:15. doi: 10.1209/epl/i2001-00117-6

Tass, P. A. (2002a). Effective desynchronization with a stimulation technique based on soft phase resetting. *Europhys. Lett.* 57:164. doi: 10.1209/epl/i2002-00557-x

Tass, P. A. (2002b). Stimulus-locked transient phase dynamics, synchronization and desynchronization of two oscillators. *Europhys. Lett.* 59:199. doi: 10.1209/epl/i2002-00226-8

Tass, P. A. (2003). A model of desynchronizing deep brain stimulation with a demand-controlled coordinated reset of neural subpopulations. *Biol. Cybern.* 89, 81–88. doi: 10.1007/s00422-003-0425-7

Tass, P. A., and Majtanik, M. (2006). Long-term anti-kindling effects of desynchronizing brain stimulation: a theoretical study. *Biol. Cybern.* 94, 58–66. doi: 10.1007/s00422-005-0028-6

Tass, P. A., Qin, L., Hauptmann, C., Dovero, S., Bezard, E., Boraud, T., et al. (2012). Coordinated reset has sustained aftereffects in Parkinsonian monkeys. *Ann. Neurol.* 72, 816–820. doi: 10.1002/ana.23663

Tehovnik, E. J. (1996). Electrical stimulation of neural tissue to evoke behavioral responses. *J. Neurosci. Methods* 65, 1–17. doi: 10.1016/0165-0270(95)00131-X

Terra, H. C. B., Borges, F. S., Moraes, M. F. D., and Cota, V. R. (2022). "Implementation of intra and extracellular nonperiodic scale-free stimulation in silico for the NEURON simulator," in *Computational Neuroscience Communications in Computer and Information Science*, eds P. R. A. Ribeiro, V. R. Cota, D. A. C. Barone, and A. C. M. Oliveira (Cham: Springer International Publishing) doi: 10.1007/978-3-031-08443-0_8

Theodore, W. H., and Fisher, R. S. (2004). Brain stimulation for epilepsy. *Lancet Neurol.* 3, 111–118. doi: 10.1016/S1474-4422(03)00664-1

Tiede, J., Brown, L., Gekht, G., Vallejo, R., Yearwood, T., and Morgan, D. (2013). Novel spinal cord stimulation parameters in patients with predominant back pain. *Neuromodulation J. Int. Neuromodulation Soc.* 16, 370–375. doi: 10.1111/ner.12032

Truccolo, W., Donoghue, J. A., Hochberg, L. R., Eskandar, E. N., Madsen, J. R., Anderson, W. S., et al. (2011). Single-neuron dynamics in human focal epilepsy. *Nat. Neurosci.* 14, 635–641. doi: 10.1038/nn.2782

Turski, W. A., Cavalheiro, E. A., Schwarz, M., Czuczwar, S. J., Kleinrok, Z., and Turski, L. (1983). Limbic seizures produced by pilocarpine in rats: behavioural, electroencephalographic and neuropathological study. *Behav. Brain Res.* 9, 315–335. doi: 10.1016/0166-4328(83)90136-5

Uhlhaas, P. J., and Singer, W. (2006). Neural synchrony in brain disorders: relevance for cognitive dysfunctions and pathophysiology. *Neuron* 52, 155–168. doi: 10.1016/j.neuron.2006.09.020

Uhlhaas, P. J., Linden, D. E. J., Singer, W., Haenschel, C., Lindner, M., Maurer, K., et al. (2006). Dysfunctional long-range coordination of neural activity during gestalt perception in schizophrenia. *J. Neurosci.* 26:8168. doi: 10.1523/JNEUROSCI.2002-06.2006

Varela, F., Lachaux, J.-P., Rodriguez, E., and Martinerie, J. (2001). The brainweb: phase synchronization and large-scale integration. *Nat. Rev. Neurosci.* 2, 229–239. doi: 10.1038/35067550

Velasco, F., Saucedo-Alvarado, P. E., Vazquez-Barron, D., Trejo, D., and Velasco, A. L. (2022). Deep brain stimulation for refractory temporal lobe epilepsy. Current Status and Future Trends. *Front. Neurol.* 13:796846. doi: 10.3389/fneur.2022.796846

Vida, I., Bartos, M., and Jonas, P. (2006). Shunting inhibition improves robustness of gamma oscillations in hippocampal interneuron networks by homogenizing firing rates. *Neuron* 49, 107–117. doi: 10.1016/j.neuron.2005.11.036

von der Malsburgl, C. (1994). "The correlation theory of brain function," in *Models of Neural Networks. Physics of Neural Networks*, eds Domany, E., van Hemmen, J.L., Schulten, K (New York, NY: Springer) doi: 10.1007/978-1-4612-4320-5_2

Vonck, K., Boon, P., Achten, E., De Reuck, J., and Caemaert, J. (2002). Long-term amygdalohippocampal stimulation for refractory temporal lobe epilepsy. *Ann. Neurol.* 52, 556–565. doi: 10.1002/ana.10323

Vonck, K., Boon, P., Claeys, P., Dedeurwaerdere, S., Achten, R., and Van Roost, D. (2005). Long-term deep brain stimulation for refractory temporal lobe epilepsy. *Epilepsia* 46(Suppl. 5), 98–99. doi: 10.1111/j.1528-1167.2005.01016.x

Vonck, K., Boon, P., Goossens, L., Dedeurwaerdere, S., Claeys, P., Gossiaux, F., et al. (2004). Neurostimulation for refractory epilepsy. *Acta Neurol. Belg.* 103, 213–217.

Wang, J., Nebeck, S., Muralidharan, A., Johnson, M. D., Vitek, J. L., and Baker, K. B. (2016). Coordinated reset deep brain stimulation of subthalamic nucleus produces

long-lasting, dose-dependent motor improvements in the 1-Methyl-4-phenyl-1,2,3,6-tetrahydropyridine non-human primate model of parkinsonism. *Brain Stimulat.* 9, 609–617. doi: 10.1016/j.brs.2016.03.014

Womelsdorf, T., Schoffelen, J.-M., Oostenveld, R., Singer, W., Desimone, R., Engel, A. K., et al. (2007). Modulation of neuronal interactions through neuronal synchronization. *Science* 316, 1609–1612. doi: 10.1126/science.1139597

Wyckhuys, T., Boon, P., Raedt, R., Van Nieuwenhuyse, B., Vonck, K., and Wadman, W. (2010). Suppression of hippocampal epileptic seizures in the kainate rat by poisson distributed stimulation. *Epilepsia* 51, 2297–2304. doi: 10.1111/j.1528-1167.2010.02750.x

Yu, T., Wang, X., Li, Y., Zhang, G., Worrell, G., Chauvel, P., et al. (2018). High-frequency stimulation of anterior nucleus of thalamus desynchronizes epileptic network in humans. *Brain* 141, 2631–2643. doi: 10.1093/brain/awy187

Zhang, D. W., Moraidis, A., and Klingberg, T. (2022). Individually tuned theta HD-tACS improves spatial performance. *Brain Stimulat.* 15, 1439–1447. doi: 10.1016/j.brs.2022.10.009

frontiers | Frontiers in Neuroinformatics

TYPE Review
PUBLISHED 21 June 2023
DOI 10.3389/fninf.2023.1156818

OPEN ACCESS

EDITED BY
Hemant Bokil,
Boston Scientific, United States

REVIEWED BY
J. Luis Lujan,
Mayo Clinic, United States
Anders J. Asp,
Mayo Clinic, United States

*CORRESPONDENCE
J. Nicole Bentley
✉ nbentl@uab.edu

RECEIVED 01 February 2023
ACCEPTED 06 June 2023
PUBLISHED 21 June 2023

CITATION
Najera RA, Mahavadi AK, Khan AU, Boddeti U, Del Bene VA, Walker HC and Bentley JN (2023) Alternative patterns of deep brain stimulation in neurologic and neuropsychiatric disorders. *Front. Neuroinform.* 17:1156818. doi: 10.3389/fninf.2023.1156818

Alternative patterns of deep brain stimulation in neurologic and neuropsychiatric disorders

Ricardo A. Najera[1], Anil K. Mahavadi[1], Anas U. Khan[1], Ujwal Boddeti[2], Victor A. Del Bene[3], Harrison C. Walker[3] and J. Nicole Bentley[1]*

[1]Department of Neurosurgery, University of Alabama at Birmingham, Birmingham, AL, United States, [2]Department of Neurosurgery, University of Maryland School of Medicine, Baltimore, MD, United States, [3]Department of Neurology, University of Alabama at Birmingham, Birmingham, AL, United States

Deep brain stimulation (DBS) is a widely used clinical therapy that modulates neuronal firing in subcortical structures, eliciting downstream network effects. Its effectiveness is determined by electrode geometry and location as well as adjustable stimulation parameters including pulse width, interstimulus interval, frequency, and amplitude. These parameters are often determined empirically during clinical or intraoperative programming and can be altered to an almost unlimited number of combinations. Conventional high-frequency stimulation uses a continuous high-frequency square-wave pulse (typically 130–160 Hz), but other stimulation patterns may prove efficacious, such as continuous or bursting theta-frequencies, variable frequencies, and coordinated reset stimulation. Here we summarize the current landscape and potential clinical applications for novel stimulation patterns.

KEYWORDS

theta-burst stimulation, deep brain stimulation, coordinated reset stimulation (CRS), paired pulses, closed-loop, interleaved stimulation, neuromodulation, cycling stimulation

Introduction

Deep brain stimulation (DBS) uses implantable depth electrodes to modulate neuronal firing in subcortical structures, eliciting downstream effects in human brain circuits (Figure 1). Intraoperative placement is followed by device programming where parameters such as pulse width, interstimulus interval (ISI), frequency, and amplitude are titrated to improve pathologic symptoms and avoid adverse side effects. Current DBS applications target motor symptoms of Parkinson's disease (PD), essential tremor (ET), and various forms of dystonia as well as neuropsychiatric symptoms of treatment-resistant obsessive-compulsive disorder (OCD), Tourette syndrome (TS), and treatment-resistant depression (TRD) with continuous high-frequency stimulation (HFS; typically, 130–160 Hz) (Figure 2). Although its exact mechanism of action is unknown, numerous theories exist. Some studies suggest that HFS may exert its effects *via* desynchronization or reorganization of pathologic network oscillations (Wilson and Moehlis, 2015; Ozturk et al., 2021). Similarly, Rosenbaum et al. (2014) theorized that HFS works through short-term depression and decoupling of specific circuits. Other groups have theorized that HFS directly inhibits neural activity (Benazzouz and Hallett, 2000; Jensen and Durand, 2009), while some suggest the opposite,

that it acts through direct excitation of neural activity (Hashimoto et al., 2003; McIntyre et al., 2004). Another theory is that HFS introduces an "information lesion," producing similar effects to neural ablation that is also used to treat the same disease processes (e.g., PD, OCD, etc.) (Grill et al., 2004; Agnesi et al., 2013; Lowet et al., 2022), however, to date, there is no single accepted theory on the mechanism of action of HFS and further work is required to elucidate its mechanism (Hammond et al., 2008; Lozano et al., 2019).

While the benefits of HFS are well-established for motor outcomes, its impact on cognitive control is less clear. Cernera et al. (2019) reviewed studies of how DBS impacts various aspects of cognitive function and found heterogenous results within and between neurocognitive metrics based on sample size, DBS target, and disease pathology. General trends suggested declines in verbal fluency, assessed by various measures such as "phonemic fluency" (ability to recall words starting with a specific letter) and "semantic fluency" (ability to recall words related to a certain category of knowledge). These declines occurred regardless of whether the DBS target was the subthalamic nucleus (STN), globus pallidus interna (GPi), or various thalamic nuclei (Ostrem et al., 2011; Pedrosa et al., 2014; Dinkelbach et al., 2015). Other global metrics such as mini-mental state examination (MMSE) or measures of executive function such as Wisconsin Card Sorting Test (WCST) have yielded mixed results (Cernera et al., 2019). In contrast, STN low-frequency stimulation (LFS) in the theta-range has been shown to improve VF in PD patients (Lee et al., 2021). Negative impacts of HFS on verbal fluency and other aspects of cognitive function challenge the notion of expanding DBS or other neuromodulation therapies for cognitive dysfunction in patients with movement disorders and other complex neuropsychiatric diseases.

These relative shortcomings of HFS, as well as a need to avoid sensorimotor side effects, have prompted investigation of non-continuous, or "patterned," stimulation paradigms such as theta burst stimulation (TBS) (Titiz et al., 2017; Horn et al., 2020), paired pulse stimulation (Birdno et al., 2007; Awad et al., 2021), variable frequency stimulation (VFS) (Jia et al., 2015; Zhang et al., 2019), interleaved stimulation (ILS) (Barbe et al., 2014; Kern et al., 2018), burst cycling stimulation (Velasco et al., 2007; Kuncel et al., 2012), coordinated reset stimulation (CR-DBS) (Adamchic et al., 2014), temporally optimized stimulation (Brocker et al., 2017; Okun et al., 2022), and adaptive, or "closed-loop" stimulation (aDBS/CL-DBS) (Little et al., 2016a; Piña-Fuentes et al., 2019) as alternatives. These paradigms were derived either from more physiologic patterns of neuronal firing or feedback-based systems that were computationally designed to better disrupt pathologic circuits. In this review, we provide an overview of alternative stimulation patterns and their potential applications.

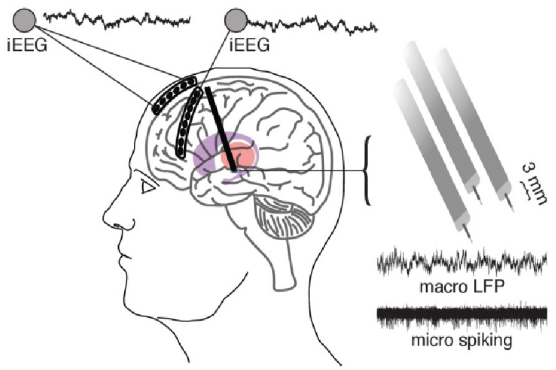

FIGURE 1
A standard DBS setup including the use of a six-contact ECoG strip over anterior PFC and eight-contact strip over lateral PFC which can be used to simultaneously record and stimulate from the DBS electrodes. DBS electrodes in this case are 3 separate macro/micro pairs which allow the recording of LFP (macro) and action potentials (micro). Adapted from Zavala et al. (2017).

Methods

We conducted PubMed searches in November 2022 (TBS, paired pulse, VFS, CR-DBS, aDBS) and March 2023 (ILS,

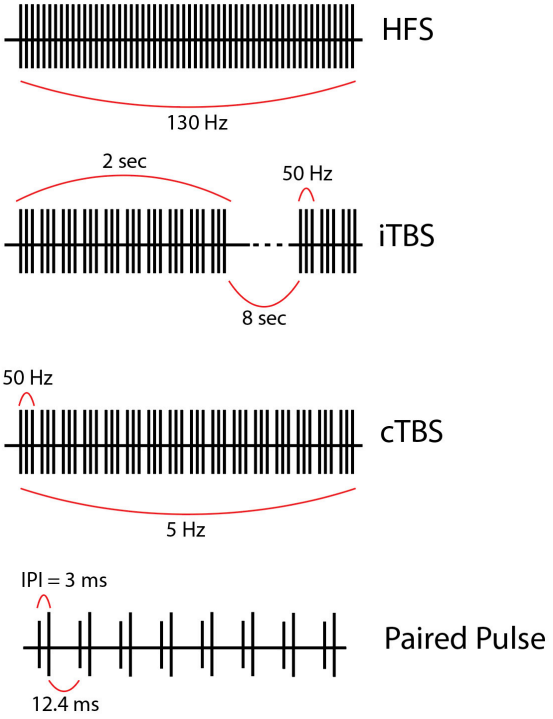

FIGURE 2
(First row) High frequency stimulation (HFS) is the current gold-standard and consists of continuous regular pulses with equal spacing at a high frequency (in this case 130 Hz). **(Second row)** Intermittent theta-burst stimulation (iTBS) usually given as 3 pulses at 50 Hz grouped into bursts delivered at a theta frequency (5 Hz) within a train. Each train lasts 2 s and contains 10 bursts. Trains are separated by 8 s intervals in this example but could be longer or shorter. **(Third row)** Continuous theta burst stimulation (cTBS) is like iTBS in that stimulation is delivered as three 50-Hz pulses grouped into bursts which are delivered at a theta frequency. However, the trains are not separated by a long (8 s) period. Instead, the stimulation is one long train. **(Fourth row)** Paired pulse stimulation utilizes biphasic paired pulses separated by short interstimulus intervals (ISI), the time from the first to the second stimulus within a single paired pulse (ISI = 3 ms in this example, but this value varies). Of note, the stimulation parameters used to create the figures for each alternative pattern of stimulation presented here are examples of possible parameters; however, these vary greatly across studies.

burst cycling, temporally optimized stimulation) to review the existing literature on alternative patterns of DBS. Search terms included: TBS {[("Deep Brain Stimulation"[Mesh]) OR ("Deep Brain Stimulation")] AND [("theta burst stimulation") OR ("intermittent theta burst") OR ("intermittent theta burst stimulation") OR ("continuous theta burst stimulation") OR ("continuous theta burst") OR ("iTBS") OR ("cTBS") OR ("theta burst")]}; paired pulse {[("Deep Brain Stimulation"[Mesh]) OR ("Deep Brain Stimulation")] AND [("paired pulse stimulation") OR ("paired pulse")]}; VFS {[("Deep Brain Stimulation"[Mesh]) OR ("Deep Brain Stimulation")] AND [("variable frequency stimulation") OR ("variable frequency")]}; ILS {[("Deep Brain Stimulation"[Mesh]) OR ("Deep Brain Stimulation")] AND [("interleaving") OR ("interleaved stimulation")]}; burst cycling {[("Deep Brain Stimulation"[Mesh]) OR ("Deep Brain Stimulation")] AND [("cycling") OR ("cyclical stimulation") OR ("burst cycling") OR ("cycling stimulation")]}; CR-DBS {[("Deep Brain Stimulation"[Mesh]) OR ("Deep Brain Stimulation")] AND [("coordinated reset stimulation") OR ("coordinated reset") OR ("CR-DBS")]}; temporally optimized stimulation {[("Deep Brain Stimulation"[Mesh]) OR ("Deep Brain Stimulation")] AND [("temporally optimized stimulation") OR ("temporally optimized patterned stimulation")]}; aDBS {[("Deep Brain Stimulation"[Mesh]) OR ("Deep Brain Stimulation")] AND [("closed loop stimulation") OR ("closed loop") OR ("closed-loop") OR ("adaptive stimulation") OR ("adaptive DBS") OR ("aDBS") OR ("adaptive deep brain stimulation") OR ("closed-loop stimulation")]}.

Studies meeting these search criteria with original clinical data on human subjects undergoing DBS were included. Exclusion criteria included animal studies, computational models, reviews, non-DBS studies (i.e., transcranial magnetic stimulation, responsive neurostimulation), DBS studies using only HFS and not the alternative pattern of interest, and non-English manuscripts. Abstracts and full texts were manually screened by a single author using the inclusion and exclusion criteria mentioned above. Our goals were to qualitatively review the current literature on alternative neuromodulation techniques, and therefore we did not utilize Preferred Reporting Items for Systematic Reviews and Meta-Analyses (PRISMA) guidelines.

Results

Literature search

Our literature search of TBS yielded 29 studies, six of which were included (Miller et al., 2015; Titiz et al., 2017; Kim et al., 2018; Bentley et al., 2020; Horn et al., 2020; Sáenz-Farret et al., 2021). Of the excluded studies, 11 were reviews, seven were non-human animal studies, three were TMS studies without DBS, and two were editorials or commentaries with no original clinical data. The paired pulse search yielded 28 studies, of which three were included (Baker et al., 2002; Birdno et al., 2007; Awad et al., 2021). Of the excluded studies, nine were non-human animal studies, six did not use paired pulse stimulation, five were reviews, and five were TMS studies without DBS. The search for VFS resulted in 12 studies, five of which were included (Jia et al., 2015, 2017, 2018; Zhang et al., 2019; Chang et al., 2021). Of the excluded studies, two used stimulation modalities other than DBS (e.g., TMS), two were protocols for upcoming studies with no original clinical data, one was a review, one was a non-human animal study, and one did not utilize VFS. For ILS, our search yielded 27 results, of which 16 were included (Wojtecki et al., 2011; Baumann et al., 2012; Kovács et al., 2012; Barbe et al., 2014; Miocinovic et al., 2014; Ramirez-Zamora et al., 2015; Zhang et al., 2016, 2018; Kern et al., 2018; Shu et al., 2018; Aquino et al., 2019; França et al., 2019; Karl et al., 2019, 2020; Goftari et al., 2020; Zafar et al., 2021). Of the excluded studies, five were reviews, three did not use ILS, one was *in silico* (i.e., no human subjects), one was a video, and one was not in English. For burst cycling, the search found 32 studies, of which 14 were included (Montgomery, 2005; Velasco et al., 2007; Tai et al., 2011; Kuncel et al., 2012; Min et al., 2013; Boongird et al., 2016; Huang et al., 2019; Enatsu et al., 2020; Kaufmann et al., 2020; Dayal et al., 2021; Vázquez-Barrón et al., 2021; Wong et al., 2021; Dalic et al., 2022; Loeffler et al., 2022). Of the excluded studies, five did not report clinical outcomes (e.g., imaging study with fMRI), four did not use burst cycling, four did not use DBS, three were reviews, one was a conceptual study with no human subjects, and one combined VNS and DBS. For CR-DBS, our search found 32 studies, but only one was included (Adamchic et al., 2014). Of the excluded studies, 21 tested computational or theoretical models of coordinated reset, six were non-human animal studies, two were reviews, and two used stimulation modalities other than DBS (e.g., TMS). For temporally optimized stimulation, our search yielded 93 results, of which two were included (Brocker et al., 2017; Okun et al., 2022). Of those excluded, 25 were reviews, 21 did not utilize temporally optimized stimulation, 15 did not use DBS, 13 were animal studies, nine did not provide clinical outcomes, seven were computational models, and one was theoretical/conceptual with no human subjects. Finally, our literature search of aDBS yielded 576 studies, of which 31 were included (Little et al., 2013, 2016a,b; Rosa et al., 2015, 2017; Malekmohammadi et al., 2016; Cagnan et al., 2017; Herron et al., 2017a; Piña-Fuentes et al., 2017, 2019, 2020a,b; Tinkhauser et al., 2017; Arlotti et al., 2018, 2021; Swann et al., 2018; Velisar et al., 2019; Castaño-Candamil et al., 2020; Ferleger et al., 2020; He et al., 2020; Opri et al., 2020; Petrucci et al., 2020; Gilron et al., 2021; Johnson et al., 2021; Louie et al., 2021; Molina et al., 2021; Nakajima et al., 2021; Sasaki et al., 2021; Scangos et al., 2021; Cagle et al., 2022; Sarikhani et al., 2022). Of the excluded studies, 180 were reviews, 139 did not use closed-loop systems, 112 tested purely theoretical or computational models of closed-loop stimulation, 51 were non-human animal studies, seven explored stimulation modalities other than DBS (e.g., TMS), and 56 were excluded for various other reasons (e.g., editorials, commentaries, study protocols, non-English language studies). Results from the literature search are summarized in **Table 1**.

Theta burst stimulation

TBS began in the context of transcranial magnetic stimulation, most notably when Huang et al. applied repetitive TMS (rTMS) to modulate motor networks. TBS can be delivered in a continuous or intermittent fashion (cTBS or iTBS), consisting of repeated trains

TABLE 1 Literature review of alternative patterns of stimulation.

Author (Year)	*N*	Diagnosis	Pattern of stimulation
Miller et al. (2015)	4	Epilepsy	TBS
Titiz et al. (2017)	13	Epilepsy	TBS
Kim et al. (2018)	4	Epilepsy	TBS
Horn et al. (2020)	17	PD	TBS
Bentley et al. (2020)	7	PD	TBS
Sáenz-Farret et al. (2021)	10	PD, ET, Dystonia	TBS
Baker et al. (2002)	5	PD, Epilepsy	Paired pulse
Birdno et al. (2007)	5	ET	Paired pulse
Awad et al. (2021)	17	PD, ET	Paired pulse
Adamchic et al. (2014)	6	PD	CR-DBS
Jia et al. (2015)	1	PD	VFS
Jia et al. (2017)	1	PD	VFS
Jia et al. (2018)	4	PD	VFS
Zhang et al. (2019)	1	PD	VFS
Chang et al. (2021)	1	PD	VFS
Wojtecki et al. (2011)	1	PD	ILS
Baumann et al. (2012)	1	PD, ET	ILS
Kovács et al. (2012)	4	Dystonia	ILS
Miocinovic et al. (2014)	3	PD	ILS
Barbe et al. (2014)	10	ET	ILS
Ramirez-Zamora et al. (2015)	9	PD	ILS
Zhang et al. (2016)	12	PD	ILS
Kern et al. (2018)	50	PD, ET, Dystonia	ILS
Shu et al. (2018)	1	Meige syndrome	ILS
Zhang et al. (2018)	1	Dystonia	ILS
Aquino et al. (2019)	20	PD	ILS
Karl et al. (2019)	76	PD	ILS
França et al. (2019)	17	PD	ILS
Karl et al. (2020)	20	PD	ILS
Goftari et al. (2020)	1	PD	ILS
Zafar et al. (2021)	19	PD	ILS
Montgomery (2005)	7	PD	Burst cycling
Velasco et al. (2007)	22	Epilepsy	Burst cycling
Tai et al. (2011)	1	Dystonia	Burst cycling
Kuncel et al. (2012)	10	ET	Burst cycling
Min et al. (2013)	2	Epilepsy	Burst cycling
Boongird et al. (2016)	1	Epilepsy	Burst cycling
Huang et al. (2019)	3	Chronic Pain	Burst cycling
Kaufmann et al. (2020)	23	Epilepsy	Burst cycling
Enatsu et al. (2020)	3	PD	Burst cycling
Wong et al. (2021)	10	PD	Burst cycling
Dayal et al. (2021)	6	PD, Progressive Supranuclear Palsy	Burst cycling
Vázquez-Barrón et al. (2021)	6	Epilepsy	Burst cycling
Dalic et al. (2022)	20	Epilepsy	Burst cycling
Loeffler et al. (2022)	1	Spinocerebellar Ataxia	Burst cycling
Brocker et al. (2017)	26	PD	TOPS
Okun et al. (2022)	8	PD	TOPS
Little et al. (2013)	8	PD	aDBS
Rosa et al. (2015)	1	PD	aDBS
Little et al. (2016a)	4	PD	aDBS
Malekmohammadi et al. (2016)	5	PD	aDBS
Little et al. (2016b)	10	PD	aDBS
Cagnan et al. (2017)	9	ET, Dystonia	aDBS
Tinkhauser et al. (2017)	13*	PD	aDBS
Herron et al. (2017a)	1	ET	aDBS
Rosa et al. (2017)	10	PD	aDBS
Piña-Fuentes et al. (2017)	1	PD	aDBS
Arlotti et al. (2018)	13	PD	aDBS
Swann et al. (2018)	2	PD	aDBS
Piña-Fuentes et al. (2019)	13	PD, Dystonia	aDBS
Velisar et al. (2019)	13	PD	aDBS
He et al. (2020)	3	ET	aDBS
Petrucci et al. (2020)	1	PD	aDBS
Piña-Fuentes et al. (2020a)	7	Dystonia	aDBS
Piña-Fuentes et al. (2020b)	13	PD	aDBS
Castaño-Candamil et al. (2020)	3	ET	aDBS
Opri et al. (2020)	3	ET	aDBS
Ferleger et al. (2020)	2	ET	aDBS
Sasaki et al. (2021)	12	PD	aDBS
Louie et al. (2021)	16	PD	aDBS
Molina et al. (2021)	5	PD	aDBS
Gilron et al. (2021)	5	PD	aDBS
Scangos et al. (2021)	1	TRD	aDBS
Johnson et al. (2021)	1	Dystonia	aDBS
Arlotti et al. (2021)	3	PD	aDBS
Nakajima et al. (2021)	1	PD	aDBS
Sarikhani et al. (2022)	15	ET, PD	aDBS
Cagle et al. (2022)	4	TS	aDBS

*Some patients included in other Little et al. studies.

of 5 Hz bursts, each consisting of three pulses at 50 Hz. In cTBS, these bursts occur regularly at 5 Hz intervals, whereas iTBS consists of repeated trains of 5 Hz bursts for 2 s followed by an 8-s pause interval (**Figure 2**) (Huang et al., 2005).

Since then, TBS has been applied successfully in several neurologic disorders and has been shown to modulate neuronal activity and associated cognitive functions. Our group found that subcortical iTBS can evoke theta oscillatory activity, known to be important in cognitive domains such as decision making and memory (Zavala et al., 2017; Jones et al., 2020; Vivekananda et al., 2021; Zeng et al., 2021; Chen et al., 2022), in connected dorsolateral prefrontal cortex (Bentley et al., 2020). Others expanded on this and found that cortical TBS evokes frequency-specific oscillations (Solomon et al., 2021), such that 5 Hz TBS maximally increases 5 Hz power. Behavioral modulation with TBS is evident with studies showing improvements in visual-spatial memory with fornix stimulation (Miller et al., 2015) and declarative memory with entorhinal stimulation (Titiz et al., 2017). Titiz et al. additionally states that delivering stimulation through microwires as opposed to large DBS stimulation electrodes can yield improved outcomes in various cognitive functions such as face categorization and learning rate during reinforcement learning. Kim et al. (2018) found differential effects on which components of memory were recalled by identifying and stimulating network nodes that were involved in these processes using theta coherence as a marker. For example, they were able to specifically impair ability to recall spatial details of a memory while sparing recall of temporal details.

Paired-pulse stimulation

Paired stimulus pulses have been used for decades to investigate neural refractoriness, augmentation, and plasticity (Zucker and Regehr, 2002; Bueno-Junior and Leite, 2018). These paradigms typically consist of a "conditioning" pulse followed by a "test" pulse separated by a specific ISI (**Figure 2**). The goal is to record short-term changes in neural activities that propagate through the engaged network. At certain ISIs, paired pulses likely increase presynaptic influx of calcium ions (Ca^{2+}), and, in turn, enhance secretory exocytosis of neurotransmitters into the synaptic cleft (Zucker and Regehr, 2002). Paired pulses can be studied rapidly and elicit diverse neural responses, such that they are a versatile tool to study network dynamics and mechanisms of action in various circuits of interest (Paek et al., 2013), including the STN, GPi (Baker et al., 2002; Yamawaki et al., 2012; Awad et al., 2020; Campbell et al., 2022), and the ventrolateral thalamus (Anderson et al., 2006; Birdno et al., 2007).

Baker et al. (2002) demonstrated that paired-pulse stimulation is feasible in humans in both PD and drug-resistant epilepsy (n = 4), using externalized DBS leads and custom external pulse generators. Awad et al. (2021) investigated the mechanism of action of DBS using paired pulses in PD (n = 8) and essential tremor (ET; n = 6). The authors validated the neural origin of short- and long-latency tissue responses and suggested that paired DBS pulses increase local tissue electrophysiologic synchrony. Specifically, they observed that certain properties (e.g., long latency, amplitude) of later oscillatory response [i.e., evoked resonant neural activity (ERNA)] mirrored properties consistent with orthodromic synaptic activity and vesicle release. Moreover, ERNA was faster at specific ISIs (~5–10 ms), which corresponded with the timing of therapeutic stimulation frequencies (100–200 Hz), suggesting that the timing of prior effective stimulation may facilitate recruitment of subsequent responses within the same local circuit. Thus, the authors concluded that ERNA evokes short-term facilitation/plasticity in the STN-GPi circuit in various movement disorders and showed a positive correlation with both clinical efficacy and resting beta power. Campbell et al. (2022) investigated the effects of pulse timing on DBS evoked potentials within the basal ganglia-thalamocortical (BGTC) circuit using a wide range of ISIs in a paired pulse stimulation paradigm in patients with PD (n = 5). They demonstrated that ISIs with frequencies > 250 Hz significantly impacted evoked potentials recorded from the STN (*via* DBS leads) and motor cortex (*via* scalp EEG). Specifically, ISIs from 1.0 to 3.0 ms produced enhanced activation (i.e., greater wavelet amplitude), while ISIs outside of this range yielded no significant changes.

Birdno et al. (2007) evaluated the effects of pulse-to-pulse changes in DBS frequency in ET (n = 5) using biphasic paired pulses (ISI 0.3–7.7 ms). They applied monopolar stimulation for 40–60 s in blinded subjects and found that tremor suppression decreased as "IPI_{diff}" increased. In other words, as the ISI increased and/or the time between each pair of pulses increased, paired pulse stimulation became less effective than continuous HFS for treatment of ET [for more on "IPI_{diff}," see Birdno et al. (2007)]. Furthermore, continuous HFS at 130 Hz with regular temporal spacing was more effective at reducing tremor than paired pulse stimulation with irregular ISIs at the same overall rate (130 pulses per second). This and similar studies suggest that DBS is dependent not only on the average frequency but also on the temporal spacing of DBS pulses (Birdno et al., 2008).

Variable frequency stimulation

While HFS DBS effectively treats PD motor symptoms (i.e., bradykinesia, rigidity, and tremor) (Perestelo-Pérez et al., 2014; Xie et al., 2016), it is less beneficial for levodopa-unresponsive elements of gait dysfunction, freezing of gait (FOG), postural instability, and speech disorders (e.g., dysarthria, hypophonia) (Benabid et al., 2009; Schlenstedt et al., 2017). Moreover, HFS may exacerbate existing symptoms or cause side effects such as decreased verbal fluency (Parsons et al., 2006). Studies investigating LFS (<100 Hz) provide evidence for greater improvements in speech, dysphagia, gait dysfunction, and FOG versus HFS (Yu et al., 2020; Conway et al., 2021; Razmkon et al., 2022). Additionally, a double-blind study found that LFS was associated with improved speech intelligibility, prosody, and both semantic and phonemic verbal fluency (Grover et al., 2019; Lee et al., 2021). One meta-analysis reported that while HFS did have more pronounced effects on tremor reduction, LFS was significantly more effective in treatment of gait dysfunction, FOG, and akinesia (Su et al., 2018). However, some studies show that the benefits of LFS versus HFS decrease with long-term use and may depend on PD phenotype (Vallabhajosula et al., 2015; Xie et al., 2018).

To address these issues, researchers have experimented with VFS, with the rationale that combined elements of HFS and LFS might more optimally improve both appendicular and axial symptoms of PD. The VFS paradigm alternates between high (>100 Hz) and low (<100 Hz) frequencies within a stimulation cycle (<60 s) (**Figure 3**). Three studies from a single group (n = 6)

demonstrated the feasibility of VFS in the context of bilateral STN DBS for PD. They delivered VFS, cycling between HFS and LFS patterns with a variable duty cycle (≤300 s; PINS Medical, Beijing), in patients who had previously undergone HFS DBS optimization without resolution of axial motor symptoms or with development of side effects. Their VFS paradigm involved 10–50 s trains of alternating HFS and LFS (e.g., 130 Hz for 30 s and 60 Hz for 20 s per 50 s cycle). VFS increased gait speed, mitigated FOG, and improved bradykinesia, while tremor and rigidity either remained stable or further improved compared to HFS alone (Jia et al., 2015, 2017, 2018). In two cases, HFS-associated decline in verbal fluency and dysarthria resolved with VFS without diminishing HFS-related improvement in primary appendicular motor symptoms (Jia et al., 2017; Zhang et al., 2019). An additional case report showed improvement in freezing and limb dyskinesia in a single patient with bilateral STN and GPi leads programmed for VFS, which did not occur with HFS alone (Chang et al., 2021). In ET, HFS was superior to LFS for tremor reduction but worsened verbal fluency, while LFS was more effective at enhancing verbal fluency compared to DBS-OFF and HFS ($p = 0.0119$), but had no significant incremental effects on tremor (Pedrosa et al., 2014) and in some cases actually exacerbated the tremor (Pedrosa et al., 2013). Thus, while VFS appears promising in PD, its potential seems less promising for ET with the frequency range and duty cycles previously applied in PD patients. Larger, prospective randomized controlled trials of VFS versus HFS for PD are currently underway (Jia et al., 2019; Karl et al., 2019).

Interleaved stimulation

Standard DBS contact configurations are either monopolar, where the contact serves as the cathode, or bipolar, where two different contacts serve as an anode and cathode, respectively. The shape or coverage of the generated stimulation field can be modified by alternating between these two settings. Suboptimal position of an electrode can result in inadequate coverage of the target with overlap into anatomic regions that cause side effects. If adjusting between monopolar, double monopolar, bipolar, and double bipolar stimulation or changing stimulation parameters fails to achieve therapeutic effect, ILS can be used to contour the stimulation field and avoid unwanted overlap with non-target regions. ILS is a novel strategy that is supported in newer- generation DBS electrodes and involves rapidly alternating between two different stimulation settings using two different contacts on the same lead. Contacts can be programmed to deliver different amplitudes and pulse widths, however, the combined frequency is set to a maximum of 250 Hz per device by manufacturers to avoid potentially harmful charge delivery. ILS has been successfully used in PD to improve rigidity, bradykinesia, tremor (Wojtecki et al., 2011; Miocinovic et al., 2014; Ramirez-Zamora et al., 2015; Zhang et al., 2016; França et al., 2019; Karl et al., 2019), and gait (e.g., FOG) symptoms (Zhang et al., 2016; Karl et al., 2019; Zafar et al., 2021), as well as to decrease unwanted side effects such as dysarthria (Wojtecki et al., 2011; Ramirez-Zamora et al., 2015; Zhang et al., 2016), dyskinesias (Ramirez-Zamora et al., 2015; Zhang et al., 2016; Kern et al., 2018; Aquino et al., 2019; França et al., 2019; Goftari et al., 2020), and diplopia or paresthesias (Miocinovic et al., 2014).

Baumann et al. described a case of concomitant PD and ET where initially one set of stimulation parameters relieved PD but not ET symptoms and another set of parameters did the opposite. However, ILS using alternating unipolar pulses with different amplitudes at opposite poles of the STN and ventrolateral anterior thalamic region relieved both PD and ET symptoms (Baumann et al., 2012). Barbe et al. reported the successful use of ILS in several ET patients to relieve stimulation-induced dysarthria while maintaining therapeutic tremor suppression (Barbe et al., 2014).

Kovács et al. (2012) published the first case series ($n = 4$) of successful ILS use to treat dystonia in patients who had not previously responded to conventional high-frequency pallidal DBS. Zhang et al. (2018) later published a case report with similar findings, supporting the need for further exploration of ILS use in dystonia patients not responding to HFS DBS. Finally, Shu et al. (2018) described a case of pallidal DBS for Meige syndrome where ILS settings greatly improved the patient's symptoms compared to HFS DBS.

Burst cycling

Unlike traditional continuous HFS DBS (Deuschl et al., 2006; Okun et al., 2009), a temporal pattern of "burst cycling" stimulation ON and OFF has also gained traction (**Figure 3**). This pattern has been tested in a variety of neurologic disorders with varying results. For PD-associated tremor, there is some evidence that cycling stimulation (10s/1s or 30s/5s ON/OFF) in the STN or thalamus may help prevent tremor rebound and tolerance to DBS (Enatsu et al., 2020). A later study found that the implementation of a cycling stimulation pattern improved FOG in one PD patient who had developed tolerance to DBS (Dayal et al., 2021). On the other hand, Wong et al. (2021) did not find significant differences between cycling and conventional HFS in the treatment of FOG in patients with PD. Montgomery et al. found that continuous HFS of the STN provided greater symptom relief than burst cycling, showing a linear relationship between cycling interval and motor performance, with increasing efficacy of cycling from 0.1 to 0.5 s, both of which were inferior to continuous HFS. However, their results were likely underpowered and did not provide definitive conclusion (Montgomery, 2005). While stimulating the thalamus in the treatment of postural tremor, Kuncel et al. (2012) similarly found that cycling parameters more closely matching continuous HFS produced the greatest reduction in tremor power.

In dystonia, burst cycling has shown some therapeutic effects while increasing battery life and reducing the frequency of battery replacements (Tai et al., 2011). Loeffler et al. employed a unique cycling stimulation paradigm in an attempt to treat tremor in a patient with FGF-14 associated spinocerebellar ataxia. Their cycling paradigm used HFS (180 Hz) during the day and switched to LFS at night (30 Hz). This group found that alternating high and low frequency in the daytime and nighttime, respectively, led to a significantly better tremor response than with stimulation OFF at night (Loeffler et al., 2022). Burst cycling has also been used to treat non-motor conditions, the most common being various forms of drug-related epilepsy (DRE). Velasco et al. (2007) applied a burst cycling paradigm consisting of 1 min ON and 4 min OFF in the centromedian nucleus of the thalamus to effectively treat

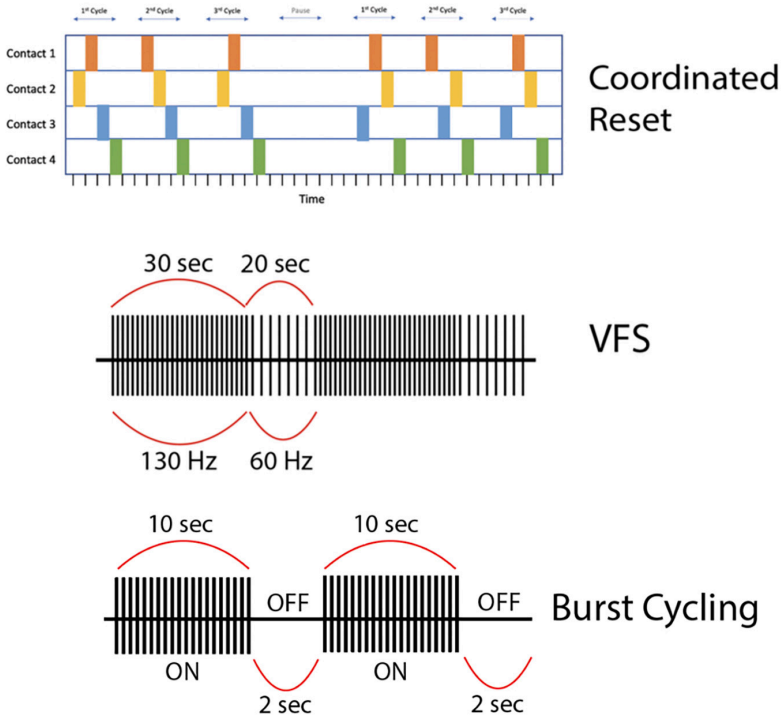

FIGURE 3
(First row) This is a representation of high-frequency (HF) Coordinated-Reset (CR) Deep Brain Stimulation (DBS). Specifically, we depict a shuffling pattern of stimulation, during which each cycle of stimulation has a new order in which the electrode contacts are stimulated. We also show how the CR-DBS paradigm typically consists of a series of ON cycles interspersed with OFF cycles. **(Second row)** This is a representation of variable frequency stimulation (VFS). During a stimulation cycle lasting 50 s, stimulation alternates between high frequency (130 Hz) and low frequency (60 Hz). **(Third row)** This is a representation of burst cycling stimulation with alternating ON/OFF periods (10 s/2 s). Of note, the stimulation parameters used to create the figures for each alternative pattern of stimulation presented here are examples of possible parameters; however, these vary greatly across studies.

generalized tonic-clonic seizures and atypical absence seizures in Lennox-Gastaut syndrome. A double-blind, randomized control trial (ESTEL trial) found cycling 145 Hz for 1 min ON and 5 min OFF significantly reduced seizures in Lennox-Gastaut syndrome compared to no stimulation (Dalic et al., 2022). The stimulation parameters selected for this trial were in large part influenced by a prior double-blind, randomized control trial (SANTE trial) that found a significant reduction in seizure frequency in patients with refractory epilepsy using cycling stimulation of the thalamus (Fisher et al., 2010). These findings have been corroborated by other groups, such as Boongird et al. (2016), who showed a 60% seizure reduction 24 months after surgery with a 145 Hz 1 min ON, 5 min OFF cycling paradigm. A similar cycling paradigm (1 min ON, 4 min OFF) was used with success to stimulate the subiculum in six patients with mesial temporal lobe epilepsy associated with hippocampal sclerosis (Vázquez-Barrón et al., 2021). This is in line with conclusion of another study with mesial temporal lobe epilepsy patients where amygdalohippocampal cycling stimulation (1 min ON, 3 min OFF) resulted in seizure reductions at 2 and 18 months (Min et al., 2013). When directly comparing anterior nucleus of thalamus cycling stimulation to conventional stimulation in DRE patients, Kaufmann et al. (2020) observed no significant difference in seizure frequency; however, they found an increase in restlessness with increased cycling frequency (shorter duration OFF period). Finally, cycling stimulation has been shown to be useful to avoid after-discharges and resultant seizures when using anterior cingulate DBS to treat chronic pain (Huang et al., 2019).

Coordinated reset

Synchronous neuronal firing is thought to underlie critical behavioral processes such as memory formation. In fact, recent studies suggest that greater neuronal synchrony between mesial temporal lobe structures correlates with improved memory performance (Jutras and Buffalo, 2010). However, hypersynchronous activity in neural circuits may also underlie pathological brain states, such as PD, epilepsy, and tinnitus (Ebert et al., 2014). For example, synchronization among populations of neurons in the thalamus and basal ganglia in PD and ET is associated with characteristic pathological movements that are typically seen in these movement disorders. More importantly, studies exploring pharmacological interventions with dopaminergic drugs (e.g., Levodopa) and/or surgical interventions with DBS have recently shown a direct correlation between reduced synchronized oscillatory activity in the β-band (8–35 Hz) and improved motor performance, suggesting the potentially critical role that synchronized neuronal activity may play in the pathogenesis of movement disorders such as PD (Chung et al., 2018).

CR-DBS is an alternative stimulation protocol that delivers intermittent high-frequency bursts to disrupt hypersynchronous neuronal firing (**Figure 3**). Typical CR-DBS parameters consist of high-frequency trains with an intra-burst frequency of 130 Hz (current: 2.0–4.0 mA), cycle repetition rate of 3–20 Hz, and pulse width ranging from 60 to 120 μs. Each pulse train typically consists of three to five pulses and the total duration of a pulse train ranges from 23 to 38 ms (Adamchic et al., 2014). This pattern of stimulation can be applied to electrode contacts in either a serial (non-shuffled) or shuffled (random order stimulation of electrode contacts) fashion (Wang et al., 2022). Developed in 2003, the rationale of CR-DBS is to desynchronize neuronal populations in the basal ganglia-motor cortical circuit to achieve therapeutic benefits in movement disorders such as PD (Tass, 2003). In a proof-of-concept study by Adamchic et al. (2014), six PD patients underwent bilateral implantation of quadripolar DBS electrodes in the STN. The patients were evaluated before and after once-daily 2-h CR-DBS treatments for a total of 3 days. Their CR-DBS stimulation protocol (detailed above) was specifically delivered to the three distal contacts of the electrode. They demonstrated that after 3 days of CR-DBS treatment, there was a significant reduction in β-band activity, with a mean reduction in β-power of 42% (p = 0.03), and an associated significant improvement in motor function [mean Unified Parkinson's Disease Rating Scale (UPDRS) score reduction of 58%, p = 0.03] (Adamchic et al., 2014). It is important to note that this study was limited by a lack of comparison to traditional HFS DBS, however, it is the first to show the therapeutic efficacy of CR-DBS in managing PD motor symptoms.

Temporally optimized stimulation

Traditional HFS DBS parameters are selected empirically based on individual patient testing and programmer experience. Newer alternative patterns have focused on using biomarkers or computational models to predict the "best settings" for a stimulation paradigm. Temporally optimized stimulation is a non-standardized computationally optimized pattern of DBS. In theory, a temporally optimized pattern of stimulation would significantly reduce energy consumption and frequency of implantable pulse generator (IPG) replacement, improving overall clinical outcomes.

In 2013, Brocker et al. (2013) tested a wide variety of temporally irregular DBS patterns in PD patients (n = 10) while assessing motor outcomes *via* a finger-tapping task in the operating room. This group found that stimulation pattern, and not rate, more significantly impacted DBS efficacy. Interestingly, they employed several patterns that relieved motor symptoms more effectively than temporally regular HFS, including "absence," "presence," "unipeak," and "uniform," with varying pulse entropy and frequencies (see Brocker et al., 2013 for detailed review).

Later, in a proof-of-concept study, Brocker et al. used model-based computational evolution to develop a temporally optimized stimulation paradigm (Brocker et al., 2017). They coupled a model of the basal ganglia with a genetic algorithm (GA) thought to operate similarly to evolution, with "natural selection" occurring to optimize stimulation. Three patterns were tested: temporally regular 185 Hz HFS, temporally regular 45 Hz LFS, and the optimized, GA pattern of stimulation, with an average frequency of 45 Hz. In a finger-tapping task in bradykinesia-dominant PD patients (n = 4), there was no significant difference in the rate and regularity of finger tapping between the HFS and GA groups, though both improved these parameters compared to baseline. Similarly, in the tremor-dominant PD subjects (n = 4), they found no significant difference in the reduction of tremor between the HFS and GA groups, though both significantly decreased tremor compared to baseline. Thus, despite significant study limitations, GA was tentatively deemed equivalent to HFS in terms of efficacy, but superior to HFS in terms of energy efficiency and battery life preservation (Brocker et al., 2017).

Recently, in a prospective, randomized, cross-over, multi-center feasibility study (n = 26), Okun et al. tested both versions of temporally optimized stimulation (TOPS) from the two aforementioned Brocker et al. studies [TOPS1 (Brocker et al., 2017) and TOPS2 (Brocker et al., 2013)] (Okun et al., 2022). They defined TOPS as pulse trains with a repeating sequence of non-regular and non-random intervals between pulses. TOPS2 used a long burst sequence (inter-burst interval ∼50 ms) followed by a short burst sequence (inter-burst interval ∼5 ms), with an average frequency of ∼158 Hz [see "absence" in Brocker et al. (2013)]. Like Brocker et al., this group found that TOPS reduced motor symptoms as effectively as conventional HFS DBS (Okun et al., 2022). As this was a safety and feasibility study, the results were not powered to provide statistically significant conclusion on efficacy. Nonetheless, the promising findings of potential non-inferiority of TOPS vs. HFS, with the added knowledge that TOPS is more energy efficient, should lead to well-powered randomized, controlled clinical trials comparing TOPS against HFS.

Closed-loop and adaptive stimulation

Current DBS systems use open-loop stimulation in which stimulation is always ON. Closed-loop adaptive neuromodulation relies on a control signal to initiate changes in stimulation parameters in real-time. Biomarker-controlled DBS may be useful, as symptoms fluctuate throughout the day in many neurologic and neuropsychiatric disorders. In PD, tremors occur at rest and rigidity occurs with the onset of movement (Reich and Savitt, 2019), whereas in ET, tremor occurs with movement (Shanker, 2019). In neuropsychiatric conditions such as treatment-resistant OCD, symptoms fluctuate throughout the day, with obsessive fixation alternating with ritualistic compulsive behaviors, all of which vary widely from patient to patient (Goodman et al., 2014). In treatment-resistant depression (TRD), symptoms may be more pronounced in times of stress and minimally present at rest, though this disease is also characterized by highly heterogeneous symptoms (Filatova et al., 2021). In Tourette syndrome (TS), tics emerge frequently when the patient is under high stress, but manifest in different areas of the body, with variable duration and intensity (Jankovic and Kurlan, 2011). Thus, neuromodulation strategies for these diseases might be more effective, more efficient, or better tolerated with on-demand stimulation paradigms. The goal of adaptive DBS (aDBS) is to treat each patient's constellation of symptoms in an individualized manner, to reduce stimulation-induced side effects (including during sleep), and to prolong battery life through more efficient energy consumption.

The majority of studies in aDBS focus on PD (Little et al., 2013, 2016a,b; Rosa et al., 2015, 2017; Malekmohammadi et al., 2016; Piña-Fuentes et al., 2017, 2019, 2020b; Tinkhauser et al., 2017; Arlotti et al., 2018, 2021; Swann et al., 2018; Velisar et al., 2019; Petrucci et al., 2020; Gilron et al., 2021; Molina et al., 2021; Nakajima et al., 2021; Sasaki et al., 2021; Sarikhani et al., 2022). Several groups suggest that STN aDBS is equivalent or non-inferior to open-loop or constant DBS (cDBS) in reducing the UPDRS score in PD (Little et al., 2016a; Piña-Fuentes et al., 2017, 2020b; Rosa et al., 2017; Arlotti et al., 2018; Swann et al., 2018; Velisar et al., 2019; Sasaki et al., 2021; Sarikhani et al., 2022). Some studies found greater score reductions with aDBS compared to cDBS (Little et al., 2013, 2016b; Rosa et al., 2015; Malekmohammadi et al., 2016). A potentially important limitation of these studies is that they were conducted with externalized leads and experimental pulse generators in a controlled research environment in the immediate post-lead-implantation period. Further studies are needed to demonstrate the generalizability of these findings in long-term studies and non-clinical environments.

Adaptive DBS is also of interest in neurocognitive aspects of PD. Little et al. (2016b) investigated a binary (ON-OFF) aDBS paradigm in eight PD patients with bilateral STN leads. They developed a threshold-based algorithm using beta oscillations (13–30 Hz) that switched ON and OFF automatically with a ramp up/down time of 250 ms (Little et al., 2013). They administered a speech intelligibility test (SIT) at baseline, during cDBS, and during aDBS (15-min duration) to measure speech-related side effects and improvement. They found that aDBS was associated with improved SIT scores compared to both baseline and cDBS (baseline SIT 67.9%; aDBS 70.4%; cDBS 60.5%; $p = 0.02$).

In ET, several studies report outcomes of unilateral VIM or zona incerta aDBS combined with recordings from subdural strip electrodes over primary motor cortex (Herron et al., 2017a,b; Castaño-Candamil et al., 2020; Ferleger et al., 2020; He et al., 2020, 2021; Opri et al., 2020). Two studies showed greater tremor suppression with aDBS (Castaño-Candamil et al., 2020; Ferleger et al., 2020) and one study showed aDBS to be equivalent or non-inferior to cDBS (Opri et al., 2020). On the other hand, Herron et al. (2017a) demonstrated decreased tremor control with aDBS compared to cDBS.

Dystonia presents both opportunities and challenges for aDBS applications. Piña-Fuentes et al. (2020a) found that short-term GPi aDBS ($n = 7$) did not lead to acute changes in low frequency oscillations (4–12 Hz) or to any significant clinical changes. However, dystonia typically has a delayed response to cDBS such that aDBS effects could be difficult to extrapolate in the context of short-term stimulation. DBS programming in dystonia patients is often more complex than for PD or ET, such that robust, effective closed loop stimulation strategies could play a useful role in these patients.

In neuropsychiatric disease, aDBS has been described in TRD (Scangos et al., 2021) and TS (Cagle et al., 2022). In TRD, Scangos et al. (2021) demonstrated safety and feasibility of a fully integrated aDBS system in a single patient. They found that bilateral amygdala gamma power is correlated to elevated symptom severity with high reproducibility. Stimulating at the VC/VS, they demonstrated improved depressive symptoms correlating to reduced amygdala gamma power in two of five stimulation trials. Cagle et al. (2022) compared aDBS to cDBS in four TS patients with bilateral centromedian-parafascicular complex thalamic leads. Using a subdural strip overlying M1 and thalamic leads, they found increased low-frequency thalamic power (3–10 Hz) at the onset of involuntary tics that was not present during voluntary movements. Though there was no statistically significant difference between the two, both cDBS and aDBS significantly reduced symptoms compared to DBS OFF, suggesting possible non-inferiority of aDBS versus cDBS in TS. As in all indications, seeking a suitable control signal presents challenges, but recent studies show that aDBS for OCD may be on the horizon (Provenza et al., 2019, 2021). For example, Provenza et al. (2021) recently found that delta-band (0–4 Hz) power showed a strong negative correlation with symptom severity in five patients with OCD implanted with sensing-capable IPGs and bilateral ventral capsule/ventral striatum (VC/VS) electrodes. Though this remains to be tested with aDBS, this finding may represent a suitable biomarker. While aDBS is of increasing interest, these studies are all limited by small sample sizes and require more robust investigation.

Discussion

As our familiarity with continuous high-frequency DBS, the gold-standard stimulation paradigm in the treatment of both neurologic and neuropsychiatric disorders, grows, clinicians and scientists increasingly recognize the need for programming optimization and improved efficacy, which has led to the development of numerous alternative patterns of stimulation. In this review, we provide a snapshot of current human evidence supporting these patterns–including TBS, paired pulse, VFS, ILS, burst cycling, CR-DBS, TOPS, and aDBS–as possible alternatives to HFS DBS. With small case series in most cases, the existing literature is not sufficient to reach definitive conclusion regarding non-inferiority/superiority of an alternative pattern versus HFS DBS. However, based on our findings, in addition to these being safe and technically feasible, they generally present two specific advantages over HFS DBS: (1) optimization leads to a more energy-efficient delivery of stimulation, prolonging battery life and reducing the frequency of costly IPG replacements; (2) non-continuous paradigms have the potential to simultaneously deliver therapeutic levels of stimulation, treating both motor and non-motor symptoms of various neurologic and neuropsychiatric diseases, while mitigating stimulation-induced side effects. By the temporal nature of their designs (i.e., non-continuous), many of the alternative patterns of stimulation discussed here would draw less power from an IPG than continuous HFS DBS when delivering stimulation. In TBS, specifically iTBS, stimulation trains or bursts are followed by pauses (DBS OFF periods) (Huang et al., 2005). Similar to iTBS, VFS presumably would draw less electrical energy than HFS alone because of the alternating periods of LFS and HFS in a given cycle. However, though theoretically iTBS and VFS would consume less battery life than cTBS or HFS DBS alone, direct evidence of this is limited. Continuous TBS appears to improve motor PD symptoms, although the therapeutic threshold is higher with low intraburst frequencies (~50 Hz vs. 100 Hz) (Horn et al., 2020). The impact of burst cycling on battery longevity has been directly investigated, and one of the main motivations for using burst cycling stimulation over conventional

continuous HFS has been to conserve device battery and decrease the frequency of IPG replacements (Kuncel et al., 2012; Wong et al., 2021). In the case of TOPS and aDBS battery life is conserved in a more indirect approach, using computational modeling or biomarker-driven auto-regulating systems, respectively, which ultimately leads to more efficient energy consumption. Studies of ILS have shown conflicting results, with some indicating that ILS may lead to higher energy consumption and decreased battery life (Kern et al., 2018; Karl et al., 2019), and others showing evidence that certain ILS settings may conserve energy relative to continuous HFS DBS (Karl et al., 2020). In contrast to the primary motivation of increasing battery longevity, several studies focused on the potential mitigation of stimulation-induced side effects provided by these non-traditional paradigms, specifically VFS, ILS, burst cycling, CR-DBS, and aDBS. Many VFS studies showed improvement in gait dysfunction, FOG, and stimulation-induced speech disorders (e.g., dysarthria, hypophonia) with the use of VFS. Additionally, ILS studies observed improvements in rigidity, bradykinesia, tremor, and gait (e.g., FOG) symptoms as well as mitigation of unwanted side effects such as dysarthria, dyskinesias, diplopia, and paresthesias.

Finally, we found that some alternative patterns of stimulation may mimic a more physiologic neuronal firing pattern, which may be an explanation for why some alternative stimulation patterns seem to better address cognitive or memory-related symptoms of movement disorders and other neuropsychiatric disorders. For example, there is evidence that dorsolateral prefrontal cortex TBS can modulate networks involved in mood and cognitive function (e.g., memory). The ability to increase theta-power on-demand may provide a way to modulate specific neuronal populations, since it is believed that higher power theta oscillations can entrain high-frequency activity more efficiently (Kahana et al., 1999). Indeed, theta-gamma coupling (and theta band activity entraining single neuron firing) has functional relevance for cognition in humans across multiple domains including memory and decision making.

We acknowledge that our broad review of alternative patterns of stimulation has some methodological limitations. The most important limitation of this study is that, though we hope to review all alternative patterns of stimulation with published human data in a comprehensive manner, we are unable to account for those patterns for which we did not search. Additionally, there are likely some alternative patterns which may not have a standard naming convention and thus are difficult to review. For example, Akbar et al. (2016) conducted a study using square biphasic pulses and other irregular pulse patterns in PD (n = 8) and ET (n = 3) patients. Briefly, their findings showed that certain non-conventional patterns of stimulation may extend battery life and minimize stimulation-associated side effects. The goal of their randomized, blinded pilot study was to provide a framework for rigorously testing non-HFS patterns of stimulation; however, they specify that further testing is needed to assess efficacy of alternative patterns of stimulation and compare them to conventional HFS (Akbar et al., 2016).

Conclusion

Alternative patterns of stimulation such as theta burst, paired pulse, variable frequency, interleaving, burst cycling, coordinated reset, temporally optimized stimulation, and adaptive DBS are promising novel patterns of stimulation that may provide improved efficacy for both motor and non-motor symptoms of neurologic and neuropsychiatric disorders. In doing so, these patterns may also extend battery life and lead to fewer replacements, ultimately improving quality of life for these patients. However, current evidence is limited and warrants rigorous trials before implementing in the clinical domain.

Author contributions

RN, AM, AK, UB, VD, HW, and JB: conceptualization, writing—original draft preparation, and writing—review and editing. VD, HW, and JB: supervision. All authors have read and agreed to the published version of the manuscript.

Conflict of interest

The authors declare that the research was conducted in the absence of any commercial or financial relationships that could be construed as a potential conflict of interest.

Publisher's note

References

Adamchic, I., Hauptmann, C., Barnikol, U. B., Pawelczyk, N., Popovych, O., Barnikol, T. T., et al. (2014). Coordinated reset neuromodulation for Parkinson's disease: proof-of-concept study. *Mov. Disord.* 29, 1679–1684. doi: 10.1002/mds.25923

Agnesi, F., Johnson, M. D., and Vitek, J. L. (2013). Deep brain stimulation: how does it work? *Handb. Clin. Neurol.* 116, 39–54. doi: 10.1016/B978-0-444-53497-2.00004-8

Akbar, U., Raike, R. S., Hack, N., Hess, C. W., Skinner, J., Martinez-Ramirez, D., et al. (2016). Randomized, blinded pilot testing of nonconventional stimulation patterns and shapes in Parkinson's Disease and Essential Tremor: Evidence for Further Evaluating Narrow and Biphasic Pulses. *Neuromodulation J. Int. Neuromodulation Soc.* 19, 343–356. doi: 10.1111/ner.1397

Anderson, T. R., Hu, B., Iremonger, K., and Kiss, Z. H. T. (2006). Selective attenuation of afferent synaptic transmission as a mechanism of thalamic deep brain stimulation-induced tremor arrest. *J. Neurosci.* 26, 841–850. doi: 10.1523/JNEUROSCI.3523-05.2006

Aquino, C. C., Duffley, G., Hedges, D. M., Vorwerk, J., House, P. A., Ferraz, H. B., et al. (2019). Interleaved deep brain stimulation for dyskinesia management in Parkinson's disease. *Mov. Disord.* 34, 1722–1727. doi: 10.1002/mds.27839

Arlotti, M., Colombo, M., Bonfanti, A., Mandat, T., Lanotte, M. M., Pirola, E., et al. (2021). A new implantable closed-loop clinical neural interface: First application in Parkinson's Disease. *Front. Neurosci.* 15:763235. doi: 10.3389/fnins.2021.763235

Arlotti, M., Marceglia, S., Foffani, G., Volkmann, J., Lozano, A. M., Moro, E., et al. (2018). Eight-hours adaptive deep brain stimulation in patients with Parkinson disease. *Neurology* 90, e971–e976. doi: 10.1212/WNL.0000000000005121

Awad, M. Z., Irwin, Z. T., Vaden, R. J., Guthrie, B. L., and Walker, H. C. (2020). Short latency cortical evoked potentials elicited by subthalamic nucleus deep brain stimulation: Commentary and results from paired pulse studies. *Clin. Neurophysiol.* 131, 465–467. doi: 10.1016/j.clinph.2019.11.015

Awad, M. Z., Vaden, R. J., Irwin, Z. T., Gonzalez, C. L., Black, S., Nakhmani, A., et al. (2021). Subcortical short-term plasticity elicited by deep brain stimulation. *Ann. Clin. Transl. Neurol.* 8, 1010–1023. doi: 10.1002/acn3.51275

Baker, K. B., Montgomery, E. B., Rezai, A. R., Burgess, R., and Lüders, H. O. (2002). Subthalamic nucleus deep brain stimulus evoked potentials: physiological and therapeutic implications. *Mov. Disord.* 17, 969–983. doi: 10.1002/mds.10206

Barbe, M. T., Dembek, T. A., Becker, J., Raethjen, J., Hartinger, M., Meister, I. G., et al. (2014). Individualized current-shaping reduces DBS-induced dysarthria in patients with essential tremor. *Neurology* 82, 614–619. doi: 10.1212/WNL.0000000000000127

Baumann, C. R., Imbach, L. L., Baumann-Vogel, H., Uhl, M., Sarnthein, J., and Sürücü, O. (2012). Interleaving deep brain stimulation for a patient with both Parkinson's disease and essential tremor. *Mov. Disord.* 27, 1700–1701. doi: 10.1002/mds.25221

Benabid, A. L., Chabardes, S., Mitrofanis, J., and Pollak, P. (2009). Deep brain stimulation of the subthalamic nucleus for the treatment of Parkinson's disease. *Lancet Neurol.* 8, 67–81. doi: 10.1016/S1474-4422(08)70291-6

Benazzouz, A., and Hallett, M. (2000). Mechanism of action of deep brain stimulation. *Neurology* 55, S13–S16.

Bentley, J. N., Irwin, Z. T., Black, S. D., Roach, M. L., Vaden, R. J., Gonzalez, C. L., et al. (2020). Subcortical Intermittent Theta-Burst Stimulation (iTBS) Increases Theta-Power in Dorsolateral Prefrontal Cortex (DLPFC). *Front. Neurosci.* 14:41. doi: 10.3389/fnins.2020.00041

Birdno, M. J., Cooper, S. E., Rezai, A. R., and Grill, W. M. (2007). Pulse-to-pulse changes in the frequency of deep brain stimulation affect tremor and modeled neuronal activity. *J. Neurophysiol.* 98, 1675–1684. doi: 10.1152/jn.00547.2007

Birdno, M. J., Kuncel, A. M., Dorval, A. D., Turner, D. A., and Grill, W. M. (2008). Tremor varies as a function of the temporal regularity of deep brain stimulation. *Neuroreport* 19, 599–602. doi: 10.1097/WNR.0b013e3282f9e45e

Boongird, A., Boongird, A., Khongkhatithum, C., Thampratankul, L., and Visudtibhan, A. (2016). Deep Brain Stimulation of Anterior Thalamic Nuclei for Intractable Epilepsy in Thailand: Case Report. *J. Med. Assoc. Thail. Chotmaihet Thangphaet* 99, S126–S129.

Brocker, D. T., Swan, B. D., So, R. Q., Turner, D. A., Gross, R. E., and Grill, W. M. (2017). Optimized temporal pattern of brain stimulation designed by computational evolution. *Sci. Transl. Med.* 9:3532. doi: 10.1126/scitranslmed.aah3532

Brocker, D. T., Swan, B. D., Turner, D. A., Gross, R. E., Tatter, S. B., Koop, M. M., et al. (2013). Improved efficacy of temporally non-regular deep brain stimulation in Parkinson's disease. *Exp. Neurol.* 239, 60–67. doi: 10.1016/j.expneurol.2012.09.008

Bueno-Junior, L. S., and Leite, J. P. (2018). Input convergence, synaptic plasticity and functional coupling across hippocampal-prefrontal-thalamic circuits. *Front. Neural Circuits* 12:40. doi: 10.3389/fncir.2018.00040

Cagle, J. N., Okun, M. S., Cernera, S., Eisinger, R. S., Opri, E., Bowers, D., et al. (2022). Embedded human closed-loop deep brain stimulation for tourette syndrome: A nonrandomized controlled trial. *JAMA Neurol.* 79, 1064–1068. doi: 10.1001/jamaneurol.2022.2741

Cagnan, H., Pedrosa, D., Little, S., Pogosyan, A., Cheeran, B., Aziz, T., et al. (2017). Stimulating at the right time: phase-specific deep brain stimulation. *Brain J. Neurol.* 140, 132–145. doi: 10.1093/brain/aww286

Campbell, B. A., Favi Bocca, L., Escobar Sanabria, D., Almeida, J., Rammo, R., Nagel, S. J., et al. (2022). The impact of pulse timing on cortical and subthalamic nucleus deep brain stimulation evoked potentials. *Front. Hum. Neurosci.* 16:1009223. doi: 10.3389/fnhum.2022.1009223

Castaño-Candamil, S., Ferleger, B. I., Haddock, A., Cooper, S. S., Herron, J., Ko, A., et al. (2020). A Pilot Study on Data-Driven Adaptive Deep Brain Stimulation in Chronically Implanted Essential Tremor Patients. *Front. Hum. Neurosci.* 14:541625. doi: 10.3389/fnhum.2020.541625

Cernera, S., Okun, M. S., and Gunduz, A. (2019). A review of cognitive outcomes across movement disorder patients undergoing deep brain stimulation. *Front. Neurol.* 10:419. doi: 10.3389/fneur.2019.00419

Chang, B., Mei, J., Xiong, C., Chen, P., Jiang, M., and Niu, C. (2021). Bilateral globus pallidus interna combined with subthalamic nucleus variable frequency deep brain stimulation in the treatment of young-onset Parkinson's Disease with refractory dyskinesia: A case report. *Front. Neurosci.* 15:782046. doi: 10.3389/fnins.2021.782046

Chen, K.-H., Tang, A. M., Gilbert, Z. D., Martin Del Campo-Vera, R., Sebastian, R., Gogia, A. S., et al. (2022). Theta low-gamma phase amplitude coupling in the human orbitofrontal cortex increases during a conflict-processing task. *J. Neural Eng.* 19:ac4f9b. doi: 10.1088/1741-2552/ac4f9b

Chung, J. W., Burciu, R. G., Ofori, E., Coombes, S. A., Christou, E. A., Okun, M. S., et al. (2018). Beta-band oscillations in the supplementary motor cortex are modulated by levodopa and associated with functional activity in the basal ganglia. *Neuroimage Clin.* 19, 559–571. doi: 10.1016/j.nicl.2018.05.021

Conway, Z. J., Silburn, P. A., Perera, T., O'Maley, K., and Cole, M. H. (2021). Low-frequency STN-DBS provides acute gait improvements in Parkinson's disease: a double-blinded randomised cross-over feasibility trial. *J. Neuroengineering Rehabil.* 18:125. doi: 10.1186/s12984-021-00921-4

Dalic, L. J., Warren, A. E. L., Bulluss, K. J., Thevathasan, W., Roten, A., Churilov, L., et al. (2022). DBS of Thalamic Centromedian Nucleus for Lennox–Gastaut Syndrome (ES^{TEL} Trial). *Ann. Neurol.* 91, 253–267. doi: 10.1002/ana.26280

Dayal, V., Rajabian, A., Jahanshahi, M., Aviles-Olmos, I., Cowie, D., Peters, A., et al. (2021). Pedunculopontine nucleus deep brain stimulation for Parkinsonian disorders: A Case Series. *Stereotact. Funct. Neurosurg.* 99, 287–294. doi: 10.1159/000511978

Deuschl, G., Schade-Brittinger, C., Krack, P., Volkmann, J., Schäfer, H., Bötzel, K., et al. (2006). A randomized trial of deep-brain stimulation for Parkinson's Disease. *N. Engl. J. Med.* 355, 896–908. doi: 10.1056/NEJMoa060281

Dinkelbach, L., Mueller, J., Poewe, W., Delazer, M., Elben, S., Wolters, A., et al. (2015). Cognitive outcome of pallidal deep brain stimulation for primary cervical dystonia: One year follow up results of a prospective multicenter trial. *Parkinsonism Relat. Disord.* 21, 976–980. doi: 10.1016/j.parkreldis.2015.06.002

Ebert, M., Hauptmann, C., and Tass, P. A. (2014). Coordinated reset stimulation in a large-scale model of the STN-GPE circuit. *Front. Comput. Neurosci.* 8:154. doi: 10.3389/FNCOM.2014.00154/BIBTEX

Enatsu, R., Kitagawa, M., Morishita, T., Sasagawa, A., Kuribara, T., Hirano, T., et al. (2020). Effect of cycling thalamosubthalamic stimulation on tremor habituation and rebound in Parkinson Disease. *World Neurosurg.* 144, 64–67. doi: 10.1016/j.wneu.2020.08.141

Ferleger, B. I., Houston, B., Thompson, M. C., Cooper, S. S., Sonnet, K. S., Ko, A. L., et al. (2020). Fully implanted adaptive deep brain stimulation in freely moving essential tremor patients. *J. Neural Eng.* 17:56026. doi: 10.1088/1741-2552/abb416

Filatova, E. V., Shadrina, M. I., and Slominsky, P. A. (2021). Major depression: One brain, one disease, one set of intertwined processes. *Cells* 10:1283. doi: 10.3390/cells10061283

Fisher, R., Salanova, V., Witt, T., Worth, R., Henry, T., Gross, R., et al. (2010). Electrical stimulation of the anterior nucleus of thalamus for treatment of refractory epilepsy. *Epilepsia* 51, 899–908. doi: 10.1111/j.1528-1167.2010.02536.x

França, C., Barbosa, E. R., Iglesio, R., Teixeira, M. J., and Cury, R. G. (2019). Interleaving Stimulation in Parkinson Disease: Interesting to Whom? *World Neurosurg.* 130, e786–e793. doi: 10.1016/j.wneu.2019.06.223

Gilron, R., Little, S., Perrone, R., Wilt, R., de Hemptinne, C., Yaroshinsky, M. S., et al. (2021). Long-term wireless streaming of neural recordings for circuit discovery and adaptive stimulation in individuals with Parkinson's disease. *Nat. Biotechnol.* 39, 1078–1085. doi: 10.1038/s41587-021-00897-5

Goftari, M., Kim, J., Johnson, E., Patriat, R., Palnitkar, T., Harel, N., et al. (2020). Pallidothalamic tract activation predicts suppression of stimulation-induced dyskinesias in a case study of Parkinson's disease. *Brain Stimulat.* 13, 1821–1823. doi: 10.1016/j.brs.2020.09.022

Goodman, W. K., Grice, D. E., Lapidus, K. A. B., and Coffey, B. J. (2014). Obsessive-compulsive disorder. *Psychiatr. Clin. North Am.* 37, 257–267. doi: 10.1016/j.psc.2014.06.004

Grill, W. M., Snyder, A. N., and Miocinovic, S. (2004). Deep brain stimulation creates an informational lesion of the stimulated nucleus. *Neuroreport* 15, 1137–1140. doi: 10.1097/00001756-200405190-00011

Grover, T., Georgiev, D., Kalliola, R., Mahlknecht, P., Zacharia, A., Candelario, J., et al. (2019). Effect of low versus high frequency subthalamic deep brain stimulation on speech intelligibility and verbal fluency in Parkinson's Disease: A double-blind study. *J. Park. Dis.* 9, 141–151. doi: 10.3233/JPD-181368

Hammond, C., Ammari, R., Bioulac, B., and Garcia, L. (2008). Latest view on the mechanism of action of deep brain stimulation. *Mov. Disord.* 23, 2111–2121. doi: 10.1002/mds.22120

Hashimoto, T., Elder, C. M., Okun, M. S., Patrick, S. K., and Vitek, J. L. (2003). Stimulation of the subthalamic nucleus changes the firing pattern of pallidal neurons. *J. Neurosci.* 23, 1916–1923. doi: 10.1523/JNEUROSCI.23-05-01916.2003

He, S., Baig, F., Mostofi, A., Pogosyan, A., Debarros, J., Green, A. L., et al. (2021). Closed-Loop deep brain stimulation for essential tremor based on thalamic local field potentials. *Mov. Disord.* 36, 863–873. doi: 10.1002/mds.28513

He, S., Debarros, J., Khawaldeh, S., Pogosyan, A., Mostofi, A., Baig, F., et al. (2020). Closed-loop DBS triggered by real-time movement and tremor decoding based on thalamic LFPs for essential tremor. *Annu. Int. Conf. IEEE Eng. Med. Biol. Soc.* 2020, 3602–3605. doi: 10.1109/EMBC44109.2020.9175433

Herron, J. A., Thompson, M. C., Brown, T., Chizeck, H. J., Ojemann, J. G., and Ko, A. L. (2017a). Chronic electrocorticography for sensing movement intention

and closed-loop deep brain stimulation with wearable sensors in an essential tremor patient. *J. Neurosurg.* 127, 580–587. doi: 10.3171/2016.8.JNS16536

Herron, J. A., Thompson, M. C., Brown, T., Chizeck, H. J., Ojemann, J. G., and Ko, A. L. (2017b). Cortical brain-computer interface for closed-loop deep brain stimulation. *IEEE Trans. Neural Syst. Rehabil. Eng.* 25, 2180–2187. doi: 10.1109/TNSRE.2017.2705661

Horn, M. A., Gulberti, A., Gülke, E., Buhmann, C., Gerloff, C., Moll, C. K. E., et al. (2020). A New Stimulation Mode for Deep Brain Stimulation in Parkinson's Disease: Theta Burst Stimulation. *Mov. Disord.* 35, 1471–1475. doi: 10.1002/mds.28083

Huang, Y., Cheeran, B., Green, A. L., Denison, T. J., and Aziz, T. Z. (2019). Applying a sensing-enabled system for ensuring safe anterior cingulate deep brain stimulation for pain. *Brain Sci.* 9:150. doi: 10.3390/brainsci9070150

Huang, Y.-Z., Edwards, M. J., Rounis, E., Bhatia, K. P., and Rothwell, J. C. (2005). Theta burst stimulation of the human motor cortex. *Neuron* 45, 201–206. doi: 10.1016/j.neuron.2004.12.033

Jankovic, J., and Kurlan, R. (2011). Tourette syndrome: evolving concepts. *Mov. Disord.* 26, 1149–1156. doi: 10.1002/mds.23618

Jensen, A. L., and Durand, D. M. (2009). High frequency stimulation can block axonal conduction. *Exp. Neurol.* 220, 57–70. doi: 10.1016/j.expneurol.2009.07.023

Jia, F., Guo, Y., Wan, S., Chen, H., Hao, H., Zhang, J., et al. (2015). Variable frequency stimulation of subthalamic nucleus for freezing of gait in Parkinson's disease. *Parkinsonism Relat. Disord.* 21, 1471–1472. doi: 10.1016/j.parkreldis.2015.10.002

Jia, F., Guo, Y., Wan, S., and Li, L. (2017). Severe subthalamic stimulation-induced dysarthria alleviated by a novel paradigm: A case report. *J. Neurol. Sci.* 372, 270–271. doi: 10.1016/j.jns.2016.11.048

Jia, F., Wagle Shukla, A., Hu, W., Almeida, L., Holanda, V., Zhang, J., et al. (2018). Deep Brain Stimulation at Variable Frequency to Improve Motor Outcomes in Parkinson's Disease. *Mov. Disord. Clin. Pract.* 5, 538–541. doi: 10.1002/mdc3.12658

Jia, F., Zhang, J., Wang, H., Liang, Z., Liu, W., Wang, X., et al. (2019). Variable- versus constant-frequency deep-brain stimulation in patients with advanced Parkinson's disease: study protocol for a randomized controlled trial. *Trials* 20:749. doi: 10.1186/s13063-019-3884-4

Johnson, V., Wilt, R., Gilron, R., Anso, J., Perrone, R., Beudel, M., et al. (2021). Embedded adaptive deep brain stimulation for cervical dystonia controlled by motor cortex theta oscillations. *Exp. Neurol.* 345:113825. doi: 10.1016/j.expneurol.2021.113825

Jones, K. T., Johnson, E. L., and Berryhill, M. E. (2020). Frontoparietal theta-gamma interactions track working memory enhancement with training and tDCS. *NeuroImage* 211:116615. doi: 10.1016/j.neuroimage.2020.116615

Jutras, M. J., and Buffalo, E. A. (2010). Synchronous neural activity and memory formation. *Curr. Opin. Neurobiol.* 20, 150–155. doi: 10.1016/j.conb.2010.02.006

Kahana, M. J., Sekuler, R., Caplan, J. B., Kirschen, M., and Madsen, J. R. (1999). Human theta oscillations exhibit task dependence during virtual maze navigation. *Nature* 399, 781–784. doi: 10.1038/21645

Karl, J. A., Ouyang, B., Goetz, S., and Metman, L. V. (2020). A Novel DBS Paradigm for Axial Features in Parkinson's Disease: A Randomized Crossover Study. *Mov. Disord.* 35, 1369–1378. doi: 10.1002/mds.28048

Karl, J. A., Ouyang, B., and Verhagen Metman, L. (2019). A Novel Dual-Frequency Deep Brain Stimulation Paradigm for Parkinson's Disease. *Neurol. Ther.* 8, 483–489. doi: 10.1007/s40120-019-0140-5

Kaufmann, E., Bötzel, K., Vollmar, C., Mehrkens, J.-H., and Noachtar, S. (2020). What have we learned from 8 years of deep brain stimulation of the anterior thalamic nucleus? Experiences and insights of a single center. *J. Neurosurg.* [Epub ahead of print]. doi: 10.3171/2020.6.JNS20695

Kern, D. S., Picillo, M., Thompson, J. A., Sammartino, F., di Biase, L., Munhoz, R. P., et al. (2018). Interleaving Stimulation in Parkinson's Disease, Tremor, and Dystonia. *Stereotact. Funct. Neurosurg.* 96, 379–391. doi: 10.1159/000494983

Kim, K., Schedlbauer, A., Rollo, M., Karunakaran, S., Ekstrom, A. D., and Tandon, N. (2018). Network-based brain stimulation selectively impairs spatial retrieval. *Brain Stimulat.* 11, 213–221. doi: 10.1016/j.brs.2017.09.016

Kovács, N., Janszky, J., Nagy, F., and Balás, I. (2012). Changing to interleaving stimulation might improve dystonia in cases not responding to pallidal stimulation. *Mov. Disord.* 27, 163–165. doi: 10.1002/mds.23962

Kuncel, A. M., Birdno, M. J., Swan, B. D., and Grill, W. M. (2012). Tremor reduction and modeled neural activity during cycling thalamic deep brain stimulation. *Clin. Neurophysiol.* 123, 1044–1052. doi: 10.1016/j.clinph.2011.07.052

Lee, D. J., Drummond, N. M., Saha, U., De Vloo, P., Dallapiazza, R. F., Gramer, R., et al. (2021). Acute low frequency dorsal subthalamic nucleus stimulation improves verbal fluency in Parkinson's disease. *Brain Stimulat.* 14, 754–760. doi: 10.1016/j.brs.2021.04.016

Little, S., Beudel, M., Zrinzo, L., Foltynie, T., Limousin, P., Hariz, M., et al. (2016a). Bilateral adaptive deep brain stimulation is effective in Parkinson's disease. *J. Neurol. Neurosurg. Psychiatry* 87, 717–721. doi: 10.1136/jnnp-2015-310972

Little, S., Tripoliti, E., Beudel, M., Pogosyan, A., Cagnan, H., Herz, D., et al. (2016b). Adaptive deep brain stimulation for Parkinson's disease demonstrates reduced speech side effects compared to conventional stimulation in the acute setting. *J. Neurol. Neurosurg. Psychiatry* 87, 1388–1389. doi: 10.1136/jnnp-2016-313518

Little, S., Pogosyan, A., Neal, S., Zavala, B., Zrinzo, L., Hariz, M., et al. (2013). Adaptive deep brain stimulation in advanced Parkinson disease. *Ann. Neurol.* 74, 449–457. doi: 10.1002/ana.23951

Loeffler, M. A., Synofzik, M., Cebi, I., Klocke, P., Hormozi, M., Gasser, T., et al. (2022). Case Report: Deep brain stimulation improves tremor in FGF-14 associated spinocerebellar ataxia. *Front. Neurol.* 13:1048530. doi: 10.3389/fneur.2022.1048530

Louie, K. H., Lu, C., Abdallah, T., Guzior, J. C., Twedell, E., Netoff, T. I., et al. (2021). Gait phase triggered deep brain stimulation in Parkinson's disease. *Brain Stimulat.* 14, 420–422. doi: 10.1016/j.brs.2021.02.009

Lowet, E., Kondabolu, K., Zhou, S., Mount, R. A., Wang, Y., Ravasio, C. R., et al. (2022). Deep brain stimulation creates informational lesion through membrane depolarization in mouse hippocampus. *Nat. Commun.* 13:7709. doi: 10.1038/s41467-022-35314-1

Lozano, A. M., Lipsman, N., Bergman, H., Brown, P., Chabardes, S., Chang, J. W., et al. (2019). Deep brain stimulation: current challenges and future directions. *Nat. Rev. Neurol.* 15, 148–160. doi: 10.1038/s41582-018-0128-2

Malekmohammadi, M., Herron, J., Velisar, A., Blumenfeld, Z., Trager, M. H., Chizeck, H. J., et al. (2016). Kinematic adaptive deep brain stimulation for resting tremor in Parkinson's Disease. *Mov. Disord.* 31, 426–428. doi: 10.1002/mds.26482

McIntyre, C. C., Savasta, M., Kerkerian-Le Goff, L., and Vitek, J. L. (2004). Uncovering the mechanism(s) of action of deep brain stimulation: Activation, inhibition, or both. *Clin. Neurophysiol.* 115, 1239–1248. doi: 10.1016/j.clinph.2003.12.024

Miller, J. P., Sweet, J. A., Bailey, C. M., Munyon, C. N., Luders, H. O., and Fastenau, P. S. (2015). Visual-spatial memory may be enhanced with theta burst deep brain stimulation of the fornix: a preliminary investigation with four cases. *Brain J. Neurol.* 138, 1833–1842. doi: 10.1093/brain/awv095

Min, B., Guoming, L., and Jian, Z. (2013). Treatment of mesial temporal lobe epilepsy with amygdalohippocampal stimulation: A case series and review of the literature. *Exp. Ther. Med.* 5, 1264–1268. doi: 10.3892/etm.2013.968

Miocinovic, S., Khemani, P., Whiddon, R., Zeilman, P., Martinez-Ramirez, D., Okun, M. S., et al. (2014). Outcomes, management, and potential mechanisms of interleaving deep brain stimulation settings. *Parkinsonism Relat. Disord.* 20, 1434–1437. doi: 10.1016/j.parkreldis.2014.10.011

Molina, R., Hass, C. J., Cernera, S., Sowalsky, K., Schmitt, A. C., Roper, J. A., et al. (2021). Closed-Loop deep brain stimulation to treat medication-refractory freezing of gait in Parkinson's Disease. *Front. Hum. Neurosci.* 15:633655. doi: 10.3389/fnhum.2021.633655

Montgomery, E. B. (2005). Effect of subthalamic nucleus stimulation patterns on motor performance in Parkinson's disease. *Parkinsonism Relat. Disord.* 11, 167–171. doi: 10.1016/j.parkreldis.2004.12.002

Nakajima, A., Shimo, Y., Fuse, A., Tokugawa, J., Hishii, M., Iwamuro, H., et al. (2021). Case Report: Chronic adaptive deep brain stimulation personalizing therapy based on Parkinsonian State. *Front. Hum. Neurosci.* 15:702961. doi: 10.3389/fnhum.2021.702961

Okun, M. S., Fernandez, H. H., Wu, S. S., Kirsch-Darrow, L., Bowers, D., Bova, F., et al. (2009). Cognition and Mood in Parkinson Disease in STN versus GPi DBS: The COMPARE Trial. *Ann. Neurol.* 65, 586–595. doi: 10.1002/ana.21596

Okun, M. S., Hickey, P. T., Machado, A. G., Kuncel, A. M., and Grill, W. M. (2022). Temporally optimized patterned stimulation (TOPS®) as a therapy to personalize deep brain stimulation treatment of Parkinson's disease. *Front. Hum. Neurosci.* 16:929509. doi: 10.3389/fnhum.2022.929509

Opri, E., Cernera, S., Molina, R., Eisinger, R. S., Cagle, J. N., Almeida, L., et al. (2020). Chronic embedded cortico-thalamic closed-loop deep brain stimulation for the treatment of essential tremor. *Sci. Transl. Med.* 12:eaay7680. doi: 10.1126/scitranslmed.aay7680

Ostrem, J. L., Racine, C. A., Glass, G. A., Grace, J. K., Volz, M. M., Heath, S. L., et al. (2011). Subthalamic nucleus deep brain stimulation in primary cervical dystonia. *Neurology* 76, 870–878. doi: 10.1212/WNL.0b013e31820f2e4f

Ozturk, M., Viswanathan, A., Sheth, S. A., and Ince, N. F. (2021). Electroceutically induced subthalamic high-frequency oscillations and evoked compound activity may explain the mechanism of therapeutic stimulation in Parkinson's disease. *Commun. Biol.* 4:393. doi: 10.1038/s42003-021-01915-7

Paek, S. B., Knight, E. J., Chang, S.-Y., Lujan, J. L., Jang, D. P., Bennet, K. E., et al. (2013). Dopamine measurement during prolonged deep brain stimulation: a proof-of-principle study of paired pulse voltammetry. *Biomed. Eng. Lett.* 3, 22–31. doi: 10.1007/s13534-013-0086-y

Parsons, T. D., Rogers, S. A., Braaten, A. J., Woods, S. P., and Tröster, A. I. (2006). Cognitive sequelae of subthalamic nucleus deep brain stimulation in Parkinson's disease: a meta-analysis. *Lancet Neurol.* 5, 578–588. doi: 10.1016/S1474-4422(06)70475-6

Pedrosa, D. J., Auth, M., Eggers, C., and Timmermann, L. (2013). Effects of low-frequency thalamic deep brain stimulation in essential tremor patients. *Exp. Neurol.* 248, 205–212. doi: 10.1016/j.expneurol.2013.06.009

Pedrosa, D. J., Auth, M., Pauls, K. A. M., Runge, M., Maarouf, M., Fink, G. R., et al. (2014). Verbal fluency in essential tremor patients: the effects of deep brain stimulation. *Brain Stimulat.* 7, 359–364. doi: 10.1016/j.brs.2014.02.012

Perestelo-Pérez, L., Rivero-Santana, A., Pérez-Ramos, J., Serrano-Pérez, P., Panetta, J., and Hilarion, P. (2014). Deep brain stimulation in Parkinson's disease: meta-analysis of randomized controlled trials. *J. Neurol.* 261, 2051–2060. doi: 10.1007/s00415-014-7254-6

Petrucci, M. N., Neuville, R. S., Afzal, M. F., Velisar, A., Anidi, C. M., Anderson, R. W., et al. (2020). Neural closed-loop deep brain stimulation for freezing of gait. *Brain Stimulat.* 13, 1320–1322. doi: 10.1016/j.brs.2020.06.018

Piña-Fuentes, D., Beudel, M., Little, S., Brown, P., Oterdoom, D. L. M., and van Dijk, J. M. C. (2019). Adaptive deep brain stimulation as advanced Parkinson's disease treatment (ADAPT study): protocol for a pseudo-randomised clinical study. *BMJ Open* 9:e029652. doi: 10.1136/bmjopen-2019-029652

Piña-Fuentes, D., Beudel, M., Van Zijl, J. C., Van Egmond, M. E., Oterdoom, D. L. M., Van Dijk, J. M. C., et al. (2020a). Low-frequency oscillation suppression in dystonia: Implications for adaptive deep brain stimulation. *Parkinsonism Relat. Disord.* 79, 105–109. doi: 10.1016/j.parkreldis.2020.08.030

Piña-Fuentes, D., van Dijk, J. M. C., van Zijl, J. C., Moes, H. R., van Laar, T., Oterdoom, D. L. M., et al. (2020b). Acute effects of adaptive Deep Brain Stimulation in Parkinson's disease. *Brain Stimulat.* 13, 1507–1516. doi: 10.1016/j.brs.2020.07.016

Piña-Fuentes, D., Little, S., Oterdoom, M., Neal, S., Pogosyan, A., Tijssen, M. A. J., et al. (2017). Adaptive DBS in a Parkinson's patient with chronically implanted DBS: A proof of principle. *Mov. Disord.* 32, 1253–1254. doi: 10.1002/mds.26959

Provenza, N. R., Matteson, E. R., Allawala, A. B., Barrios-Anderson, A., Sheth, S. A., Viswanathan, A., et al. (2019). The Case for Adaptive Neuromodulation to Treat Severe Intractable Mental Disorders. *Front. Neurosci.* 13:152. doi: 10.3389/fnins.2019.00152

Provenza, N. R., Sheth, S. A., Dastin-van Rijn, E. M., Mathura, R. K., Ding, Y., Vogt, G. S., et al. (2021). Long-term ecological assessment of intracranial electrophysiology synchronized to behavioral markers in obsessive-compulsive disorder. *Nat. Med.* 27, 2154–2164. doi: 10.1038/s41591-021-01550-z

Ramirez-Zamora, A., Kahn, M., Campbell, J., DeLaCruz, P., and Pilitsis, J. G. (2015). Interleaved programming of subthalamic deep brain stimulation to avoid adverse effects and preserve motor benefit in Parkinson's disease. *J. Neurol.* 262, 578–584. doi: 10.1007/s00415-014-7605-3

Razmkon, A., Abdollahifard, S., Taherifard, E., Roshanshad, A., and Shahrivar, K. (2022). Effect of deep brain stimulation on freezing of gait in patients with Parkinson's disease: a systematic review. *Br. J. Neurosurg.* [Epub ahead of print]. doi: 10.1080/02688697.2022.2077308

Reich, S. G., and Savitt, J. M. (2019). Parkinson's Disease. *Med. Clin. North Am.* 103, 337–350. doi: 10.1016/j.mcna.2018.10.014

Rosa, M., Arlotti, M., Ardolino, G., Cogiamanian, F., Marceglia, S., Di Fonzo, A., et al. (2015). Adaptive deep brain stimulation in a freely moving Parkinsonian patient. *Mov. Disord.* 30, 1003–1005. doi: 10.1002/mds.26241

Rosa, M., Arlotti, M., Marceglia, S., Cogiamanian, F., Ardolino, G., Fonzo, A. D., et al. (2017). Adaptive deep brain stimulation controls levodopa-induced side effects in Parkinsonian patients. *Mov. Disord.* 32, 628–629. doi: 10.1002/mds.26953

Rosenbaum, R., Zimnik, A., Zheng, F., Turner, R. S., Alzheimer, C., Doiron, B., et al. (2014). Axonal and synaptic failure suppress the transfer of firing rate oscillations, synchrony and information during high frequency deep brain stimulation. *Neurobiol. Dis.* 62, 86–99. doi: 10.1016/j.nbd.2013.09.006

Sáenz-Farret, M., Loh, A., Boutet, A., Germann, J., Elias, G. J. B., Kalia, S. K., et al. (2021). Theta burst deep brain stimulation in movement disorders. *Mov. Disord. Clin. Pract.* 8, 282–285. doi: 10.1002/mdc3.13130

Sarikhani, P., Ferleger, B., Mitchell, K., Ostrem, J., Herron, J., Mahmoudi, B., et al. (2022). Automated deep brain stimulation programming with safety constraints for tremor suppression in patients with Parkinson's disease and essential tremor. *J. Neural Eng.* 19, ac86a2. doi: 10.1088/1741-2552/ac86a2

Sasaki, F., Oyama, G., Sekimoto, S., Nuermaimaiti, M., Iwamuro, H., Shimo, Y., et al. (2021). Closed-loop programming using external responses for deep brain stimulation in Parkinson's disease. *Parkinsonism Relat. Disord.* 84, 47–51. doi: 10.1016/j.parkreldis.2021.01.023

Scangos, K. W., Khambhati, A. N., Daly, P. M., Makhoul, G. S., Sugrue, L. P., Zamanian, H., et al. (2021). Closed-loop neuromodulation in an individual with treatment-resistant depression. *Nat. Med.* 27, 1696–1700. doi: 10.1038/s41591-021-01480-w

Schlenstedt, C., Shalash, A., Muthuraman, M., Falk, D., Witt, K., and Deuschl, G. (2017). Effect of high-frequency subthalamic neurostimulation on gait and freezing of gait in Parkinson's disease: a systematic review and meta-analysis. *Eur. J. Neurol.* 24, 18–26. doi: 10.1111/ene.13167

Shanker, V. (2019). Essential tremor: diagnosis and management. *BMJ* 366:14485. doi: 10.1136/bmj.l4485

Shu, W., Li, Y., Li, J., and Zhang, Y. (2018). Interleaving programming in pallidal deep brain stimulation improves outcomes in a patient with Meige syndrome. *Br. J. Neurosurg.* 32, 661–662. doi: 10.1080/02688697.2018.1504883

Solomon, E. A., Sperling, M. R., Sharan, A. D., Wanda, P. A., Levy, D. F., Lyalenko, A., et al. (2021). Theta-burst stimulation entrains frequency-specific oscillatory responses. *Brain Stimulat.* 14, 1271–1284. doi: 10.1016/j.brs.2021.08.014

Su, D., Chen, H., Hu, W., Liu, Y., Wang, Z., Wang, X., et al. (2018). Frequency-dependent effects of subthalamic deep brain stimulation on motor symptoms in Parkinson's disease: a meta-analysis of controlled trials. *Sci. Rep.* 8:14456. doi: 10.1038/s41598-018-32161-3

Swann, N. C., de Hemptinne, C., Thompson, M. C., Miocinovic, S., Miller, A. M., Gilron, R., et al. (2018). Adaptive deep brain stimulation for Parkinson's disease using motor cortex sensing. *J. Neural Eng.* 15:46006. doi: 10.1088/1741-2552/aabc9b

Tai, C.-H., Wu, R.-M., Liu, H.-M., Tsai, C.-W., and Tseng, S.-H. (2011). Meige syndrome relieved by bilateral pallidal stimulation with cycling mode: case report. *Neurosurgery* 69, E1333–E1337. doi: 10.1227/NEU.0b013e31822a9ad2

Tass, P. A. (2003). A model of desynchronizing deep brain stimulation with a demand-controlled coordinated reset of neural subpopulations. *Biol. Cybern.* 89, 81–88. doi: 10.1007/s00422-003-0425-7

Tinkhauser, G., Pogosyan, A., Little, S., Beudel, M., Herz, D. M., Tan, H., et al. (2017). The modulatory effect of adaptive deep brain stimulation on beta bursts in Parkinson's disease. *Brain J. Neurol.* 140, 1053–1067. doi: 10.1093/brain/awx010

Titiz, A. S., Hill, M. R. H., Mankin, E. A., Aghajan, M. Z., Eliashiv, D., Tchemodanov, N., et al. (2017). Theta-burst microstimulation in the human entorhinal area improves memory specificity. *eLife* 6:e29515. doi: 10.7554/eLife.29515

Vallabhajosula, S., Haq, I. U., Hwynn, N., Oyama, G., Okun, M., Tillman, M. D., et al. (2015). Low-frequency versus high-frequency subthalamic nucleus deep brain stimulation on postural control and gait in Parkinson's disease: a quantitative study. *Brain Stimulat.* 8, 64–75. doi: 10.1016/j.brs.2014.10.011

Vázquez-Barrón, D., Cuéllar-Herrera, M., Velasco, F., and Velasco, A. L. (2021). Electrical Stimulation of Subiculum for the Treatment of Refractory Mesial Temporal Lobe Epilepsy with Hippocampal Sclerosis: A 2-Year Follow-Up Study. *Stereotact. Funct. Neurosurg.* 99, 40–47. doi: 10.1159/000510295

Velasco, F., Velasco, A. L., Velasco, M., Jiménez, F., Carrillo-Ruiz, J. D., and Castro, G. (2007). Deep brain stimulation for treatment of the epilepsies: the centromedian thalamic target. *Acta Neurochir. Suppl.* 97, 337–342. doi: 10.1007/978-3-211-33081-4_38

Velisar, A., Syrkin-Nikolau, J., Blumenfeld, Z., Trager, M. H., Afzal, M. F., Prabhakar, V., et al. (2019). Dual threshold neural closed loop deep brain stimulation in Parkinson disease patients. *Brain Stimulat.* 12, 868–876. doi: 10.1016/j.brs.2019.02.020

Vivekananda, U., Bush, D., Bisby, J. A., Baxendale, S., Rodionov, R., Diehl, B., et al. (2021). Theta power and theta-gamma coupling support long-term spatial memory retrieval. *Hippocampus* 31, 213–220. doi: 10.1002/hipo.23284

Wang, J., Fergus, S. P., Johnson, L. A., Nebeck, S. D., Zhang, J., Kulkarni, S., et al. (2022). Shuffling Improves the Acute and Carryover Effect of Subthalamic Coordinated Reset Deep Brain Stimulation. *Front. Neurol.* 13:716046. doi: 10.3389/fneur.2022.716046

Wilson, D., and Moehlis, J. (2015). Clustered Desynchronization from High-Frequency Deep Brain Stimulation. *PLoS Comput. Biol.* 11:e1004673. doi: 10.1371/journal.pcbi.1004673

Wojtecki, L., Vesper, J., and Schnitzler, A. (2011). Interleaving programming of subthalamic deep brain stimulation to reduce side effects with good motor outcome in a patient with Parkinson's disease. *Parkinsonism Relat. Disord.* 17, 293–294. doi: 10.1016/j.parkreldis.2010.12.005

Wong, J. K., Hu, W., Barmore, R., Lopes, J., Moore, K., Legacy, J., et al. (2021). Safety and Tolerability of Burst-Cycling Deep Brain Stimulation for Freezing of Gait in Parkinson's Disease. *Front. Hum. Neurosci.* 15:651168. doi: 10.3389/fnhum.2021.651168

Xie, C.-L., Shao, B., Chen, J., Zhou, Y., Lin, S.-Y., and Wang, W.-W. (2016). Effects of neurostimulation for advanced Parkinson's disease patients on motor symptoms: A multiple-treatments meta-analysas of randomized controlled trials. *Sci. Rep.* 6:25285. doi: 10.1038/srep25285

Xie, T., Bloom, L., Padmanaban, M., Bertacchi, B., Kang, W., MacCracken, E., et al. (2018). Long-term effect of low frequency stimulation of STN on dysphagia, freezing of gait and other motor symptoms in PD. *J. Neurol. Neurosurg. Psychiatry* 89, 989–994. doi: 10.1136/jnnp-2018-318060

Yamawaki, N., Magill, P. J., Woodhall, G. L., Hall, S. D., and Stanford, I. M. (2012). Frequency selectivity and dopamine-dependence of plasticity at glutamatergic synapses in the subthalamic nucleus. *Neuroscience* 203, 1–11. doi: 10.1016/j.neuroscience.2011.12.027

Yu, H., Takahashi, K., Bloom, L., Quaynor, S. D., and Xie, T. (2020). Effect of Deep Brain Stimulation on Swallowing Function: A Systematic Review. *Front. Neurol.* 11:547. doi: 10.3389/fneur.2020.00547

Zafar, S. M., Rajan, R., Krishnan, S., Kesavapisharady, K., and Kishore, A. (2021). Interleaved Stimulation for Freezing of Gait in Advanced Parkinson's Disease. *Neurol. India* 69, 457–460. doi: 10.4103/0028-3886.314570

Zavala, B., Damera, S., Dong, J. W., Lungu, C., Brown, P., and Zaghloul, K. A. (2017). Human Subthalamic Nucleus Theta and Beta Oscillations Entrain Neuronal Firing During Sensorimotor Conflict. *Cereb. Cortex N. Y. N.* 27, 496–508.

Zeng, K., Drummond, N. M., Ghahremani, A., Saha, U., Kalia, S. K., Hodaie, M., et al. (2021). Fronto-subthalamic phase synchronization and cross-frequency coupling during conflict processing. *Neuroimage* 238:118205.

Zhang, C., Pan, Y., Zhou, H., Xie, Q., Sun, B., Niu, C. M., et al. (2019). Variable High-Frequency Deep Brain Stimulation of the Subthalamic Nucleus for Speech Disorders in Parkinson's Disease: A Case Report. *Front. Neurol.* 10:379.

Zhang, S., Wang, Y., Li, P., and Wang, W. (2018). Interleaving pallidal deep brain stimulation improves the degree of benefit obtained in a patient with dystonia. *Neurol. India* 66, S138–S141. doi: 10.4103/0028-3886.226442

Zhang, S., Zhou, P., Jiang, S., Wang, W., and Li, P. (2016). Interleaving subthalamic nucleus deep brain stimulation to avoid side effects while achieving satisfactory motor benefits in Parkinson disease: A report of 12 cases. *Medicine* 95:e5575. doi: 10.1097/MD.0000000000005575

Zucker, R. S., and Regehr, W. G. (2002). Short-term synaptic plasticity. *Annu. Rev. Physiol.* 64, 355–405. doi: 10.1146/annurev.physiol.64.092501.114547

frontiers | Frontiers in Neuroinformatics

TYPE Original Research
PUBLISHED 22 August 2023
DOI 10.3389/fninf.2023.1217786

OPEN ACCESS

EDITED BY
Fu-Ming Zhou,
University of Tennessee Health Science Center (UTHSC), United States

REVIEWED BY
Alexander K. Kozlov,
Royal Institute of Technology, Sweden
Atefeh Asadi,
Institute for Advanced Studies in Basic Sciences (IASBS), Iran

*CORRESPONDENCE
Justus A. Kromer
✉ jkromer@stanford.edu

RECEIVED 05 May 2023
ACCEPTED 31 July 2023
PUBLISHED 22 August 2023

CITATION
Kromer JA, Bokil H and Tass PA (2023) Synaptic network structure shapes cortically evoked spatio-temporal responses of STN and GPe neurons in a computational model. *Front. Neuroinform.* 17:1217786. doi: 10.3389/fninf.2023.1217786

Synaptic network structure shapes cortically evoked spatio-temporal responses of STN and GPe neurons in a computational model

Justus A. Kromer[1]*, Hemant Bokil[2] and Peter A. Tass[1]

[1]Department of Neurosurgery, Stanford University, Stanford, CA, United States, [2]Boston Scientific Neuromodulation, Valencia, CA, United States

Introduction: The basal ganglia (BG) are involved in motor control and play an essential role in movement disorders such as hemiballismus, dystonia, and Parkinson's disease. Neurons in the motor part of the BG respond to passive movement or stimulation of different body parts and to stimulation of corresponding cortical regions. Experimental evidence suggests that the BG are organized somatotopically, i.e., specific areas of the body are associated with specific regions in the BG nuclei. Signals related to the same body part that propagate along different pathways converge onto the same BG neurons, leading to characteristic shapes of cortically evoked responses. This suggests the existence of functional channels that allow for the processing of different motor commands or information related to different body parts in parallel. Neurological disorders such as Parkinson's disease are associated with pathological activity in the BG and impaired synaptic connectivity, together with reorganization of somatotopic maps. One hypothesis is that motor symptoms are, at least partly, caused by an impairment of network structure perturbing the organization of functional channels.

Methods: We developed a computational model of the STN-GPe circuit, a central part of the BG. By removing individual synaptic connections, we analyzed the contribution of signals propagating along different pathways to cortically evoked responses. We studied how evoked responses are affected by systematic changes in the network structure. To quantify the BG's organization in the form of functional channels, we suggested a two-site stimulation protocol.

Results: Our model reproduced the cortically evoked responses of STN and GPe neurons and the contributions of different pathways suggested by experimental studies. Cortical stimulation evokes spatio-temporal response patterns that are linked to the underlying synaptic network structure. Our two-site stimulation protocol yielded an approximate functional channel width.

Discussion/conclusion: The presented results provide insight into the organization of BG synaptic connectivity, which is important for the development of computational models. The synaptic network structure strongly affects the processing of cortical signals and may impact the generation of pathological rhythms. Our work may motivate further experiments to analyze the network structure of BG nuclei and their organization in functional channels.

KEYWORDS

basal ganglia, evoked responses, functional channels, network connectivity, multichannel stimulation, neural networks

1. Introduction

The BG are a sub-cortical complex that consists of several nuclei, such as the subthalamic nucleus (STN) and the globus pallidus (Soghomonian and Jagaroo, 2016). Due to different synaptic projections, the latter is divided into internal (GPi) and external segments (GPe). The BG play an important role in decision-making, motor control, and motor learning. Several neurological disorders are associated with abnormal BG activity, such as excessive synchronization in Parkinson's disease, and alternations in synaptic connectivity (Hammond et al., 2007; Madadi Asl et al., 2022b). The STN and GPe circuit is in the center of the BG and is believed to be critical for the generation of oscillations (Plenz and Kital, 1999; Bevan et al., 2002; Crompe et al., 2020). Furthermore, the STN is a major target for high-frequency deep brain stimulation, the current standard of care for medically refractory Parkinson's disease (Krack et al., 2003).

The STN receives topographically organized glutamatergic inputs from the cerebral cortex via the cortico-STN hyperdirect pathway, and gamma-aminobutyric acid (GABA)ergic inputs from the GPe via the cortico-striato-GPe-STN indirect pathway (see Figure 1) (Jeon et al., 2022). Additionally, synaptic input to the BG nuclei is organized somatotopically (Nambu, 2011), i.e., motor cortical neurons in regions representing different body parts project to different regions in these nuclei (Monakow et al., 1978; Nambu et al., 1996, 2002; Miyachi et al., 2006). On the other hand, BG neurons respond to motor cortex stimulation (Nambu et al., 2000; Kita and Kita, 2011; Polyakova et al., 2020) and to active and passive movement of corresponding body parts (DeLong et al., 1985). These characteristics are harnessed during stereotaxic surgery for electrode placement for deep brain stimulation as a treatment for movement disorders such as Parkinson's disease (Kaplitt et al., 2003; Krack et al., 2003).

Experimental studies in primates and rodents analyzed the response of STN and GPe neurons to electrical stimulation of different cortical areas, including the limb regions of the motor cortex, the primary sensory cortex, and the supplementary motor area (Nambu et al., 2000; Kita et al., 2004; Kita and Kita, 2011; Polyakova et al., 2020). The effect of local injections of glutamate and GABA antagonists into the STN (Polyakova et al., 2020), the GPe (Kita et al., 2004) as well as into the putamen and the GPe (Polyakova et al., 2020) on evoked responses was studied to get further insight into the involved pathways (Kita et al., 2004; Jaeger and Kita, 2011; Polyakova et al., 2020). Responding STN neurons showed complex response patterns characterized by an early and a late excitation followed by a late inhibition. These patterns indicated that signals from the stimulated cortical region reach STN neurons via two pathways: the monosynaptic cortico-STN pathway and the polysynaptic cortico-striato-GPe-STN pathway (Nambu et al., 2000; Kita and Kita, 2011; Polyakova et al., 2020). Furthermore, responding GPe neurons show characteristic responses consisting of an early excitation, an inhibition, and a late excitation (Nambu et al., 2000; Jaeger and Kita, 2011; Kita and Kita, 2011). The analysis of these evoked responses revealed the complex interplay of synaptic pathways in the cortico-basal ganglia circuit.

Evidence from animal models suggests that Parkinson's disease is not only accompanied by abnormal neuronal synchrony (Hammond et al., 2007) but also by alterations of synaptic connectivity in the BG (Fan et al., 2012; Chu et al., 2015, 2017; Madadi Asl et al., 2022b) and impaired somatotopy (Filion et al., 1988; Boraud et al., 2000; Cho et al., 2002). Furthermore, characteristic features of cortically evoked responses change in 6-hydroxydopamine (6-OHDA) lesioned rats, an animal model for Parkinson's disease (Kita and Kita, 2011). Besides Parkinson's disease, abnormal alterations of the somatotopic organization of the BG and their cortical inputs have been observed in other movement disorders (Bronfeld and Bar-Gad, 2011), such as motor tics (McCairn et al., 2009), appearing as a symptom, for instance, in Tourette syndrome, and dystonia (Tamburin et al., 2002; Delmaire et al., 2005). This suggests that alterations of synaptic connectivity shape cortically evoked responses, and likely affect the processing of cortical stimuli.

In the present paper, we build on these results and explore to which extent cortically evoked responses of STN and GPe neurons can be used to infer characteristics of the underlying synaptic network structure. In a computational model, we show that a characteristic width of parallel "functional channels" in the BG, which allow for parallel processing of multiple stimulation-induced cortical inputs, can be obtained based on the cortically evoked responses of STN and GPe neurons. Considering the underlying channel structure may be advantageous for the parameter adjustment and stimulation contact usage during multisite deep brain stimulation, for instance, for the delivery of coordinated reset stimulation in animal models for Parkinson's disease (Tass et al., 2012; Wang et al., 2016, 2022; Bore et al., 2022) or Parkinson's disease patients (Adamchic et al., 2014).

To study the relation between synaptic connectivity and cortically evoked responses, we developed a computational model of the BG that incorporates a simplified type of somatotopy (Nambu, 2011), where neurons tend to project to neurons that represent similar body parts characterized by similar (spatial) coordinates, as well as two modified somatotopy variants. Our model produces cortically evoked responses that mimic experimental data from rats (Kita and Kita, 2011). We analyzed the spatio-temporal pattern of cortically evoked responses and explored how it is affected by perturbations of the synaptic network structure. To quantify the width of parallel functional channels in the BG, we suggest a two-site stimulation approach in which two cortical stimuli cause two evoked responses in the STN and GPe. We quantify the modulation of the evoked response to a test stimulus by the presence of a priming stimulus and show how an approximate channel width can be inferred. The latter measures the minimum distance between cortical areas whose input to the BG is processed independently.

The present paper is organized as follows. First, we introduce our computational model and present details on the incorporated experimental data on synaptic connectivity as well as the suggested two-site stimulation technique. Next, we show that our computational model reproduces the experimentally observed characteristic sequence of excitations and inhibitions. Then, we analyze the spatio-temporal response pattern and study how it is affected by variations of the synaptic network structure. We present simulation results on evoked responses of STN and GPe neurons during two-site cortical stimulation and show how an estimate of

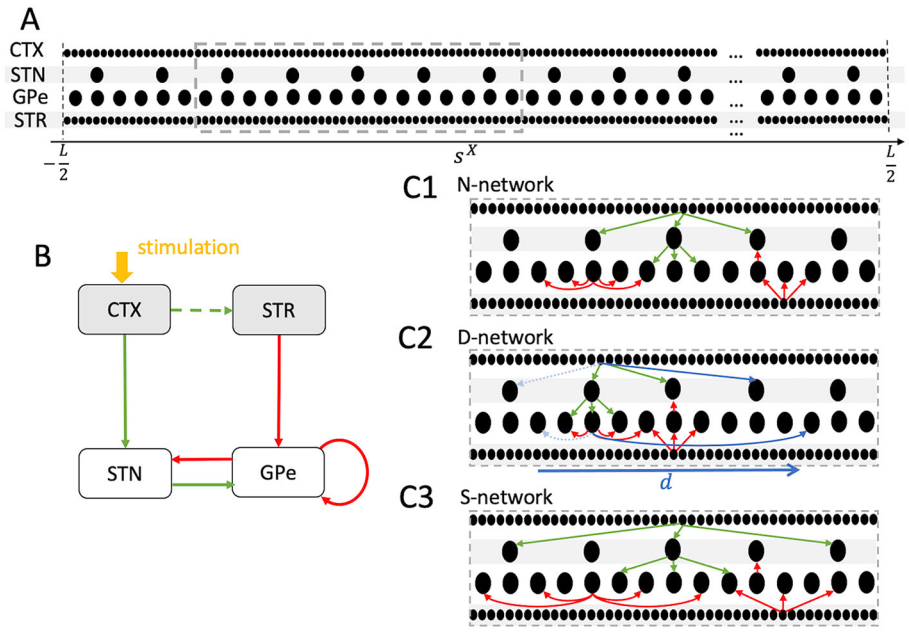

FIGURE 1
Schematics of neuron placement and the three network structures considered throughout the paper. **(A)** Neurons (black dots) were placed in the interval $[-L/2, L/2]$ (Model and methods). Similar coordinates, s^X, refer to neurons representing similar body parts. A total of 10^3 cortical (CTX), 100 STN, 300 GPe, and 10^3 striatal (STR) medium spiny neurons (MSN) was considered. **(B)** Schematic of the STN-GPe circuit and its CTX and STR Poisson input (gray). Green arrows indicate glutamatergic and red arrows GABAergic synaptic interaction. Stimulation (yellow) is delivered to the CTX Poisson spike generators and leads to a transient increase of spiking activity in the cortex. Excitatory CTX input to the striatum is modeled by increasing STR MSN activity following CTX stimulation (see Model and methods). **(C1–C3)** Schematics of *nearest postsynaptic neurons* networks (N-networks) **(C1)**, *displaced postsynaptic neurons* networks (D-networks) **(C2)**, and *skip postsynaptic neurons* networks (S-networks) **(C3)**. A small number of connections of each type are shown for a single presynaptic neuron in a small portion of the network (dashed gray box in **A**). The actual numbers of connections are given in Table 2. In N-networks **(C1)**, neurons project to postsynaptic neurons at similar coordinates. In D-networks **(C2)**, 10% of the synaptic connections are randomly selected to connect to postsynaptic neurons with coordinates shifted by d (blue, see Model and Methods). Connections before shifting are marked by dashed light blue arrows. In S-networks **(C3)**, neurons project to postsynaptic neurons with similar coordinates except that every second postsynaptic neuron is skipped.

the width of functional channels in the cortico-BG network can be obtained. Finally, we discuss our results.

2. Model and methods

We developed a computational model of the STN-GPe circuit that accounts for topographically organized synaptic connections. Following earlier studies, individual neurons were modeled by adaptive quadratic integrated-and-fire neurons to ensure low computational costs (Lindahl et al., 2013; Fountas and Shanahan, 2017). The organization of synaptic connections was partly motivated by earlier computational studies (Terman et al., 2002; Hahn and McIntyre, 2010; Kumaravelu et al., 2016), partly based on experimental data on the synaptic connectivity in the STN-GPe circuit (Oorschot, 1996; Sadek et al., 2007; Baufreton et al., 2009; Kita and Kita, 2011; Koshimizu et al., 2013; Ketzef and Silberberg, 2021), and partly obtained from parameter optimization to reproduce experimentally observed mean firing rates of the neurons (Fountas and Shanahan, 2017). Note that firing rates of BG neurons in rats vary depending on the state, e.g., awake, anesthetized, resting. Whenever possible, we considered the data from Kita and Kita (2011) in anesthetized rats, as they provide a detailed analysis of cortically evoked responses.

2.1. Neural network model

2.1.1. Dynamics of membrane potentials

Following the approach of Lindahl et al. (2013) and Fountas and Shanahan (2017), individual neurons were modeled using adaptive quadratic integrate-and-fire neurons. This class of models was found to reproduce a wide class of neuronal spiking and bursting behavior (Izhikevich, 2003). The dynamics of the membrane potential, v_i, of the ith GPe neuron was modeled as follows (Fountas and Shanahan, 2017)

$$\begin{aligned} C_i^{\mathrm{GPe}} \frac{d}{dt} v_i &= k^{\mathrm{GPe}}(v_i - v^{\mathrm{r,GPe}})(v_i - v^{\mathrm{t,GPe}}) - u_{1i} + I_{\mathrm{GPe}}, \\ \frac{d}{dt} u_{1i} &= a^{\mathrm{GPe}}(b^{\mathrm{GPe}}(v_i - v^{\mathrm{r,GPe}}) - u_{1i}). \end{aligned} \tag{1}$$

C_i^{GPe} is the membrane capacitance, I_{GPe} the applied current, and u_{1i} is a slow recovery variable with time scale given by $1/a^{\mathrm{GPe}}$. $v^{\mathrm{r,GPe}}$ is the resting potential and $v^{\mathrm{t,GPe}}$ corresponds to the threshold potential. The other parameters adjust the shape of the nullclines and were chosen according to Fountas and Shanahan (2017).

We considered the parameter set for GPe neurons that exhibited periods of high frequency discharges (referred to as "GPe type B" neurons in Fountas and Shanahan (2017). These correspond to prototypic GPe neurons which present the largest neuronal population in the GPe and project to the STN (Mallet et al., 2012; Abdi et al., 2015). Neurons with this type of dynamics were observed more often than others in experiments in monkeys at rest (≈ 85% of GPe neurons in DeLong, 1972). Abdi et al. found that about two-thirds of GPe neurons are prototypic neurons in dopamine-intact rats (Abdi et al., 2015).

Whenever the membrane potential passed a threshold $v_{\text{peak}}^{\text{GPe}}$, the state variables were reset, i.e., $v_i \rightarrow c^{\text{GPe}}$ and $u_{1i} \rightarrow u_{1i} + d^{\text{GPe}}$ (Fountas and Shanahan, 2017).

To describe the dynamics of the membrane potential of the ith STN neuron, an additional slow variable was introduced (Fountas and Shanahan, 2017):

$$\begin{aligned} C_i^{\text{STN}} \frac{d}{dt} v_i &= k^{\text{STN}}(v_i - v^{\text{r,STN}})(v_i - v^{\text{t,STN}}) - u_{1i} - w^{\text{STN}} u_{2i} \\ &\quad + I^{\text{STN}}, \\ \frac{d}{dt} u_{1i} &= a_{\text{STN}}(b^{\text{STN}}(v_i - v^{\text{r,STN}}) - u_{1i}), \\ \frac{d}{dt} u_{2i} &= \tilde{a}^{\text{STN}}(G(v_i)\tilde{b}^{\text{STN}}(v_i - \tilde{v}^{\text{r,STN}}) - u_{2i}). \end{aligned} \tag{2}$$

The first two equations describe the dynamics of the membrane potential and a recovery variable, similar to the dynamics of GPe neurons given in Equation (1). In addition, a second recovery variable u_{2i} is used to describe the dynamics of STN neurons. $G(v_i)$ is the Heaviside step function, $H(\tilde{v}^{\text{r,STN}} - v_i)$, such that u_{2i} activates below $\tilde{v}^{\text{r,STN}}$ and causes a rebound response (Fountas and Shanahan, 2017).

In rat brain slices, the majority of STN neurons was found to produce rebound burst firing after removal of a hyperpolarizing current (17 out of 20 neurons in Bevan et al., 2000). We modeled such STN neurons using the parameter set for rebound bursting STN neurons from Fountas and Shanahan (2017).

Whenever the membrane potential passed a threshold $v_{\text{peak}}^{\text{STN}} + Uu_{2i}$, the state variables of STN neurons were reset $v_i \rightarrow c^{\text{STN}} - Uu_{2i}$, $u_{1i} \rightarrow u_{1i} + d^{\text{STN}}$, and $u_{2i} \rightarrow u_{2i} + \tilde{d}^{\text{STN}}$ (Fountas and Shanahan, 2017). Here, $U = (w^{\text{STN}}|u_{2i}| + 1/w^{\text{STN}})^{-1}$ (Fountas and Shanahan, 2017).

To ensure heterogeneity, the membrane capacitances of neurons of each type X=STN or X=GPe were distributed according to a Gaussian distribution with mean $\langle C_j^{\text{X}} \rangle$ and standard deviation $0.1\langle C_j^{\text{X}} \rangle$. A complete list of the parameter values used to model GPe and STN neurons can be found in Table 1.

Cortical (CTX) neurons and striatal medium spiny neurons (MSN)s expressing D2 receptors were modeled as Poisson spike generators with baseline firing rates r^{CTX} and r^{MSN}, respectively. We used $r^{\text{CTX}} = 4$ Hz since Dejean et al. (2008) reported 4.1 ± 1.3 spikes per second in freely moving rats. In addition, we selected $r^{\text{MSN}} = 0.67$ Hz, representing the firing rate of spontaneously active medium spiny D2 neurons in anesthetized rats in the dopamine-intact state in Kita and Kita (2011). Note that r^{MSN} is well in the range of 0.8 ± 0.2 Hz reported by Dejean et al. (2008) for freely moving rats.

TABLE 1 Parameters for single-neuron dynamics according to Fountas and Shanahan (2017).

	GPe	STN
$\langle C_j^{\text{STN / GPe}} \rangle$ (pF)	68.0	23.0
$k^{\text{STN / GPe}}$ (nS/mV)	0.943	0.439
$v^{r,\text{STN / GPe}}$ (mV)	−53.0	−56.2
$\tilde{v}^{r,\text{STN / GPe}}$ (mV)		−60.0
$v^{t,\text{STN / GPe}}$ (mV)	−44.0	−41.4
$I_{\text{bias}}^{\text{STN / GPe}}$ (pA)	64.0	56.1
$w^{\text{STN / GPe}}$		0.1
$w^{\text{STN}\tilde{}\text{ / GPe}}$		0.0
$a^{\text{STN / GPe}}$ (1/ms)	0.0045	0.021
$b^{\text{STN / GPe}}$ (nS)	3.895	4.0
$\tilde{a}^{\text{STN / GPe}}$ (1/ms)		0.123
$\tilde{b}^{\text{STN / GPe}}$ (nS)		0.015
$v_{\text{peak}}^{\text{STN / GPe}}$ (mV)	25.0	15.4
$c^{\text{STN / GPe}}$ (ms)	−58.36	−47.7
$d^{\text{STN / GPe}}$ (pA)	0.353	17.1
$\tilde{d}^{\text{STN / GPe}}$ (pA)		−68.4
$\theta^{\text{STN / GPe}}$	3.0	0.5

In our computational model, we simulated 10^3 CTX and 10^3 MSN Poisson spike generators that provided synaptic input to the STN and GPe, respectively. The STN consisted of 100 neurons and the GPe of 300 neurons. The ratio of the total numbers of STN and GPe model neurons was selected to reproduce the ratio observed in young adult rats by Oorschot (1996). There, the total number of STN neurons was estimated as $(13.56 \pm 1.41) \times 10^3$ (mean ± std.) and the total number of GPe neurons as $(45.96 \pm 5.12) \times 10^3$ (mean ± std.).

2.1.2. Synaptic dynamics

To model synaptic connections, we considered the time-dependent conductances $g_j^{\text{X,Y}}(t)$, with dynamics given by

$$\tau^{\text{X,Y}} \frac{dg_j^{\text{X,Y}}}{dt} = -g_j^{\text{X,Y}}. \tag{3}$$

$\tau^{\text{X,Y}}$ is the synaptic time scale. $g_j^{\text{X,Y}}(t)$ describes the total input conductance for synaptic inputs from neurons in nucleus X to the neuron j in nucleus Y. $g_j^{\text{X,Y}}$ was increased instantaneously at all spike arrival times: $g_j^{\text{X,Y}} \rightarrow g_j^{\text{X,Y}} + G^{\text{X,Y}}$, at times $t_i + \lambda^{\text{X,Y}}$. Here, t_i is the spike time of a presynaptic neuron and $\lambda^{\text{X,Y}}$ is the synaptic transmission delay between presynaptic spike time and the arrival of the action potential at the synapse.

We considered GABAergic synapses and two types of receptors for glutamatergic synapses: alpha-amino-3-hydroxy-5-methyl-4-isoxazolepropionic acid (AMPA) receptors and slower N-methyl-D-aspartic acid (NMDA) receptors. As GABA and AMPA are considered rather fast, we neglect the rise time of the corresponding

synaptic conductances. The resulting postsynaptic currents were given by Fountas and Shanahan (2017)

$$I_{Z,j}^{X,Y} = g_j^{X,Y}(E^{X,Y} - v_j), \quad Z = \text{GABA,AMPA}. \tag{4}$$

$E^{X,Y}$ is the synaptic reversal potential. The dynamics of $g_j^{X,Y}$ is given by Equation (3) and the corresponding $\tau^{X,Y}$ is the decay time of the synaptic potentials.

In contrast, NMDA receptors are rather slow and the rise time of the corresponding conductance is of the order of the decay times for GABA and AMPA currents (Kumaravelu et al., 2016). We therefore modeled the rise and the decay of the corresponding synaptic conductances after each spike arrival:

$$I_{Z,j}^{X,Y}(v_j) = (g_{\text{slow},j}^{X,Y} - g_{\text{fast},j}^{X,Y})(E^{X,Y} - v_j), \quad Z = \text{NMDA}. \tag{5}$$

The dynamics of both the slow, $g_{\text{slow},j}^{X,Y}$, and fast conductance, $g_{\text{fast},j}^{X,Y}$, were given by Equation (3), and the corresponding synaptic time scales quantify the fast rise and the slow decay of the total synaptic conductance $g_{\text{slow},j}^{X,Y} - g_{\text{fast},j}^{X,Y}$, respectively, for the resulting postsynaptic currents. In addition, we considered a voltage-dependent magnesium plug for the NMDA receptors given by Fountas and Shanahan (2017)

$$B(v) = 1.0/(1.0 + 0.28\exp(-0.062\,v)). \tag{6}$$

The total postsynaptic current I_j^Y into neuron j in Equations (1) and (2) was then given by

$$\begin{aligned} I_j^{GPe} = \quad & I_{AMPA,j}^{STN,GPe}(v_j) + B(v_j)\, I_{NMDA,j}^{STN,GPe}(v_j) + I_{GABA,j}^{MSN,GPe}(v_j) \\ + \quad & I_{GABA,j}^{GPe,GPe}(v_j) + I_{bias}^{GPe} + \sqrt{2\theta^{GPe}}C_j^{GPe}\xi_j(t) \end{aligned} \tag{7}$$

and

$$\begin{aligned} I_j^{STN} = \quad & I_{AMPA,j}^{CTX,STN}(v_j) + B(v_j)\, I_{NMDA,j}^{CTX,STN}(v_j) + I_{GABA,j}^{GPe,STN}(v_j) + I_{bias}^{STN} \\ + \quad & \sqrt{2\theta^{STN}}C_j^{STN}\xi_j(t), \end{aligned} \tag{8}$$

respectively. Here, I_{bias}^{STN} and I_{bias}^{GPe} are constant bias currents that adjust the baseline activity of STN and GPe neurons, respectively. $\xi_j(t)$ is zero mean, white Gaussian noise with amplitude scaled by θ^X. All parameter values related to the synaptic dynamics are given in Table 2.

2.1.3. Synaptic network structure

Synaptic connections in the BG are somatotopically organized (Nambu, 2011). To incorporate somatotopy in our computational model, we introduced coordinates s^X, where X denotes the corresponding nucleus, as before. The maximal range of these coordinates is denoted by L and will be set to one. For a given neuron, s^X represents the *feature* that is represented, e.g., the body part or motor program. Similar coordinate values of different neurons refer to similar features. Alternatively, given that synaptic connections in the BG are organized somatotopically (Nambu, 2011), s^X can be interpreted as a spatial coordinate. Neurons in each nucleus were equidistantly placed in the interval $[-L/2, L/2]$.

In our reference scenario, which will be referred to as N-network throughout the paper, neurons connect to postsynaptic neurons with similar features, i.e., $s^X \approx s^Y$, where X refers to the presynaptic nucleus and Y to the postsynaptic nucleus. Thus, the somatotopic organization of synaptic connections is intact. In the computational model, we fixed the number of outgoing connections per neuron, $N^{X,Y}$, according to the values given in Table 2. Below, we give more details on the choices of $N^{X,Y}$. Then, for each presynaptic neuron, we chose the postsynaptic neurons such that the difference in coordinates $|s^Y - s^X|$ was minimal among all possible postsynaptic neurons.

Parkinson's disease and other neurological disorders impact many aspects of the nervous system. Here, as discussed below, we focus on synaptic reorganization. We compared the results for N-networks with perturbed network structures in which a portion of synaptic connections was rearranged. Specifically, we considered D-networks and S-networks, which were constructed as follows.

- **D-networks:** The first type of perturbation of N-networks was a *displacement* of a fraction of connections. Specifically, we randomly selected a portion $\mathcal{P}$ of the connections and rearranged them such that $|(s^Y - d) - s^X|$ was minimal (see Figure 1C2 for an illustration). Thus, these connections then targeted postsynaptic neurons that were displaced by d. Throughout the present paper, we chose $\mathcal{P} = 0.1$ and $d = 0.15L$. Connections were randomly selected for displacement according to a uniform probability distribution. D-networks mimic the situation were the somatotopy is perturbed such that a region representing a certain body part also forms projections to a region that represents a different body part. This was motivated by results in the 1-methyl-4-phenyl-l,2,3,6-tetrahydropyridine (MPTP) monkey model of Parkinson's disease, where pallidal neurons in control conditions responded to movement of a single joint but neurons responded to movement of multiple joints after MPTP intoxication (Filion et al., 1988; Boraud et al., 2000; Pessiglione et al., 2005; Bronfeld and Bar-Gad, 2011).
- **S-networks:** The second type of perturbation of the network structure was a skipping of neurons in the postsynaptic nucleus (see Figure 1C3 for an illustration). This led to an increase in the projection area in the postsynaptic nucleus. In the present paper, we considered the case where every second postsynaptic neuron was skipped. Thus, synaptic connections were implemented as in N-networks, except that each presynaptic neuron projected only to every second postsynaptic neuron, starting with the one for which $|s^Y - s^X|$ was minimal (see Figure 1C3). This network structure was motivated by experimental studies on striatal neurons in the 6-OHDA rat model for Parkinson's disease (Cho et al., 2002). There, neurons related to a certain body part occurred in clusters in healthy controls. After 6-OHDA lesion, the cluster size shrank and some of the neurons at the borders became related to different body parts, suggesting a larger overlap of regions representing different body parts.

TABLE 2 Parameters used to model synaptic interaction.

	$\tau^{X,Y}$ (ms)	$\lambda^{X,Y}$ (ms)	$G^{X,Y}$ (nS)	$E^{X,Y}$ (mV)	$N^{X,Y}$
CTX→STN (AMPA)	2 [1]	1.0[1]	opt.	0 [1]	3 [1]
CTX→STN (NMDA)	2 [3], 100 [1]	$\lambda_{AMPA}^{CTX,STN}$	0.6 $G_{AMPA}^{CTX,STN}$	0 [1]	3 [1]
STN→GPe (AMPA)	2 [1]	1.0[2]	opt.	0 [1]	
STN→GPe (NMDA)	2 [3], 100 [1]	$\lambda_{AMPA}^{STN,GPe}$	0.36 $G_{AMPA}^{STN,GPe}$	0 [1]	
GPe→GPe	5 [4]	5.0 [5]	opt.	−85 [3]	20 [6]
MSN→GPe	5 [3]	7.4 [5][3]	opt.	−85[3]	10 [1]
GPe→STN	8 [4]	$\lambda^{STN,GPe}$	opt.	−84 [4]	1 [7]
CTX→MSN		10.5 [2]			

For NMDA receptors, the first synaptic time scale $\tau^{X,Y}$ represents the rise and the second the decay time. Values obtained from numerical optimization ("opt.") are given in Table 3. $N^{STN,GPe}$ was a free parameter. References: [1] Fountas and Shanahan (2017), [2] Kita and Kita (2011), [3] Kumaravelu et al. (2016), [4] Lindahl et al. (2013). [5] Ketzef and Silberberg (2021), [6] Kita (2007), and [7] Baufreton et al. (2009).

1. Was adjusted such that the onset of the early excitation in cortically evoked response occurs at ∼5 − 6 ms [2].
2. Was adjusted such that the onset of the early excitation in cortically evoked response occurs at ∼7 − 10 ms [2].
3. Onset delay of prototypic neurons to striatial stimulation was 7.34 ± 0.35 ms and that of arkypallidal cells 8.6 ± 0.43 ms [5]. Here, we only considered prototypic neurons.

To ensure that the obtained network did not depend on the order in which synaptic connections were added between neurons, we added small random offsets to the neurons' coordinates that were uniformly distributed between zero and $10^{-4}L$ for CTX and MSN Poisson spike generators and between zero and $10^{-3}L$ for STN and GPe neurons. This way, there were no two neuron pairs that had identical distances to each other. Then, pairs of pre- and postsynaptic neurons were sorted according to the distances between them, and synaptic connections were added.

The numbers of outgoing connections per presynaptic neuron, $N^{X,Y}$, were either motivated by experimental data, taken from earlier computational studies, or obtained from parameter optimization.

- For the outgoing synaptic connections of the two populations of Poisson spike generators, we chose $N^{CTX,STN} = 3$ and $N^{MSN,GPe} = 10$, which reproduced the connection probabilities used for random connections in Fountas and Shanahan (2017), where the connection probability for CTX to STN connections was 0.03 and the connection probability for MSN to GPe connections was 0.033.
- Baufreton et al. (2009) studied GPe→STN connections. They found that these connections were sparse but highly selective. Based on the number of synaptic boutons per GPe neuron in the STN, they estimated that each GPe neuron forms only enough synaptic boutons to contact < 2% of the STN neurons. Furthermore, they reported that GPe neurons form many synapses with each postsynaptic STN neuron. Their data also suggest that neighboring STN neurons rarely receive input from the same GPe neuron. Based on these findings, we chose $N^{GPe,STN} = 1$.
- Kita (2007) observed that large areas of somata and dendrites of the GPe projection neurons are covered with synaptic boutons. The majority of which belonged to striatal axons. We chose $N^{GPe,GPe} = 20$ outgoing GPe→GPe connections per GPe neuron such that the majority of GABAergic synapses came from striatal neurons.
- The numbers of outgoing STN→GPe connections differ substantially among previous computational models. Hahn and McIntyre (2010) considered rather focused projections of STN neurons to GPe neurons, resembling a high degree of specificity of STN→GPe connections in functionally related areas in the GPe as observed experimentally in monkeys (Shink et al., 1996). In their computational model, STN neurons only project to GPe neurons in the same channel, i.e., each STN neuron projected to the three closest GPe neurons ($N^{STN,GPe} = 3$). Other computational studies considered more diffuse STN→GPe connections, e.g., in Fountas and Shanahan (2017) each STN neuron projected to 30% of the GPe neurons (corresponding to 90 STN→GPe connections per STN neuron). In Lindahl et al. (2013), each STN neuron had 30 STN→GPe connections. These latter numbers were motivated by experimental data on the organization of STN and STR synaptic terminals in the GPe obtained from earlier labeling studies in monkeys (Hazrati and Parent, 1992; Parent and Hazrati, 1993). In these studies, it was suggested that STN→GPe and STR→GPe connections are highly organized and that STN excitation targets larger groups of GPe neurons. In contrast, STR inhibition specifically targets subsets of these groups. Later, STN projections were studied in more detail in rat brain segments (Koshimizu et al., 2013). There, STN neurons were found to form large numbers of axon boutons inside the GPe. Furthermore, boutons were highly clustered in groups indicating projections to localized groups of pallidal neurons. Furthermore, there was high variability in the number of axon boutons formed per STN neuron. Throughout the present paper, we varied the number of STN-GPe connections to study to which extent our results depend on $N^{STN,GPe}$. Specifically, we considered the cases $N^{STN,GPe} = 3$ (Hahn and McIntyre, 2010) and $N^{STN,GPe} = 30$ (Lindahl et al., 2013), spanning the range from highly focused (each STN neurons targets 1% of GPe neurons) onto a small cluster of GPe neurons to diffuse projections onto a macroscopic portion of the GPe (each STN neurons targets 10% of GPe neurons).

The values of all maximal synaptic conductances, $G^{X,Y}$, were chosen such that experimental data for the stationary mean firing rate of STN and GPe neurons were reproduced. In particular, we followed Fountas and Shanahan (2017) and considered a sequence of scenarios in which different neuronal populations were inhibited. Following, we describe the resulting parameter adjustment algorithm:

1. **Estimation of $G^{CTX,STN}$:** In the first step, we applied a parameter optimization algorithm to find values of $G^{CTX,STN}$ such that the mean firing rate of STN neurons was close to experimental data from Farries et al. (2010) in rats *in vivo*. In these rats, a large excitotoxic lesion was applied to the GPe. In our computational model, this was implemented by considering only the CTX spike generators and the STN neurons, i.e., the STN was isolated from the GPe by setting $G^{GPe,STN} = 0$ nS. Farries et al. (2010) reported STN firing rates of 20.7 ± 5.2 Hz during these experiments, which was about twice as large as the firing rate of STN neurons measured in rats with intact GPe (9.5 ± 3.5 Hz). The parameter optimization procedure was performed as follows: The firing rate of STN neurons was estimated by performing simulations of the computational model for 40 s and 12 different initial conditions. Each initial condition had a random realization of membrane capacitances, initial values of membrane potentials, and slow variables. To reduce finite size effects, neurons close to the borders of the interval for s^X were ignored and only spikes of the center third of STN neurons were recorded (STN neurons with indices $33-66$) during the time interval $t \in [30, 40)$ s. Then, an estimate of the average mean firing rate r_{est}^{STN} was obtained based on the spike count. These simulations were repeated for different values of $G^{CTX,STN}$ and the difference between r_{est}^{STN} and 20.7 Hz (Farries et al., 2010) was minimized using the python function "scipy.optimize.minimize" (scipy version 1.5.4) with "Nelder-Mead" method and a tolerance of 0.1. We used $G^{CTX,STN} = 1$ nS as the initial guess. This procedure led to $G^{CTX,STN} = 0.125$ nS.
2. **Estimation of $G^{GPe,STN}$:** To estimate the value of $G^{GPe,STN}$, we followed the approach of Fountas and Shanahan (2017) and added the GPe to the model from (1) using $G^{CTX,STN} = 0.125$ nS. For this step, the GPe neurons were modeled by a population of 300 Poisson spike generators with mean firing rate of 30.4 Hz (Kita and Kita, 2011, anesthetized rats). Then, we applied a similar algorithm as described in the previous paragraph optimizing the value of $G^{GPe,STN}$ such that the firing rate of STN neurons became close to 11.8 Hz. Kita and Kita (2011) measured 11.8 ± 9.1 Hz in rats that were anesthetized with isoflurane. The initial guess was $G^{GPe,STN} = 6.82$ nS which was the peak conductance measured by Baufreton et al. (2009). Baufreton et al. reported a range for $G^{GPe,STN}$ of $0.51 - 25.33$ nS). This optimization led to $G^{GPe,STN} = 1.11$ nS
3. **Estimation of $G^{STN,GPe}$:** Next, we adjusted the parameters $G^{STN,GPe}$ and $N^{STN,GPe}$. For $N^{STN,GPe}$, we considered two values that were taken from previous computational studies: $N^{STN,GPe} = 3$ (Hahn and McIntyre, 2010) and $N^{STN,GPe} = 30$ (Lindahl et al., 2013). For both values of $N^{STN,GPe}$, $G^{STN,GPe}$ was adjusted by considering the CTX-STN-GPe network without GABAergic inputs to GPe neurons. Celada et al. (1999) found that local bicuculline infusion, a GABA antagonist, into the globus pallidus of anesthetized rats led to a $\approx$ 55% increase of the mean firing rate of neurons in the globus pallidus. Note that the firing rate of these neurons in anesthetized rats might differ from the one in awake rats. Motivated by these experiments, we performed a similar optimization algorithm as in the previous paragraphs. During optimization, we replaced the STN neurons with a population of Poisson neurons firing with a mean firing rate of 11.8 Hz. This implicitly assumed that altered spiking of pallidal neurons in response to local bicuculline infusion had little effect on the majority of STN neurons. During optimization, the value of $G^{STN,GPe}$ was varied such that GPe firing rates were 55% higher than in control conditions. For the control case, we used the firing rates from Kita and Kita (2011), who measured 30.4 ± 11.4 Hz in rats anesthetized with isoflurane. Thus, our target firing rate for GPe neurons was 47.12 Hz. To tune $G^{STN,GPe}$, we ran the parameter optimization algorithm to find a value of $G^{STN,GPe}$ for which the GPe firing rate was close to the target values. For $N^{STN,GPe} = 3$ the algorithm led to $G^{STN,GPe} = 15.8$ nS for which we obtained $r_{est}^{GPe} \approx 47.1$ Hz. For $N^{STN,GPe} = 30$, we found $G^{STN,GPe} = 1.5$ nS resulting in $r_{est}^{GPe} \approx 47.0$ Hz.
4. **Estimation of $G^{MSN,GPe}$ and $G^{GPe,GPe}$:** For the two different values of $N^{STN,GPe}$ described in the previous paragraph and their corresponding values of $G^{STN,GPe}$, we searched for values of the maximal conductances $G^{MSN,GPe}$ and $G^{GPe,GPe}$ such that the STN firing rate was close to the target value 11.8 Hz (Kita and Kita, 2011, anesthetized rats) and the GPe firing rate was close to the target value 30.4 Hz (Kita and Kita, 2011, anesthetized rats) in the intact STN-GPe circuit (Figure 1). We minimized

$$\Delta R = \left| \frac{r^{STN} - 11.8\ \text{Hz}}{\sigma_{STN}} \right| + \left| \frac{r^{GPe} - 30.4\ \text{Hz}}{\sigma_{GPe}} \right|, \tag{9}$$

with $\sigma_{STN} = 9.1$ Hz and $\sigma_{GPe} = 11.4$ Hz being the estimated standard deviations of single neuron baseline firing rates obtained from Kita and Kita (2011) (anesthetized rats) (see Tables 1, 2 in Kita and Kita, 2011). Using a similar optimization algorithm as in the previous paragraphs, we found that $G^{MSN,GPe} = 5.54$ nS and $G^{GPe,GPe} = 0.44$ nS minimized ΔR for $N^{STN,GPe} = 3$ (the resulting firing rates were $r_{est}^{STN} \approx 13.6$ Hz and $r_{est}^{GPe} \approx 30.5$ Hz). For $N^{STN,GPe} = 30$, we found that $G^{MSN,GPe} = 12.0$ nS and $G^{GPe,GPe} = 0.21$ nS minimized ΔR, which led to $r_{est}^{STN} \approx 11.8$ Hz and $r_{est}^{GPe} \approx 30.4$ Hz.

2.2. Cortical stimulation

Cortical stimulation was modeled by temporally increasing the firing rate of cortical Poisson spike generators. We implemented a spatial stimulus profile that determined the probability $P(s_i^{CTX}|s_0)$ at which a cortical Poisson spike generator at coordinate s_i^{CTX} spikes in response to a stimulus delivered to s_0

$$P(s_i^{CTX}|s_0) = \left(1 + \left(\frac{s_i^{CTX} - s_0}{\sigma_s}\right)^2\right)^{-1}. \tag{10}$$

TABLE 3 Parameters for network connectivity.

Parameter	Value	Source
$N^{\mathrm{CTX,STN}}$	3	(Fountas and Shanahan, 2017)
$N^{\mathrm{MSN,GPe}}$	10	(Fountas and Shanahan, 2017)
$N^{\mathrm{GPe,STN}}$	1	(Baufreton et al., 2009)
$N^{\mathrm{GPe,GPe}}$	20	estimated, (Sadek et al., 2007; Baufreton et al., 2009)
$N^{\mathrm{STN,GPe}}$	3	(Hahn and McIntyre, 2010)
	30	(Lindahl et al., 2013)
$G^{\mathrm{CTX,STN}}$	$0.125\mu_{\mathrm{scale}}$ nS	Result of optimization (1)
$G^{\mathrm{GPe,STN}}$	$1.11\mu_{\mathrm{scale}}$ nS	Result of optimization (2)
$G^{\mathrm{STN,GPe}}$	$15.8\mu_{\mathrm{scale}}$ nS	Result of optimization (3) for $N^{\mathrm{STN,GPe}} = 3$
	$1.5\mu_{\mathrm{scale}}$ nS	Result of optimization (3) for $N^{\mathrm{STN,GPe}} = 30$
$G^{\mathrm{MSN,GPe}}$	$5.81\mu_{\mathrm{scale}}$ nS	Result of optimization (4) for $N^{\mathrm{STN,GPe}} = 3$
	$12.0\mu_{\mathrm{scale}}$ nS	Result of optimization (4) for $N^{\mathrm{STN,GPe}} = 30$
$G^{\mathrm{GPe,GPe}}$	$0.44\mu_{\mathrm{scale}}$ nS	Result of optimization (4) for $N^{\mathrm{STN,GPe}} = 3$
	$0.21\mu_{\mathrm{scale}}$ nS	Result of optimization (4) for $N^{\mathrm{STN,GPe}} = 30$

We introduced a scale factor of $\mu_{\mathrm{scale}} = 0.85$.

This profile was motivated by the shape of the profile of electrical stimuli used in Lysyansky et al. (2013). σ_s is the width of the stimulus profile and will be set to $\sigma_s = 0.05L/\pi$ if not mentioned otherwise.

In experiments, cortical stimulation of the limb region resulted in a response of STR MSNs (Kita and Kita, 2011). We modeled the effect of the cortex on MSN activity by modifying the firing rate of the MSNs in response to afferent cortical neurons. Specifically, the MSN spike generator that was the closest to a cortical spike generator that spiked at time t_0 in response to the stimulus, fired a spike between time t and time $t + h$ with probability

$$P(t|s_i^{\mathrm{MSN}}, t_0) = \begin{cases} p(t - t_0 - \lambda^{\mathrm{CTX,MSN}})h, & \text{spike of closest cortical spike generator at } t_0 \\ r^{\mathrm{MSN}}, & \text{otherwise} \end{cases} \quad (11)$$

Here, $p(t - t_0)$ was chosen such that it approximated the shape of the probability density for a striatal spike after a stimulus at time 0 given in Figure 4A of Kita and Kita, 2011

$$p(t) = \begin{cases} \eta e^{\frac{-(t-\mu)^2}{2\sigma^2}}, & t < 2\mu \\ 0, & 2\mu \le t < 2\mu + t_{\mathrm{start}} \\ \frac{t - t_{\mathrm{start}}}{t_{\mathrm{end}} - t_{\mathrm{start}}}, & 2\mu + t_{\mathrm{start}} \le t < 2\mu + t_{\mathrm{end}} \\ r^{\mathrm{MSN}}, & t \ge 2\mu + t_{\mathrm{end}} \end{cases}, \quad t > 0, \quad (12)$$

with $\eta = 0.145$, $\mu = 2.1$, $\sigma = \mu/3$. We used $t_{\mathrm{start}} = 100$ ms and $t_{\mathrm{end}} = 300$ ms.

Cortical activation consisted of periodic sequences of 500 stimulus pulses delivered every 1.7 s (Kita and Kita, 2011). We also considered two-pulse stimulation where two pulses were delivered every 1.7 s. We refer to the first of the two pulses as *priming stimulus* and to the second pulse as *test stimulus*. The priming stimulus was centered at $s^{\mathrm{CTX}} = -\Delta s/2$ and the test stimulus was delivered after Δt and centered at $s^{\mathrm{CTX}} = \Delta s/2$. Δs and Δt were varied. The two-pulse stimulation setup is illustrated in Figure 2.

2.3. Numerical details

Numerical integration was performed using the Euler–Maruyama method (Kloeden and Platen, 1992) with an integration time step of 0.05 ms. Numerical integration and data analysis was done in python. The times when the dynamics of individual neurons was reset were considered as the spike times.

The peristimulus time histograms (PSTHs) in Figures 3, 4 were calculated as follows: first, simulations were run for five different trials, i.e., while the same realizations of single neuron parameters and network realizations were used in each trial, different realizations of the noisy input currents and Poisson inputs were considered. After, 40 s of simulated time the stimulation was started. A total of 500 stimuli was delivered for one-site stimulation. From the recorded spike trains, PSTHs were calculated by estimating the probability of a spike of the neuron in the very center of the s^{X} axes during a certain time bin of width 1 ms relative to the closest stimulus onset. Results are shown in Figures 3, 4.

To estimate the distributions of single-neuron mean firing rates (Figure 6), we performed simulations of 96 trials for each of the networks and each value of $N^{\mathrm{STN,GPe}}$. For each neuron, the mean firing rate was estimated by calculating the number of spikes during a time interval of nine seconds starting after 31 seconds of simulated time. Results in Figure 6, show a histogram of the single-neuron mean firing rates of the center 30 STN ($-1/6 < s_i^{\mathrm{STN}} < 1/6$) and the center 100 GPe neurons ($-1/6 < s_i^{\mathrm{GPe}} < 1/6$).

To estimate the spatio-temporal responses in Figures 5, 7, 8, we performed simulations for 24 trials and calculated PSTHs as in Figures 3, 4 for neurons at different coordinates s^{X}. From these PSTHs, the probability for a neuron with coordinate between s^{X} and $s^{\mathrm{X}} + 0.01/L$ (STN and GPe) and s^{X} and $s^{\mathrm{X}} + 0.001/L$ (CTX and MSN) at a time lag between t and $t + 1$ ms relative to the closest stimulus onset was estimated by calculating the average number of spikes in that time and coordinate bin per trial and stimulus from the set of obtained single-neuron PSTHs. For one-site stimulation (Figures 5, 7) 500 stimuli were delivered, as in Figures 3, 4. For two-site stimulation (Figure 8), 500 pairs of stimuli were delivered.

For each data point in Figure 9, we performed simulations similar to the ones in Figure 8 for two scenarios. In the first scenario, one-site stimulation was delivered to the cortical location $\Delta s/2$ and in the second one two-site stimulation was delivered to $\pm\Delta s/2$, respectively. Then, $\mathcal{L}^{\mathrm{X}}_{\mathrm{base}}$ (Equation 13) and $\mathcal{L}^{\mathrm{X}}_{\mathrm{re}}$ (Equation 14) were calculated as described in Section 3.6.

3. Results

Responses of STN and GPe neurons evoked by cortical stimulation were studied in monkeys (Nambu et al., 2000; Kita et al., 2004; Polyakova et al., 2020) and in rodents (Kita and Kita, 2011). Electrical stimuli were delivered to the motor cortex

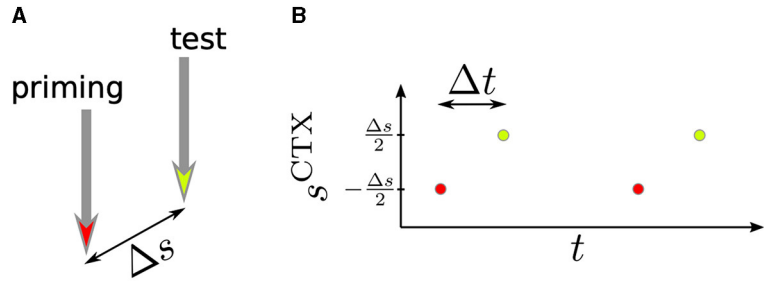

FIGURE 2
Schematics of two-pulse stimulation. **(A)** The priming stimulus (red) and the test stimulus (yellow) were delivered to two cortical locations. The distance between these locations was Δs. **(B)** We delivered periodic sequences of priming and test stimuli and studied how the time lag, Δt, and the distance between stimuli, Δs, affected the response of BG neurons.

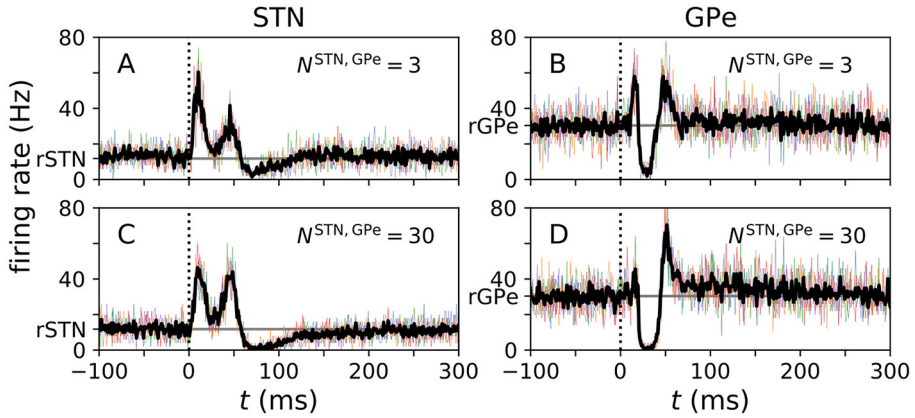

FIGURE 3
PSTHs obtained from computational model. **(A–D)** PSTHs for the center STN **(A, C)** and the center GPe **(B, D)** neuron obtained from simulations for the N-network. Colored curves show single-neuron PSTHs for five different trials. In each trial 500 stimuli were delivered and the center neurons' PSTHs were recorded. The black curves show averages of these trials. Simulations were performed for two N-networks with different numbers of STN to GPe connections, $N^{STN,GPe}$, corresponding to a small projection area ($N^{STN,GPe} = 3$ as used in Hahn and McIntyre, 2010) and to a large projection area ($N^{STN,GPe} = 30$ as used in Lindahl et al., 2013), respectively. The vertical dotted line marks the stimulus delivery at $t = 0$ and the horizontal gray line marks the baseline firing rates r^{STN} and r^{GPe} in the absence of stimulation.

(Nambu et al., 2000; Kita et al., 2004; Kita and Kita, 2011; Polyakova et al., 2020) and the primary sensory cortex (Nambu et al., 2000) and PSTHs of responding STN and GPe neurons were recorded.

Responses of STN neurons showed an early and a late excitation followed by a long inhibition, whereas responses of GPe neurons showed an early excitation, an inhibition, and a late excitation. These characteristics were observed in rodents and in monkeys. Combining cortical stimulation with local drug injection, experiments in monkeys revealed that these characteristic features result from the interplay of two pathways: the cortico-STN glutamatergic hyperdirect pathway and the cortico-striato-GPe-STN indirect pathway (Kita et al., 2004; Kita, 2007; Jaeger and Kita, 2011; Polyakova et al., 2020).

Using our computational model, we explored how the characteristics of motor cortical stimulation-evoked responses depend on synaptic network connectivity. To this end, we mimicked the experimental setup in our computational model and studied PSTHs of STN and GPe neurons. We delivered cortical stimulation (Model and methods). Cortical stimuli were centered at $s^{CTX} = 0$, if not mentioned otherwise.

3.1. Evoked responses in computational model

PSTHs obtained from simulations of our computational model are shown in Figure 3. PSTHs of STN and GPe neurons show the typical characteristics observed in experiments. In particular, the characteristic sequence of an early excitation, a late excitation, and a long inhibition in responding STN neurons (Figures 3A, C) and the sequence of an early excitation, an inhibition, and a late excitation in responding GPe neurons (Figures 3B, D) were reproduced by our computational model.

The number of STN→GPe connections had a strong impact on how well the individual features were pronounced. The early excitation in GPe neurons was most pronounced for $N^{STN,GPe} = 3$ (Figure 3B), whereas it became less pronounced for large $N^{STN,GPe}$ (Figure 3D). This was because the model with $N^{STN,GPe} = 3$ had stronger excitatory STN to GPe connections. The corresponding maximal conductance was chosen such that the STN and GPe firing rates were close to experimental data. Consequently, a small number of STN inputs strongly excited postsynaptic GPe neurons (see Table 3).

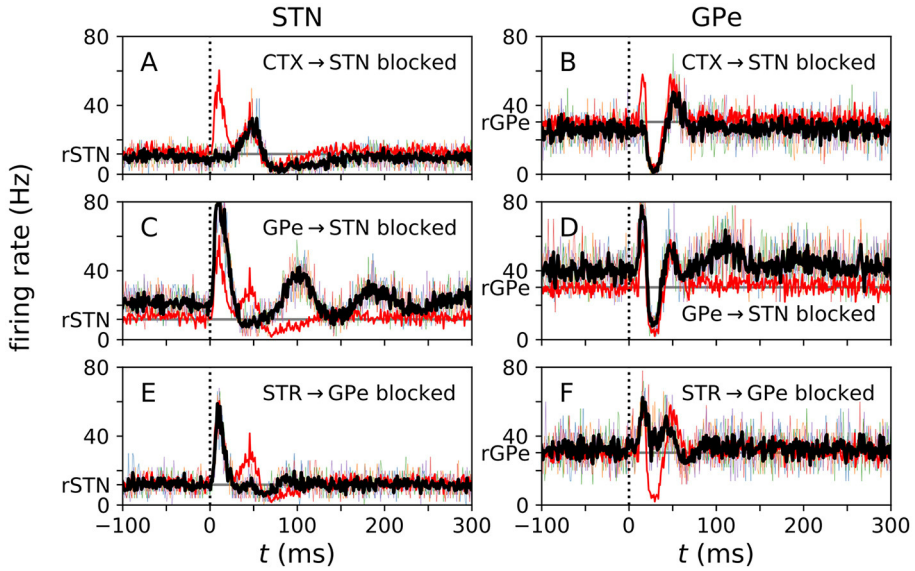

FIGURE 4
Local blockage of incoming connections affects evoked responses. **(A–F)** PSTHs for center STN **(A, C, E)** and center GPe **(B, D, F)** neurons obtained from simulations of the N-network, when incoming connections of respective types were blocked. Thin colored curves show single-neuron PSTHs from five different trials, each averaged over 500 stimuli. Black curve shows average over PSTHs from different trials. The red curve shows the control case (same as black curves in Figures 3A, B). Simulations were performed for three different cases: (top) all incoming cortical connections to the center three STN neurons were blocked; (center) all incoming GPe connections to the center three STN neurons were blocked; and (bottom) all incoming STR MSN connections to the center three GPe neurons were blocked. The vertical dotted line marks the stimulus delivery at $t = 0$ and the horizontal gray line marks baseline firing rates in the absence of stimulation. Parameters: $N^{\mathrm{STN,GPe}} = 3$.

3.2. Glutamatergic and GABAergic inputs shape cortically evoked responses

Experimental studies explored the origin of the characteristic pattern of excitations and inhibitions in the PSTHs. In monkeys, incoming connections were blocked by local injection of GABA and glutamate antagonists (Kita et al., 2004; Polyakova et al., 2020). In our computational model, we created similar scenarios by cutting incoming connections to individual STN or GPe neurons. The resulting PSTHs are shown in Figure 4.

Cutting cortical inputs to single STN neurons led to a reduction of the amplitude of the early excitation in the response of these neurons to cortical stimuli (Figure 4A). Furthermore, their mean firing rate decreased. In responding GPe neurons, cutting cortical input to STN neurons reduced the amplitude of the early excitation substantially (Figure 4B).

Cutting all GPe inputs to the responding STN neurons strongly diminished the amplitude of the second excitation and the late inhibition. Furthermore, it increased the mean firing rate of STN neurons (Figure 4C). It also led to slow, damped oscillations of the instantaneous firing rate following the initial early excitation (Figure 4C). In responding GPe neurons, we also found an increase in the mean firing rate. Furthermore, the amplitude of the early excitation increased, and slow oscillations occurred after the second excitation (Figure 4D).

Finally, cutting striatal inputs to responding GPe neurons led to a reduction of the amplitude of the second excitation of responding STN neurons and to a shortening of the late inhibition (Figure 4E). In responding GPe neurons, it strongly suppressed the inhibition between early and late excitations (Figure 4F).

3.3. Spatio-temporal characteristics of cortical stimulation-evoked responses

Next, we studied the spatio-temporal characteristics of cortically evoked responses in the computational model. To this end, we analyzed the trial-averaged responses of BG neurons with different coordinates (see schematics in Figure 1).

In Figure 5, we show the trial-averaged instantaneous firing rate, $p(t, s^{\mathrm{X}})$, of a neuron with coordinate s^{X} in nucleus X. For comparison, we marked the mean firing rate of cortical neurons (4 Hz), STR MSNs (0.67 Hz), STN neurons (11.8 Hz), and of GPe neurons (30.4 Hz) on the color axes in Figure 5. The response of BG neurons strongly depended on their baseline firing rate and on $|s^{\mathrm{X}}|$, i.e., the coordinated difference to the stimulus center. Neurons with similar coordinates as the stimulated cortical neurons, $s^{\mathrm{X}} \approx 0$, possessed the characteristic responses presented in Figure 3. STN neurons with small $|s^{\mathrm{STN}}|$ showed a pronounced late inhibition (Figure 5B). In the GPe, neurons with moderate $|s^{\mathrm{GPe}}|$ showed a substantially shorter late excitation than GPe neurons with $|s^{\mathrm{GPe}}| \approx 0$. The dependence of cortically evoked responses on the coordinate s^{X} was more pronounced for large $N^{\mathrm{STN,GPe}} = 30$ (Figures 4C, D).

Motivated by the impact of $N^{\mathrm{STN,GPe}}$ on the evoked responses of BG neurons, we studied the impact of the network structure on the distributions of single-neuron mean firing rates and the spatio-temporal characteristics of cortically evoked responses.

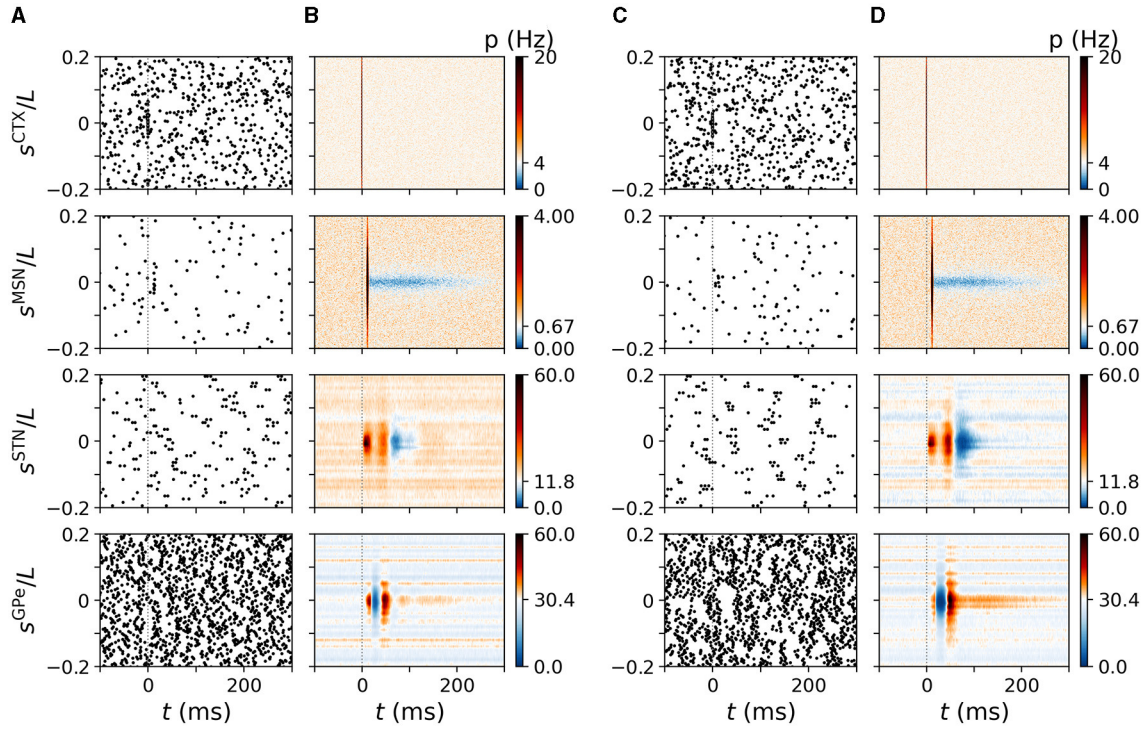

FIGURE 5
Cortically evoked spatio-temporal responses in a simulated N-network. Rows show responses of inner CTX (top), MSN (second to top), STN (second to bottom), and GPe neurons (bottom). Columns **(A, B)** show results of the computational model for $N^{STN,GPe} = 3$ and columns **(C, D)** show results for $N^{STN,GPe} = 30$. **(A)** Raster plots of spiking activity in the computational model triggered by a cortical stimulus at $t = 0$. y-axes shows neuron coordinates, s^X. **(B)** trial-averaged instantaneous firing rate $p(t, s^X)$ of neurons at location s^X obtained by averaging over 500 stimuli and 24 realizations of noise and Poisson input. Color code indicates firing rate changes relative to baseline firing rate in the absence of stimulation (white). Increases in firing rate are shown in red/black and decreases in blue. **(C, D)** Same as **(A, B)** but for $N^{STN,GPe} = 30$. Parameters: $N^{STN,GPe} = 3$ **(A, B)** and $N^{STN,GPe} = 30$ **(C, D)**. CTX stimuli were centered at $s^{CTX} = 0$.

3.4. Network structure shapes distribution of single-neuron mean firing rates

Next, we analyzed how the network connectivity affected the dynamics of STN and GPe neurons. We considered three network structures: N-networks, D-networks, and S-networks. N-networks were obtained by implementing outgoing synaptic connections such that the presynaptic neurons connect to postsynaptic neurons with similar coordinates. D-networks were obtained in the same way, except that 10% of synaptic connections were randomly selected and displaced systematically (Model and methods). Lastly, S-networks were obtained like N-networks except that neurons were only allowed to project to every second neuron in the postsynaptic nucleus (see Model and methods for more details).

Estimated distributions of single-neuron mean firing rates of STN and GPe neurons obtained from simulations of the computational model are shown in Figure 6. Firing rate distributions were unimodal except for D-networks and small $N^{STN,GPe}$. For the latter, individual STN to GPe connections were strong, and random displacement of connections in the D-network led to variability in the number of incoming STN connections per GPe neuron. Few incoming connections resulted in low mean firing rates, whereas many incoming connections resulted in high mean firing rates. This led to the additional peaks in Figure 6B.

Following, we will restrict our analysis to networks with $N^{STN,GPe} = 3$, thereby modeling a high degree of specificity of STN→ GPe connections as reported by experimental studies in monkeys (Shink et al., 1996). We continue by analyzing how the network structure affects the spatio-temporal pattern of evoked responses.

3.5. Network structure shapes evoked spatio-temporal responses

We studied cortically evoked responses in N-networks, D-networks, and S-networks. Figure 7 shows simulated responses of BG neurons to cortical stimuli for the three network structures. Column A shows the results for the N-network from Figure 5B. In the D-network, a displacement of randomly selected connections by $d = 0.15L$ led to additional responses of STN neurons near $s^{STN} = 0.15L$ and responses of GPe neurons near $s^{GPe} = 0.15L$ (Figure 7B). We also find that the evoked response of neurons with lower baseline activity deviated from the characteristic response patterns (blue horizontal lines in Figure 7B). In contrast, in an S-network, neurons showed less pronounced response patterns than in N-networks and overall reduced baseline activity (Figure 7C).

The strong variability of single-GPe neurons' mean firing rates in D-networks (see also Figure 6) can be seen in Figure 7B.

10.3389/fninf.2023.1217786

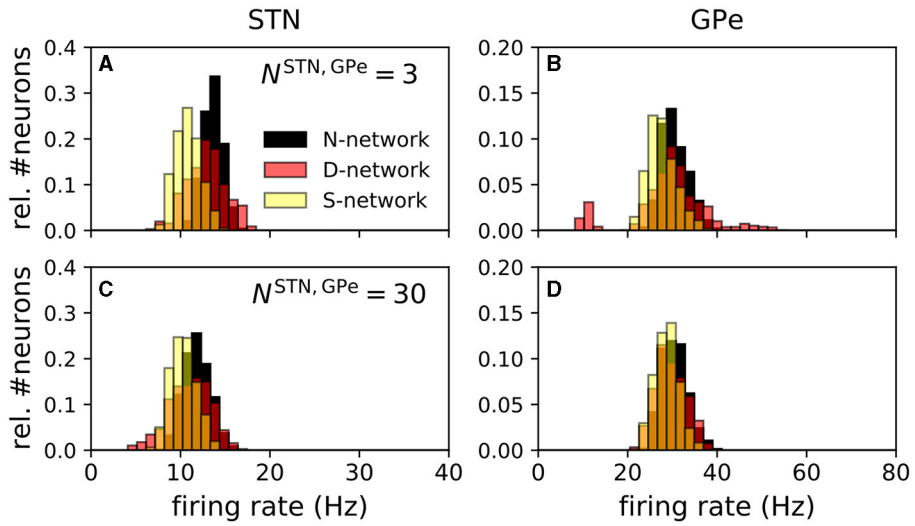

FIGURE 6
Distribution of single-neuron mean firing rates depended on network structure. Panels **(A–D)** show distributions of single-neuron mean firing rates for an N-network, a D-network, and an S-networks. The left column shows simulation results for STN and the right column results for GPe neurons. Panels **(A, B)** show results for $N^{STN,GPe} = 3$ and panels **(C, D)** for $N^{STN,GPe} = 30$. Estimates of single-neuron mean firing rates were obtained by counting the number of spikes in a simulated time window of 9 s. Prior to that a 31 s time window was simulated to ensure stationary dynamics. Mean firing rates of the inner 30 STN neurons ($-1/6 < s_i^{STN} < 1/6$) **(A, C)** and the inner 100 GPe neurons ($-1/6 < s_i^{GPe} < 1/6$) **(B, D)** for a total of 96 realizations of the noise and the Poisson input are shown.

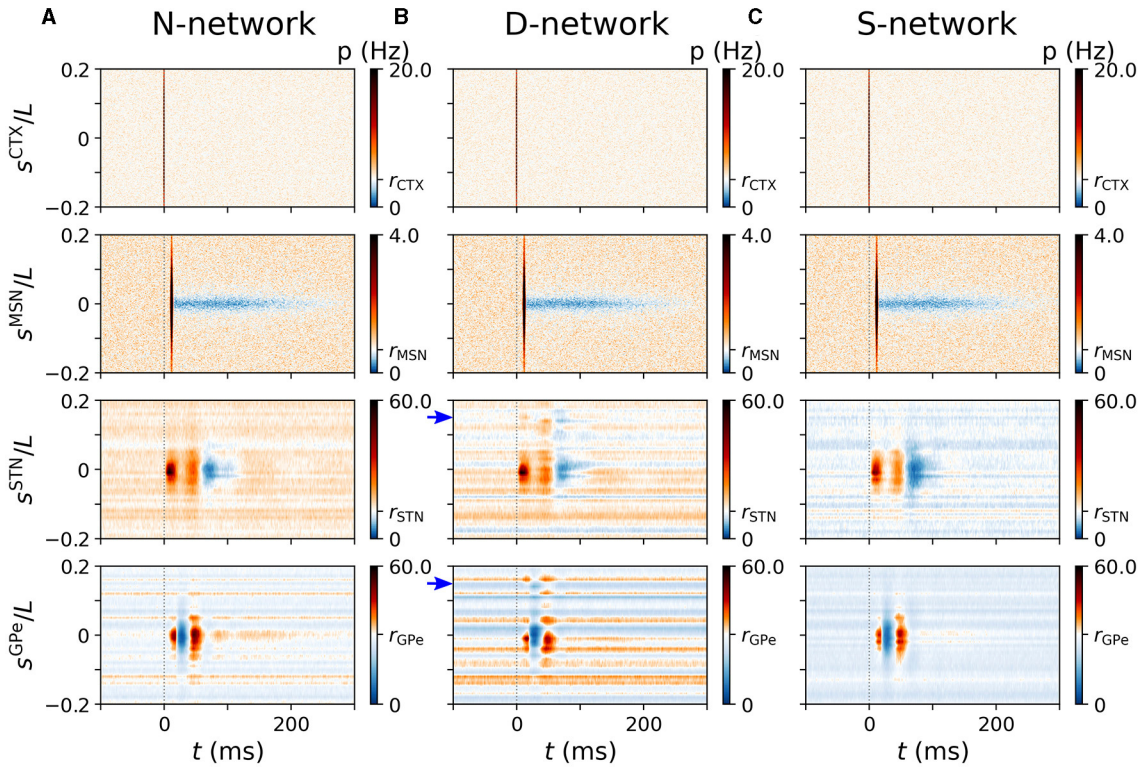

FIGURE 7
Representative cortically evoked spatio-temporal responses in an N-network, a D-network, and an S-network. Rows show spatio-temporal response patterns of CTX (top), MSN (second to top), STN (second to bottom), and GPe neurons (bottom). Columns **(A–C)** show results from simulations of the computational model for an N-network **(A)**, a D-network **(B)**, and an S-network **(C)**. Blue arrows mark displacement $d = 0.15L$ in D-network. Results were averaged over 24 trials with different realizations of noise and Poisson input. For each trial results were averaged over a sequence of 500 stimuli. Cortical stimuli were centered at $s^{CTX} = 0$. Responses of individual STN and GPe neurons strongly depended on, $|s^X|$, with X=STN,GPe (see also Figure 5).

While neurons at some coordinates, s^{GPe}, fired at a low rate and responded only weakly to cortical stimuli, others were highly active and showed strong responses. In our computational model, this resulted in high trial-averaged instantaneous firing rates $p(t, s^{\mathrm{GPe}})$ for certain s^{GPe} and low $p(t, s^{\mathrm{GPe}})$ for others.

So far, our results suggest that alterations of the network connectivity lead to changes in the evoked spatio-temporal response pattern. We studied two types of alterations: first, in D-networks, we randomly selected 10% of the connections and exchanged the postsynaptic neurons by postsynaptic neurons at different locations (shifted by d relative to the original postsynaptic neuron). This led to a weaker response in the original target region and an additional response in another region. Second, in S-networks, the responding region was larger; however, responses to cortical stimulation were weaker as a whole.

3.6. BG responses to cortical two-site stimulation

Next, we delivered a sequence of pairs of priming and test stimuli to different cortical coordinates. This mimicked the stimulation of neuronal populations representing different features. In our computational model, this was implemented by delivering the priming stimulus to a cortical population centered at $s_{\mathrm{I}}^{\mathrm{CTX}} = -\Delta s/2$ and the test stimulus to a population centered at $s_{\mathrm{II}}^{\mathrm{CTX}} = \Delta s/2$ (Figure 2). The stimulus profiles were given by Equation (10).

Representative spatio-temporal responses for $\Delta s = 0.1L$ are shown in Figure 8. For a rather large time lag of $\Delta t = 100$ ms, each stimulus caused spatio-temporal responses that were similar to the ones caused by a single stimulus in the respective network (compare Figures 7, 8).

Next, we performed a more detailed analysis of the response patterns. To this end, we compared two cases: (i) only the test stimulus was delivered to $s_{\mathrm{II}}^{\mathrm{CTX}} = \Delta s/2$ at time t_{s} and (ii) the priming stimulus and the test stimulus were delivered: the priming stimulus to $s_{\mathrm{I}}^{\mathrm{CTX}} = -\Delta s/2$ at time $t_{\mathrm{s}} - \Delta t$ and the test stimulus to $s_{\mathrm{II}}^{\mathrm{CTX}} = \Delta s/2$ at time t_{s}. Note that we only considered positive inter-stimulus intervals, $\Delta t > 0$. In what follows, we mark quantities corresponding to case (i) by the index "i" and quantities corresponding to case (ii) by the index "ii".

For our analysis, we averaged the trial-averaged PSTHs of all neurons with coordinates that were close to $s_{\mathrm{II}}^{\mathrm{CTX}}$, i.e., $s^{\mathrm{X}} \in [\Delta s/2 - A/2, \Delta s/2 + A/2]$, with X=STN,GPe. Here, A is the width of the coordinate range over which responses were averaged. In the case (i), only the test stimulus was delivered at time t_{s} to the stimulation site at $\Delta s/2$. We denote the average response of BG neurons in nucleus X with $s^{\mathrm{X}} \in [\Delta s/2 - A/2, \Delta s/2 + A/2]$ at time t as $\mathcal{F}_{(\mathrm{i})}^{\mathrm{X}}(t|\Delta s/2)$. In case (ii), an additional priming stimulus was delivered to the stimulation site at $-\Delta s/2$ at time $t_{\mathrm{s}} - \Delta t$. We denote the average response of BG neurons in nucleus X with $s^{\mathrm{X}} \in [\Delta s/2 - A/2, \Delta s/2 + A/2]$ at time t as $\mathcal{F}_{(\mathrm{ii})}^{\mathrm{X}}(t|\Delta s/2, -\Delta s/2, \Delta t)$. We used $A = 0.045L$.

To study how much the presence of the priming stimulus alters the response evoked by the test stimulus, we evaluated two quantities. The first quantity was

$$\mathcal{L}_{\mathrm{base}}^{\mathrm{X}}(\Delta t, \Delta s) := \int_{t_{\mathrm{s}}-T^-}^{t_{\mathrm{s}}} dt \left| \mathcal{F}_{(\mathrm{ii})}^{\mathrm{X}}\left(t \middle| \frac{\Delta s}{2}, -\frac{\Delta s}{2}, \Delta t\right) - \mathcal{F}_{(\mathrm{i})}^{\mathrm{X}}\left(t \middle| \frac{\Delta s}{2}\right)\right|^2. \quad (13)$$

Here, $T^- > 0$ is the time range prior to the test stimulus during which the change of the neurons' trial-averaged instantaneous firing rate due to the presence of the priming stimulus was evaluated. $\mathcal{L}_{\mathrm{base}}^{\mathrm{X}}(\Delta t, \Delta s)$ measures how much the presence of the priming stimulus affects spiking of neurons in nucleus X shortly before their evoked response to the test stimulus. It therefore provides information on how much the baseline activity of neurons in nucleus X is affected by the priming stimulus. The second quantity we evaluated was

$$\mathcal{L}_{\mathrm{re}}^{\mathrm{X}}(\Delta t, \Delta s) := \int_{t_{\mathrm{s}}}^{t_{\mathrm{s}}+T^+} dt \left| \mathcal{F}_{(\mathrm{ii})}^{\mathrm{X}}\left(t \middle| \frac{\Delta s}{2}, -\frac{\Delta s}{2}, -\Delta t\right) - \mathcal{F}_{(\mathrm{i})}^{\mathrm{X}}\left(t \middle| \frac{\Delta s}{2}\right)\right|^2. \quad (14)$$

$\mathcal{L}_{\mathrm{re}}^{\mathrm{X}}(\Delta t, \Delta s)$ measures how much the presence of the priming stimulus affected the responses of neurons in nucleus X evoked by the test stimulus.

In Figure 9, we show results for $\mathcal{L}_{\mathrm{base}}^{\mathrm{X}}(\Delta t, \Delta s)$ and $\mathcal{L}_{\mathrm{re}}^{\mathrm{X}}(\Delta t, \Delta s)$ for an N-network, a D-network, and an S-network obtained from simulations of our computational model. $\mathcal{L}_{\mathrm{base}}^{\mathrm{X}}(\Delta t, \Delta s)$ and $\mathcal{L}_{\mathrm{re}}^{\mathrm{X}}(\Delta t, \Delta s)$ showed different dependencies on Δt and Δs. For short inter-stimulus intervals, Δt, $\mathcal{L}_{\mathrm{base}}^{\mathrm{X}}(\Delta t, \Delta s)$ was close to zero, indicating that the baseline activity prior to the test stimulus was not affected by the presence of the priming stimulus. For long inter-stimulus intervals, $\mathcal{L}_{\mathrm{base}}^{\mathrm{X}}(\Delta t, \Delta s)$ increased and finally saturated for fixed Δs as more and more of the response evoked by the priming stimulus impacts the baseline activity of neurons before their response to the test stimulus. The saturation for large Δt indicates that the impact of the response evoked by the priming stimulus was over before neurons responded to the test stimulus. Additionally, increasing the coordinate difference, Δs, between stimulated cortical subpopulations reduced the impact the priming stimulus had on neurons responding to the test stimulus in N-networks and S-networks. Accordingly, a characteristic width of functional channels in which cortical inputs are processed independently may be derived. In contrast, in D-networks $\mathcal{L}_{\mathrm{base}}^{\mathrm{X}}(\Delta t, \Delta s)$ attained another local maximum as a function of Δs when Δs was close to the displacement, d, of synaptic connections (Figures 9E, G).

Remarkably, $\mathcal{L}_{\mathrm{re}}^{\mathrm{X}}(\Delta t, \Delta s)$ showed a more complex dependence on Δt and Δs than $\mathcal{L}_{\mathrm{base}}^{\mathrm{X}}(\Delta t, \Delta s)$. Several local maxima occurred at small Δs and at $\Delta t \approx 5 - 10$ ms, $\Delta t \approx 30 - 40$ ms, and $\Delta t \approx 50 - 60$ ms for STN neurons (Figure 9B) and at $\Delta t \approx 10 - 15$ ms for GPe neurons. A comparison of these times with the PSTHs in Figure 3 suggested that they correspond to the timings of the two excitations and the gap in between in the PSTHs of STN neurons (Figure 3A) and the timing of the first excitation in the PSTHs of GPe neurons (Figure 3B). However, the delay between STN and GPe neurons needs to be considered (1 ms in simulations; however, it took about 5 ms for the postsynaptic neurons to respond to

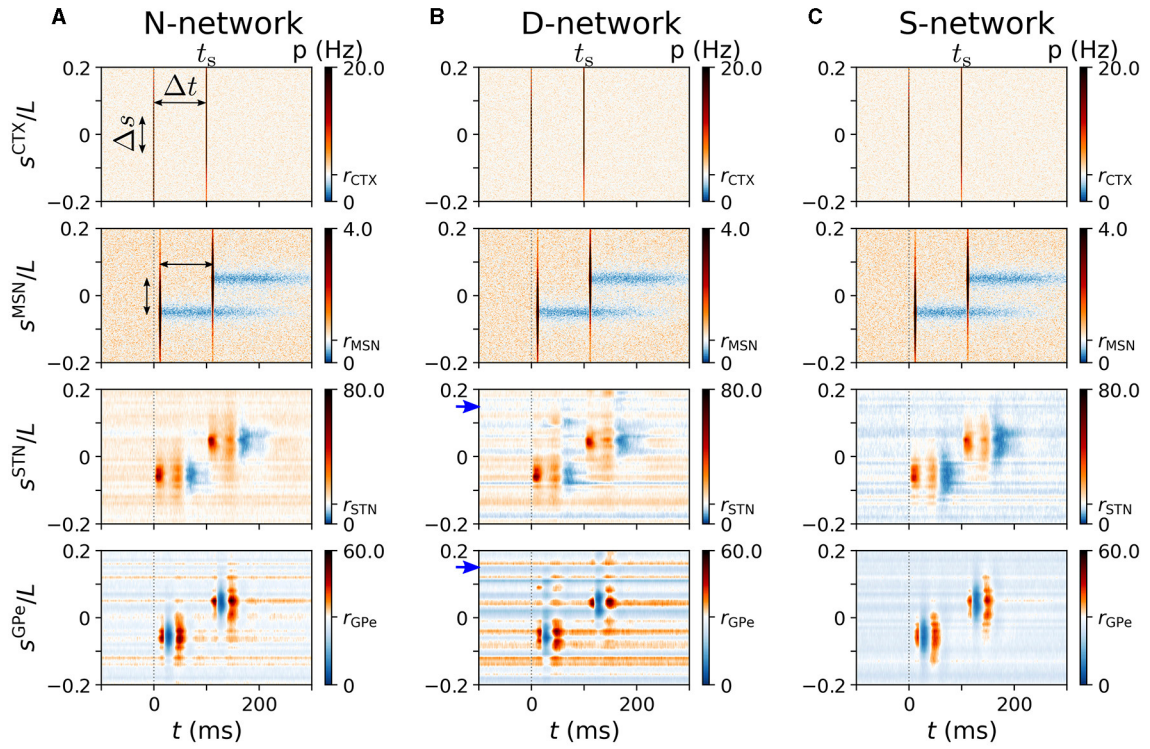

FIGURE 8
Spatio-temporal response to cortical two-site stimulation. Panels **(A–C)** show representative trial-averaged responses of simulated BG and cortical neurons at different locations, s^X, to cortical two-site stimulation. Stimulation sites were at $\pm\Delta s/2$ and the inter-stimulus interval was Δt. Column **(A)** shows results for an N-network, column **(B)** results for a D-network, and column **(C)** results for an S-network. Blue arrows mark displacement $d = 0.15L$ in D-network. Rows show the instantaneous firing rates of neurons at location s^X in the cortex, the striatum, the STN, and the GPe (from top to bottom). Parameters: $\sigma_s = 0.05L/\pi$, $\Delta s = 0.1L$, $\Delta t = 100$ ms, $N^{STN,GPe} = 3$. Results were averaged over 500 stimuli and 24 realizations of noise and Poisson input.

incoming excitatory input due to the finite time constant of the membrane potential).

Most remarkable, for all considered network structures, $\mathcal{L}^{STN}_{re}(\Delta t, \Delta s)$ was more sensitive than $\mathcal{L}^{X}_{base}(\Delta t, \Delta s)$ or $\mathcal{L}^{GPe}_{re}(\Delta t, \Delta s)$ in the sense that the influence of the priming stimulus was measurable for larger Δs, i.e., when stimulation sites were further apart. In particular, an inter-stimulus interval of about $30 - 40$ ms between the stimulus deliveries led to the largest coordinate difference between stimulation sites for which the influence of the second stimulus was measurable using $\mathcal{L}^{STN}_{re}(\Delta t, \Delta s)$ (Figures 9B, F, J). Note that this time interval also corresponded to the inter-stimulus intervals for which $\mathcal{L}^{STN}_{re}(\Delta t, \Delta s)$ showed a local maximum for at $\Delta s \approx d$ in D-networks (Figure 9F).

4. Discussion

Cortically evoked responses of STN and GPe neurons exhibit characteristic sequences of excitations and inhibitions that were observed in rodents (Kita and Kita, 2011) and primates (Nambu et al., 2000; Kita, 2007; Jaeger and Kita, 2011; Polyakova et al., 2020). We developed a computational model of the STN-GPe circuit that reproduced these response characteristics and related them to aspects of the topology of synaptic connections. Furthermore, we presented a one- and a two-site stimulation technique to quantify the width of functional channels in the BG network. Our results suggest that details of the synaptic connectivity are critical for the processing of cortical signals. They further support the use of computational models that include synaptic connectivity that is derived from experimental findings rather than random connections. The presented one- and two-site stimulation protocols enable probing of connectivity patterns in preclinical experiments. Based on our computational results on the effect of alterations of network connectivity on cortically-evoked responses, one may design preclinical experiments to falsify or verify our predictions. With such a combined computational and experimental approach, one may reveal further characteristics of synaptic connectivity in the BG and may identify patterns of synaptic reorganization in neurological diseases, e.g., Parkinson's disease.

The characteristic pattern of excitations and inhibitions in cortically evoked responses of STN and GPe neurons was studied experimentally (Nambu et al., 2000; Kita et al., 2004; Kita, 2007; Kita and Kita, 2011; Polyakova et al., 2020). Cortical stimulation triggered characteristic responses of STN neurons that consisted of an early excitation and a late excitation, which were separated by a gap, and a long, late inhibition (Nambu et al., 2000; Polyakova et al., 2020). In GPe neurons, responses showed an early excitation that was followed by an inhibition and a late excitation (Nambu et al.,

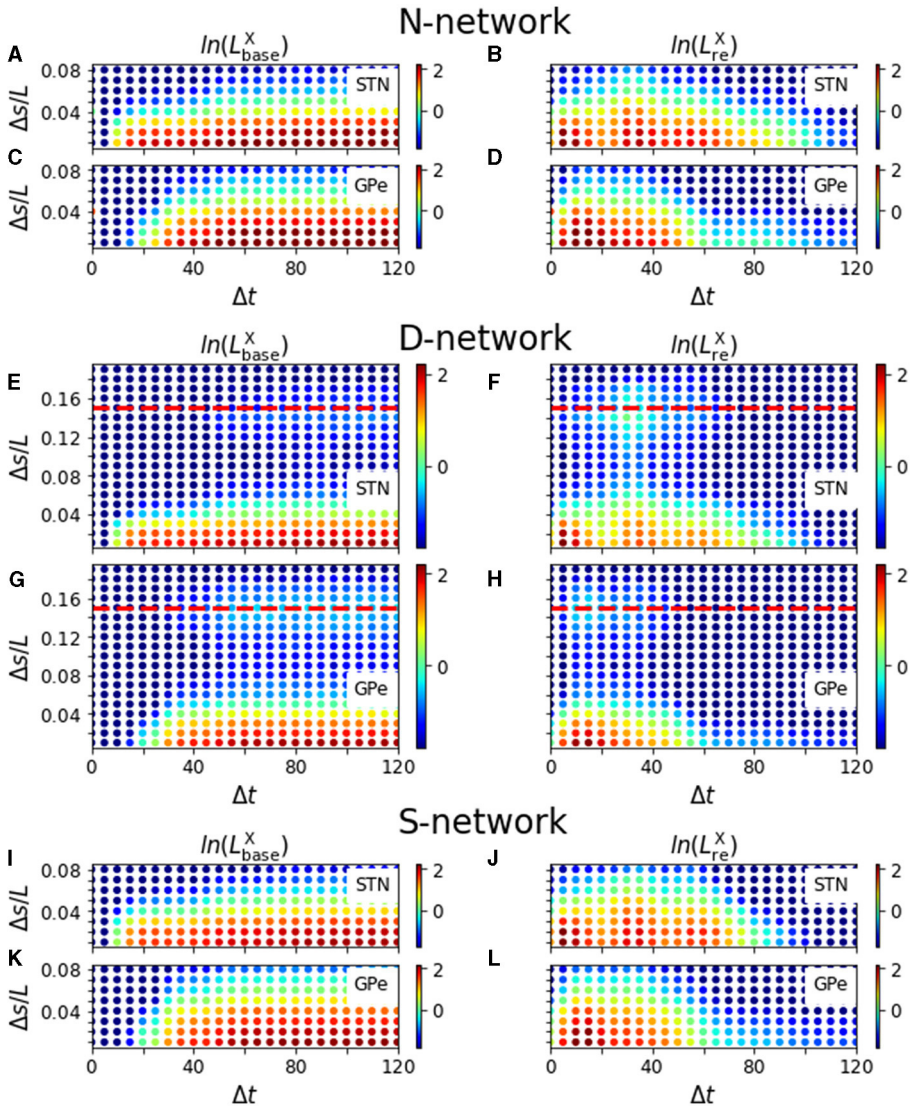

FIGURE 9
Modulation of evoked responses by a priming stimulus. Panels **(A–D)** show results for N-networks, panels **(E–H)** for D-networks, and panels **(I–L)** for S-networks. In the left column, we show the natural logarithm of $\mathcal{L}^X_{\text{base}}(\Delta t, \Delta s)$ and in the right column the natural logarithm of $\mathcal{L}^X_{\text{re}}(\Delta t, \Delta s)$ for $X = \text{STN}$ and $X = \text{GPe}$, respectively. Parameters: $N^{\text{STN,GPe}} = 3$. PSTHs used for the calculation of $\mathcal{L}^X_{\text{base}}(\Delta t, \Delta s)$ and $\mathcal{L}^X_{\text{re}}(\Delta t, \Delta s)$ were averaged over sequences of 500 stimuli and over 24 realizations of noise and Poisson input. For D-networks, we used $d = 0.15L$ (red, dashed line). $T^+ = 200$ ms and $T^- = 190$ ms.

2000; Kita, 2007; Jaeger and Kita, 2011). These features were well reproduced by our computational model (Figure 3).

Polyakova et al. (2020) found that local injection of glutamate receptor antagonists into the STN diminished the early excitation, and that the injection of muscimol (a GABA receptor agonist) into the striatum or the GPe diminished the late excitation. Their results supported the suggestions of earlier studies that the early excitation in the evoked response of STN neurons is caused by glutamatergic input via the cortico-STN hyperdirect pathway and the late excitation results from disinhibition due to GABAergic input via the cortico-striato-GPe-STN indirect pathway (Nambu et al., 2000). In our computational model, we modeled these experiments by cutting glutamate inputs to single STN neurons (to mimic the local injection of glutamate receptor antagonists) and by cutting inhibitory inputs to STN neurons (to mimic the local injection of GABA antagonists) (Figure 4). In accordance with Polyakova et al. (2020) we observed a suppression of the early excitation in the former case (Figure 4A) and a suppression of the late excitation in the latter case (Figure 4C). However, in our computational model, the latter case also led to damped beta oscillations in the instantaneous firing rate of STN neurons (Figure 4C). Such damped oscillations were not reported by Polyakova et al. (2020). However, Polyakova et al. reported high variability in the amplitude of the early and late excitations in the responses of STN neurons after local injection of a GABA antagonist. In our computational model, cutting GPe inputs to STN neurons destabilized the characteristic

response pattern of excitations and inhibitions in both responding STN and GPe neurons (Figures 4C, D). A similar destabilizing effect may occur in the experiments and may cause high variability of the amplitudes of excitations among responding STN neurons (Polyakova et al., 2020). Together, these findings suggest that the GPe→STN connections are critical for the GPe-STN network to process cortical input and stabilize baseline activity. The results from our computational model further suggest that cutting STR MSN inputs to single GPe neurons would diminish the inhibition in the GPe neurons' responses (Figure 4F) and also reduce the amplitude of the late excitation in the evoked response of STN neurons (Figure 4E). These results are in accordance with other experiments by Polyakova et al. (2020) in which the injection of muscimol into the putamen reduced the amplitude of the second excitation in STN neurons substantially. Our results on the effect of cutting STR MSN inputs to GPe neurons are also in line with the experimental results of Kita et al. (2004); however, Kita et al. injected a GABA antagonist locally into the GPe, which also reduced GABAergic input from other GPe neurons and not only STR MSN input. In our computational model, only STR MSN inputs were cut, which resulted in a substantial weakening of the inhibition in the response of GPe neurons (Figure 4F). Furthermore, our computational results suggest that the late excitation in the GPe may be partly due to excitatory input from the STN and partly due to disinhibition after striatal inhibition. This is in accordance with previous results by Kita and colleagues (Kita et al., 2004; Kita, 2007).

The variability of the STN and GPe neurons' baseline firing rates contributed to the variability of single-neuron responses to cortical stimuli in our computational model. In more detail, the characteristic features of neuronal responses were most pronounced among neurons with high baseline activity (see Figures 5, 7). Unfortunately, it is difficult to compare the responses of STN or GPe neurons with low mean firing rates to cortical stimuli to experimental data, because such neurons were often excluded from the analysis in experimental studies (Kita et al., 2004; Kita and Kita, 2011; Polyakova et al., 2020).

N-networks and S-networks resulted in unimodal distributions of single-neuron mean firing rates for STN and GPe neurons (Figure 6). In contrast, in D-networks, baseline firing rates of GPe neurons showed a multimodal distribution (Figure 6B). The shapes of these distributions obtained from our computational model reproduced experimental data for STN neurons as observed in studies in rat brain slices qualitatively; a histogram of single-neuron firing rates of tonically spiking STN neurons in rat brain slices can be found in Beurrier et al. (1999). However, the mean firing rate in that study was higher than in our model, as our model was fitted to experimental data from anesthetized rats presented in Kita and Kita (2011). A histogram of single-neuron mean firing rates of GPe neurons can be found in Figure 8B of Miguelez et al. (2012). There, a significant portion of GPe neurons did not spike ($\approx$ 25% in Miguelez et al., 2012), and the broad distribution of single-neuron mean firing rates of GPe neurons suggests high variability of single-neuron mean firing rates. In our model, GPe neurons with a small number of incoming STN connections possessed very low firing rates (Figure 6B). High variability of single-neuron mean firing rates occurred due to variability in the number of incoming STN→GPe connections, which was only realized in D-networks for a small number of STN→GPe connections, $N^{\mathrm{STN,GPe}} = 3$. For the latter, individual connections were substantially stronger than for $N^{\mathrm{STN,GPe}} = 30$ because parameters were adjusted to fit the STN and GPe firing rates to experimental data (Figure 5B). The random displacement of connections in D-networks led to broader distributions of single-neuron mean firing rates in D-networks than in N-networks or in S-networks.

Our results suggest that cortical stimulation results in complex spatio-temporal response patterns in the STN and GPe. These patterns result from the propagation of signals along the cortico-STN hyperdirect pathway and along the cortico-striato-GPe-STN indirect pathway (Figure 1B), and the convergence of these pathways onto the same regions in the STN and the GPe. In our computational model, these patterns strongly depended on the underlying structure of synaptic connections (Figure 7). Evidence from animal models suggests that the synaptic network structure in the BG nuclei is impaired in the dopamine-depleted state in animal models for Parkinson's disease (Fan et al., 2012; Miguelez et al., 2012; Chu et al., 2015; Pamukcu et al., 2020). Modulation of evoked responses of individual BG neurons in the dopamine-depleted state has been reported and analyzed by Kita and Kita (2011) in a rodent model for Parkinson's disease. The authors observed that the characteristic patterns of excitations and inhibitions were strongly affected by dopamine depletion. Our results suggest that dopamine depletion may also affect the spatio-temporal pattern of evoked responses and affect the structure of parallel functional channels in the BG.

In the present paper, we studied three types of networks: a base case with an intact functional channel structure and two cases in which this structure was perturbed. In the base case, neurons projected to neurons expressing similar features. This was realized in N-networks by connecting neurons with similar (spatial) coordinates s^{X} (Figure 1C1). This mimicked an intact somatotopic organization of synaptic connections (Nambu, 2011) and precise reciprocal loops between STN and GPe (Kita, 2007). In addition, we considered two types of altered network structures: First, in D-networks a shift in synaptic connectivity was induced for a fraction of the neurons such that they would connect to neurons with shifted (spatial) coordinates $s^{\mathrm{X}} + d$ (Figure 1C2). Second, in S-networks, neurons projected to an enlarged area in the postsynaptic nucleus such that neurons with less similar coordinates were also targeted (Figure 1C3). The described changes in the network structure had a strong impact on cortically evoked spatio-temporal responses of STN and GPe neurons. While cortical stimulation in N-networks only triggered responses of neurons with similar coordinates, a second neuronal population expressing different features responded in D-networks. Interpreting these results, stimulation or activation of a cortical region corresponding to a certain body part or motor program would also activate neuronal populations representing different body parts or motor programs in D-networks. Such a perturbation of the BG structure may lead to the inability to activate these body parts independently. In contrast, in S-networks, cortical stimuli triggered less pronounced responses but of a bigger neuronal population. Such an alteration of the BG structure may correspond to less coordinated motor movements in response to cortical activation. Evidence from animal models

suggests that a reorganization of network connectivity emerges in several BG related movement disorders, e.g., Parkinson's disease (Bronfeld and Bar-Gad, 2011). Experimental studies in the MPTP monkey model suggest that both types of impairment, i.e., responses to different body parts (D-network) and broadening of the projection region (S-network), may occur in the BG in Parkinson's disease. Boraud et al. (2000) reported that, under normal conditions, arm- and leg-related GPi neurons occurred in clusters and were linked to a single joint. In contrast, in the MPTP monkey model for Parkinson's disease, the overall number of responding neurons increased, and most responding neurons were linked to multiple joints (Boraud et al., 2000). Filion et al. (1988) reported that in MPTP monkeys, more globus pallidus neurons responded to the movement of a certain body part. Also, neuronal responses were elicited by the movement of more than one joint and by movements in different directions. Furthermore, some neurons responded to the movement of both upper and lower limbs on both the ipsi- and the contralateral sides. In contrast, in healthy animals, responses were only caused by the movement of a single joint on the contralateral side and in one direction (Filion et al., 1988). In rats, Cho et al. (2002) analyzed the reorganization in the lateral striatum (sensorimotor striatum) following 6-OHDA lesion. In controls, STR neurons that responded to the same body part were organized in clusters. However, after 6-OHDA lesion, the cluster size was reduced, and the portion of STR neurons that responded to more than one body part increased by a factor of 16 (Cho et al., 2002). These findings supported a hypothesis advanced by Mink (1996) that the BG's primary role may be the focused selection of the "correct" motor program and inhibition of competing ones. Synaptic reorganization in disorders such as Parkinson's disease would diminish action selection and cause motor symptoms.

Of particular interest for further analysis of the synaptic network structure of the BG would be to measure aspects of the synaptic connectivity in experiments. In earlier studies, the organization of cortico-STN connections was analyzed in tracer studies in monkeys (Monakow et al., 1978; Nambu et al., 1996). Furthermore, in Jeon et al. (2022), neuroanatomical techniques were used to construct 3D connectivity maps in mice and compare them to results from 7T MRI and tractography studies in humans. In the present study, we suggested a two-site stimulation protocol in which a test and a priming stimulus are delivered to two cortical stimulation sites at a certain distance and with a certain inter-stimulus interval. Analyzing how the priming stimulus influences the response of neurons to the test stimulus, we found that if the priming stimulus is applied long ($>$ 100 ms) before the test stimulus, varying the spatial distance between cortical stimulation sites yields an approximate "channel width," characterizing the width of the cortical area in which stimulation activates the considered area in the STN or GPe (Figures 9A, C). This method may be used to analyze the spatial characteristics of the somatotopic organization in the BG. To realize two-site stimulation in an experiment, the response of single BG neurons to cortical stimuli would be measured, similar to the experiments performed by Nambu et al. (2000); Kita et al. (2004); Jaeger and Kita (2011); Kita and Kita (2011); and Polyakova et al. (2020). Then a priming stimulus would be administered with a time lag Δt and at a distance Δs from the original, test stimulus. Measuring the BG neuron's PSTH for a long sequence of stimuli and comparing it to the one in the absence of the priming stimulus yields estimates of the quantities $\mathcal{L}^{\mathrm{x}}_{\mathrm{base}}(\Delta t, \Delta s)$ and $\mathcal{L}^{\mathrm{x}}_{\mathrm{re}}(\Delta t, \Delta s)$. Evaluating, these quantities for different Δt and Δs yields similar data as the one shown in Figure 9 for each responding BG neuron.

The presented two-site stimulation protocol also allowed us to measure the displacement of synaptic connections in D-networks. In these networks, neurons in the considered region of the STN or GPe responded to stimulation of two distinct cortical regions (Figures 9E–H). Our computational results suggest that this method is most sensitive when the modulation of the evoked response of STN neurons by an earlier cortical stimulus rather than the modulation of their baseline activity is considered (Figures 9B, F, J), in particular for an inter-stimulus interval of about 30 $-$ 40 ms. This time interval may be affected by synaptic transmission delays and needs to be verified experimentally. In our computational model, an approximate of the width of functional channels was also obtained if the modulation of the baseline activity of STN or GPe neurons by the presence of the cortical priming stimulus was studied (Figures 9A, E, I). This approach may also be realized by applying only one cortical stimulus and studying variations of neuronal activity from their baseline activity. However, the baseline activity may vary over time, whereas evoked responses possess characteristic features. In general, two-site stimulation may help to get a deeper understanding of the topology of synaptic connections in the BG, the somatotopic organization of the cortico-BG circuits, and to which extent this structure is impaired in animal models of neurological disorders, e.g., Parkinson's disease.

More detailed information on the organization of synaptic connections could inform future computational models. Current computational models often either consider random connectivity between nuclei, e.g., Lindahl et al. (2013); Ebert et al. (2014); Madadi Asl et al. (2022a); Adam et al. (2022); Salehi et al. (2023), or they incorporate parallel channels either by considering macroscopic parallel circuits of randomly connected subpopulations, e.g., Leblois et al. (2006); Fountas and Shanahan (2017), or by constructing parallel channels on the scale of the individual neurons, e.g., Terman et al. (2002); Hahn and McIntyre (2010); Lourens et al. (2015). The latter is somewhat comparable to the synaptic connectivity used in the present study. Our results suggest that differences in the organization of synaptic connections in computational models strongly impact cortically evoked responses and likely affect other characteristics of neuronal activity, such as synchronization or the existence of pathological oscillations. An accurate implementation of synaptic connections may be critical for generating clinically relevant hypotheses, e.g., about the response to brain stimulation.

Recently, Schmidt et al. (2020) related the shape of deep brain stimulation-evoked potentials to the involved pathways. While no information on somatotopic maps was revealed, the authors suggested that the shape of deep brain stimulation-evoked potentials may serve as a biomarker for adaptive deep brain stimulation, or may guide parameter selection and electrodes placement for deep brain stimulation in Parkinson's disease

(Schmidt et al., 2020; Dale et al., 2022). Our results may motivate preclinical and clinical studies to use cortical as well as BG one- or two-site stimulation to analyze the spatial arrangement of synaptic connections between BG nuclei. Such insight may help to improve computational models of the BG and models on high-frequency deep brain stimulation as a treatment for medically refractory Parkinson's disease significantly.

To reduce complexity, we did not consider some aspects of the STN and GPe nuclei during the derivation of our computational model. For instance, recent experimental studies reported the existence of multiple neuron types with distinct functionality in the STN (Jeon et al., 2022) and the GPe (Mallet et al., 2012; Abdi et al., 2015; Mastro et al., 2017), which may affect network functionality such as the processing of cortical responses and rhythm generation (Suryanarayana et al., 2019; Gast et al., 2021). Neuron types in the GPe include prototypic neurons and arkypallidal neurons (Mallet et al., 2012; Abdi et al., 2015). While prototypic neurons have been found to project mainly to the STN and down-stream nuclei, arkypallidal neurons project to the striatum thereby providing feedback to this upstream nucleus. Anatomical studies also reported projections of STN neurons to the striatum (Beckstead, 1983; Kita and Kitai, 1987). Here, we neglected upstream synaptic connections of the STN-GPe circuit and focused on the most common neuron type in the GPe, i.e., prototypic neurons. There is also evidence from anatomical studies that STN neurons form local axon collaterals suggesting recurrent STN connections (Hammond and Yelnik, 1983; Gouty-Colomer et al., 2018); However, recent studies performing simultaneous multi-cell recordings in rat brain slices reported the absence of functional intra-STN connectivity (Steiner et al., 2019). Therefore, we did not consider synaptic connections between STN neurons in our computational model. Another simplification is the assumption of a one-dimensional arrangement of the neurons along the s^{X}-axes. The STN and GPe are three-dimensional structures and evidence from experimental studies suggests non-homogeneous synaptic connectivity along different directions. For instance, STN axons form band-like terminal fields in the globus pallidus that are aligned with those of striatal axons (Hazrati and Parent, 1992). This would likely impact spatio-temporal characteristics of cortically evoked responses and the orientation of functional channels. Furthermore, the somatotopic organization of STN and GPe nuclei are more complex. For instance it includes multiple body maps for inputs from the primary motor cortex and the supplementary motor area, respectively (Nambu, 2011). Some experimental evidence also suggests that within regions that represent a certain body part neurons encoding similar motor features are sometimes spread out across a larger area instead of clustering together (DeLong et al., 1985). Further studies are required to understand how these factors impact the spatio-temporal response patterns evoked by cortical stimulation studied in the present paper.

As explained above, the functional channels used in this study are related to the impact, specifically spatial range and coverage of electrical stimuli on parts of brain circuits (see Figure 2). These functional channels are not meant to be building blocks of a neural code as, e.g., activity sequences corresponding to sub-second behavioral motifs (Markowitz et al., 2018). However, disease-related changes as reflected by the width of these functional channels may impact behaviorally relevant activity sequences. Accordingly, functional channels may help elucidate neuronal information processing under physiological as well as pathological conditions.

In a future study, we want to address how characteristic measures, such as the width of functional channels, can be harnessed to calibrate multisite deep brain stimulation, for instance, coordinated reset stimulation (Tass, 2003; Tass et al., 2012; Adamchic et al., 2014; Wang et al., 2016, 2022; Bore et al., 2022), random reset stimulation (Kromer and Tass, 2020; Khaledi-Nasab et al., 2021a), and other multisite stimulation protocols (Khaledi-Nasab et al., 2021b, 2022; Weerasinghe et al., 2021; Kromer and Tass, 2022) for improving desynchronizing effects, especially in the presence of reorganized somatotopic maps. In computational studies, the desynchronization effect of coordinated reset stimulation was more pronounced when individual stimuli were delivered to segregated neuronal subpopulations (Popovych and Tass, 2012; Lysyansky et al., 2013; Ebert et al., 2014; Zeitler and Tass, 2015) suggesting that effective stimulation requires appropriate spacing of stimulation sites, e.g., minimal distances between the latter. This is in accordances with results from preclinical studies on coordinated reset deep brain stimulation in the MPTP monkey model, where weaker stimulation led to more pronounced long-lasting effects (Tass et al., 2012), and findings obtained in a clinical study on acoustic coordinated reset stimulation in tinnitus patients, where larger gaps between stimulus frequencies were correlated with better acute reduction of tinnitus loudness and annoyance after 16 min of sound treatment (Tass et al., 2019; Munjal et al., 2021). Future computational and pre-clinical studies might use the functional channel width, as introduced here, to determine optimal stimulation site spacing.

Data availability statement

The original contributions presented in the study are included in the article/supplementary material, further inquiries can be directed to the corresponding author.

Author contributions

JK, HB, and PT conceived the idea and designed the study, analyzed and interpreted the numerical data, and revised and finalized the manuscript. JK performed the numerical simulations and prepared the initial draft. All authors contributed to the article and approved the submitted version.

Funding

We gratefully acknowledge support of this study by Boston Scientific Neuromodulation (Stanford Project 127674). PT gratefully acknowledges support by the John A. Blum Foundation, the Alda Parkinson's Research Fund, the Ravi Neuro Research Fund, and the Vaughn Bryson Research Fund.

Acknowledgments

We are grateful to Stanford University and Stanford's Sherlock Computing cluster for computational resources and support that contributed to these research results.

Conflict of interest

PT worked as a consultant for Boston Scientific Neuromodulation. HB is an employee of and owns stock in Boston Scientific. All authors filed a patent related to the presented two-site stimulation method.

Publisher's note

All claims expressed in this article are solely those of the authors and do not necessarily represent those of their affiliated organizations, or those of the publisher, the editors and the reviewers. Any product that may be evaluated in this article, or claim that may be made by its manufacturer, is not guaranteed or endorsed by the publisher.

References

Abdi, A., Mallet, N., Mohamed, F. Y., Sharott, A., Dodson, P. D., Nakamura, K. C., et al. (2015). Prototypic and arkypallidal neurons in the dopamine-intact external globus pallidus. *J. Neurosci.* 35, 6667–6688. doi: 10.1523/JNEUROSCI.4662-14.2015

Adam, E. M., Brown, E. N., Kopell, N., and McCarthy, M. M. (2022). Deep brain stimulation in the subthalamic nucleus for Parkinson's disease can restore dynamics of striatal networks. *Proc. Nat. Acad. Sci. U. S. A.* 119, e2120808119. doi: 10.1073/pnas.2120808119

Adamchic, I., Hauptmann, C., Barnikol, U. B., Pawelczyk, N., Popovych, O., Barnikol, T. T., et al. (2014). Coordinated reset neuromodulation for Parkinson's disease: proof-of-concept study. *Mov. Disord.* 29, 1679–1684. doi: 10.1002/mds.25923

Bahadori-Jahromi, F., Salehi, S., Madadi Asl, M., andValizadeh, A., et al. (2023). Efficient suppression of parkinsonian beta oscillations in a closed-loop model of deep brain stimulation with amplitude modulation. *Front. Hum. Neurosci.* 16, 871. doi: 10.3389/fnhum.2022.1013155

Baufreton, J., Kirkham, E., Atherton, J. F., Menard, A., Magill, P. J., Bolam, J. P., et al. (2009). Sparse but selective and potent synaptic transmission from the globus pallidus to the subthalamic nucleus. *J. Neurophysiol.* 102, 532. doi: 10.1152/jn.00305.2009

Beckstead, R. M. (1983). A reciprocal axonal connection between the subthalamic nucleus and the neostriatum in the cat. *Brain Res.* 275, 137–142. doi: 10.1016/0006-8993(83)90425-0

Beurrier, C., Congar, P., Bioulac, B., and Hammond, C. (1999). Subthalamic nucleus neurons switch from single-spike activity to burst-firing mode. *J. Neurosci.* 19, 599–609. doi: 10.1523/JNEUROSCI.19-02-00599.1999

Bevan, M. D., Magill, P. J., Terman, D., Bolam, J. P., and Wilson, C. J. (2002). Move to the rhythm: oscillations in the subthalamic nucleus-external globus pallidus network. *Trends Neurosci.* 25, 525–531. doi: 10.1016/S0166-2236(02)02235-X

Bevan, M. D., Wilson, C. J., Bolam, J. P., and Magill, P. J. (2000). Equilibrium potential of gabaa current and implications for rebound burst firing in rat subthalamic neurons *in vitro*. *J. Neurophysiol.* 83, 3169–3172. doi: 10.1152/jn.2000.83.5.3169

Boraud, T., Bezard, E., Bioulac, B., and Gross, C. (2000). Ratio of inhibited-to-activated pallidal neurons decreases dramatically during passive limb movement in the mptp-treated monkey. *J. Neurophysiol.* 83, 1760–1763. doi: 10.1152/jn.2000.83.3.1760

Bore, J. C., Campbell, B. A., Cho, H., Pucci, F., Gopalakrishnan, R., Machado, A. G., et al. (2022). Long-lasting effects of subthalamic nucleus coordinated reset deep brain stimulation in the non-human primate model of parkinsonism: A case report. *Brain Stimul.* 15, 598–600.

Bronfeld, M., and Bar-Gad, I. (2011). Loss of specificity in basal ganglia related movement disorders. *Front. Syst. Neurosci.* 5, 38. doi: 10.3389/fnsys.2011.00038

Celada, P., Paladini, C., and Tepper, J. (1999). Gabaergic control of rat substantia nigra dopaminergic neurons: role of globus pallidus and substantia nigra pars reticulata. *Neuroscience* 89, 813–825. doi: 10.1016/S0306-4522(98)00356-X

Cho, J., Duke, D., Manzino, L., Sonsalla, P. K., and West, M. O. (2002). Dopamine depletion causes fragmented clustering of neurons in the sensorimotor striatum: evidence of lasting reorganization of corticostriatal input. *J. Comp. Neurol.* 452, 24–37. doi: 10.1002/cne.10349

Chu, H.-Y., Atherton, J. F., Wokosin, D., Surmeier, D. J., and Bevan, M. D. (2015). Heterosynaptic regulation of external globus pallidus inputs to the subthalamic nucleus by the motor cortex. *Neuron* 85, 364–376. doi: 10.1016/j.neuron.2014.12.022

Chu, H.-Y., McIver, E. L., Kovaleski, R. F., Atherton, J. F., and Bevan, M. D. (2017). Loss of hyperdirect pathway cortico-subthalamic inputs following degeneration of midbrain dopamine neurons. *Neuron* 95, 1306–1318. doi: 10.1016/j.neuron.2017.08.038

Crompe, B., d. l., Aristieta, A., Leblois, A., Elsherbiny, S., Boraud, T., et al. (2020). The globus pallidus orchestrates abnormal network dynamics in a model of parkinsonism. *Nat. Commun.* 11, 1570. doi: 10.1038/s41467-020-15352-3

Dale, J., Schmidt, S. L., Mitchell, K., Turner, D. A., and Grill, W. M. (2022). Evoked potentials generated by deep brain stimulation for Parkinson's disease. *Brain Stimul.* 15, 1040–1047. doi: 10.1016/j.brs.2022.07.048

Dejean, C., Gross, C. E., Bioulac, B., and Boraud, T. (2008). Dynamic changes in the cortex-basal ganglia network after dopamine depletion in the rat. *J. Neurophysiol.* 100, 385–396. doi: 10.1152/jn.90466.2008

Delmaire, C., Krainik, A., Du Montcel, S. T., Gerardin, E., Meunier, S., Mangin, J.-F., et al. (2005). Disorganized somatotopy in the putamen of patients with focal hand dystonia. *Neurology* 64, 1391–1396. doi: 10.1212/01.WNL.0000158424.01299.76

DeLong, M. R. (1972). Activity of basal ganglia neurons during movement. *Brain Res.* 40, 127–135. doi: 10.1016/0006-8993(72)90118-7

DeLong, M. R., Crutcher, M. D., and Georgopoulos, A. P. (1985). Primate globus pallidus and subthalamic nucleus: functional organization. *J. Neurophysiol.* 53, 530–543. doi: 10.1152/jn.1985.53.2.530

Ebert, M., Hauptmann, C., and Tass, P. A. (2014). Coordinated reset stimulation in a large-scale model of the stn-gpe circuit. *Front. Comput. Neurosci.* 8, 154. doi: 10.3389/fncom.2014.00154

Fan, K. Y., Baufreton, J., Surmeier, D. J., Chan, C. S., and Bevan, M. D. (2012). Proliferation of external globus pallidus-subthalamic nucleus synapses following degeneration of midbrain dopamine neurons. *J. Neurosci.* 32, 13718–13728. doi: 10.1523/JNEUROSCI.5750-11.2012

Farries, M. A., Kita, H., and Wilson, C. J. (2010). Dynamic spike threshold and zero membrane slope conductance shape the response of subthalamic neurons to cortical input. *J. Neurosci.* 30, 13180–13191. doi: 10.1523/JNEUROSCI.1909-10.2010

Filion, M., Tremblay, L., and Bédard, P. J. (1988). Abnormal influences of passive limb movement on the activity of globus pallidus neurons in parkinsonian monkeys. *Brain Res.* 444, 165–176. doi: 10.1016/0006-8993(88)90924-9

Fountas, Z., and Shanahan, M. (2017). The role of cortical oscillations in a spiking neural network model of the basal ganglia. *PLoS ONE* 12, e0189109. doi: 10.1371/journal.pone.0189109

Gast, R., Gong, R., Schmidt, H., Meijer, H. G., and Knösche, T. R. (2021). On the role of arkypallidal and prototypical neurons for phase transitions in the external pallidum. *J. Neurosci.* 41, 6673–6683. doi: 10.1523/JNEUROSCI.0094-21.2021

Gouty-Colomer, L.-A., Michel, F. J., Baude, A., Lopez-Pauchet, C., Dufour, A., Cossart, R., et al. (2018). Mouse subthalamic nucleus neurons with local axon collaterals. *J. Comp. Neurol.* 526, 275–284. doi: 10.1002/cne.24334

Hahn, P. J., and McIntyre, C. C. (2010). Modeling shifts in the rate and pattern of subthalamopallidal network activity during deep brain stimulation. *J. Comput. Neurosci.* 28, 425–441. doi: 10.1007/s10827-010-0225-8

Hammond, C., Bergman, H., and Brown, P. (2007). Pathological synchronization in Parkinson's disease: networks, models and treatments. *Trends Neurosci.* 30, 357–364. doi: 10.1016/j.tins.2007.05.004

Hammond, C., and Yelnik, J. (1983). Intracellular labelling of rat subthalamic neurones with horseradish peroxidase: computer analysis of dendrites and characterization of axon arborization. *Neuroscience* 8, 781–790. doi: 10.1016/0306-4522(83)90009-X

Hazrati, L.-N., and Parent, A. (1992). Convergence of subthalamic and striatal efferents at pallidal level in primates: an anterograde double-labeling study with biocytin and pha-l. *Brain Res.* 569, 336–340. doi: 10.1016/0006-8993(92)90648-S

Izhikevich, E. M. (2003). Simple model of spiking neurons. *IEEE Transact. Neural Netw.* 14, 1569–1572. doi: 10.1109/TNN.2003.820440

Jaeger, D., and Kita, H. (2011). Functional connectivity and integrative properties of globus pallidus neurons. *Neuroscience* 198, 44–53. doi: 10.1016/j.neuroscience.2011.07.050

Jeon, H., Lee, H., Kwon, D.-H., Kim, J., Tanaka-Yamamoto, K., Yook, J. S., et al. (2022). Topographic connectivity and cellular profiling reveal detailed input pathways and functionally distinct cell types in the subthalamic nucleus. *Cell Rep.* 38, 110439. doi: 10.1016/j.celrep.2022.110439

Kaplitt, M. G., Hutchison, W. D., and Lozano, A. M. (2003). "Target localization in movement disorders surgery?" in *Surgical Treatment of Parkinson's Disease and Other Movement Disorders*, ed D. Tarsy (Totowa, NJ: Humana Press Inc.), 87–98.

Ketzef, M., and Silberberg, G. (2021). Differential synaptic input to external globus pallidus neuronal subpopulations *in vivo*. *Neuron* 109, 516–529. doi: 10.1016/j.neuron.2020.11.006

Khaledi-Nasab, A., Kromer, J., and Tass, P. A. (2021a). Long-lasting desynchronization of plastic neural networks by random reset stimulation. *Front. Physiol.* 11, 622620. doi: 10.3389/fphys.2020.622620

Khaledi-Nasab, A., Kromer, J. A., and Tass, P. A. (2021b). Long-lasting desynchronization effects of coordinated reset stimulation improved by random jitters. *Front. Physiol.* 12, 719680. doi: 10.3389/fphys.2021.719680

Khaledi-Nasab, A., Kromer, J. A., and Tass, P. A. (2022). Long-lasting desynchronization of plastic neuronal networks by double-random coordinated reset stimulation. *Front. Netw. Physiol.* 2, 864859. doi: 10.3389/fnetp.2022.864859

Kita, H. (2007). Globus pallidus external segment. *Prog. Brain Res.* 160, 111–133. doi: 10.1016/S0079-6123(06)60007-1

Kita, H., and Kita, T. (2011). Cortical stimulation evokes abnormal responses in the dopamine-depleted rat basal ganglia. *J. Neurosci.* 31, 10311–10322. doi: 10.1523/JNEUROSCI.0915-11.2011

Kita, H., and Kitai, S. (1987). Efferent projections of the subthalamic nucleus in the rat: light and electron microscopic analysis with the pha-l method. *J. Comp. Neurol.* 260, 435–452. doi: 10.1002/cne.902600309

Kita, H., Nambu, A., Kaneda, K., Tachibana, Y., and Takada, M. (2004). Role of ionotropic glutamatergic and gabaergic inputs on the firing activity of neurons in the external pallidum in awake monkeys. *J. Neurophysiol.* 92, 3069–3084. doi: 10.1152/jn.00346.2004

Kloeden, P. E., and Platen, E. (1992). *Numerical Solution of Stochastic Differential Equations*. Berlin: Springer-Verlag.

Koshimizu, Y., Fujiyama, F., Nakamura, K. C., Furuta, T., and Kaneko, T. (2013). Quantitative analysis of axon bouton distribution of subthalamic nucleus neurons in the rat by single neuron visualization with a viral vector. *J. Comp. Neurol.* 521, 2125–2146. doi: 10.1002/cne.23277

Krack, P., Batir, A., Van Blercom, N., Chabardes, S., Fraix, V., Ardouin, C., et al. (2003). Five-year follow-up of bilateral stimulation of the subthalamic nucleus in advanced Parkinson's disease. *N. Engl. J. Med.* 349, 1925–1934. doi: 10.1056/NEJMoa035275

Kromer, J. A., and Tass, P. A. (2020). Long-lasting desynchronization by decoupling stimulation. *Phys. Rev. Res.* 2, 033101. doi: 10.1103/PhysRevResearch.2.033101

Kromer, J. A., and Tass, P. A. (2022). Synaptic reshaping of plastic neuronal networks by periodic multichannel stimulation with single-pulse and burst stimuli. *PLoS Comput. Biol.* 18, e1010568. doi: 10.1371/journal.pcbi.1010568

Kumaravelu, K., Brocker, D. T., and Grill, W. M. (2016). A biophysical model of the cortex-basal ganglia-thalamus network in the 6-ohda lesioned rat model of Parkinson's disease. *J. Comput. Neurosci.* 40, 207–229. doi: 10.1007/s10827-016-0593-9

Leblois, A., Boraud, T., Meissner, W., Bergman, H., and Hansel, D. (2006). Competition between feedback loops underlies normal and pathological dynamics in the basal ganglia. *J. Neurosci.* 26, 3567–3583. doi: 10.1523/JNEUROSCI.5050-05.2006

Lindahl, M., Kamali Sarvestani, I., Ekeberg, Ö, and Kotaleski, J. H. (2013). Signal enhancement in the output stage of the basal ganglia by synaptic short-term plasticity in the direct, indirect, and hyperdirect pathways. *Front. Comput. Neurosci.* 7, 76. doi: 10.3389/fncom.2013.00076

Lourens, M. A., Schwab, B. C., Nirody, J. A., Meijer, H. G., and van Gils, S. A. (2015). Exploiting pallidal plasticity for stimulation in Parkinson's disease. *J. Neural Eng.* 12, 026005. doi: 10.1088/1741-2560/12/2/026005

Lysyansky, B., Popovych, O. V., and Tass, P. A. (2013). Optimal number of stimulation contacts for coordinated reset neuromodulation. *Front. Neuroeng.* 6, 5. doi: 10.3389/fneng.2013.00005

Madadi Asl, M., Asadi, A., Enayati, J., and Valizadeh, A. (2022a). Inhibitory spike-timing-dependent plasticity can account for pathological strengthening of pallido-subthalamic synapses in Parkinson's disease. *Front. Physiol.* 13, 915626. doi: 10.3389/fphys.2022.915626

Madadi Asl, M., Vahabie, A. H., Valizadeh, A., and Tass, P. A. (2022b). Spike-timing-dependent plasticity mediated by dopamine and its role in Parkinson's disease pathophysiology. *Front. Netw. Physiol.* 2, 817524. doi: 10.3389/fnetp.2022.817524

Mallet, N., Micklem, B. R., Henny, P., Brown, M. T., Williams, C., Bolam, J. P., et al. (2012). Dichotomous organization of the external globus pallidus. *Neuron* 74, 1075–1086. doi: 10.1016/j.neuron.2012.04.027

Markowitz, J. E., Gillis, W. F., Beron, C. C., Neufeld, S. Q., Robertson, K., Bhagat, N. D., et al. (2018). The striatum organizes 3D behavior via moment-to-moment action selection. *Cell* 174, 44–58. doi: 10.1016/j.cell.2018.04.019

Mastro, K. J., Zitelli, K. T., Willard, A. M., Leblanc, K. H., Kravitz, A. V., and Gittis, A. H. (2017). Cell-specific pallidal intervention induces long-lasting motor recovery in dopamine-depleted mice. *Nat. Neurosci.* 20, 815–823. doi: 10.1038/nn.4559

McCairn, K. W., Bronfeld, M., Belelovsky, K., and Bar-Gad, I. (2009). The neurophysiological correlates of motor tics following focal striatal disinhibition. *Brain* 132, 2125–2138. doi: 10.1093/brain/awp142

Miguelez, C., Morin, S., Martinez, A., Goillandeau, M., Bezard, E., Bioulac, B., et al. (2012). Altered pallido-pallidal synaptic transmission leads to aberrant firing of globus pallidus neurons in a rat model of parkinson's disease. *J. Physiol.* 590, 5861–5875. doi: 10.1113/jphysiol.2012.241331

Mink, J. W. (1996). The basal ganglia: focused selection and inhibition of competing motor programs. *Prog. Neurobiol.* 50, 381–425. doi: 10.1016/S0301-0082(96)00042-1

Miyachi, S., Lu, X., Imanishi, M., Sawada, K., Nambu, A., and Takada, M. (2006). Somatotopically arranged inputs from putamen and subthalamic nucleus to primary motor cortex. *Neurosci. Res.* 56, 300–308. doi: 10.1016/j.neures.2006.07.012

Monakow, K., Akert, K., and Künzle, H. (1978). Projections of the precentral motor cortex and other cortical areas of the frontal lobe to the subthalamic nucleus in the monkey. *Exp. Brain Res.* 33, 395–403. doi: 10.1007/BF00235561

Munjal, T., Silchenko, A. N., Pfeifer, K. J., Han, S. S., Yankulova, J. K., Fitzgerald, M. B., et al. (2021). Treatment tone spacing and acute effects of acoustic coordinated reset stimulation in tinnitus patients. *Front. Netw. Physiol.* 1, 734344. doi: 10.3389/fnetp.2021.734344

Nambu, A. (2011). Somatotopic organization of the primate basal ganglia. *Front. Neuroanat.* 5, 26. doi: 10.3389/fnana.2011.00026

Nambu, A., Kaneda, K., Tokuno, H., and Takada, M. (2002). Organization of corticostriatal motor inputs in monkey putamen. *J. Neurophysiol.* 88, 1830–1842. doi: 10.1152/jn.2002.88.4.1830

Nambu, A., Takada, M., Inase, M., and Tokuno, H. (1996). Dual somatotopical representations in the primate subthalamic nucleus: evidence for ordered but reversed body-map transformations from the primary motor cortex and the supplementary motor area. *J. Neurosci.* 16, 2671–2683. doi: 10.1523/JNEUROSCI.16-08-02671.1996

Nambu, A., Tokuno, H., Hamada, I., Kita, H., Imanishi, M., Akazawa, T., et al. (2000). Excitatory cortical inputs to pallidal neurons via the subthalamic nucleus in the monkey. *J. Neurophysiol.* 84, 289–300. doi: 10.1152/jn.2000.84.1.289

Oorschot, D. E. (1996). Total number of neurons in the neostriatal, pallidal, subthalamic, and substantia nigral nuclei of the rat basal ganglia: a stereological study using the cavalieri and optical disector methods. *J. Comp. Neurol.* 366, 580–599. doi: 10.1002/(SICI)1096-9861(19960318)366:4<580::AID-CNE3>3.0.CO;2-0

Pamukcu, A., Cui, Q., Xenias, H. S., Berceau, B. L., Augustine, E. C., Fan, I., et al. (2020). Parvalbumin+ and npas1+ pallidal neurons have distinct circuit topology and function. *J. Neurosci.* 40, 7855–7876. doi: 10.1523/JNEUROSCI.0361-20.2020

Parent, A., and Hazrati, L.-N. (1993). Anatomical aspects of information processing in primate basal ganglia. *Trends Neurosci.* 16, 111–116. doi: 10.1016/0166-2236(93)90135-9

Pessiglione, M., Guehl, D., Rolland, A.-S., François, C., Hirsch, E. C., Féger, J., et al. (2005). Thalamic neuronal activity in dopamine-depleted primates: evidence for a loss of functional segregation within basal ganglia circuits. *J. Neurosci.* 25, 1523–1531. doi: 10.1523/JNEUROSCI.4056-04.2005

Plenz, D., and Kital, S. T. (1999). A basal ganglia pacemaker formed by the subthalamic nucleus and external globus pallidus. *Nature* 400, 677–682. doi: 10.1038/23281

Polyakova, Z., Chiken, S., Hatanaka, N., and Nambu, A. (2020). Cortical control of subthalamic neuronal activity through the hyperdirect and indirect pathways in monkeys. *J. Neurosci.* 40, 7451–7463. doi: 10.1523/JNEUROSCI.0772-20.2020

Popovych, O. V., and Tass, P. A. (2012). Desynchronizing electrical and sensory coordinated reset neuromodulation. *Front. Hum. Neurosci.* 6, 58. doi: 10.3389/fnhum.2012.00058

Sadek, A. R., Magill, P. J., and Bolam, J. P. (2007). A single-cell analysis of intrinsic connectivity in the rat globus pallidus. *J. Neurosci.* 27, 6352–6362. doi: 10.1523/JNEUROSCI.0953-07.2007

Schmidt, S. L., Brocker, D. T., Swan, B. D., Turner, D. A., and Grill, W. M. (2020). Evoked potentials reveal neural circuits engaged by human deep brain stimulation. *Brain Stimul.* 13, 1706–1718. doi: 10.1016/j.brs.2020.09.028

Shink, E., Bevan, M., Bolam, J., and Smith, Y. (1996). The subthalamic nucleus and the external pallidum: two tightly interconnected structures that control the output of the basal ganglia in the monkey. *Neuroscience* 73, 335–357. doi: 10.1016/0306-4522(96)00022-X

Soghomonian, J.-J., and Jagaroo, V. (2016). "Introduction: overview of the basal ganglia and structure of the volume," in *The Basal Ganglia, Chapter 1*, ed J.-J. Soghomonian (Cham: Springer International Publishing), 1–8.

Steiner, L. A., Tomás, F. J. B., Planert, H., Alle, H., Vida, I., and Geiger, J. R. (2019). Connectivity and dynamics underlying synaptic control of the subthalamic nucleus. *J. Neurosci*. 39, 2470–2481. doi: 10.1523/JNEUROSCI.1642-18.2019

Suryanarayana, S. M., Kotaleski, J. H., Grillner, S., and Gurney, K. N. (2019). Roles for globus pallidus externa revealed in a computational model of action selection in the basal ganglia. *Neural Netw*. 109, 113–136. doi: 10.1016/j.neunet.2018.10.003

Tamburin, S., Manganotti, P., Marzi, C. A., Fiaschi, A., and Zanette, G. (2002). Abnormal somatotopic arrangement of sensorimotor interactions in dystonic patients. *Brain* 125, 2719–2730. doi: 10.1093/brain/awf279

Tass, P. A. (2003). A model of desynchronizing deep brain stimulation with a demand-controlled coordinated reset of neural subpopulations. *Biol. Cybern*. 89, 81–88. doi: 10.1007/s00422-003-0425-7

Tass, P. A., Qin, L., Hauptmann, C., Dovero, S., Bezard, E., Boraud, T., et al. (2012). Coordinated reset has sustained aftereffects in parkinsonian monkeys. *Ann. Neurol*. 72, 816–820. doi: 10.1002/ana.23663

Tass, P. A., Silchenko, A. N., and Popelka, G. R. (2019). Acoustic coordinated reset therapy for tinnitus with perceptually relevant frequency spacing and levels. *Sci. Rep*. 9, 13607. doi: 10.1038/s41598-019-49945-w

Terman, D., Rubin, J. E., Yew, A., and Wilson, C. (2002). Activity patterns in a model for the subthalamopallidal network of the basal ganglia. *J. Neurosci*. 22, 2963–2976. doi: 10.1523/JNEUROSCI.22-07-02963.2002

Wang, J., Fergus, S. P., Johnson, L. A., Nebeck, S. D., Zhang, J., Kulkarni, S., et al. (2022). Shuffling improves the acute and carryover effect of subthalamic coordinated reset deep brain stimulation. *Front. Neurol*. 13, 716046. doi: 10.3389/fneur.2022.716046

Wang, J., Nebeck, S., Muralidharan, A., Johnson, M. D., Vitek, J. L., and Baker, K. B. (2016). Coordinated reset deep brain stimulation of subthalamic nucleus produces long-lasting, dose-dependent motor improvements in the 1-methyl-4-phenyl-1, 2, 3, 6-tetrahydropyridine non-human primate model of parkinsonism. *Brain Stimul*. 9, 609–617. doi: 10.1016/j.brs.2016.03.014

Weerasinghe, G., Duchet, B., Bick, C., and Bogacz, R. (2021). Optimal closed-loop deep brain stimulation using multiple independently controlled contacts. *PLoS Comput. Biol*. 17, e1009281. doi: 10.1371/journal.pcbi.1009281

Zeitler, M., and Tass, P. A. (2015). Augmented brain function by coordinated reset stimulation with slowly varying sequences. *Front. Syst. Neurosci*. 9, 49. doi: 10.3389/fnsys.2015.00049

frontiers | Frontiers in Neuroinformatics

TYPE Original Research
PUBLISHED 24 August 2023
DOI 10.3389/fninf.2023.1205529

OPEN ACCESS

EDITED BY
Peter A. Tass,
Stanford University, United States

REVIEWED BY
Alireza Valizadeh,
Institute for Advanced Studies in Basic Sciences (IASBS), Iran
Md. Ariful Islam,
University of Dhaka, Bangladesh

*CORRESPONDENCE
Jie Zhou
✉ sxuj_zhou@163.com

RECEIVED 14 April 2023
ACCEPTED 10 August 2023
PUBLISHED 24 August 2023

CITATION
Zhang X, Dong S, Shen Q, Zhou J and Min J (2023) Deep extreme learning machine with knowledge augmentation for EEG seizure signal recognition. *Front. Neuroinform.* 17:1205529. doi: 10.3389/fninf.2023.1205529

Deep extreme learning machine with knowledge augmentation for EEG seizure signal recognition

Xiongtao Zhang[1,2], Shuai Dong[1,2], Qing Shen[1,2], Jie Zhou[3]* and Jingjing Min[4]

[1]School of Information Engineering, Huzhou University, Huzhou, China, [2]Zhejiang Province Key Laboratory of Smart Management and Application of Modern Agricultural Resources, Huzhou University, Huzhou, China, [3]Department of Computer Science and Engineering, Shaoxing University, Shaoxing, China, [4]Department of Neurology, The First People's Hospital of Huzhou, First Affiliated Hospital of Huzhou University, Huzhou, China

Introduction: Intelligent recognition of electroencephalogram (EEG) signals can remarkably improve the accuracy of epileptic seizure prediction, which is essential for epileptic diagnosis. Extreme learning machine (ELM) has been applied to EEG signals recognition, however, the artifacts and noises in EEG signals have a serious effect on recognition efficiency. Deep learning is capable of noise resistance, contributing to removing the noise in raw EEG signals. But traditional deep networks suffer from time-consuming training and slow convergence.

Methods: Therefore, a novel deep learning based ELM (denoted as DELM) motivated by stacking generalization principle is proposed in this paper. Deep extreme learning machine (DELM) is a hierarchical network composed of several independent ELM modules. Augmented EEG knowledge is taken as complementary component, which will then be mapped into next module. This learning process is so simple and fast, meanwhile, it can excavate the implicit knowledge in raw data to a greater extent. Additionally, the proposed method is operated in a single-direction manner, so there is no need to perform parameters fine-tuning, which saves the expense of time.

Results: Extensive experiments are conducted on the public Bonn EEG dataset. The experimental results demonstrate that compared with the commonly-used seizure prediction methods, the proposed DELM wins the best average accuracies in 13 out of the 22 data and the best average F-measure scores in 10 out of the 22 data. And the running time of DELM is more than two times quickly than deep learning methods.

Discussion: Therefore, DELM is superior to traditional and some state-of-the-art machine learning methods. The proposed architecture demonstrates its feasibility and superiority in epileptic EEG signal recognition. The proposed less computationally intensive deep classifier enables faster seizure onset detection, which is showing great potential on the application of real-time EEG signal classification.

KEYWORDS

multilayer extreme learning machine, deep network, knowledge utilization, EEG, seizure recognition

1. Introduction

Epilepsy is a common chronic neurological disease caused by sudden abnormal discharge of neurons in human brain (Sanei and Chambers, 2013). Most epileptic patients have no difference from common people when epileptic seizure does not appear, but epilepsy has a serious effect on quality of human life, or even causes fatal harm

(Iasemidis et al., 2003). Rapid and accurate diagnosis of epilepsy is essential for the treatment of patients and the risk reduction of potential seizures, and its relevant technique is urgently expected in current society. Electroencephalogram (EEG) shows the electrical activity of human brain recorded by amplifying voltage differences between electrodes placed on the scalp or cerebral cortex. In traditional epilepsy detection by doctors, visual marking of long EEG recordings is a tedious and high-cost task with high misjudgment rate, especially taking into account the subjectiveness of experts (Wang et al., 2018).

EEG signal recognition plays an important role in the assessment and auxiliary diagnosis of epilepsy (Ghosh-Dastidar et al., 2007; Ahmadlou and Adeli, 2011; Ayman et al., 2023). Careful analysis of the electroencephalograph records can provide valuable insight and improved understanding of the mechanisms causing epileptic disorders. Machine learning methods, such as neural network (Subasi and Ercelebi, 2005; Kumar et al., 2010), fuzzy system (Güler and Übeyli, 2005), support vector machine (Panda et al., 2010; Nicolaou and Georgiou, 2012; Kumar et al., 2014), and extreme learning machine (Liang et al., 2006b; Yuan et al., 2011; Song and Zhang, 2013), have been extensively used in EEG signal recognition. But some of the existing intelligent methods perform poor in terms of classification accuracy, real-time prediction and so on. As a novel paradigm of learning method, ELM can not only learn rapidly with good generalization performance, but also effectively overcome the inherent drawbacks of some intelligent technologies. In recent years, ELM and its variants (Huang et al., 2004, 2006, 2011a,b; Liang et al., 2006a; Betthauser et al., 2017) have received increasing attention. However, its shallow structure is deficient in extracting the significant implicit information from the original data, which becomes the main bottleneck restricting its development. As a popular trend in machine learning, deep learning has confirmed that pattern recognition can remarkably benefit from the knowledge learned via hierarchical feature representation. Typical deep networks include deep belief network (Hinton and Salakhutdinov, 2006; Hinton et al., 2006; Plis et al., 2014), convolutional neural network (Khan et al., 2017; Acharya et al., 2018; Choi et al., 2019), stack autoencoder (Bengio et al., 2007; Vincent et al., 2010; Xu et al., 2015), etc. There are many artifacts and noises in EEG signals, which can seriously decrease recognition efficiency (Bengio, 2009; Zhou and Chan, 2016; Bhattacharyya and Pachori, 2017). Deep learning is exactly able to resist noise in recognition process and can remove noise from EEG data (Huang et al., 2013; Deng et al., 2016). However, conventional deep learning algorithm is time-consuming with complicated structure and can easily lead to overfitting in presence of limited available samples. In order to tackle the aforementioned problems, ELM is gradually combined with deep learning to generate a high-performance model (Tang et al., 2014, 2015; Yu et al., 2015; Zhu et al., 2015; Duan et al., 2016; McIntosh et al., 2020). However, most of the existing hierarchical ELM models can hardly effectively use the knowledge learned in previous layers.

ELM is popular for its high-speed response, real-time prediction ability, network conciseness, and excellent generalization performance. The thought of deep learning can be beneficial to excavate the invisible value of input to the greatest extent. To address the problem of lacking representational learning, deep extreme learning machine (DELM) is proposed to recognize EEG epileptic signals. The efficient deep classifier is based on stacked structure, which in essence consists of several modules whose hidden layer parameters are initialized randomly. The proposed method forms a hierarchical structure to aggregate some discrete and valuable information stepwisely into knowledge for hierarchical representation. The previous valuable information is fed into new input in the manner of available knowledge and then transmitted to current sub-model, which serves to implement the subsequent recognition task better. According to stacking generalization theory, the output of the next sub-model plus the knowledge of the previous sub-model in DELM can indeed open the manifold structure of the input space, which resulting an improved performance. DELM have accomplish fast epileptic recognition and show greater performance in EEG signal classification than traditional ELM and some of the state-of-the-art methods, which makes it possible to finish accurate epilepsy diagnosis in real time and with high precision. The main contributions of this work are as follows:

(1) DELM is a novel deep learning structure, which is the product of the fusion of ELM and deep learning. DELM is composed of original ELMs, accordingly, the new structure is inherently brief, flexible to implement, and demonstrates a superior learning performance. Additionally, the introduction of deep representation ensures that valuable knowledge is refined and not wasted. Learning rich representations efficiently is crucial for achieving better generalization performance and informative features can promote the accuracy. In our paper, the new framework can achieve classification accuracy comparable to that of existing deep network schemes in EEG recognition tasks, while DELM takes the leading position in training speed.
(2) Motivated by deep learning, the proposed DELM is used to capture useful information in multi-dimensional EEG variables. DELM is a hierarchical framework, which incorporates a stepwise knowledge augmentation strategy into original ELM. It learns knowledge in an incremental way and expands it in the manner of forward calculation. The current sub-model can exploit knowledge from all previous sub-models and the recognition results can be obtained in the last layer.
(3) DELM uses classic ELM as the basic building block, and each module is the same as the original ELM structure. Supervised learning performs throughout the whole learning process and each sample has a tendency to approach to its own class under the supervision.

The main differences of the proposed DELM and traditional and deep learning methods are summarized in Table 1. The rest of this paper is organized as follows. Section 2 presents the details of deep extreme learning machine proposed in our work and describes its learning process. Section 3 introduces the experiment conducted and compares the recognition performance of the proposed method with that of existing conventional methods on real EEG datasets. Finally, Section 4 concludes the findings of the study.

2. The proposed classifier DELM

2.1. The proposed architecture based on deep representation

ELM with L hidden neural units and activation function g(.) can approximate these N samples with zero error, which is modeled as (Huang et al., 2004):

$$\sum_{i=1}^{L} \beta_i g(w_i x_j + b_i) = t_j, j = 1, ..., N \quad (1)$$

where $x_i = [x_{i1}, x_{i2}, \ldots, x_{in}]^T \in R^n$, $t_i = [t_{i1}, t_{i2}, \ldots, t_{im}]^T \in R^m$, β_i is the weight vector connecting the ith hidden node and the output nodes, w_i is the ith hidden node and the input nodes, and b_i represents the bias of the ith hidden node. For the sake of convenience, the equation can be written in a compact form

$$H\beta = T \quad (2)$$

with $\beta = [\beta_1, \ldots, \beta_L]^T_{m\times L}$, $T = [t_1, \cdots, t_N]^T_{m\times N}$ and $H(w_1, ..., w_L, b_1, ..., b_L, x_1, ..., x_N)$

$$= \begin{pmatrix} g(w_1 \cdot x_1 + b_1) & \ldots & g(w_L \cdot x_1 + b_L) \\ \vdots & \ldots & \vdots \\ g(w_1 \cdot x_N + b_1) & \cdots & g(w_L \cdot x_N + b_L) \end{pmatrix}_{N\times L}$$

TABLE 1 Comparisons between the proposed DELM and traditional and deep learning methods.

Models	Running speed quickly	Deep learning ability
ELM	Yes	No
Adaboost	No	No
DBN	No	Yes
SAE	No	Yes
DELM	Yes	Yes

where H is the hidden layer output matrix of neural network, the ith column of H is corresponding output of the ith hidden layer unit with respect to inputs.

The solution of Equation 2 is equivalent to the next optimization problem (Liang et al., 2006a):

$$\left\| H(w_1, ..., w_L, b_1, ..., b_L)\widehat{\beta} - T \right\| = \min_{\beta} \left\| H(w_1, ..., w_L, b_1, ..., b_L)\beta - T \right\| \quad (3)$$

In most cases of practical application, the hidden layer neurons is far less than the samples need be trained, $L \ll N$. The output matrix of the hidden layer is not a square matrix, and the minimum norm least-squares solution of the above linear system can be calculated by Equation 4 (Huang et al., 2011a):

$$\widehat{\beta} = H^+ T \quad (4)$$

H^+ denotes the Moore-Penrose generalized inverse of the output matrix H. The theory of ELM is aimed at reaching not only the smallest training error but also the smallest norm of output weights.

ELM is a shallow network composed of three layers (respectively input layer, hidden layer and output layer), whose representation capability is limited. Adequate representation of the input is routinely desired to acquire an excellent performance in the idea of deep learning. On account of the flexibility and efficiency of ELMs, ELM is extended to the learning of deep neural network (DNN) to shorten the learning time dramatically and reduce the computational complexity without deserting their original excellence. The proposed architecture constructed from ELM building block is a new ELM-based stacked structure that processes information layer by layer in order to utilize the learned knowledge. Figure 1 depicts the architecture of the proposed hierarchical method.

The proposed structure inherits the simplicity of the original ELM, and then digestion and absorption of knowledge is performed in multiple sub-model. In DELM, the initial EEG epileptic signal is learned step by step in a forward manner. The representation learned from the previous layer is regarded as new knowledge and will then be taught. Upon the arrival of given input, the

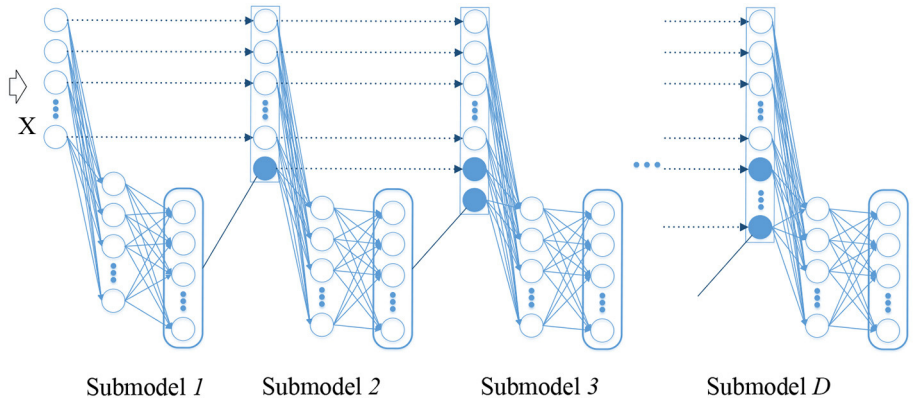

FIGURE 1
The proposed hierarchical architecture.

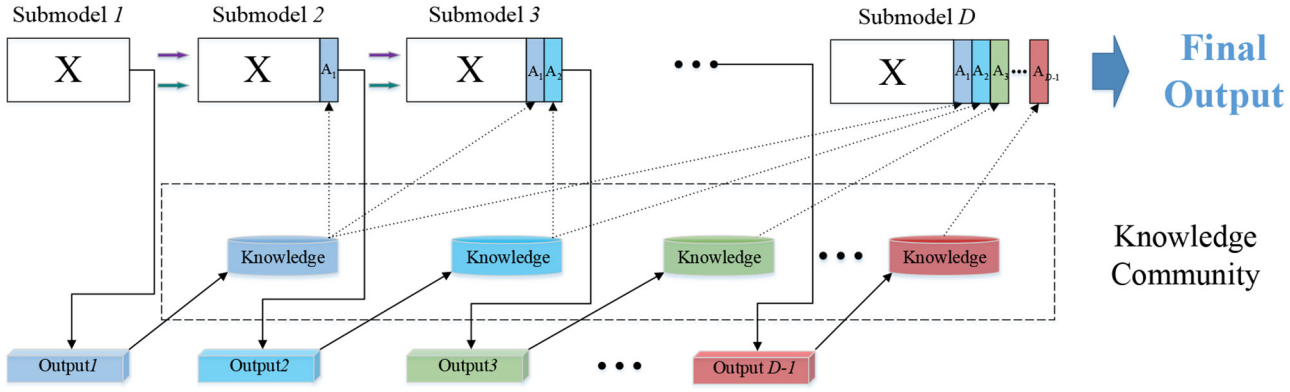

FIGURE 2
Stepwise knowledge learning in DELM.

corresponding linear system can be solved immediately in the first ELM.

In a singleton ELM module, the knowledge generation process is as follows. If H^TH is nonsingular, the orthogonal projection method can be used to calculate the generalized inverse of a matrix (Huang et al., 2011b):

$$H^+ = \left(H^TH\right)^{-1}H^T \tag{5}$$

According to Equation 4 (Betthauser et al., 2017), we can get

$$\widehat{\beta} = \left(H^TH\right)^{-1}H^TT \tag{6}$$

For binary EEG classification applications, the decision function is:

$$f(\mathrm{x}) = \mathrm{sign}(\mathrm{g}(\mathrm{x})\beta) \tag{7}$$

g(.) maps the data from input space into the L-dimensional hidden-layer feature space (ELM feature space). By inserting Equations 6 into Equation 7, we can obtain

$$f(\mathrm{x}) = \mathrm{sign}(\mathrm{g}(\mathrm{x})\left(H^TH\right)^{-1}H^TT) \tag{8}$$

For multi-class EEG classification tasks, the corresponding predicted label of sample is the index number of the output node which has the highest output value for the given instance. f_p denotes the output function of pth node, then we have the predicted class label of sample x:

$$label(x) = arg\max_{p\in\{1,2,\ldots,m\}} f_p(x) \tag{9}$$

Each sub-model in a higher layer takes information transformed from the decision output of the previous lower layers and appends them as supplementary knowledge, enabling more relevant representation to be handed over to the next generation. Deeper representation is captured to build a hierarchical network until the next additive ELM had no remarkable effect.

With deep representation in DELM, useful information is well-explored and transmitted from the initial layer to the last layer, bringing a more complete and precise expression of original input, improving the knowledge utilization rate greatly and strengthening the learning capability of ELM. Several ELMs are combined together by means of a serial link and the response can be reused in higher sub-model next to it. On the premise of meaningfulness of extended ELM, the purpose of the previous submodel is to convey the knowledge learned by previous layer. By updating the knowledge community, the original manifold can be separated apart in the end.

2.2. Knowledge augmentation based on DELM

A detailed introduction to knowledge transfer between multiple modules is provided in Figure 2. The input of n dimensional attributes provides data for the first level to construct a traditional ELM classifier. For N samples in a given dataset, x_i is the data of the ith dimension attribute corresponding to different samples, and t_i is the expected label, where $x_i = [x_{i1}, x_{i2}, \ldots, x_{in}]^T \in R^n$, $t_i = [t_{i1}, t_{i2}, \ldots, t_{im}]^T \in R^m$.

The expected label is expressed in T while the actual output Y_d calculated by the dth level model is expressed as:

$$Y_d = \begin{bmatrix} y_{11}^d & \cdots & y_{1N}^d \\ \vdots & \ddots & \vdots \\ y_{m1}^d & \cdots & y_{mN}^d \end{bmatrix} \tag{10}$$

m represents the number of categories of samples. The matrix form is as follows: $T = [t_1, \cdots, t_N]_{m\times N}^T$. After finishing the task of the first ELM, the output produced by sub-model1 is $Y_1 \in R^{m\times N}$. Resemble the process in classic ELM, the output matrix should perform a transformation here. The information acquired by current sub-model is integrated, and the fused knowledge community is stored for the next knowledge transmission. For the ith instance, take the maximum value in its each column as its class label, store the class label $x_{n+1} \in R^{1\times N}$ and merge it with the original input. The updated input is obtained in the second level Submodel2: $x_i = \left[x_{i1}, x_{i2}, \ldots, x_{in}, x_{i(n+1)}\right]^T \in R^{n+1}$. The

Input: The dataset $S_1=\{(x_i,t_i)\,|x_i \in R^n, t_i \in R^m, i=1,\ldots,N\}$, where the original input matrix is expressed as X_1, the activation function is g(.), total number of iterations is r.
Output: The output label Y.

for $k=1; k \leq r$ **do**
Step 1:
(a) Randomly initialize input weights w_i and biases of hidden layer neurons b_i;
(b) Calculate the output matrix of the hidden layer H_1;
(c) Determine the output weights analytically according to Equation 6, $\widehat{\beta}_1=H_1^+T$;
(d) Compute the classification results: $Y_1=H_1\widehat{\beta}_1$, convert the actual output to label matrix A_1, and store it into a new representation matrix $X_2=[X_1|A_1]$, so the updated dataset of input: $S_2=\{(x_i,t_i)\,|x_i \in R^{n+1}, t_i \in R^m, i=1,2,\ldots,N\}$.
Step 2:
Initialize the depth $d=2$.
Repeat
(a) Randomly initialize input weights and biases of hidden layer neurons;
(b) Calculate the new output matrix of the hidden layer H_d, d refers to the d th submodel of the current training process;
(c) The output weight of corresponding submodel is calculated: $\widehat{\beta}_d=H_d^+T$;
(d) Compute the classification output: $Y_d=H_d\widehat{\beta}_d$, the matrix after label transformation of output A_d, and store it into a new representation matrix $X_{d+1}=[X_d|A_d]$, so the updated dataset of input: $S_{d+1}=\{(x_i,t_i)\,|x_i \in R^{n+d}, t_i \in R^m, i=1,2,\ldots,N\}$.
(e) Set $d=d+1$.
until the testing error threshold between the two adjacent submodels is satisfied

Algorithm 1. DELM

TABLE 2 A brief introduction to the EEG dataset.

Condition	Set	Description
Healthy volunteer	A	EEG signals obtained from healthy volunteers with their eyes open.
	B	EEG signals obtained from healthy volunteers with their eyes closed.
Epileptic volunteer	C	EEG signals obtained from the hippocampal formation of the opposite hemisphere of the brain during seizure free intervals.
	D	EEG signals obtained from the epileptogenic zone during seizure free intervals.
	E	EEG signals obtained during the onset of epileptic seizure.

label T remains the same as the original one. Similarly, calculate the actual output Y_2. Y_2 is transformed into knowledge again,

TABLE 3 The detailed parameters used in our experiment.

Algorithm	Parameter description
SVM	$c \in \{2^{-4},2^{-3},2^{-2},2^{-1},1,2,2^2,2^3\}$
	$g \in \{2^{-5},2^{-4},2^{-3},2^{-2},2^{-1},1,2\}$
RBF	$spread \in \{2^{-1},2^0,2,2^2,2^3,2^4\}$
Adaboost	$NLearners \in \{5,10,15,20,\ldots,100,200,1000\}$
Bagging	$NLearners \in \{2,3,4,5\}$
DBN	$numepochs \in \{30,40\}$
	$batchsize \in \{20,40,80\}$
SAE	$numepochs \in \{20,30,40,50\}$
	$batchsize \in \{20,40,80\}$

and the significant information is stored in new input: $x_i = \left[x_{i1},x_{i2},\ldots,x_{in},x_{i(n+1)},x_{i(n+2)}\right]^T \in R^{n+2}$. Then, the third sub-model leverages knowledge extracted from the output of sub-model_1 and sub-model_2 to complete the classification of the model. Establish three modules or more on both training and testing sets and that can yield favorable results. The input for these modules comprises original features and appended features from all previous recognition prediction. So the augmented input for each module can be formed as:

$$\begin{aligned} X_1 &= X_1 \\ X_2 &= [X_1|A_1] \\ X_3 &= [X_2|A_2] \\ &\vdots \\ X_D &= [X_{D-1}|A_{D-1}] \end{aligned} \tag{11}$$

At each level, the predicted output of current sub-model is integrated into the input as learning experiences. In the next learning step, the new input after incorporation will be mapped into a new ELM feature space through random mapping in current sub-model to solve the least square problem. The new features, including A_1, A_2 and so on, contains discriminative information derived from lower modules, so it is helpful in forcing the manifold structure apart in original EEG input. In this course of knowledge augmentation, DELM is aimed at learning a more reasonable decision basis from raw data in classification tasks.

2.3. Specialty of DELM pattern classifier

We are motivated by the idea of deep learning and stacking generalization theory, and establish a hierarchical ELM-based stacked architecture. Each sub-model has the same supervised learning process as classic ELM and several ELMs are integrated into a deep network. ELM in each level is an elegant original model, which is respectively composed of input layer, hidden layer and output layer in our paper. Under the guidance of the corresponding expected labels, DELM can better pull each sample to its own class cluster, hence, samples have a tendency to approach their own field gradually after knowledge augmentation. In other words, it makes it easier for the samples belonging to some class

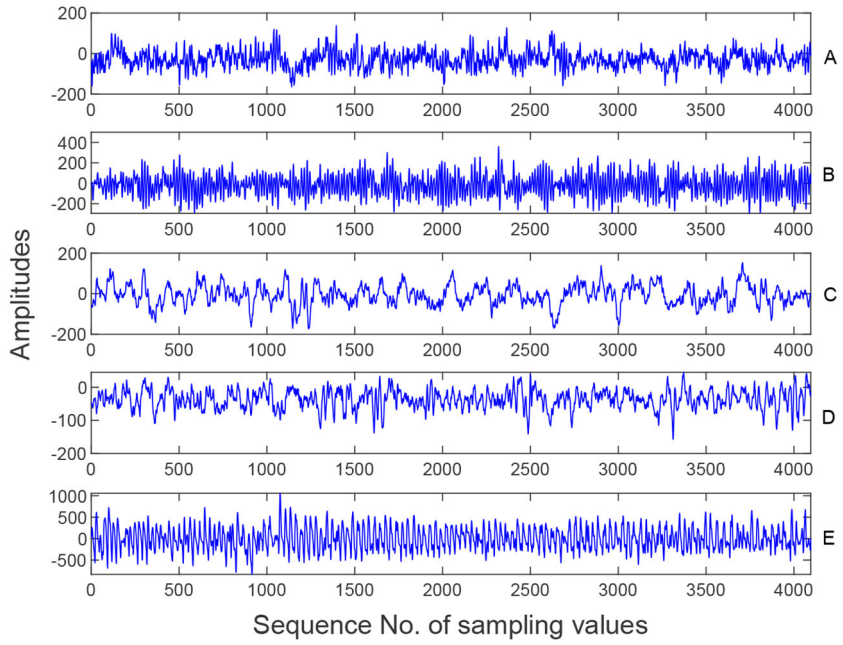

FIGURE 3
Samples from five EEG sets **(A–E)**.

to be identified as belonging to its true class by DELM pattern classifier. Accordingly, the output generated in previous submodel performs knowledge transformation first, and then it is regarded as a supplement to the input. DELM is targeted at achieving a richer form of representation from raw data, which enables the sequential propagation of knowledge in a forward way and provides a method to automatically discover valuable implied patterns. With the valuable information extracted from the instances, the whole model is directed to study the internal information of instances, and constantly approach the ideal output with stepwise learning.

Noise caused by electrode movement or others often appears in the practical EEG signal, resulting in poor recognition results. The proposed framework has the anti-noise capability of deep network in practice in contrast to the traditional ELM algorithm, which can stand against the noise to a certain extent. With stepwise transformation of input EEG epileptic information, the dimension of the input expands continuously, and the pollution in the original data is gradually reduced or eliminated. Stepwise knowledge is continuously strengthened, more reasonable features are generated, and the final classification accuracy of epileptic EEG signals is improved.

The entire network consists of several stacked independent ELM modules. The stacked approach is one of the most effective ensemble learning strategies. Our model trains several submodels in a serial way, and each submodel still preserve the output of the previous submodel for deep representation learning, which shares the same philosophy as stacked generalization (Wolpert, 1992; Wang et al., 2017; Hang et al., 2020).

Our model is aimed at reducing the loss of effective information in the original data and greatly economizing the time required for classification under the premise of ensuring certain accuracy. The information is extracted, grows in refinement and richness, and is accepted to be vital members of the knowledge community ultimately. The sub-model that organizes the higher layer has additional input features involving the classification output from all previous sub-models. DELM learns reasonable and effective features from a large number of complex raw data, and the newly generated features are absorbed by our deep network into its own knowledge, which can achieve satisfactory results in most cases when faced with practical application problems.

In the previous phase, multi submodels are adopted for knowledge augmentation and knowledge are automatically captured through feature expansion. In the latter phase, the original input and the generated knowledge in previous modules are used to accomplish the modeling and the classification tasks. The deep learning algorithm of the proposed DELM is summarized in Algorithm 1.

2.4. Time complexity analysis

In order to exhibit the time complexity of the proposed deep learning algorithm, we start with the classic ELM algorithm first. The time complexity of classic ELM algorithm mainly lies in the solution of Moore-Penrose generalized inverse of hidden output matrix. In terms of Equation 5, $O\left(N^2L\right)$ can be required to compute the H^TH. It requires $O\left(N^3\right)$ to calculate the inverse. So the time complexity in ELM becomes $O\left(N^3+N^2L+NnL+1\right)$. The proposed DELM introduces the concept of deep learning, which is composed of several building units. Obviously, the time complexity of the entire DELM can be indicated as $\mathrm{O}\left(\sum_{d=1}^{D}\left(N^3+N^2L+NnL+1\right)\right)$, where D is the final value of

TABLE 4 Average testing accuracy in our experiment.

	SVM	RBF	Adaboost	Bagging	DBN	SAE	Basic ELM	DELM (D = 3)	DELM
A/E	0.9277	0.8745	0.9317	**0.9443**	0.9279	0.9123	0.8866	0.9174	0.9307
	(0.0080)	(0.0064)	(0.0147)	(0.0099)	(0.1501)	(0.0095)	(0.0100)	(0.0051)	(0.0067)
B/E	0.9067	0.8678	0.8727	0.9020	0.9086	0.9039	0.8754	0.9091	**0.9180**
	(0.0065)	(0.0087)	(0.0082)	(0.0152)	(0.0083)	(0.0181)	(0.0154)	(0.0073)	(0.0091)
C/E	0.9135	0.8641	0.9007	0.9165	0.8978	0.9098	0.8764	0.9050	**0.9196**
	(0.0089)	(0.0087)	(0.0061)	(0.0076)	(0.0350)	(0.0125)	(0.0102)	(0.0124)	(0.0065)
D/E	0.8603	0.8311	0.8730	0.8887	0.8993	0.8545	0.8400	0.8737	**0.9137**
	(0.0083)	(0.0067)	(0.0115)	(0.0076)	(0.0219)	(0.0134)	(0.0093)	(0.0103)	(0.0096)
AB/E	0.9377	0.9028	0.9116	0.9305	0.9286	0.9345	0.9055	0.9326	**0.9415**
	(0.0057)	(0.0020)	(0.0059)	(0.0117)	(0.0271)	(0.0101)	(0.0065)	(0.0058)	(0.0070)
AC/E	0.9004	0.9023	0.9333	0.9341	0.9032	0.9388	0.9043	0.9301	**0.9395**
	(0.0091)	(0.0067)	(0.0076)	(0.0056)	(0.0778)	(0.0044)	(0.0057)	(0.0041)	(0.0050)
AD/E	0.8746	0.8832	0.9106	0.9249	**0.9354**	0.9042	0.8796	0.9078	0.9157
	(0.0086)	(0.0092)	(0.0099)	(0.0091)	(0.0126)	(0.0062)	(0.0077)	(0.0065)	(0.0073)
BC/E	0.8978	0.8972	0.9084	0.9201	0.9357	0.9102	0.9003	0.9269	**0.9367**
	(0.0105)	(0.0075)	(0.0081)	(0.0060)	(0.0099)	(0.0086)	(0.0094)	(0.0072)	(0.0074)
BD/E	**0.9220**	0.8830	0.8834	0.9001	0.9210	0.9002	0.8767	0.9050	0.9111
	(0.0056)	(0.0068)	(0.0078)	(0.0067)	(0.0089)	(0.0089)	(0.0099)	(0.0079)	(0.0076)
CD/E	**0.9312**	0.8788	0.8993	0.9151	0.9280	0.9033	0.8802	0.9085	0.9122
	(0.0052)	(0.0079)	(0.0053)	(0.0035)	(0.0089)	(0.0081)	(0.0098)	(0.0083)	(0.0056)
ABC/E	0.9390	0.9254	0.9263	0.9398	0.9347	0.9370	0.9260	0.9460	**0.9497**
	(0.0046)	(0.0052)	(0.0066)	(0.0046)	(0.0580)	(0.0055)	(0.0051)	(0.0048)	(0.0055)
ABD/E	0.9202	0.9076	0.9154	0.9284	**0.9556**	0.9334	0.9067	0.9277	0.9320
	(0.0063)	(0.0030)	(0.0064)	(0.0050)	(0.0058)	(0.0072)	(0.0073)	(0.0060)	(0.0058)
ACD/E	0.9243	0.9102	0.9228	0.9324	0.9269	0.9285	0.9098	0.9282	**0.9329**
	(0.0061)	(0.0034)	(0.0064)	(0.0052)	(0.0627)	(0.0060)	(0.0055)	(0.0071)	(0.0051)
BCD/E	0.9209	0.9085	0.9112	0.9176	**0.9536**	0.9424	0.9061	0.9277	0.9299
	(0.0057)	(0.0088)	(0.0052)	(0.0076)	(0.0038)	(0.0032)	(0.0058)	(0.0048)	(0.0056)
ABCD/E	0.9390	0.9212	0.9243	0.9357	0.9224	0.9418	0.9235	0.9396	**0.9442**
	(0.0028)	(0.0044)	(0.0089)	(0.0060)	(0.0066)	(0.0069)	(0.0073)	(0.0046)	(0.0035)
A/B/E	0.7406	**0.7519**	0.6392	0.6894	0.7225	0.6746	0.6919	0.7071	0.7142
	(0.0134)	(0.0158)	(0.0223)	(0.0111)	(0.0422)	(0.0172)	(0.0086)	(0.0120)	(0.0107)
A/C/E	**0.6975**	0.6665	0.6481	0.6771	0.6829	0.6717	0.6524	0.6750	0.6797
	(0.0123)	(0.0169)	(0.0262)	(0.0132)	(0.0387)	(0.0194)	(0.0084)	(0.0104)	(0.0128)
A/D/E	0.6530	0.6322	0.6457	0.6738	0.6329	0.6673	0.6436	0.6658	**0.6708**
	(0.0107)	(0.0133)	(0.0259)	(0.0114)	(0.0319)	(0.0191)	(0.0104)	(0.0099)	(0.0116)
B/C/E	0.7052	0.6275	0.6058	0.7193	0.6839	0.6812	0.7176	0.7350	**0.7371**
	(0.0124)	(0.0148)	(0.0192)	(0.0115)	(0.0421)	(0.0215)	(0.0141)	(0.0103)	(0.0166)
B/D/E	0.6641	0.5032	0.5838	0.7143	**0.7288**	0.6486	0.6717	0.6961	0.7002
	(0.0124)	(0.0210)	(0.0073)	(0.0134)	(0.0231)	(0.0168)	(0.0107)	(0.0142)	(0.0107)
C/D/E	0.6278	0.5787	0.6060	0.6262	0.6263	0.6045	0.6068	0.6273	**0.6306**
	(0.0152)	(0.0077)	(0.0086)	(0.0102)	(0.0075)	(0.0100)	(0.0147)	(0.0097)	(0.0134)
A/B/C/D/E	0.4954	0.3557	0.3994	0.4058	0.4883	0.4227	0.4585	0.4722	**0.5058**
	(0.0048)	(0.0098)	(0.0116)	(0.0126)	(0.0239)	(0.0184)	(0.0087)	(0.0102)	(0.0127)

The best results are marked in bold.

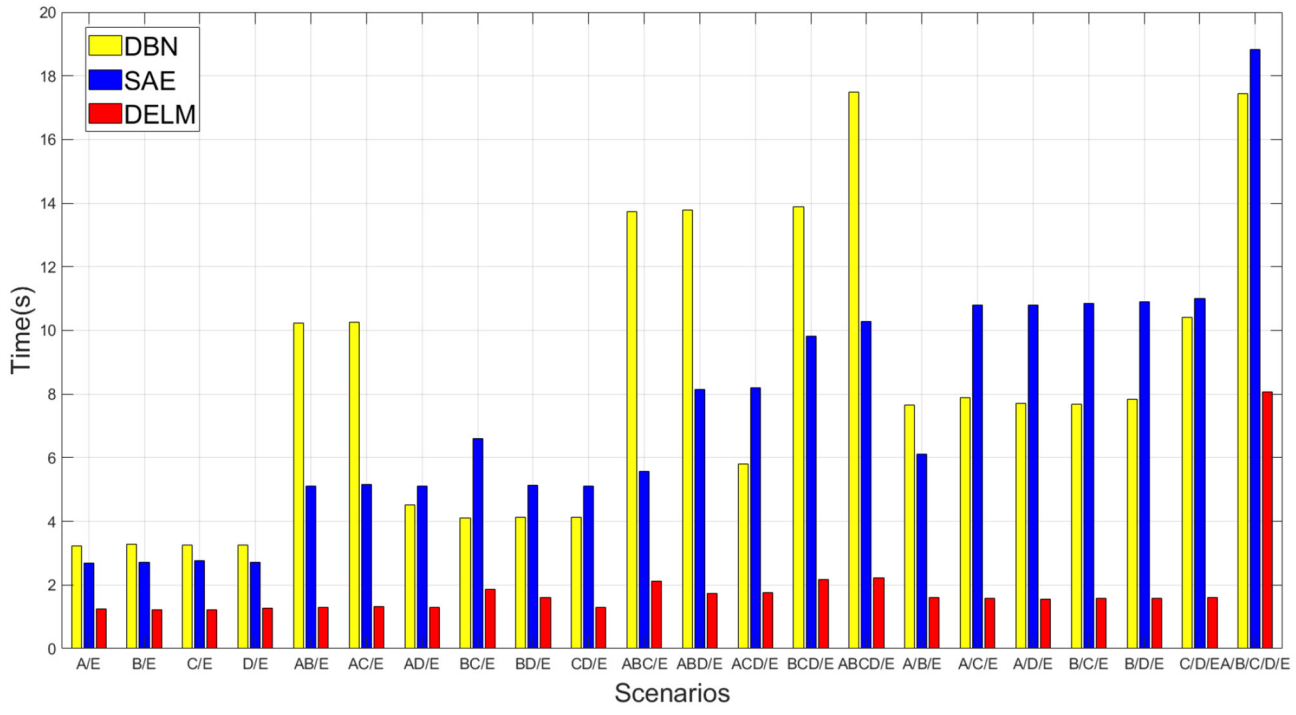

FIGURE 4
Average time consumed by deep networks in our experiment.

depth, L is the number of hidden layer neural network units and N is the number of instances.

3. Experiment studies

In this section, we will demonstrate the effectiveness of our proposed hierarchical model DELM by reporting the experiment result from Bonn dataset. In our experimental study, DELM is sequentially compared with some machine learning algorithms and popular deep learning networks such as DBN, and so on. The final performance evaluation is performed according to the result. In our experiment, all adopted methods were implemented using MATLAB 2019a on a personal computer with Intel Core i5-9400 2.90 GHz CPU and 8.0G RAM.

3.1. Epileptic EEG dataset

The EEG signals used in the paper are derived from Department of Epileptology, Bonn University, Germany. The dataset has been described in detail by Andrzejak et al. (2001). The EEG signals were collected under various conditions with five healthy volunteers and five epileptic patients. The details information of five groups are summarized in Table 2, in which each group contains 2,300 samples.

The dataset consists of five groups of data (A, B, C, D, and E) where each containing 100 single-channel EEG segments. EEG data were recorded using the same 128-channel amplifier system with a sampling rate of 173.6 Hz and a 12-bit resolution. Each EEG segment contained 4,096 sampling points and lasted 23.6 s. The five samples in Figure 3 come from Set A, B, C, D and E respectively, as shown below.

In our experiment, three kinds of EEG signals are employed, namely normal (A and B), interictal (C and D), and ictal (E), to evaluate the proposed epilepsy detection framework.

3.2. Data preparation and normalization

Firstly, the EEG signals are segmented into 178 sampling points by means of moving windows, among which there is no overlapping of sampling windows. Therefore, 23 epochs can be obtained from each segment. The remaining points in each segment are dismissed. Different features extracted from the original EEG signals have different scales after data segmentation, so it is necessary to use normalization processing to normalize all attribute features.

3.3. Experiment setup

In our experimental organization, the processed dataset is firstly randomly divided into two parts: training and testing set. In each scenario, we randomly selected 80% of the data as the training data, and the remaining 20% as the testing data. The experiment is repeated 20 times in various scenarios and then the average experimental results of some other schemes are also collected as contrast. In our experiment, SVM, RBF and some ensemble algorithms such as Adaboost are used. Meanwhile, experimental

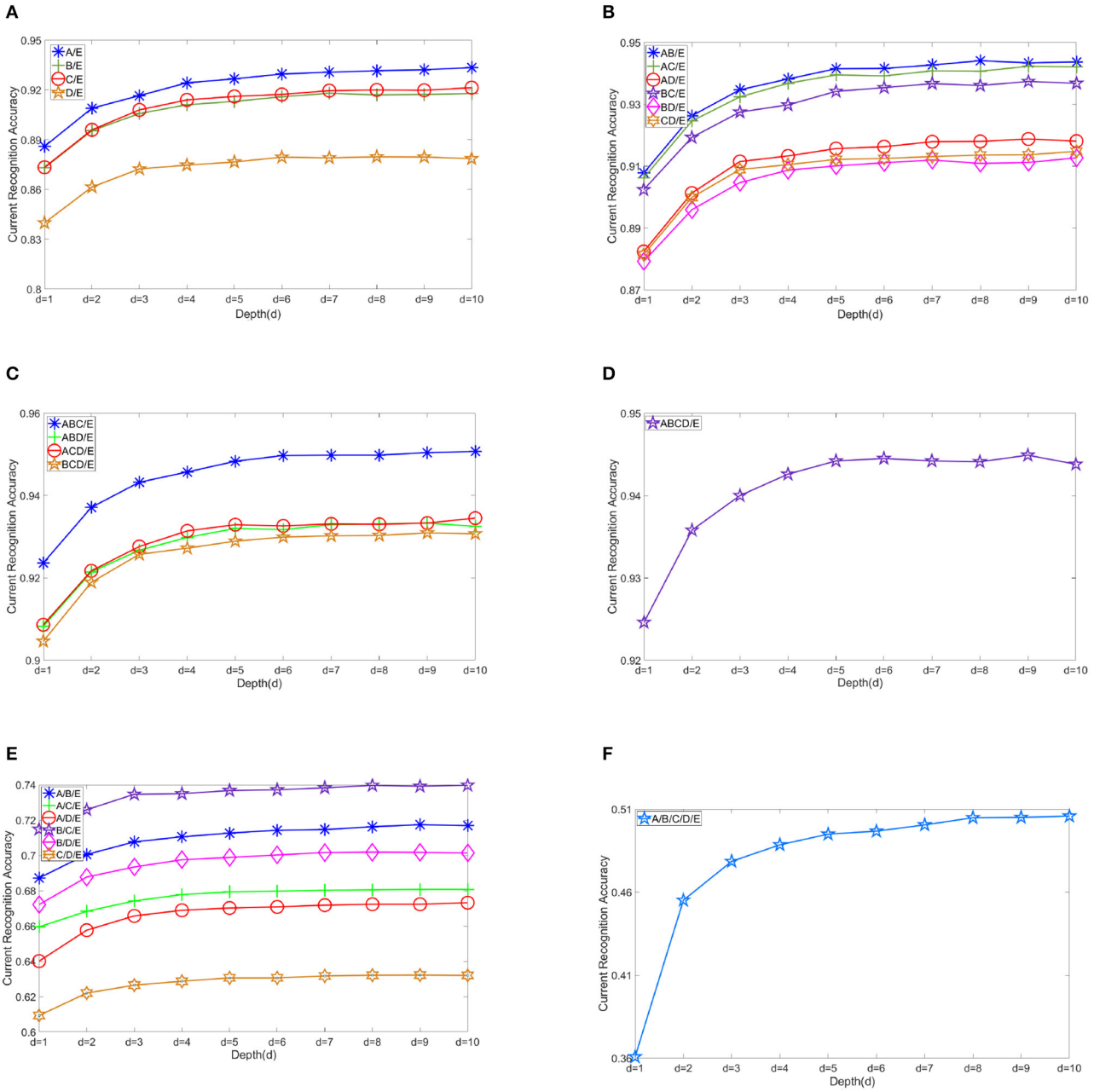

FIGURE 5
Changes in recognition accuracy along with stacked depth of modules in various scenarios. **(A)** Another individual group vs. ictal A/E, B/E, C/E, and D/E. **(B)** Two other groups vs. ictal AB/E, AC/E, AD/E, BC/E, BD/E, and CD/E. **(C)** Three other groups vs. ictal ABC/E, ABD/E, ACD/E, and BCD/E. **(D)** All other groups vs. ictal ABCD/E. **(E)** A/B/E, A/C/E, A/D/E, B/C/E, B/D/E, and C/D/E. **(F)** A/B/C/D/E.

results of well-known deep networks, such as DBN and SAE, are also adopted as comparison in our experiment in order to demonstrate the superiority of the proposed DELM.

To reasonably evaluate our method, the performance metrics adopted here are *Accuracy* and $F-measure$, which are defined as follows:

$$Accuracy=\frac{TP+TN}{TP+TN+FP+FN}; \tag{12}$$

$$F-measure=\frac{2\times TP}{2\times TP+FN+FP}; \tag{13}$$

where TP (true positive) represents the number of segments detected as seizure correctly, FN (false negative) represents the number of segments detected as non-seizure incorrectly, TN (true negative) represents the number of segments detected as non-seizure correctly, and FP (false positive) is the number of segments detected as seizure incorrectly.

In terms of recognition accuracy, our DELM model can achieve great classification accuracy comparable to that of deep learning schemes. Running time is one of the key evaluation indexes which can perform excellent performance in DELM. The classic ELM is qualified for real-time recognition

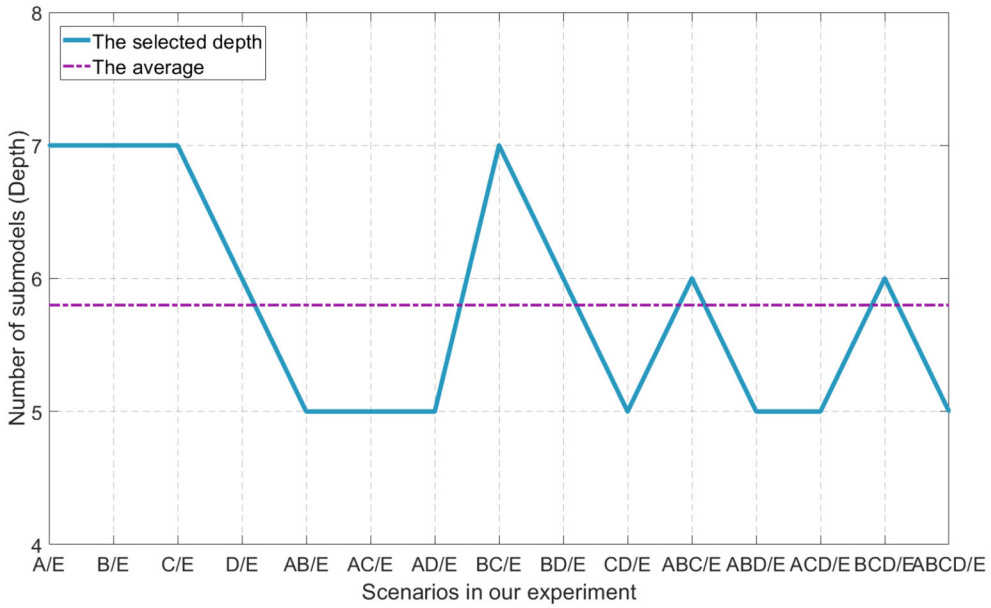

FIGURE 6
Different parameters of depth used in our experiment.

TABLE 5 *F − measure* scores of the comaparative methods.

Method	SVM	RBFN	Adaboost	Bagging	DBN	SAE	DELM
A/E	0.9225	0.8560	0.9287	**0.9431**	0.8784	0.9050	0.9262
B/E	0.8954	0.8449	0.8637	0.9071	0.9102	0.8943	**0.9103**
C/E	0.9048	0.8450	0.8961	**0.9215**	0.9071	0.9016	0.9122
D/E	0.8481	0.8120	0.8690	0.8953	0.8985	0.8388	**0.9056**
AB/E	0.8975	0.8290	0.8544	0.9024	0.8811	0.8916	**0.9027**
AC/E	0.8200	0.8271	0.8923	0.8998	0.8091	0.8997	**0.9000**
AD/E	0.7727	0.8001	0.8550	0.8961	**0.9037**	0.8407	0.8597
BC/E	0.8177	0.8240	0.8480	0.8886	0.8916	0.8443	**0.8939**
BD/E	0.8716	0.7986	0.8060	0.8612	**0.8799**	0.8356	0.8525
CD/E	**0.8892**	0.7880	0.8334	0.8830	0.8886	0.8366	0.8536
ABC/E	0.8594	0.8216	0.8384	0.8875	0.8287	0.8584	**0.8888**
ABD/E	0.8172	0.7830	0.8142	0.8667	**0.9112**	0.8524	0.8473
ACD/E	0.8274	0.7897	0.8333	**0.8769**	0.8048	0.8415	0.8511
BCD/E	0.8203	0.7872	0.8016	0.8486	**0.9054**	0.8785	0.8445
ABCD/E	0.8251	0.7695	0.7884	0.8524	**0.9120**	0.8412	0.8447
A/B/E	0.7268	**0.7573**	0.5920	0.6809	0.6853	0.6677	0.7151
A/C/E	0.6774	0.6752	0.5975	0.6602	0.6366	0.6429	**0.6836**
A/D/E	0.5872	0.6414	0.6083	**0.6578**	0.6266	0.6229	0.6476
B/C/E	0.6924	0.6237	0.5518	0.7037	0.6421	0.6705	**0.7405**
B/D/E	0.6677	0.5121	0.5375	0.7002	**0.7124**	0.6257	0.7074
C/D/E	0.5800	0.5874	0.5990	0.6034	0.5484	0.5873	**0.6274**
A/B/C/D/E	0.4709	0.3163	0.3411	0.4013	0.4494	0.3849	**0.5047**

The best results are marked in bold.

requirements and so does our hierarchical model. Extremely fast recognition ability can still be exhibited in DELM, meanwhile traditional deep networks are too far behind to catch with.

Among all the competing schemes, SVM, RBF, and ensemble algorithms were implemented by toolbox in MATLAB. And traditional deep learning algorithms are implemented by MATLAB which is encapsulated in the DeepLearning Toolbox. The parameters settings are summarized in Table 3.

In each sub-model, all input weights and hidden biases are set to the pseudo random values drawn from the uniform distribution on the interval $(-1, 1)$ and $(0, 1)$. Such scheme is in accordance with the standard methodology of ELM, which simplifies the learning process. In each ELM, the hidden layer adopts the same number of hidden nodes and the same activation function. Sigmoid function is chosen as the activation function g(.) in each submodel. The number of hidden units is usually scenario-specific and determined by experience or by continuous attempts. We need to find a point as balanced as possible between the number of hidden units and time. As a result, DELM can acquire a relatively mature knowledge system, which can well meet the accuracy requirements of classification. The optimal amount of hidden units in all sub-models is uniformly set to a fixed value 500. Considering the difficulty of recognition in five class problem, the number of hidden units is set to 800. More ELMs can be cascaded to modules, if desired, for the purpose of adequate knowledge. So we dynamically determine the depth of network. The stacking process will be aborted if the difference between the current and upper level in the experiment is <0.1. It is clear that DELM simply involves a few parameters, which greatly reduces the cost of parameter adjustment. To evaluate DELM comprehensively and precisely, classification tasks in various scenarios are designed here.

3.4. Epileptic EEG signal recognition

3.4.1. Two class problem

Classification of four combinations between A and E, B and E, C and E, and D and E are considered to distinguish normal from seizure. Epileptic seizure segments E was selected to compare with one of the remaining EEG sets from the dataset for classification. Then select two or more sets in the database and conduct trials again. The combinations are as follows: AB and E, AC and E, AD and E, BC and E, BD and E, CD and E, ABC and E, ABD and E, ACD and E, BCD and E, and ABCD and E.

3.4.2. Three class problem

In three class problems, the selected combinations are: A, B, E and A, C, E and A, D, E and B, C, E and B, D, E and C, D, E.

3.4.3. Five class problem

In five class problem, each group is regarded as an independent class for testing.

3.5. Experimental results and statistical analysis

Table 4 shows us the accuracy in the sense of both the mean and standard deviation in DELM and deep networks. The results are also presented when the depth d of DELM is 3. But the result in the case is still a certain gap from the ideal, and more ELMs are required to assure higher accuracy. In terms of accuracy, DELM can compete with conventional intelligent methods. It can be noted in the results that the proposed method has certain advantages over traditional methods and is generally comparable to traditional deep networks. We attribute this advancement in recognition performance to the embedded knowledge. The accuracy is greatly improved by extending the vertical network layers and the model gradually acquires a better command of the implication of knowledge. Table 4 also report the accuracy of common machine learning algorithms on our datasets.

Since DELM can inherit advantages of ELM, extremely fast learning speed is one of its remarkable characteristics. In the aspect of computational efficiency, the slight increase of learning time (extremely short seconds) in DELM compared to the original ELM is inappreciable, especially when considering the added improvement in classification accuracy. DELM is about sacrificing a little time and tolerating a cascade of multi modules in exchange for final performance, so we just need to draw comparison between our ELM-based deep network and traditional deep network. The experimental results show that the time needed in DELM is much less than that of the traditional deep networks after the accuracy is guaranteed to meet the requirements. In some designed scenarios, the speed of DELM in training and testing is approximately a dozen times faster than traditional deep networks.

Figure 4 reports time efficiency during learning process, and the result is average learning time of models. As observed from both Table 4 and Figure 4, the accuracy performance is almost similar in DELM and traditional deep methods. However, the time consumed by the proposed classifier is the least. Taking into account both accuracy and computational effort simultaneously, the proposed DELM demonstrates tremendous potential in EEG classification and may be a competitive choice.

Figure 5 shows the changes in recognition accuracy along with current stacked depth of modules in different EEG classification scenarios. There is no doubt that the EEG classification accuracy increases with the addition of sub-models. The number of submodels we use is namely the depth of DELM. Depth is denoted by d, and the result shows the classification accuracy from $d = 1$ to $d = 10$. It is shown that the improvement in accuracy can be relatively evident in the first three levels. Modest improvement can still be obtained in the subsequent expansion of ELMs, but DELM will gradually lose competitiveness in real-time tasks. Without rapid classification performance, what we think of as our inherent excellence in our model, several serial ELM network modules in our model, would make no sense and our previous efforts would not worth it. By starting from $d = 1$, ordinary extreme learning machine, excellent features can be well-preserved and classification effect is gradually improved. Performance augmentation can be seen in these figures.

The depth is the key aspect to knowledge augmentation in DELM. In our experimental organization, different depths are adopted in binary class problems, while $D = 6$ is uniformly adopted in three and five class problems in order to obtain better classification accuracy. Setting a threshold for DELM is because excessive accumulation of layers is not productive any more. The average depth of binary class problems is $d_{AVG} = 5.8$. The selection of depth parameters are shown in Figure 6.

Table 5 presents $F - measure$ scores obtained by traditional deep learning methods in different scenarios. From the perspective of $F - measure$ scores, DELM outperforms several deep networks used for comparison. In other scenarios, DELM is slightly worse than deep networks, but it still performs well and is comparable to deep networks.

DELM enjoys extremely fast speed of ELM while providing deeper representation of original signals. Experiments show that our algorithm consistently outperforms several existing state-of-art schemes in terms of accuracy and execution time.

4. Conclusion

A novel deep extreme learning machine DELM is proposed for the recognition of EEG epileptic signals in our paper. DELM stepwisely transmits the response to the next submodel through fusion of knowledge derived from previous sub-models. Such a process is beneficial to mine the valuable information of the original EEG data, so as to better accomplish the subsequent EEG recognition tasks. The proposed model operates in a forward way with an increment form to strive for an increasingly efficient performance and its computation speed is considerably fast. ELM is introduced as the basic building block, making the whole learning process flexible and effective. As available knowledge, the classification results of the previous multi-module can enhance the classification performance of the subsequent modules. Our experimental results demonstrate that the proposed method is a promising candidate for epileptic EEG-based recognition. Compared with traditional methods, the proposed DELM is motivated by deep learning and stack generalization theory, which can obtain excellent classification results and outperform the traditional methods. According to stacking generalization theory, the output of the next sub-model plus the knowledge of the previous sub-model in DELM can indeed open the manifold structure of the input space, which resulting an improved performance. Moreover, knowledge augmentation can effectively extract the implied knowledge in each sub-model and obtain increasing performance.

However, it is still not clear the reason for the improvement of knowledge augmentation throughout the training process. In the future work, we will spare no efforts to theoretically demonstrate how the prediction output in each ELM module can be helpful with EEG epileptic signal recognition.

Data availability statement

The datasets presented in this study can be found in online repositories. The names of the repository/repositories and accession number(s) can be found at: http://epileptologie-bonn.de/cms/upload/workgroup/lehnertz/eegdata.html.

Author contributions

XZ and JZ conceived and designed the theoretical framework of this paper. All authors participated the experimentation and analysis process and drafted the manuscript. All authors contributed to the article and approved the submitted version.

Funding

This work was supported by the National Natural Science Foundation of China under Grant: 62101645, Zhejiang Provincial Natural Science Foundation of China under Grant: LQ22F020024, Zhejiang Medicine and Health Science and Technology Project: 2020RC118, and Huzhou Municipal Science and Technology Bureau Public Welfare Application Research Project: 2019GZ40.

Conflict of interest

The authors declare that the research was conducted in the absence of any commercial or financial relationships that could be construed as a potential conflict of interest.

Publisher's note

All claims expressed in this article are solely those of the authors and do not necessarily represent those of their affiliated organizations, or those of the publisher, the editors and the reviewers. Any product that may be evaluated in this article, or claim that may be made by its manufacturer, is not guaranteed or endorsed by the publisher.

References

Acharya, U. R., Oh, S. L., Hagiwara, Y., Tan, J. H., and Adeli, H. (2018). Deep convolutional neural network for the automated detection and diagnosis of seizure using EEG signals. *Comput. Biol. Med.* 100, 270–278. doi: 10.1016/j.compbiomed.2017.09.017

Ahmadlou, M., and Adeli, H. (2011). Functional community analysis of brain: a new approach for EEG-based investigation of the brain pathology. *Neuroimage* 58, 401–408. doi: 10.1016/j.neuroimage.2011.04.070

Andrzejak, R. G., Lehnertz, K., Mormann, F., Rieke, C., David, P., and Elger, C. E. (2001). Indications of non-linear deterministic and finite-dimensional structures in time series of brain electrical activity: dependence on recording region and brain state. *Phys. Rev. E* 64, e061907. doi: 10.1103/PhysRevE.64.061907

Ayman, U., Zia, M. S., Okon, O. D., Rehman, N.-u., Meraj, T., Ragab, A. E., et al. (2023). Epileptic patient activity recognition system using extreme learning machine method. *Biomedicines* 11, 30816. doi: 10.3390/biomedicines11030816

Bengio, Y. (2009). *Learning Deep Architectures for AI*. Delft: Now Publishers Inc.

Bengio, Y., Lamblin, P., Popovici, D., Larochelle, H., et al. (2007). Greedy layer-wise training of deep networks. *Adv. Neural Inform. Process. Syst.* 19, 153. doi: 10.7551/mitpress/7503.003.0024

Betthauser, J. L., Hunt, C. L., Osborn, L. E., Masters, M. R., Lévay, G., Kaliki, R. R., et al. (2017). Limb position tolerant pattern recognition for myoelectric prosthesis control with adaptive sparse representations from extreme learning. *IEEE Trans. Biomed. Eng.* 65, 770–778. doi: 10.1109/TBME.2017.2719400

Bhattacharyya, A., and Pachori, R. B. (2017). A multivariate approach for patient-specific EEG seizure detection using empirical wavelet transform. *IEEE Trans. Biomed. Eng.* 64, 2003–2015. doi: 10.1109/TBME.2017.2650259

Choi, G., Park, C., Kim, J., Cho, K., Kim, T.-J., Bae, H., et al. (2019). "A novel multi-scale 3D CNN with deep neural network for epileptic seizure detection," in *2019 IEEE International Conference on Consumer Electronics (ICCE)* (Las Vegas, NV: IEEE), 1–2.

Deng, Y., Ren, Z., Kong, Y., Bao, F., and Dai, Q. (2016). A hierarchical fused fuzzy deep neural network for data classification. *IEEE Trans. Fuzzy Syst.* 25, 1006–1012. doi: 10.1109/TFUZZ.2016.2574915

Duan, L., Bao, M., Miao, J., Xu, Y., and Chen, J. (2016). Classification based on multilayer extreme learning machine for motor imagery task from EEG signals. *Proc. Comput. Sci.* 88, 176–184. doi: 10.1016/j.procs.2016.07.422

Ghosh-Dastidar, S., Adeli, H., and Dadmehr, N. (2007). Mixed-band wavelet-chaos-neural network methodology for epilepsy and epileptic seizure detection. *IEEE Trans. Biomed. Eng.* 54, 1545–1551. doi: 10.1109/TBME.2007.891945

Güler, I., and Übeyli, E. D. (2005). Adaptive neuro-fuzzy inference system for classification of EEG signals using wavelet coefficients. *J. Neurosci. Methods* 148, 113–121. doi: 10.1016/j.jneumeth.2005.04.013

Hang, W., Feng, W., Liang, S., Wang, Q., Liu, X., and Choi, K.-S. (2020). Deep stacked support matrix machine based representation learning for motor imagery EEG classification. *Comput. Methods Progr. Biomed.* 193, 105466. doi: 10.1016/j.cmpb.2020.105466

Hinton, G. E., Osindero, S., and Teh, Y.-W. (2006). A fast learning algorithm for deep belief nets. *Neural Comput.* 18, 1527–1554. doi: 10.1162/neco.2006.18.7.1527

Hinton, G. E., and Salakhutdinov, R. R. (2006). Reducing the dimensionality of data with neural networks. *Science* 313, 504–507. doi: 10.1126/science.1127647

Huang, G., Kasun, L., Zhou, H., and Vong, C. (2013). Representational learning with extreme learning machine for big data. *IEEE Intell. Syst.* 28, 31–34. doi: 10.1109/MIS.2013.140

Huang, G.-B., Wang, D. H., and Lan, Y. (2011a). Extreme learning machines: a survey. *Int. J. Machine Learn. Cybernet.* 2, 107–122. doi: 10.1007/s13042-011-0019-y

Huang, G.-B., Zhou, H., Ding, X., and Zhang, R. (2011b). Extreme learning machine for regression and multiclass classification. *IEEE Trans. Syst. Man Cybernet. B* 42, 513–529. doi: 10.1109/TSMCB.2011.2168604

Huang, G.-B., Zhu, Q.-Y., and Siew, C.-K. (2004). "Extreme learning machine: a new learning scheme of feedforward neural networks," in *2004 IEEE International Joint Conference on Neural Networks (IEEE Cat. No. 04CH37541), Vol. 2* (Budapest: IEEE), 985–990.

Huang, G.-B., Zhu, Q.-Y., and Siew, C.-K. (2006). Extreme learning machine: theory and applications. *Neurocomputing* 70, 489–501. doi: 10.1016/j.neucom.2005.12.126

Iasemidis, L. D., Shiau, D.-S., Chaovalitwongse, W., Sackellares, J. C., Pardalos, P. M., Principe, J. C., et al. (2003). Adaptive epileptic seizure prediction system. *IEEE Trans. Biomed. Eng.* 50, 616–627. doi: 10.1109/TBME.2003.810689

Khan, H., Marcuse, L., Fields, M., Swann, K., and Yener, B. (2017). Focal onset seizure prediction using convolutional networks. *IEEE Trans. Biomed. Eng.* 65, 2109–2118. doi: 10.1109/TBME.2017.2785401

Kumar, S. P., Sriraam, N., Benakop, P., and Jinaga, B. (2010). Entropies based detection of epileptic seizures with artificial neural network classifiers. *Expert Syst. Appl.* 37, 3284–3291. doi: 10.1016/j.eswa.2009.09.051

Kumar, Y., Dewal, M., and Anand, R. (2014). Epileptic seizure detection using DWT based fuzzy approximate entropy and support vector machine. *Neurocomputing* 133, 271–279. doi: 10.1016/j.neucom.2013.11.009

Liang, N.-Y., Huang, G.-B., Saratchandran, P., and Sundararajan, N. (2006a). A fast and accurate online sequential learning algorithm for feedforward networks. *IEEE Trans. Neural Netw.* 17, 1411–1423. doi: 10.1109/TNN.2006.880583

Liang, N.-Y., Saratchandran, P., Huang, G.-B., and Sundararajan, N. (2006b). Classification of mental tasks from EEG signals using extreme learning machine. *Int. J. Neural Syst.* 16, 29–38. doi: 10.1142/S0129065706000482

McIntosh, J. R., Yao, J., Hong, L., Faller, J., and Sajda, P. (2020). Ballistocardiogram artifact reduction in simultaneous EEG-FMRI using deep learning. *IEEE Trans. Biomed. Eng.* 68, 78–89. doi: 10.1109/TBME.2020.3004548

Nicolaou, N., and Georgiou, J. (2012). Detection of epileptic electroencephalogram based on permutation entropy and support vector machines. *Expert Syst. Appl.* 39, 202–209. doi: 10.1016/j.eswa.2011.07.008

Panda, R., Khobragade, P., Jambhule, P., Jengthe, S., Pal, P., and Gandhi, T. (2010). "Classification of EEG signal using wavelet transform and support vector machine for epileptic seizure diction," in *2010 International Conference on Systems in Medicine and Biology* (Kharagpur: IEEE), 405–408.

Plis, S. M., Hjelm, D. R., Salakhutdinov, R., Allen, E. A., Bockholt, H. J., Long, J. D., et al. (2014). Deep learning for neuroimaging: a validation study. *Front. Neurosci.* 8, 229. doi: 10.3389/fnins.2014.00229

Sanei, S., and Chambers, J. A. (2013). *EEG Signal Processing*. Hoboken, NJ: John Wiley & Sons.

Song, Y., and Zhang, J. (2013). Automatic recognition of epileptic EEG patterns via extreme learning machine and multiresolution feature extraction. *Expert Syst. Appl.* 40, 5477–5489. doi: 10.1016/j.eswa.2013.04.025

Subasi, A., and Ercelebi, E. (2005). Classification of EEG signals using neural network and logistic regression. *Comput. Methods Progr. Biomed.* 78, 87–99. doi: 10.1016/j.cmpb.2004.10.009

Tang, J., Deng, C., and Huang, G.-B. (2015). Extreme learning machine for multilayer perceptron. *IEEE Trans. Neural Netw. Learn. Syst.* 27, 809–821. doi: 10.1109/TNNLS.2015.2424995

Tang, J., Deng, C., Huang, G.-B., and Hou, J. (2014). "A fast learning algorithm for multi-layer extreme learning machine," in *2014 IEEE International Conference on Image Processing (ICIP)* (Paris: IEEE), 175–178.

Vincent, P., Larochelle, H., Lajoie, I., Bengio, Y., Manzagol, P.-A., and Bottou, L. (2010). Stacked denoising autoencoders: learning useful representations in a deep network with a local denoising criterion. *J. Machine Learn. Res.* 11, 3371–3408. doi: 10.1016/j.mechatronics.2010.09.004

Wang, D., Ren, D., Li, K., Feng, Y., Ma, D., Yan, X., et al. (2018). Epileptic seizure detection in long-term EEG recordings by using wavelet-based directed transfer function. *IEEE Trans. Biomed. Eng.* 65, 2591–2599. doi: 10.1109/TBME.2018.2809798

Wang, G., Zhang, G., Choi, K.-S., and Lu, J. (2017). Deep additive least squares support vector machines for classification with model transfer. *IEEE Trans. Syst. Man Cybernet.* 49, 1527–1540. doi: 10.1109/TSMC.2017.2759090

Wolpert, D. H. (1992). Stacked generalization. *Neural Netw.* 5, 241–259.

Xu, J., Xiang, L., Liu, Q., Gilmore, H., Wu, J., Tang, J., et al. (2015). Stacked sparse autoencoder (SSAE) for nuclei detection on breast cancer histopathology images. *IEEE Trans. Med. Imag.* 35, 119–130. doi: 10.1109/TMI.2015.2458702

Yu, W., Zhuang, F., He, Q., and Shi, Z. (2015). Learning deep representations via extreme learning machines. *Neurocomputing* 149, 308–315. doi: 10.1016/j.neucom.2014.03.077

Yuan, Q., Zhou, W., Li, S., and Cai, D. (2011). Epileptic EEG classification based on extreme learning machine and nonlinear features. *Epilepsy Res.* 96, 29–38. doi: 10.1016/j.eplepsyres.2011.04.013

Zhou, P.-Y., and Chan, K. C. (2016). Fuzzy feature extraction for multichannel EEG classification. *IEEE Trans. Cogn. Dev. Syst.* 10, 267–279. doi: 10.1109/TCDS.2016.2632130

Zhu, W., Miao, J., Qing, L., and Huang, G.-B. (2015). "Hierarchical extreme learning machine for unsupervised representation learning," in *2015 International Joint Conference on Neural Networks (ijcnn)* (Killarney: IEEE), 1–8.

frontiers | Frontiers in Neuroinformatics

TYPE Original Research
PUBLISHED 24 August 2023
DOI 10.3389/fninf.2023.1185723

OPEN ACCESS

EDITED BY
Peter A. Tass,
Stanford University, United States

REVIEWED BY
Sabato Santaniello,
University of Connecticut, United States
Justus Alfred Kromer,
Stanford University, United States
Yasmine Kehnemouyi,
Stanford University, United States,
in collaboration with reviewer JK

*CORRESPONDENCE
Jing Wang
✉ wang3444@umn.edu

RECEIVED 13 March 2023
ACCEPTED 01 August 2023
PUBLISHED 24 August 2023

CITATION
Bosley KM, Luo Z, Amoozegar S, Acedillo K, Nakajima K, Johnson LA, Vitek JL and Wang J (2023) Effect of subthalamic coordinated reset deep brain stimulation on Parkinsonian gait. *Front. Neuroinform.* 17:1185723. doi: 10.3389/fninf.2023.1185723

Effect of subthalamic coordinated reset deep brain stimulation on Parkinsonian gait

Kai M. Bosley[1], Ziling Luo[1], Sana Amoozegar[1], Kit Acedillo[1], Kanon Nakajima[2], Luke A. Johnson[1], Jerrold L. Vitek[1] and Jing Wang[1]*

[1]Department of Neurology, University of Minnesota, Minneapolis, MN, United States, [2]Neuroscience Program, Macalester College, Saint Paul, MN, United States

Introduction: Coordinated Reset Deep Brain Stimulation (CR DBS) is a novel DBS approach for treating Parkinson's disease (PD) that uses lower levels of burst stimulation through multiple contacts of the DBS lead. Though CR DBS has been demonstrated to have sustained therapeutic effects on rigidity, tremor, bradykinesia, and akinesia following cessation of stimulation, i.e., carryover effect, its effect on Parkinsonian gait has not been well studied. Impaired gait is a disabling symptom of PD, often associated with a higher risk of falling and a reduced quality of life. The goal of this study was to explore the carryover effect of subthalamic CR DBS on Parkinsonian gait.

Methods: Three non-human primates (NHPs) were rendered Parkinsonian and implanted with a DBS lead in the subthalamic nucleus (STN). For each animal, STN CR DBS was delivered for several hours per day across five consecutive days. A clinical rating scale modified for NHP use (mUPDRS) was administered every morning to monitor the carryover effect of CR DBS on rigidity, tremor, akinesia, and bradykinesia. Gait was assessed quantitatively before and after STN CR DBS. The stride length and swing speed were calculated and compared to the baseline, pre-stimulation condition.

Results: In all three animals, carryover improvements in rigidity, bradykinesia, and akinesia were observed after CR DBS. Increased swing speed was observed in all the animals; however, improvement in stride length was only observed in NHP B2. In addition, STN CR DBS using two different burst frequencies was evaluated in NHP B2, and differential effects on the mUPDRS score and gait were observed.

Discussion: Although preliminary, our results indicate that STN CR DBS can improve Parkinsonian gait together with other motor signs when stimulation parameters are properly selected. This study further supports the continued development of CR DBS as a novel therapy for PD and highlights the importance of parameter selection in its clinical application.

KEYWORDS

Parkinson's disease, subthalamic nucleus, coordinated reset, gait, non-human primate

Introduction

Parkinson's disease (PD) is a progressive neurodegenerative disorder characterized by tremors, akinesia, bradykinesia, rigidity, and impairment in gait and posture. Deep brain stimulation (DBS) is an effective treatment for advanced PD; however, it has been associated with side effects likely caused by the current spreading into unintended brain regions (Saint-Cyr et al., 2000; Deuschl et al., 2006; van Nuenen et al., 2008; Odekerken et al., 2013). Coordinated Reset DBS (CR DBS) is an innovative approach to DBS that uses lower levels of burst stimulation over multiple contacts of the DBS lead and

was designed to desynchronize abnormal neuronal population synchrony (Tass, 2003). It has been demonstrated in preclinical and clinical studies that CR DBS in the subthalamic nucleus (STN) can induce therapeutic improvements on rigidity, tremor, akinesia, and bradykinesia that can be sustained even after stimulation cessation, i.e., carryover effect (Tass et al., 2012; Adamchic et al., 2014; Wang et al., 2016). However, the impact of CR DBS on Parkinsonian gait has not been explored. Gait impairment is a profoundly disabling symptom of PD, often associated with higher risks of falling and reduced quality of life (Gray and Hildebrand, 2000; Kelly et al., 2012). Gait disturbances in PD include shuffling gait, decreased amplitude of motion at the joints, reduced movement velocity, and shortened stride length (Svehlík et al., 2009). It has been demonstrated that Parkinsonian gait impairment is also associated with abnormal neuronal synchronization such as exaggerated beta oscillatory activity in the STN (Toledo et al., 2014; Anidi et al., 2018; Chen et al., 2019; Fim Neto et al., 2022), providing a strong rationale for applying CR DBS in order to desynchronize the neuronal activity associated with the impaired gait. We hypothesized that STN CR DBS will also produce carryover improvement on Parkinsonian gait in addition to rigidity, akinesia, and bradykinesia. In this study, we tested this hypothesis by investigating the carryover effect of STN CR DBS on a modified version of the Unified Parkinson's Disease Rating Scale (mUPDRS), as well as the stride length and swing speed during gait in the Parkinsonian non-human primate (NHP) model of PD. Stride length and swing speed (similar to gait speed) are two standard gait measures (Doyle et al., 2022) that have been used in numerous clinical studies for differentiating PD patients from healthy controls or evaluating the effect of therapeutic treatments on gait (Luo et al., 2015; di Biase et al., 2020; De Oliveira et al., 2021; Gandolfi et al., 2023; Johansson et al., 2023; Matsuno et al., 2023). In addition, we examined the relative effect of STN CR DBS using two different burst frequencies on Parkinsonian gait. This was motivated by computational modeling studies (Lysyansky et al., 2013; Manos and Zeitler, 2018; Manos et al., 2018) and our previous NHP study (Wang et al., 2022) showing that varying the CR DBS parameter settings, e.g., intensity, frequency, dosage, and shuffling time, can significantly alter the effect of CR DBS. A particular modeling study showed that changing the burst frequency of the stimulation pattern greatly impacted the desynchronizing effect of CR stimulation (Manos and Zeitler, 2018). Taken altogether, our results suggest that STN CR DBS may produce carryover improvement in Parkinsonian gait when the stimulation parameters are properly selected.

Materials and methods

Animal care complied with the National Institutes of Health Guide for the Care and Use of Laboratory Animals, and all procedures were performed under a protocol approved by the Institutional Animal Care and Use Committee of the University of Minnesota.

Animals and surgical procedures

Three adult female rhesus monkeys (Macaca mulatta; Animal P, 6 kg; B1, 10.5 kg; B2, 8.2 kg) were used. Each animal was implanted with a head restraint system and a scaled-down version of the DBS lead (NuMed Inc.) targeting the STN (0.63 mm diameter, 0.5 mm contact height, and 0.5 mm space between contacts; total contact number: 4 for P, 8 for B1&B2) using techniques established in the laboratory (Wang et al., 2016, 2022). In brief, pre-operative high-resolution CT and MRI images were merged to identify the STN and make the surgical plan. A chamber and head restraint post were implanted during an aseptic surgery following which microelectrode recording and stimulation techniques were used to map the sensorimotor region and the borders of the STN. A final recording track was made to determine the lead placement depth after which a DBS lead was implanted. The cable of the DBS lead was then routed to a separate dry chamber which allows connection to a programmable pulse generator (Animal P: Abbott; Animal B1&B2: Boston Scientific) for the delivery of CR DBS.

Animals were rendered Parkinsonian through intracarotid and intramuscular injections of the neurotoxin 1-methyl-4-phenyl-1,2,3,6-tetrahydropyridine (MPTP). The severity of Parkinsonian motor signs on the side of the body contralateral to the site of DBS implantation was assessed using a version of the Unified Parkinson's Disease Rating Scale modified for NHP use (mUPDRS). On a 4-point scale (0–3; 0 = unimpaired), the mUPDRS was used to rate rigidity, bradykinesia, akinesia, and tremor for both the upper and lower limbs, as well as food retrieval for the upper limb only (maximum = 27 points). Prior to DBS testing, all animals reached a mild to moderate Parkinsonian state (Yu et al., 2021), demonstrating mainly rigidity, akinesia, and bradykinesia [mUPDRS: 17.3 ± 0.5 (mean ± SD) in NHP P, 7.6 ± 0.2 in NHP B1 and 10.4 ± 0.4 in NHP B2]. Animal B1 and B2 did not present tremors while animal P had mild tremors. These mUPDRS assessments were performed 12 times across 4 weeks in animal P, 10 times over 2 weeks in animal B1, and 14 times across 4 weeks in animal B2.

At the end of the study, animals P and B2 were euthanized, and histology was performed. For NHP P, 50 μm coronal sections were stained with cresyl violet to identify the location of the DBS lead (Figure 1B left). For NHP B2, 40 μm coronal sections were imaged and visualized in a 3D slicer, with the sagittal view extracted to show the DBS lead location (Figure 1B right). Histology was not available for NHP B1, so a post-implantation CT was merged with the pre-operative MRI to verify the location of lead (Figure 1B middle).

Experiment protocol

For each animal, CR DBS was delivered for 2 (NHP B1&B2) or 4 (NHP P) h per day for five consecutive days, followed by a period of post-treatment observation (at least 5 days) to characterize the carryover effects (post-CR days). The daily stimulation duration was chosen based on the time needed in each animal to observe therapeutic effects during CR DBS on a separate day before the study. The shortest time needed for the

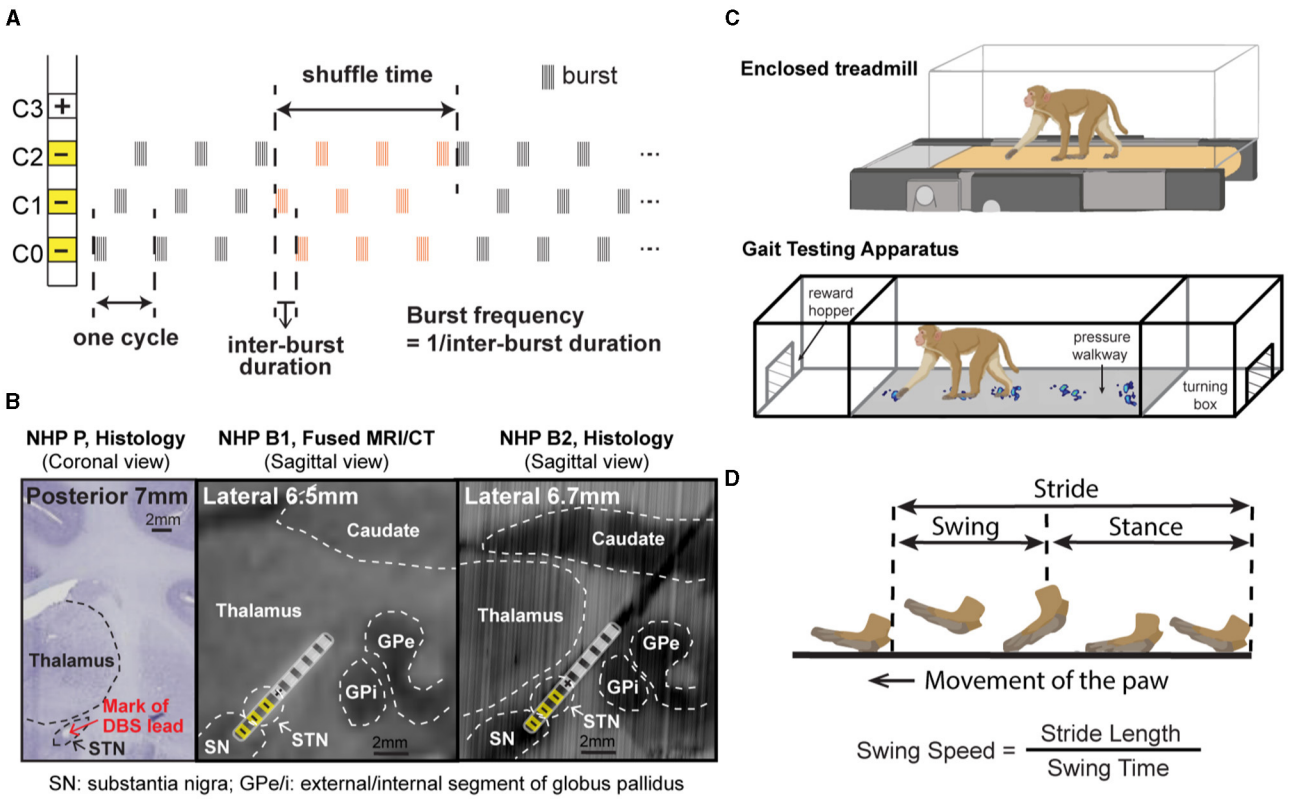

FIGURE 1
(A) CR DBS pattern showing the definition of shuffle time and burst frequency. **(B)** Histology or merged MRI/CT showing the location of the DBS lead in each animal. (Left) Coronal section from NHP P illustrating the relative location of the mark (red arrow) left by placement of the DBS lead in the STN. (Middle) Sagittal view of the merged MRI and CT images showing the estimated location of the DBS lead in NHP B1. (Right) Sagittal view of the DBS lead location reconstructed from the histology for NHP B2. Stimulation contacts used for CR DBS are indicated in yellow. **(C)** Demonstration of the treadmill system (top) used for NHP P and the Habit Trail system (bottom) used for NHP B1 and B2 for the assessment of gait. Both systems were enclosed using plexiglass. Modified from Doyle et al. (2022). **(D)** Definition of the swing and stance phases of gait and the calculation of swing speed.

TABLE 1 Parameter settings for CR DBS.

Parameters	NHP		
	P	B1	B2
Intensity (mA)	0.2	0.1	0.16
Pulse width (μs)	125	120	120
Pulses/bursts	5	6	6
Intra-burst rate (Hz)	150	150	150
Burst frequency (Hz)	21	21	21, 27
On:off pattern (cycles)	3 On: 2 Off	NA	NA
Shuffle time (s)	0.143	10	10
Daily stim duration (hour)	4	2	2

mUPDRS score to achieve its maximum reduction and plateau was chosen to be the daily stimulation duration. CR DBS parameters are demonstrated in Table 1. These parameters were determined based on previous studies (Tass et al., 2012; Wang et al., 2016, 2022) and the capability of the stimulators. CR DBS consisted of burst stimulation delivered through four most ventral contacts within the STN region (C0/C1/C2−, C3+) of the DBS lead (Figure 1A) in a pseudorandomized order. The stimulation intensity was determined as 1/3–1/2 of the intensity identified for the therapeutic traditional, isochronal DBS. The ON:OFF pattern and shuffle time used in NHP P were based on the previous studies (Tass et al., 2012; Wang et al., 2016), and those in NHP B1 and B2 were selected based on the device capability. A cycle is the time needed to deliver bursts through all selected cathodes, and the shuffle time is the time duration within which the stimulating contact order is kept the same before this order is pseudorandomly shuffled (Figure 1A). To assess the carryover effect of STN CR DBS on rigidity, bradykinesia, akinesia, and tremor, mUPDRS was performed prior to CR DBS on stimulation days and once daily in the morning on post-CR days. In NHP B2, two CR DBS settings were evaluated using the same experiment protocol, with burst frequency as the only different parameter (Table 1). In addition to the standard burst frequency (21 Hz) used in previous studies (Tass et al., 2012; Wang et al., 2016, 2022), a 27 Hz burst frequency was also evaluated. The 27 Hz burst frequency was chosen based on the oscillatory activity we observed in the local field potential signal detected in the STN that demonstrated a 27-Hz peak frequency. As modeling studies have suggested that CR DBS using a frequency at which the neuronal population is synchronized will be more effective (Tass, 2003), we

hypothesized that CR DBS with a 27-Hz burst frequency will be more effective at improving all motor signs than that with a 21-Hz burst frequency in this animal. These two evaluation sessions were 10 months apart, and each session was initiated when a stable baseline mUPDRS score mentioned above was observed.

The animal's gait was assessed using slightly different techniques due to a technical limitation at the time of the experiment. NHP P was ambulated in a treadmill system enclosed by plexiglass at a speed of 1.2 miles/hour (Figure 1C top). The movement of the animal's limbs was monitored using a motion capture system (Motion Analysis Corp.). NHPs B1 and B2 were ambulated in a gait testing apparatus (GTA) system in which natural, volitional gait data can be collected (Doyle et al., 2022). The GTA is an apparatus consisting of a plexiglass tunnel capped by two end enclosures, each of which is equipped with a hopper to deliver food or liquid reward (Figure 1C bottom). The animal's gait data were obtained using a pressure walkway mat (HR Walkway 4 VersaTek system, Tekscan, Inc.) in the tunnel. The GTA system allowed the NHP to walk naturally controlling its own pace, but the treadmill system required the NHP to walk continuously around the treadmill speed. CR DBS testing was not initiated until stable gait performance across days was observed. Prior to the DBS testing, animal P received 9 weeks of training on the treadmill, and animals B1 and B2 received 6 weeks and 4 weeks of training, respectively, in the GTA system. For all the NHPs, gait data were recorded before CR DBS, within 24 h after 5 days of CR DBS, and during the carryover period. The exact times of mUPDRS and gait assessments for each animal are shown in Figures 2A, 3A, 4A. Each gait evaluation session took ∼20 min for animal P and ∼30 min for animals B1 and B2. During the evaluation, animal P walked on the treadmill with brief breaks every 2 min, and animals B1 and B2 walked back and forward on the gait mat with brief breaks between passes.

Data analysis

All mUPDRS scores obtained were converted to a percentage of change compared to the baseline score (the score obtained immediately prior to DBS on CR day 1): percentage change in mUPDRS score = 100*(baseline score – daily score)/baseline score. Positive changes indicate improvement in the mUPDRS scores. Given the potential natural fluctuation in the severity of Parkinsonian motor signs across days, we considered any changes smaller than 10% from the baseline score as fluctuations of the baseline level. The score was considered returned to baseline when the percentage change was reduced to 10%. The carryover effects, i.e., percent changes in the mUPDRS scores from the week immediately after 5 days of stimulation, of CR DBS using different burst frequencies in NHP B2 were compared with each other using the Wilcoxon test [χ^2 (DoF, N)]. Using custom MATLAB functions, the movement trajectories at the front limb and hind limb from the motion analysis system and NHP steps collected from the pressure mat were analyzed, and gait parameters were then calculated. To evaluate changes in gait following CR DBS, we assessed the change in stride length and swing speed. As shown in Figure 1D, the distance that separated two consecutive points of initial contact of the same paw with the ground was referred to as the "stride length." The amount of time that an animal spent with its paw in the air and away from the ground was considered "swing time." "Swing speed" can be obtained by dividing "stride length" by "swing time." The carryover effect of CR DBS on each gait parameter for the front and hind limbs on the left side (the side contralateral to the site of DBS implantation) was compared to the baseline using the Wilcoxon test followed by Steel's test with control = baseline. JMP (SAS Institute Inc., North Carolina, United States) was used to conduct statistical analyses, and alpha was corrected for multiple comparisons using the Bonferroni method.

Results

Improvement in gait reflected by increased swing speed was observed in all three NHPs when STN CR DBS was delivered using a burst frequency of 21 Hz. Given the difference in gait assessment methods and experiment protocols, changes in mUPDRS ratings and gait parameters following the CR DBS are demonstrated separately for each animal.

Animal P

Carryover improvement was observed in both the mUPDRS scores and swing speed during treadmill walking following STN CR DBS. Carryover improvement was observed in the mUPDRS score including improvements in each motor subscore (Figure 2B) compared to its baseline subscore (rigidity 3.5; food retrieval 2; akinesia 4; bradykinesia 3.5; tremor 4). Changes in the mUPDRS score showed gradual improvement during 5 days of STN CR DBS, reaching an improvement of 29.4% from the baseline on CR day 5. Following 5 days of CR DBS, the improvement in the mUPDRS was sustained for 12 days. The improvement in rigidity accounted for half or more of the total motor improvement. In addition to improvement in the mUPDRS score, we observed (Figure 2C) a 20% increase in swing speed noted at the NHP's front limb after stimulation on the 3rd and 5th CR days as well as on all the post-CR days [Figure 2C top, left, Wilcoxon test $\chi^2_{(9,231)} = 108.6$, $p < 0.0001$ followed by Steel's test with control = BL, $p < 0.05$]. Opposite changes were observed in stride length at the same joint indicated by ∼10% of decrease in most post-CR days [Figure 2C bottom, left, Wilcoxon test $\chi^2_{(9,231)} = 104.6$, $p < 0.0001$ followed by Steel's test with control = BL, $p < 0.05$]. Limited changes in both parameters were observed at the hind limb, only showing significant changes in swing speed on post-CR days 3 and 12 [Wilcoxon test $\chi^2_{(9,231)} = 51.6$, $p < 0.0001$ followed by Steel's test with control = BL, $p < 0.05$] and in stride length on post-CR day 9 [Wilcoxon test $\chi^2_{(9,231)} = 29.4$, $p = 0.0005$ followed by Steel's test with control = BL, $p < 0.05$; Figure 2C right). Although the swing speed and stride length at the front limb did not return to the baseline level, their changes on post-CR days 12, 15, and 18 showed a trend of returning to the baseline.

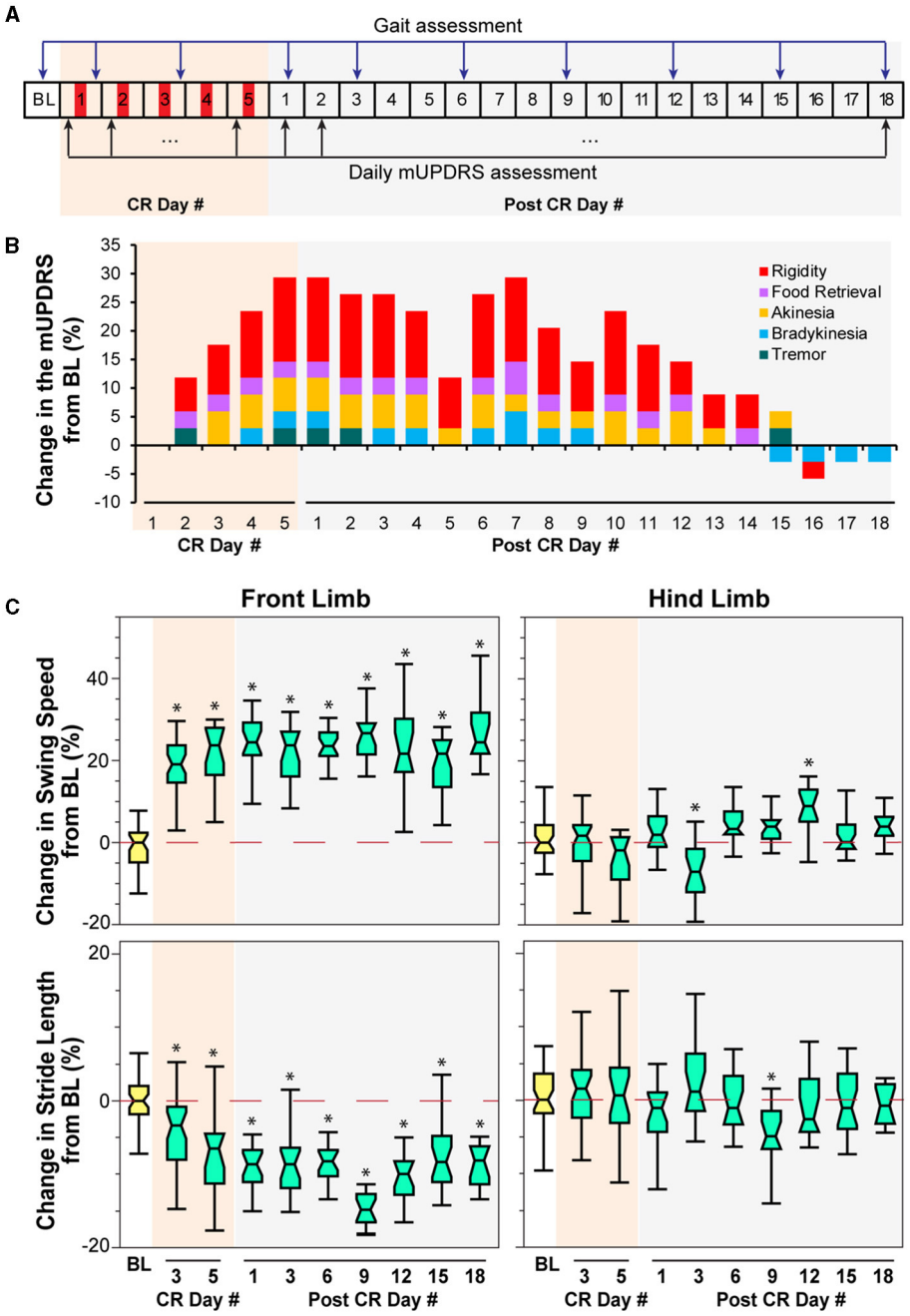

FIGURE 2
Effect of CR DBS on the mUPDRS and gait parameters in NHP P. **(A)** Schematic of the experiment protocol indicating the times when the mUPDRS and gait were assessed. Red panels: CR DBS, 4 h per Day. **(B)** Changes in the mUPDRS from baseline. The composite mUPDRS is further broken down to reveal the changes in individual subscores. **(C)** Changes in the swing speed and stride length at the front limb and hind limb from baseline. The * symbol indicates a significant difference from BL ($^*P < 0.05$).

Animal B1

Similar to that observed in animal P, STN CR DBS was associated with carryover improvements in both the mUPDRS and swing speed in animal B1 but with a shorter duration of carryover benefits. As shown in Figure 3B, significant improvement in the mUPDRS (>50%) was observed starting from CR day 4, while only limited improvement (<10%) was seen in the first 3 days of CR DBS compared to the baseline subscores (rigidity 2.8; food retrieval 1; akinesia 2; bradykinesia 2; tremor 0). The improvement was observed in rigidity, food retrieval, akinesia, and bradykinesia but not tremors as this animal did not demonstrate tremors in its Parkinsonian state. This large improvement in the mUPDRS score reduced significantly starting from the fourth day after 5 days of CR DBS and returned to a level (5%) close to the baseline. During ambulation in the habit trail system, increased swing speed at the front limb immediately after 5 days of CR DBS [Wilcoxon test $\chi^2_{(3,38)} = 8$, $p < 0.05$ followed by Steel's test with control = BL, p

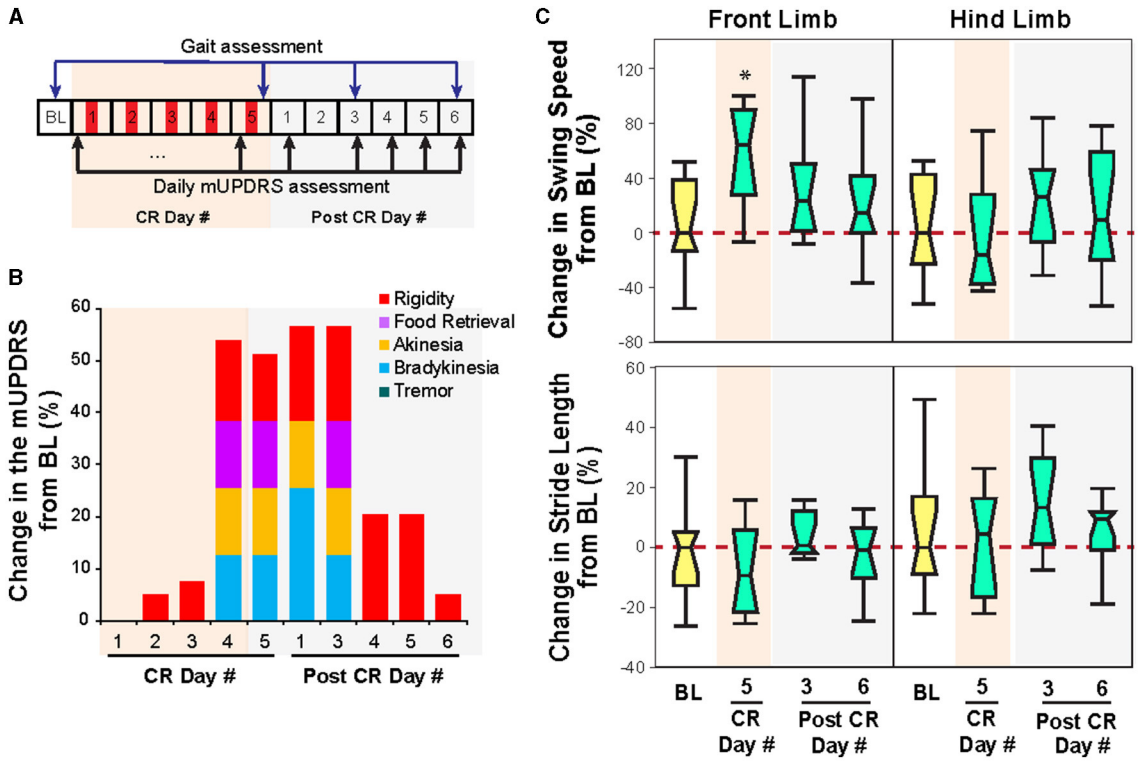

FIGURE 3
Effect of CR DBS on the mUPDRS and gait parameters in NHP B1. **(A)** Schematic of the experiment protocol. Red panels: CR DBS, 2 h per Day. **(B)** Changes in the mUPDRS and its subscores from baseline. **(C)** Changes in the swing speed and stride length at the front limb and hind limb from baseline. The *symbol indicates a significant difference from BL ($^{*}P < 0.05$).

< 0.05] was observed, while the swing speed at the hind limb and stride length did not change (Figure 3C). Consistent with the trend of change in the mUPDRS score after post-CR day 3, improvement in swing speed was only observed immediately after 5 days of CR DBS and diminished on post-CR day 3.

Animal B2

In this animal, carryover improvement in the mUPDRS score was observed in both CR sessions using 21 and 27 Hz burst frequencies; however, improvement in gait parameters was only observed after CR DBS using the 21 Hz burst frequency (Figures 4B, C). The baseline mUPDRS subscores obtained prior to the 21 Hz session were 2.425 (rigidity), 2 (food retrieval), 3 (akinesia), 3.5 (bradykinesia), and 0 (tremor), and those prior to the 27 Hz session were 3 (rigidity), 1.5 (food retrieval), 3 (akinesia), 3 (bradykinesia), and 0 (tremor). CR DBS using the 21 Hz burst frequency produced up to 25.6% of carryover improvement in the mUPDRS score relative to the baseline (Figure 4B left). This improvement reduced over time and dropped to a level of 10% on post-CR day 7. During the CR session using the 27 Hz burst frequency, up to 32% of carryover improvement in the mUPDRS score was observed (Figure 4B middle). This carryover improvement was not reduced to a level close to 10% until post-CR day 12, indicating longer carryover benefits compared to the CR session using 21Hz burst frequency. In both CR sessions, improvement was observed in all the motor subscores except for tremors. Investigating the changes in the mUPDRS in the week following 5 days of CR DBS, greater carryover improvement was observed with CR DBS using 27 Hz burst frequency [Figure 4B right, Wilcoxon test $\chi^2_{(1,13)} = 4.6$, $p = 0.03$] mostly due to the greater improvement in rigidity (Figure 4B left and middle).

In contrast to the changes in mUPDRS, changes in gait parameters demonstrated carryover improvement after CR DBS using the 21 Hz burst frequency but not with the 27 Hz burst frequency. During the CR session using the 21 Hz burst frequency, increases in the swing speed and stride length relative to the baseline were observed at both the front limb and hind limb, immediately following 5 days of CR DBS and on post-CR day 3 (Figure 4C left). Both parameters returned to the baseline level on post-CR day 6. CR DBS using 27 Hz burst frequency rather than improving swing speed and stride length had the opposite effect leading to longer swing times and shorter stride lengths on post-CR day 6 (Figure 4C right). The results of the statistical analysis on the gait parameters for NHP B2 are shown in Table 2.

Discussion

Previous studies have demonstrated the efficacy of STN CR DBS in improving Parkinsonian motor signs including rigidity, akinesia, bradykinesia, and tremor. This study demonstrates that STN CR DBS might also improve Parkinsonian gait. The differential effects

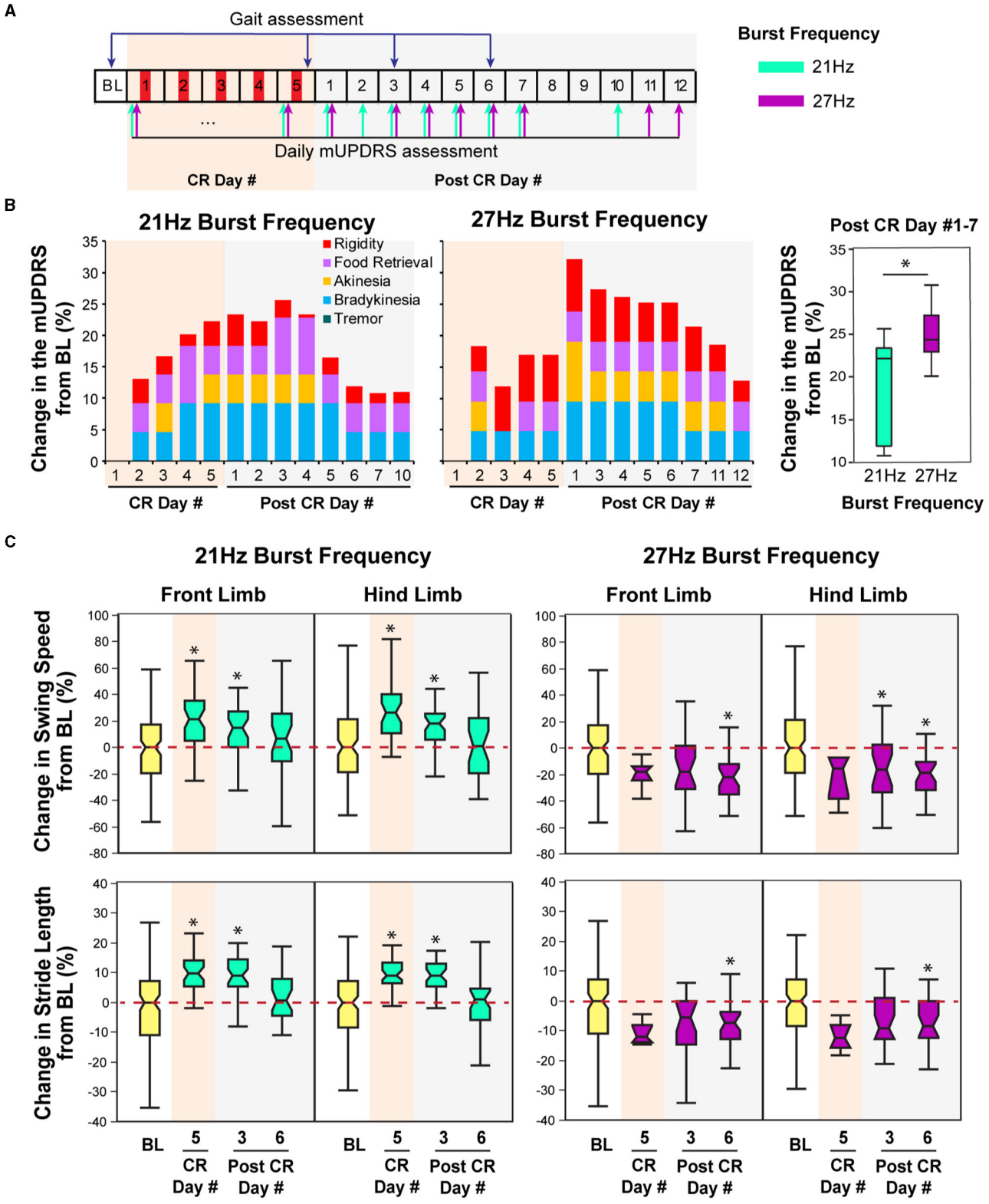

FIGURE 4
Effect of CR DBS using different burst frequencies on the mUPDRS and gait parameters in NHP B2. **(A)** Schematic of the experiment protocol. Red panels: CR DBS, 2 h per Day. The cyan and purple arrows indicate the mUPDRS assessment times for the CR DBS session using the 21 and 27 Hz burst frequencies, respectively. **(B)** Changes in the mUPDRS from baseline for the CR DBS session using 21 Hz (left) and 27Hz (middle) burst frequencies, as well as the comparison in the mUPDRS scores from post CR day #1–7 between these two sessions (right). **(C)** Changes in the swing speed and stride length at the front limb and hind limb from baseline after CR DBS using 21 Hz (left) and 27 Hz (right) burst frequencies. The *symbol indicates a significant difference from BL ($^*P < 0.05$).

TABLE 2 Statistical analysis for the gait parameters for NHP B2.

		Wilcoxon test			p-value of Steel's test with control = BL		
		χ^2	DoF, N	p-value	CR day 5	Post-CR day 3	Post-CR day 6
21 Hz burst frequency							
Swing speed	Front limb	24.1	3, 240	<0.0001	<0.0001	0.0151	0.5383
	Hind limb	34.8	3, 240	<0.0001	<0.0001	0.0054	0.9989
Stride length	Front limb	49.3	3, 240	<0.0001	<0.0001	<0.0001	0.7049
	Hind limb	52.1	3, 240	<0.0001	<0.0001	<0.0001	0.9983
27 Hz burst frequency							
Swing speed	Front limb	21.5	3, 184	<0.0001	0.1202	0.1654	<0.0001
	Hind limb	25.2	3, 184	<0.0001	0.0824	0.0249	<0.0001
Stride length	Front limb	13.8	3, 184	0.0032	0.1044	0.1009	0.0169
	Hind limb	14.3	3, 184	0.0026	0.0596	0.0564	0.0358

of CR DBS using different burst frequencies on gait parameters observed in NHP B2 (Figure 4C) also indicate that the selection of CR parameters, e.g., burst frequency, can significantly impact the efficacy of CR DBS on gait. Moreover, the potential different impact of varying the burst frequency on Parkinsonian gait and other motor signs, i.e., one burst frequency might be more efficient at improving gait, while the other might produce greater improvement on other motor signs, indicating the importance of parameters selection for treating specific PD symptoms. The findings from our research not only support our hypothesis that CR DBS can improve Parkinsonian gait but also can demonstrate the importance of parameter selection for CR DBS in order to achieve specific motor benefits.

STN CR DBS can improve Parkinsonian gait

CR stimulation was developed through computational modeling studies performed by Peter Tass' group (Tass, 2003; Tass and Majtanik, 2006; Hauptmann et al., 2007; Lysyansky et al., 2011). This stimulation approach was designed to desynchronize the neuronal population by stimulating the neuronal subpopulations with a small amount of current in a phase-shifted manner, with the stimulation frequency determined as the frequency at which neurons were synchronized. As abnormal neuronal synchronization in the basal ganglia-thalamocortical network has been associated with the development of PD motor symptoms (Connolly et al., 2015; Neumann et al., 2017; Sanabria et al., 2017; Tinkhauser et al., 2018; Lofredi et al., 2019), pilot preclinical and clinical studies were conducted to explore the effect of CR DBS on PD motor signs (Tass et al., 2012; Adamchic et al., 2014; Wang et al., 2016). These studies demonstrated the acute and carryover therapeutic effects of STN CR DBS stimulated on a wide range of Parkinsonian motor signs, but its effect on Parkinsonian gait was not examined. This study fills the gap by demonstrating the potential therapeutic carryover improvement on Parkinsonian gait of the STN CR DBS using the 21 Hz burst frequency, indicated by the improved gait speed of the front limb in all animals (Figures 2C, 3C, 4C). Stride length was also improved in NHP B2 but reduced in NHP P after CR DBS. The reduced stride length in NHP P was likely due to the different gait assessment approach. NHP P was ambulated in an enclosed treadmill system with limited space. With increased gait speed that exceeded the treadmill speed, the animal reached the front of the treadmill which prevented further movement, resulting in reduced stride length. On the other hand, improvements in both the swing speed and stride length were observed in NHP B2 when the animal was ambulating naturally in the habit trail system although stride length was not improved in NHP B1. This finding indicates the importance of a gait assessment system that can quantitatively evaluate the naturalistic, volitional gait patterns (Doyle et al., 2022).

Exploring the effect of CR DBS on Parkinsonian gait is also a critical step toward the clinical translation of this novel DBS approach. Long-term follow-up studies have shown that certain aspects of gait function improve initially with traditional high-frequency DBS but then progressively worsen resulting in more pronounced asymmetry and dyscoordination (Krack et al., 2003; Volkmann et al., 2004; van Nuenen et al., 2008; Ravi et al., 2021). Although the results are preliminary, this study supports the hypothesis that STN CR DBS can improve Parkinsonian gait while using lower stimulation intensity than traditional DBS, in addition to the benefits CR DBS induced in rigidity, akinesia, bradykinesia, and tremor. Further research on more subjects to evaluate the longer-term therapeutic effects of CR DBS will be needed to confirm our findings. Additional studies (Conway et al., 2021; Seger et al., 2021; Su et al., 2022; Cavallieri et al., 2023; Pourahmad et al., 2023) to compare the effect of CR DBS on gait with that of traditional DBS will also be required for the clinical translation of CR DBS.

Differential effects of different CR burst frequencies on gait and other motor signs

Computational modeling studies have shown that varying CR parameters, e.g., stimulation intensity, burst frequency, stimulation dosage, and number of stimulation contacts, can significantly

impact the desynchronizing effect of CR stimulation (Lysyansky et al., 2013; Manos and Zeitler, 2018; Manos et al., 2018). Our previous study also demonstrated significantly greater carryover benefits associated with shuffled CR DBS compared to the non-shuffled pattern (Wang et al., 2022). Although the results are preliminary, this study is the first to show the differential effects on gait and other motor signs (rigidity, bradykinesia, and akinesia) after CR DBS using different burst frequencies, with one parameter (burst frequency 21 Hz) producing greater carryover benefits on gait, while the other (27 Hz) produced greater benefits on other motor signs (Figure 4C). This might indicate that a specific burst frequency is required to optimize the effect of CR DBS on Parkinsonian gait, while a different burst frequency is required for achieving optimal improvement on rigidity, akinesia, and bradykinesia. As only two burst frequencies were evaluated in animal B2, it is also possible that the optimal burst frequency that can improve both gait and other motor signs has not been identified. Additional explorations in the effect of CR DBS using a wider range of burst frequencies will be needed to further investigate the impact of burst frequency on different Parkinsonian motor signs and even non-motor signs.

Limitations and future directions

Even though all three animals showed significant improvement in gait speed after CR DBS, there were some limitations within this study. The effects of STN CR DBS with different burst frequencies were not investigated in animals P and B1. This was attributable to the length of time necessary to examine each CR DBS setting and the limited time for evaluating CR DBS in these two animals. Due to the various capabilities of the device available at the time of the experiments and the varying lengths of daily stimulation necessary to produce a sustained therapeutic effect, animals P and B1/B2 were subjected to different ON:OFF patterns, shuffling times, and stimulation durations, while other CR parameters were the same. Different gait assessment systems, i.e., treadmill and habit trail systems, were used, which resulted in different observations of the change in stride length. As discussed above, the assessment of the natural gait in the habit trail system is superior to that of the passive gait movement in the treadmill, making it critical for future explorations into the effects of CR DBS (Doyle et al., 2022). Another limitation of this study is that carryover assessment was terminated when the mUPDRS score returned to the baseline and an offline gait data analysis was performed afterward to investigate the effect of CR DBS on gait. Therefore, we were not able to observe the returning of gait parameters to the baseline in animal P and the 27 Hz CR DBS session in animal B2. Future studies are needed to systematically evaluate the impact of different CR parameters on Parkinsonian gait.

Despite these limitations, this study provides valuable insight into the effect of STN CR DBS on Parkinsonian gait and the potential impact of varying CR parameters on gait and other motor signs. These findings support the development of CR DBS as a novel DBS strategy that can be customized for each patient and further advance the translation of this novel therapy into clinical application.

Data availability statement

The raw data supporting the conclusions of this article will be made available by the authors, without undue reservation.

Ethics statement

The animal study was reviewed and approved by The Institutional Animal Care and Use Committee.

Author contributions

JW conceived and designed the experiments. LJ, JW, KB, and ZL contributed to animal instrumentation. JW, KB, ZL, and KA acquired the data. KB, ZL, and KN analyzed the data. KB, SA, JW, LJ, and JV were involved in drafting the article. All authors have reviewed the article and approved the final version for submission.

Funding

This research was funded by the National Institutes of Health (R01NS117822, R01NS037019, R37NS077657, and P50NS123109), the Engdahl Family Foundation, and a fellowship from the Parkinson's Foundation.

Acknowledgments

The authors thank Sinta Fergus, Claudia Hendrix, and Adele DeNicola for their technical support in data collection and analysis. The authors thank the neuromodulation research center (nmrc.umn.edu) for the group effort on animal care and technical support.

Conflict of interest

JV serves as a consultant for Medtronic, Inc., Boston Scientific, Abbott, Surgical Information Sciences, Inc. He serves on the Executive Advisory Board for Abbott and the Scientific Advisory Board for Surgical Information Sciences and has an equity interest in Surgical Information Sciences.

The remaining authors declare that the research was conducted in the absence of any commercial or financial relationships that could be construed as a potential conflict of interest.

Publisher's note

References

Adamchic, I., Hauptmann, C., Barnikol, U. B., Pawelczyk, N., Popovych, O., Barnikol, T. T., et al. (2014). Coordinated reset neuromodulation for Parkinson's disease: proof-of-concept study. *Mov. Disord.* 29, 1679–1684. doi: 10.1002/mds.25923

Anidi, C., O'Day, J. J., Anderson, R. W., Afzal, M. F., Syrkin-Nikolau, J., Velisar, A., et al. (2018). Neuromodulation targets pathological not physiological beta bursts during gait in Parkinson's disease. *Neurobiol. Dis.* 120, 107–117. doi: 10.1016/j.nbd.2018.09.004

Cavallieri, F., Campanini, I., Gessani, A., Budriesi, C., Fioravanti, V., Di Rauso, G, et al. (2023). Long-term effects of bilateral subthalamic nucleus deep brain stimulation on gait disorders in Parkinson's disease: a clinical-instrumental study. *J. Neurol.* 270, 4342–4353. doi: 10.1007/s00415-023-11780-5

Chen, C.-C., Yeh, C.-H., Chan, H.-L., Chang, Y.-J., Tu, P.-H., Yeh, C.-H., et al. (2019). Subthalamic nucleus oscillations correlate with vulnerability to freezing of gait in patients with Parkinson's disease. *Neurobiol. Dis.* 132, 104605. doi: 10.1016/j.nbd.2019.104605

Connolly, A. T., Jensen, A. L., Bello, E. M., Netoff, T. I., Baker, K. B., Johnson, M. D., et al. (2015). Modulations in oscillatory frequency and coupling in globus pallidus with increasing Parkinsonian severity. *J. Neurosci.* 35, 6231–6240. doi: 10.1523/JNEUROSCI.4137-14.2015

Conway, Z. J., Silburn, P. A., Perera, T., O'Maley, K., and Cole, M. H. (2021). Low-frequency STN-DBS provides acute gait improvements in Parkinson's disease: a double-blinded randomised cross-over feasibility trial. *J. Neuroengineering Rehabil.* 18, 125. doi: 10.1186/s12984-021-00921-4

De Oliveira, M. P. B., Lobato, D. F. M., Smaili, S. M. C., Carvalho, C., and Borges, J. B. C. (2021). Effect of aerobic exercise on functional capacity and quality of life in individuals with Parkinson's disease: a systematic review of randomized controlled trials. *Arch. Gerontol. Geriatr.* 95, 104422. doi: 10.1016/j.archger.2021.104422

Deuschl, G., Herzog, J., Kleiner-Fisman, G., Kubu, C., Lozano, A. M., Lyons, K. E., et al. (2006). Deep brain stimulation: postoperative issues. *Mov. Disord.* 21(Suppl 14), S219–S237. doi: 10.1002/mds.20957

di Biase, L., Di Santo, A., Caminiti, M. L., De Liso, A., Shah, S. A., Ricci, L, et al. (2020). Gait Analysis in Parkinson's disease: an overview of the most accurate markers for diagnosis and symptoms monitoring. *Sensors* 20, 3529. doi: 10.3390/s20123529

Doyle, A. M., Bauer, D., Hendrix, C., Yu, Y., Nebeck, S. D., Fergus, S., et al. (2022). Spatiotemporal scaling changes in gait in a progressive model of Parkinson's disease. *Front. Neurol.* 13, 1041934. doi: 10.3389/fneur.2022.1041934

Fim Neto, A., de Luccas, J. B., Bianqueti, B. L., da Silva, L. R., Almeida, T. P., Takahata, A. K., et al. (2022). Subthalamic low beta bursts differ in Parkinson's disease phenotypes. *Clin. Neurophysiol.* 140, 45–58. doi: 10.1016/j.clinph.2022.05.013

Gandolfi, M., Fiorio, M., Geroin, C., Torneri, P., Menaspà, Z., Smania, N., et al. (2023). Dual tasking affects gait performance but not automaticity in functional gait disorders: a new diagnostic biomarker. *Parkinsonism Relat. Disord.* 108, 105291. doi: 10.1016/j.parkreldis.2023.105291

Gray, P., and Hildebrand, K. (2000). Fall risk factors in Parkinson's disease. *J. Neurosci. Nurs. J. Am. Assoc. Neurosci. Nurses* 32, 222–228. doi: 10.1097/01376517-200008000-00006

Hauptmann, C., Popovych, O., and Tass, P. A. (2007). Desynchronizing the abnormally synchronized neural activity in the subthalamic nucleus: a modeling study. *Expert. Rev. Med. Devices* 4, 633–50. doi: 10.1586/17434440.4.5.633

Johansson, H., Folkerts, A.-K., Hammarström, I., Kalbe, E., and Leavy, B. (2023). Effects of motor-cognitive training on dual-task performance in people with Parkinson's disease: a systematic review and meta-analysis. *J. Neurol.* 270, 2890–2907. doi: 10.1007/s00415-023-11610-8

Kelly, V. E., Eusterbrock, A. J., and Shumway-Cook, A. (2012). A review of dual-task walking deficits in people with Parkinson's disease: motor and cognitive contributions, mechanisms, and clinical implications. *Park. Dis.* 2012, 1–14. doi: 10.1155/2012/918719

Krack, P., Batir, A., Van Blercom, N., Chabardes, S., Fraix, V., Ardouin, C., et al. (2003). Five-year follow-up of bilateral stimulation of the subthalamic nucleus in advanced Parkinson's disease. *N. Engl. J. Med.* 349, 1925–1934. doi: 10.1056/NEJMoa035275

Lofredi, R., Neumann, W. J., Brücke, C., Huebl, J., Krauss, J. K., Schneider, G. H., et al. (2019). Pallidal beta bursts in Parkinson's disease and dystonia. *Mov. Disord.* 34, 420–424. doi: 10.1002/mds.27524

Luo, G., Zhu, Y., Wang, R., Tong, Y., Lu, W., Wang, H., et al. (2015). Bayesian classification and analysis of gait disorders using image and depth sensors of Microsoft Kinect. *Digit. Signal Process.* 47, 169–177. doi: 10.1016/j.dsp.2015.05.011

Lysyansky, B., Popovych, O. V., and Tass, P. A. (2011). Multi-frequency activation of neuronal networks by coordinated reset stimulation. *Interface Focus* 1, 75–85. doi: 10.1098/rsfs.2010.0010

Lysyansky, B., Popovych, O. V., and Tass, P. A. (2013). Optimal number of stimulation contacts for coordinated reset neuromodulation. *Front. Neuroeng.* 6, 5. doi: 10.3389/fneng.2013.00005

Manos, T., Zeitler, M., and Tass, P. A. (2018). Short-term dosage regimen for stimulation-induced long-lasting desynchronization. *Front Physiol* 9, 376. doi: 10.3389/fphys.2018.00376

Manos, T., and Zeitler, M. P. A. (2018). How stimulation frequency and intensity impact on the long-lasting effects of coordinated reset stimulation. *PLOS Comput. Biol.* 14, e1006113. doi: 10.1371/journal.pcbi.1006113

Matsuno, A., Matsushima, A., Saito, M., Sakurai, K., Kobayashi, K., Sekijima, Y., et al. (2023). Quantitative assessment of the gait improvement effect of LSVT BIG® using a wearable sensor in patients with Parkinson's disease. *Heliyon* 9, e16952. doi: 10.1016/j.heliyon.2023.e16952

Neumann, W.-J., Staub-Bartelt, F., Horn, A., Schanda, J., Schneider, G.-H., Brown, P., et al. (2017). Long term correlation of subthalamic beta band activity with motor impairment in patients with Parkinson's disease. *Clin. Neurophysiol.* 128, 2286–2291. doi: 10.1016/j.clinph.2017.08.028

Odekerken, V. J. J., van Laar, T., Staal, M. J., Mosch, A., Hoffmann, C. F. E., Nijssen, P. C. G., et al. (2013). Subthalamic nucleus versus globus pallidus bilateral deep brain stimulation for advanced Parkinson's disease (NSTAPS study): a randomised controlled trial. *Lancet Neurol.* 12, 37–44. doi: 10.1016/S1474-4422(12)70264-8

Pourahmad, R., Saleki, K., Esmaili, M., Abdollahi, A., Alijanizadeh, P., Gholinejad, M. Z., et al. (2023). Deep brain stimulation (DBS) as a therapeutic approach in gait disorders: what does it bring to the table? *IBRO Neurosci. Rep.* 14, 507–513. doi: 10.1016/j.ibneur.2023.05.008

Ravi, D. K., Baumann, C. R., Bernasconi, E., Gwerder, M., Ignasiak, N. K., Uhl, M., et al. (2021). Does subthalamic deep brain stimulation impact asymmetry and dyscoordination of gait in Parkinson's disease? *Neurorehabil. Neural Repair* 35, 1020–1029. doi: 10.1177/15459683211041309

Saint-Cyr, J. A., Trépanier, L. L., Kumar, R., Lozano, A. M., and Lang, A. E. (2000). Neuropsychological consequences of chronic bilateral stimulation of the subthalamic nucleus in Parkinson's disease. *Brain J. Neurol.* 123, 2091–2108. doi: 10.1093/brain/123.10.2091

Sanabria, D. E., Johnson, L. A., Nebeck, S. D., Zhang, J., Johnson, M. D., Baker, K. B., et al. (2017). Parkinsonism and vigilance: alteration in neural oscillatory activity and phase-amplitude coupling in the basal ganglia and motor cortex. *J. Neurophysiol.* 118, 2654–2669. doi: 10.1152/jn.00388.2017

Seger, A., Gulberti, A., Vettorazzi, E., Braa, H., Buhmann, C., Gerloff, C., et al. (2021). Short pulse and conventional deep brain stimulation equally improve the Parkinsonian gait disorder. *J. Park. Dis.* 11, 1455–1464. doi: 10.3233/JPD-202492

Su, Z. H., Patel, S., Gavine, B., Buchanan, T., Bogdanovic, M., Sarangmat, N., et al. (2022). Deep brain stimulation and levodopa affect gait variability in Parkinson disease differently. *Neuromodulation* 26, 382–393. doi: 10.1016/j.neurom.2022.04.035

Svehlík, M., Zwick, E. B., Steinwender, G., Linhart, W. E., Schwingenschuh, P., Katschnig, P., et al. (2009). Gait analysis in patients with Parkinson's disease off dopaminergic therapy. *Arch. Phys. Med. Rehabil.* 90, 1880–1886. doi: 10.1016/j.apmr.2009.06.017

Tass, P. A. (2003). A model of desynchronizing deep brain stimulation with a demand-controlled coordinated reset of neural subpopulations. *Biol. Cybern.* 89, 81–88. doi: 10.1007/s00422-003-0425-7

Tass, P. A., and Majtanik, M. (2006). Long-term anti-kindling effects of desynchronizing brain stimulation: a theoretical study. *Biol. Cybern.* 94, 58–66. doi: 10.1007/s00422-005-0028-6

Tass, P. A., Qin, L., Hauptmann, C., Dovero, S., Bezard, E., Boraud, T., et al. (2012). Coordinated reset has sustained aftereffects in Parkinsonian monkeys. *Ann. Neurol.* 72, 816–820. doi: 10.1002/ana.23663

Tinkhauser, G., Torrecillos, F., Duclos, Y., Tan, H., Pogosyan, A., Fischer, P., et al. (2018). Beta burst coupling across the motor circuit in Parkinson's disease. *Neurobiol. Dis.* 117, 217–225. doi: 10.1016/j.nbd.2018.06.007

Toledo, J. B., López-Azcárate, J., Garcia-Garcia, D., Guridi, J., Valencia, M., Artieda, J., et al. (2014). High beta activity in the subthalamic nucleus and freezing of gait in Parkinson's disease. *Neurobiol. Dis.* 64, 60–65. doi: 10.1016/j.nbd.2013.12.005

van Nuenen, B. F., Esselink, R. A., Munneke, M., Speelman, J. D., van Laar, T., Bloem, B. R., et al. (2008). Postoperative gait deterioration after bilateral

subthalamic nucleus stimulation in Parkinson's disease. *Mov. Disord.* 23, 2404–2406. doi: 10.1002/mds.21986

Volkmann, J., Allert, N., Voges, J., Sturm, V., Schnitzler, A., Freund, H. J., et al. (2004). Long-term results of bilateral pallidal stimulation in Parkinson's disease. *Ann. Neurol.* 55, 871–875. doi: 10.1002/ana.20091

Wang, J., Fergus, S. P., Johnson, L. A., Nebeck, S. D., Zhang, J., Kulkarni, S., et al. (2022). Shuffling improves the acute and carryover effect of subthalamic coordinated reset deep brain stimulation. *Front. Neurol.* 13, 716046. doi: 10.3389/fneur.2022.716046

Wang, J., Nebeck, S., Muralidharan, A., Johnson, M. D., Vitek, J. L., Baker, K. B., et al. (2016). Coordinated reset deep brain stimulation of subthalamic nucleus produces long-lasting, dose-dependent motor improvements in the 1-methyl-4-phenyl-1,2,3,6-tetrahydropyridine non-human primate model of Parkinsonism. *Brain Stimulat.* 9, 609–617. doi: 10.1016/j.brs.2016.03.014

Yu, Y., Sanabria, D. E., Wang, J., Hendrix, C. M., Zhang, J., Nebeck, S. D., et al. (2021). Parkinsonism alters beta burst dynamics across the basal ganglia-motor cortical network. *J. Neurosci.* 41, 2274–2286. doi: 10.1523/JNEUROSCI.1591-20.2021

frontiers | Frontiers in Human Neuroscience

TYPE Brief Research Report
PUBLISHED 05 October 2023
DOI 10.3389/fnhum.2023.1233565

OPEN ACCESS

EDITED BY
Peter A. Tass,
Stanford University, United States

REVIEWED BY
Jing Wang,
University of Minnesota Twin Cities, United States
Justus Alfred Kromer,
Stanford University, United States
Yasmine Kehnemouyi,
Stanford University, United States,
in collaboration with reviewer JK

*CORRESPONDENCE
Monika Pötter-Nerger
✉ m.poetter-nerger@uke.de

RECEIVED 05 June 2023
ACCEPTED 18 September 2023
PUBLISHED 05 October 2023

CITATION
Gülke E, Horn MA, Caffier J, Pinnschmidt H, Hamel W, Moll CKE, Gulberti A and Pötter-Nerger M (2023) Comparison of subthalamic unilateral and bilateral theta burst deep brain stimulation in Parkinson's disease. *Front. Hum. Neurosci.* 17:1233565. doi: 10.3389/fnhum.2023.1233565

Comparison of subthalamic unilateral and bilateral theta burst deep brain stimulation in Parkinson's disease

Eileen Gülke[1], Martin A. Horn[2], Julian Caffier[1], Hans Pinnschmidt[3], Wolfgang Hamel[4], Christian K. E. Moll[5], Alessandro Gulberti[1] and Monika Pötter-Nerger[1]*

[1]Department of Neurology, University Medical Center Hamburg-Eppendorf, Hamburg, Germany, [2]Department of Medicine, University Medical Center Hamburg-Eppendorf, Hamburg, Germany, [3]Institute of Medical Biometry and Epidemiology, University Medical Center, Hamburg-Eppendorf, Hamburg, Germany, [4]Department of Neurosurgery, University Medical Center Hamburg-Eppendorf, Hamburg, Germany, [5]Institute of Neurophysiology and Pathophysiology, University Medical Center Hamburg-Eppendorf, Hamburg, Germany

High-frequency, conventional deep brain stimulation (DBS) of the subthalamic nucleus (STN) in Parkinson's disease (PD) is usually applied bilaterally under the assumption of additive effects due to interhemispheric crosstalk. Theta burst stimulation (TBS-DBS) represents a new patterned stimulation mode with 5 Hz interburst and 200 Hz intraburst frequency, whose stimulation effects in a bilateral mode compared to unilateral are unknown. This single-center study evaluated acute motor effects of the most affected, contralateral body side in 17 PD patients with unilateral subthalamic TBS-DBS and 11 PD patients with bilateral TBS-DBS. Compared to therapy absence, both unilateral and bilateral TBS-DBS significantly improved ($p < 0.05$) lateralized Movement Disorder Society-Unified Parkinson's Disease Rating Scale part III (MDS-UPDRS III) scores. Bilateral TBS-DBS revealed only slight, but not significant additional effects in comparison to unilateral TBS-DBS on total lateralized motor scores, but on the subitem lower limb rigidity. These results indicate that bilateral TBS-DBS has limited additive beneficial effects compared to unilateral TBS-DBS in the short term.

KEYWORDS

Parkinson's disease, subthalamic nucleus, deep brain stimulation, theta burst, unilateral stimulation, bilateral stimulation

Introduction

Bilateral deep brain stimulation (DBS) of the subthalamic nucleus (STN) in a conventional, continuous, high-frequency stimulation mode is a highly effective symptomatic treatment for Parkinson's disease (PD) patients improving quality of life (Deuschl et al., 2006; Schuepbach et al., 2013). Previous studies of continuous, unilateral STN-DBS revealed insights into potential interaction of interhemispheric cross-talk, since unilateral STN-DBS was demonstrated to improve not only contralateral body side symptoms, but also ipsilateral and axial motor symptoms after 1–2 years (Kim et al., 2009; Walker et al., 2009). Besides, quality of life was significantly improved by unilateral STN-DBS (Kim et al., 2009; Walker et al., 2009). Still, heterogeneous results were obtained when clinical results of motor scores of unilateral and bilateral STN-DBS were compared.

It is unknown whether these heterogeneous results might be due to simple methodological restraints as different observation periods or potential unfavorable interhemispheric subthalamic cross-talk in terms of counteracting effects of crossing fibers on local STN circuits whitewashing local DBS effects or inconvenient resonance behavior.

Recently, a new form of STN-DBS, the so-called "Theta Burst Stimulation" (TBS-DBS) was used in previous studies in man (Horn et al., 2020; Sáenz-Farret et al., 2021). This patterned DBS mode has been inferred from theta burst stimulation studies in animal slices, *in vivo* hippocampal stimulation in animal models and from non-invasive transcranial magnetic stimulation (TMS) in man (Suppa et al., 2016). In rats, hippocampal TBS improved deficits in learning and memory (Sweet et al., 2014). In humans, continuous TBS-TMS applied to the motor cortex induced cortical inhibition outlasting the TMS train (Huang et al., 2005), probably depending on N-methyl-D-aspartate-receptor and Ca^{2+} channel activity (Suppa et al., 2016) resulting in lasting neuroplasticity. TBS was transferred from non-invasive TMS to STN-DBS, since subthalamic TBS-DBS might entrain glutamatergic hyperdirect cortical afferents and pallidal glutamatergic efferents to induce neuroplastic changes. TBS-DBS might enhance stimulation outcomes by low stimulation energy, has the potential to lower the probability of stimulation side effects and reduce battery consumption in STN-DBS patients (Horn et al., 2020).

To date, it remains unclear whether bilateral TBS-DBS application in STN-DBS patients is safe, effective, and whether it has additional beneficial effects over unilateral application. We hypothesize that bilateral application of TBS-DBS potentiates unilateral effects by modulation of interhemispheric pathways at different basal ganglia, brainstem and cortical levels through modulation of glutamatergic pathways (Arai et al., 2008; Nakajima et al., 2017).

In this brief report, we aim to compare the effect of unilateral and bilateral 200 Hz TBS-DBS on lateralized motor symptoms in postoperative PD patients with STN-DBS.

Methods

Participants

The study was approved by the local ethics committee (PV 5281, PV 6025) and conducted in agreement with the Code of Ethics of the World Medical Association (Declaration of Helsinki, 2018). Written informed consent was obtained. Inclusion criteria were: (1) diagnosis of bilateral idiopathic PD by motor assessments, (2) appropriate patients for STN-DBS along the CAPSIT protocol (Defer et al., 1999), (3) the implantation of a bilateral Medtronic system (Medtronic, Minneapolis), (4) stable postoperative condition >3 months after DBS implantation in the STN. Exclusion criteria were: (1) major psychiatric comorbidities, (2) severe dementia. All participants were tested after overnight withdrawal of short-acting dopaminergic medication (MED OFF).

Study design

This report synthesizes two clinical studies, which were single-center, randomized, double-blind, interventional assessments in chronically operated PD patients with bilateral STN-DBS. Two data sets from two different studies were retrospectively combined and then analyzed for divergent effects on the contralateral body side by either unilateral or bilateral TBS-DBS application: In the first cohort (Horn et al., 2020), unilateral TBS-DBS was applied in the STN contralateral to the most affected body side, in the second cohort we assessed the motor symptoms of the most affected body side while stimulating both STN (Table 1). For the bilateral TBS-DBS data set, the more affected body side was retrospectively defined by the highest Movement Disorder Society-Unified Parkinson's Disease Rating Scale part III (MDS-UPDRS III) sum score (items 3.3–3.8, 3.15–3.18) in the OFF condition. If left and right lateralized MDS-UPDRS III sum scores were equal, the body side with the highest rigidity score of the upper extremity in the stimulation OFF state was chosen.

In both studies, theta burst stimulation (TBS-DBS), conventional DBS (cDBS) and stimulation OFF state were compared in a randomized double-blind fashion with an inter-trial interval of 30 min. Total lateralized motor sum scores as well as subitems of the MDS-UPDRS III were assessed. The TBS pattern consists of stimulation bursts of 0.1 s duration repeated at 5 Hz with a pulse width of 60 µs (Horn et al., 2020). This is achieved by periodical switching DBS ON and OFF for 0.1 s in the cyclic mode of the chronically implanted impulse generators (IPG). Intraburst frequency was set to 200 Hz. For the current report, only TBS-DBS results of the contralateral body side were analyzed. TBS-DBS was applied at the clinically most effective electrode contact that was chronically used in every-day life conditions and confirmed by a preceding monopolar review. TBS-DBS was applied for 30 min. Because of restricted cycling options in programming, only PD patients with Medtronic Activa PC/ RC system and 3,389 leads with 4-omnidirectional contacts participated in the study. The intensity of TBS-DBS was adjusted to efficacy and side effects threshold. Amplitude could be kept constant for cTBS and TBS-DBS for unilateral application whereas we needed to adjust the amplitude slightly for bilateral TBS-DBS along the effect and side effect threshold. The study was executed by two investigators: one blinded movement disorder experienced clinician assessed the motor symptoms, while the other investigator operated the programming. Safety and tolerability of TBS-DBS was clinically assessed by the clinicians during a preceding monopolar review with assessment of side effect thresholds (dysarthria, paresthesia's, tetanic contraction or malaise) and by asking the subjects for side effects during the 30 min DBS condition.

Statistics

Statistical analysis was performed in SPSS V27.0 (IBM Corporation, SPSS, Inc., Chicago, IL). Descriptive statistics are presented as mean ± standard deviation (SD). The level of significance was $p \leq 0.05$. A Wilcoxon signed rank test was used to compare within-subject differences of stimulation conditions (TBS-DBS vs. stimulation OFF; $p \leq 0.05$). The Mann–Whitney U test was used to compare intersubject differences of stimulation conditions of the two cohorts.

Results

Patient demographics

Two PD patient cohorts were clinically assessed with either unilateral or bilateral TBS-DBS application (Table 1). The first cohort was investigated between April 2017 and January 2018 with 17 subjects

10.3389/fnhum.2023.1233565

TABLE 1 Patient characteristics and stimulation parameters of the randomized, double-blind assessment of motor performances after 30 min stimulation.

ID	Sex	Age	Years with disease	Years with DBS	cDBS 130 Hz		TBS 200 Hz		Contacts activated	
					Left Electrode	Right electrode	Left electrode	Right electrode	Left electrode	Right electrode
					Amplitude [V/mA]	Amplitude [V/mA]	Amplitude [V/mA]	Amplitude [V/mA]		
01	Female	56	4	2.8	–	3.0	–	3.0	–	10
02	Female	76	15	4.4	–	3.5	–	3.5	–	9/10
03	Female	64	23	4.6	3.3	–	3.3	–	2	–
04	Male	72	13	0 (4)	–	2.0	–	2.0	–	
05	Male	53	14	5.5	–	3.2	–	3.2	–	10
06	Male	56	17	7.3	–	2.0	–	2.0	–	10
07	Male	71	9	3.2	2.4	–	2.4	–	2	–
08	Male	74	21	3.3	2.5	–	2.5	–	2	–
09	Male	73	20	0 (10)	–	2.8	–	2.8	–	10
10	Male	66	17	2.5	3.1	–	3.1	–	2	–
11	Male	66	11	1.9	–	3.1	–	3.1	–	9
12	Male	63	9	2.6	3.0	–	3.0	–	1	–
13	Female	66	21	9.2	–		–		–	6
14	Male	64	6	3.8	–	2.5	–	2.5	–	10
15	Male	58	11	0 (9)	–	2.5	–	2.5	–	10
16	Male	58	18	3.5	–	2.6	–	2.6	–	10
17	Female	67	22	0 (6)	3.5	–	3.5	–	1	–
22	Male	56	8	1	1.0	–	1.1	–	2	–
23	Female	67	18	0 (4)	–	2.6	–	3.0	–	9
24	Male	70	18	7	2.3	–	2.6	–	3	–
25	Male	61	12	4	–	3.0	–	3.4	–	10
26	Male	73	9	5	–	2.0	–	2.3	–	10
27	Male	61	15	8	1.9	–	2.2	–	1	–
28	Female	56	13	6	3.0	–	3.5	–	2	–
29	Female	69	22	8	2.7	–	3.0	–	1	–
30	Male	61	13	12	–	2.7	–	3.0	–	10
31	Male	62	12	4	–	3.8	–	4.3	–	10
32	Male	69	30	13	–	1.9	–	2.2	–	10

Only the parameters of the more affected body side are listed. For all stimulation modes, pulse width was set to 60 µs. In brackets is given the time with DBS since surgery in months.

(five females) in the unilateral TBS-DBS study (age 64.9 ± 6.9 years, disease duration 14.8 ± 5.8 years, 3.2 ± 2.6 years since DBS surgery). The second cohort included 11 patients, which were assessed between February 2021 and May 2022 (three females) with bilateral TBS-DBS (age 64.1 ± 5.8 years, disease duration 15.4 ± 6.3 years, 6.2 ± 4.0 years since DBS surgery). Further patient characteristics are described in Table 1.

Clinical assessment of Parkinson's disease motor symptoms

The two PD patient groups of the two studies were quite similar in terms of their clinical characteristics. The activated DBS electrode contact level counting from 1 (most ventral contact) to 4 (most dorsal contact) was 2.8 ± 0.4 for the unilateral DBS cohort and 2.8 ± 0.6 for the bilateral DBS cohort (Table 1). Stimulation amplitude for the unilateral TBS-DBS was 2.8 ± 0.5 V and 2.8 ± 0.8 mA for bilateral TBS-DBS. Both unilateral and bilateral cDBS and TBS-DBS improved the clinical condition of the subjects in comparison to DBS absence (Table 2). The Mann–Whitney U test showed no significant differences in lateralized MDS-UPDRS III sum scores between the two cohorts for stimulation OFF condition ($U = 89.00$, $Z = -0.213$, $p = 0.853$), cDBS condition ($U = 79.00$, $Z = -0.686$, $p = 0.517$) and TBS-DBS condition ($U = 85.00$, $Z = -0.402$, $p = 0.711$). We therefore judged the comparison of the uni- and bilateral DBS effects in those two similar cohorts as reasonable.

The lateralized MDS-UPDRS III sum score of the more affected body side significantly improved from 15.8 ± 4.9 (STIM OFF) to 10.6 ± 4.6 with unilateral, contralateral cDBS ($n = 17$, $Z = -3.32$, $p < 0.001$) as well as with unilateral, contralateral TBS-DBS to 12.8 ± 5.0 ($n = 17$, $Z = -2.38$, $p = 0.017$). Wilcoxon signed rank test revealed a significant difference of relative changes of unilateral cDBS (31.56 ± 28.96%) compared to unilateral TBS-DBS (15.98 ± 39.80%; $p = 0.011$). Bilateral cDBS also significantly improved the lateralized MDS-UPDRS III sum score of the more affected body side from 16.7 ± 3.7 (OFF) to 11.8 ± 5.02 ($n = 11$, $Z = -2.68$, $p = 0.007$) as well as bilateral TBS-DBS, which improved to 12.4 ± 5.4 ($n = 11$, $Z = -2.14$, $p = 0.032$). Wilcoxon signed rank test revealed a non-significant difference of relative changes of bilateral cDBS (29.87 ± 25.77%) compared to bilateral TBS-DBS (26.14 ± 26.37%; $p = 0.541$). Although there was a slight tendency of more efficient improvement of the relative changes of lateralized MDS-UPDRS III by bilateral TBS-DBS (26.1 ± 26.4%) compared to unilateral TBS-DBS (16.0 ± 39.8%), the difference was not significant ($U = 74.50$, $Z = -0.895$, $p = 0.378$).

Relative changes of lateralized MDS-UPDRS III revealed a 31.56 ± 28.96% improvement by unilateral cDBS and a 29.87 ± 25.77% improvement by bilateral cDBS. The Mann–Whitney U test showed non-significant differences in lateralized MDS-UPDRS III sum scores between the 2 cohorts for cDBS stimulation ($U = 83.50$, $Z = -0.461$, $p = 0.643$). In a second step, we investigated subitems of the lateralized MDS-UPDRS III. There was a statistically significant difference in the improvement of lower limb rigidity when comparing unilateral (1.3 ± 0.7) with bilateral (0.4 ± 0.5) TBS-DBS ($U = 44.00$, $Z = -2.655$, $p = 0.012$), and a close to significance level difference of toe tapping between unilateral (1.1 ± 0.9) and bilateral (1.7 ± 0.6) TBS-DBS ($U = 56.50$, $Z = 0.000$, $p = 0.055$). Other lateralized MDS-UPDRS subitems were not significantly different between unilateral and bilateral TBS-DBS.

Discussion

In this single-center analysis, we showed that short-term application of bilateral TBS-DBS was safe and efficient. Bilateral TBS-DBS revealed slight, but not significant, additional beneficial effects on the total lateralized motor sum scores compared to unilateral TBS-DBS, and a significantly better improvement of the specific MDS-UPDRS III subitem rigidity of the lower limb. Of note, there was no increased rate of adverse events or constraint symptom improvement with bilateral TBS-DBS compared to unilateral TBS-DBS.

Further results of bilateral TBS-DBS in humans are scarce. Sáenz-Farret et al. demonstrated TBS-DBS to improve slightly gait in a minor subgroup of STN-DBS patients with refractory axial symptoms (Sáenz-Farret et al., 2021). Our short-term results also revealed a particular benefit of bilateral TBS-DBS on the subitem rigidity of the lower limbs. Still, long-term effects of TBS-DBS on axial symptoms and gait need to be assessed. On the one hand, PD symptom responsiveness is time-dependent with axial symptoms responding after hours (Herrington et al., 2016) whereas in our experiment, lower limb symptoms were assessed only with inter-trial intervals of 30 min. On the other hand, we suppose TBS-DBS to develop its full clinical

TABLE 2 Results of the calculated lateralized MDS-UPDRS III sum scores, lower extremity (LE) rigidity and toe tapping scores of the three different conditions compared are shown.

Cohort	Condition	Item							Percentile	
			N	Min	Max	M	SD	MD	25	75
Unilateral	OFF	Sum Score	17	7	23	15.76	4.92	17	12	19.5
		Rigidity LE	17	0	3	1.71	0.92	2	1.5	2
		Toe Tapping	17	0	4	1.35	1.32	1	0	2.5
	cDBS	Sum Score	17	2	16	10.59	4.57	11	7	15
		Rigidity LE	17	0	2	1.06	0.82	1	0	1
		Toe Tapping	17	0	2	0.82	0.72	1	0	1
	TBS	Sum Score	17	4	20	12.76	5.02	14	9	17
		Rigidity LE	17	0	2	1.29	0.69	1	1	2
		Toe Tapping	17	0	3	1.12	0.86	1	0.5	2
Bilateral	OFF	Sum Score	11	13	25	16.73	3.72	17	13	18
		Rigidity LE	11	0	2	1.09	0.83	1	0	2
		Toe Tapping	11	1	3	1.91	0.70	2	1	2
	cDBS	Sum Score	11	5	20	11.82	5.02	12	6	16
		Rigidity LE	11	0	2	0.55	0.68	0	0	1
		Toe Tapping	11	0	2	1.45	0.68	2	1	2
	TBS	Sum Score	11	7	24	12.45	5.36	12	7	16
		Rigidity LE	11	0	1	0.45	0.52	0	0	1
		Toe Tapping	11	1	3	1.73	0.65	2	1	2

N, number; Min, Minimum; Max, Maximum; M, Mean; MD, Median; SD, Standard Deviation; 25th and 75th percentiles are given. OFF, stimulation OFF; cDBS, conventional DBS; TBS, Theta Burst Stimulation.

efficacy after longer application due to potential neuroplastic effects of intermittent stimulation (Horn et al., 2020) as it has been demonstrated for non-invasive theta burst transcranial magnetic stimulation in humans (Huang et al., 2007; Suppa et al., 2016). We hypothesize therefore that bilateral TBS-DBS might be also beneficial for axial symptoms. However, long-term effects need to be assessed with chronic TBS-DBS in PD patients.

From previous clinical and neurophysiological studies of conventional STN-DBS in PD, there were different, interhemispheric findings. *Clinically*, there was evidence of synonymous, contra- and ipsilateral 15–28% motor improvement after 3–18 months with unilateral STN-DBS surgery (Kumar et al., 1999; Slowinski et al., 2007; Walker et al., 2009) and axial improvement of 19–39% (Kumar et al., 1999; Germano et al., 2004; Chung et al., 2006; Slowinski et al., 2007; Castrioto et al., 2011). *Electrophysiological* evidence for interhemispheric, concordant basal ganglia crosstalk was provided by perioperative DBS electrode local field potential (LFP) recordings. The STN of one hemisphere was involved in the preparation of both ipsilateral and contralateral hand movements in PD patients (Paradiso et al., 2003). Intraoperative, unilateral, high-frequency electrical STN stimulation induced and suppressed tremor in both forearms in a frequency-dependent manner, accompanied by bilateral, subthalamic, oscillatory local field potential changes (Liu et al., 2002). Unilateral STN-DBS suppressed contralateral STN beta LFPs (Hasegawa et al., 2020). In the animal model, neural subthalamic single unit firing rates were decreased bilaterally after unilateral STN-DBS in dopamine-depleted rats, indicating cross-talk between bilateral STN neurons (Shi et al., 2006). Those bilateral STN-DBS effects might be mediated by anatomical, interhemispheric projections at different levels. There are bilateral basal ganglia connections through interhemispheric pallidothalamic and pallidotegmental projections (Hazrati and Parent, 1991), bilateral, reciprocal STN connections to the brainstem pedunculopontine nucleus (Hammond et al., 1983) and bilateral cortico-striatal pathways (Wilson, 1986). Thus conventional, bilateral conventional STN-DBS might be more advantageous than unilateral STN-DBS. There was evidence of greater motor improvement of one body side with bilateral than with unilateral stimulation of the contralateral STN (Kumar et al., 1999; Samii et al., 2007). Levodopa dosages were decreased to a smaller extent by 15–19% after unilateral compared to bilateral STN-DBS (Germano et al., 2004; Chung et al., 2006). A two-year long-term observation of initially highly asymmetric PD patients revealed a 42% worsening of ipsilateral PD symptoms in the postoperative course with the need to re-increase levodopa and finally to consider all patients for second-side surgery (Kim et al., 2009). In our short-term observation, we observed only minor additive effects on lower limb rigidity of bilateral TBS-DBS compared to unilateral TBS-DBS.

There are several limitations of this study. First, the sample sizes of the two cohorts were relatively small, but comparable to other DBS studies using patterned stimulation (Adamchic et al., 2014; Akbar et al., 2016; Horn et al., 2020; Sáenz-Farret et al., 2021). Second, we assessed intersubject differences in two different cohorts and no intrasubject unilateral TBS. The clinical characteristics of the two cohorts, however, were fairly similar and not significantly different so that we still consider the comparison of TBS-DBS modes in the two cohorts reasonable. Besides, the inter-trial waiting period of 30 min might be too short to exclude DBS outlasting effects. However in previous experiments with unilateral TBS-DBS trains, there were no clinical stimulation-outlasting effects after 30 min (Horn et al., 2020), so that we assume this time period to be adequate. Another limitation in the use of TBS-DBS is the lack of knowledge of what amplitude size needs to be applied. Adjustment along the TEED might be one way, but might be of limited value in complex DBS patterns.

In summary, we demonstrated that short-term bilateral TBS-DBS with intraburst frequency of 200 Hz and interburst frequency of 5 Hz is safe and effective. In short-term observations, bilateral TBS-DBS is approximately at least equally effective on lateralized motor scores compared to unilateral TBS-DBS, with potentially additive beneficial effects on lower limb function as rigidity.

Data availability statement

The raw data supporting the conclusions of this article will be made available from the corresponding author upon reasonable request.

Ethics statement

The studies involving humans were approved by Ethikkommission Ärztekammer Hamburg, Germany. The studies were conducted in accordance with the local legislation and institutional requirements. The participants provided their written informed consent to participate in this study.

Author contributions

EG: analysis, writing, and editing of the final version of the manuscript. MH and JC: execution of the study, analysis, and editing of final version of the manuscript. WH: DBS surgery and editing of final version of the manuscript. CM: editing of final version of the manuscript. AG: writing and editing of final version of the manuscript. MP-N: design of the study, supervision of analysis, writing, and editing of final version of the manuscript. All authors contributed to the article and approved the submitted version.

Funding

This study was funded by the Deutsche Forschungsgemeinschaft (DFG, German Research Foundation) – SFB 936 – 178316478 – C8 (MP-N and CM).

Conflict of interest

EG reports honoraria (Abbvie, Abbott, Medtronic, Bial, Grifols, Zambon, Weser GmbH, Kreiskrankenhaus Gummersbach, Thieme). MP-N received lecture fees from Abbott, Abbvie, Boston Scientific and served as consultant for Medtronic, Boston Scientific, Abbott, Zambon and Abbvie.

The remaining authors declare that the research was conducted in the absence of any commercial or financial relationships that could be construed as a potential conflict of interest.

Publisher's note

References

Adamchic, I., Hauptmann, C., Barnikol, U. B., Pawelczyk, N., Popovych, O., Barnikol, T. T., et al. (2014). Coordinated reset neuromodulation for Parkinson's disease: proof-of-concept study. *Mov. Disord.* 29, 1679–1684. doi: 10.1002/mds.25923

Akbar, U., Raike, R. S., Hack, N., Hess, C. W., Skinner, J., Martinez-Ramirez, D., et al. (2016). Randomized, blinded pilot testing of nonconventional stimulation patterns and shapes in Parkinson's disease and essential tremor: evidence for further evaluating narrow and biphasic pulses. *Neuromodulation* 19, 343–356. doi: 10.1111/ner.12397

Arai, N., Yokochi, F., Ohnishi, T., Momose, T., Okiyama, R., Taniguchi, M., et al. (2008). Mechanisms of unilateral STN-DBS in patients with Parkinson's disease: a PET study. *J. Neurol.* 255, 1236–1243. doi: 10.1007/s00415-008-0906-7

Castrioto, A., Meaney, C., Hamani, C., Mazzella, F., Poon, Y. Y., Lozano, A. M., et al. (2011). The dominant-STN phenomenon in bilateral STN DBS for Parkinson's disease. *Neurobiol. Dis.* 41, 131–137. doi: 10.1016/j.nbd.2010.08.029

Chung, S. J., Jeon, S. R., Kim, S. R., Sung, Y. H., and Lee, M. C. (2006). Bilateral effects of unilateral subthalamic nucleus deep brain stimulation in advanced Parkinson's disease. *Eur. Neurol.* 56, 127–132. doi: 10.1159/000095704

Defer, G. L., Widner, H., Marie, R. M., Remy, P., and Levivier, M. (1999). Core assessment program for surgical interventional therapies in Parkinson's disease (CAPSIT-PD). *Mov. Disord.* 14, 572–584. doi: 10.1002/1531-8257(199907)14:4<572::AID-MDS1005>3.0.CO;2-C

Deuschl, G., Herzog, J., Kleiner-Fisman, G., Kubu, C., Lozano, A. M., Lyons, K. E., et al. (2006). Deep brain stimulation: postoperative issues. *Mov. Disord.* 21, S219–S237. doi: 10.1002/mds.20957

Germano, I. M., Gracies, J. M., Weisz, D. J., Tse, W., Koller, W. C., and Olanow, C. W. (2004). Unilateral stimulation of the subthalamic nucleus in Parkinson disease: a double-blind 12-month evaluation study. *J. Neurosurg.* 101, 36–42. doi: 10.3171/jns.2004.101.1.0036

Hammond, C., Rouzaire-Dubois, B., Feger, J., Jackson, A., and Crossman, A. R. (1983). Anatomical and electrophysiological studies on the reciprocal projections between the subthalamic nucleus and nucleus tegmenti pedunculopontinus in the rat. *Neuroscience* 9, 41–52. doi: 10.1016/0306-4522(83)90045-3

Hasegawa, H., Fischer, P., Tan, H., Pogosyan, A., Samuel, M., Brown, P., et al. (2020). The effect of unilateral subthalamic nucleus deep brain stimulation on contralateral subthalamic nucleus local field potentials. *Neuromodulation* 23, 509–514. doi: 10.1111/ner.13155

Hazrati, L. N., and Parent, A. (1991). Contralateral pallidothalamic and pallidotegmental projections in primates: an anterograde and retrograde labeling study. *Brain Res.* 567, 212–223. doi: 10.1016/0006-8993(91)90798-Z

Herrington, T. M., Cheng, J. J., and Eskandar, E. N. (2016). Mechanisms of deep brain stimulation. *J. Neurophysiol.* 115, 19–38. doi: 10.1152/jn.00281.2015

Horn, M. A., Gulberti, A., Gülke, E., Buhmann, C., Gerloff, C., Moll, C. K. E., et al. (2020). A new stimulation mode for deep brain stimulation in Parkinson's disease: Theta burst stimulation. *Mov. Disord.* 35, 1471–1475. doi: 10.1002/mds.28083

Huang, Y. Z., Chen, R. S., Rothwell, J. C., and Wen, H. Y. (2007). The after-effect of human theta burst stimulation is NMDA receptor dependent. *Clin. Neurophysiol.* 118, 1028–1032. doi: 10.1016/j.clinph.2007.01.021

Huang, Y. Z., Edwards, M. J., Rounis, E., Bhatia, K. P., and Rothwell, J. C. (2005). Theta burst stimulation of the human motor cortex. *Neuron* 45, 201–206. doi: 10.1016/j.neuron.2004.12.033

Kim, H. J., Paek, S. H., Kim, J. Y., Lee, J. Y., Lim, Y. H., Kim, D. G., et al. (2009). Two-year follow-up on the effect of unilateral subthalamic deep brain stimulation in highly asymmetric Parkinson's disease. *Mov. Disord.* 24, 329–335. doi: 10.1002/mds.22211

Kumar, R., Lozano, A. M., Sime, E., Halket, E., and Lang, A. E. (1999). Comparative effects of unilateral and bilateral subthalamic nucleus deep brain stimulation. *Neurology* 53, 561–566. doi: 10.1212/WNL.53.3.561

Liu, X., Ford-Dunn, H. L., Hayward, G. N., Nandi, D., Miall, R. C., Aziz, T. Z., et al. (2002). The oscillatory activity in the parkinsonian subthalamic nucleus investigated using the macro-electrodes for deep brain stimulation. *Clin. Neurophysiol.* 113, 1667–1672. doi: 10.1016/S1388-2457(02)00256-0

Nakajima, A., Shimo, Y., Uka, T., and Hattori, N. (2017). Subthalamic nucleus and globus pallidus interna influence firing of tonically active neurons in the primate striatum through different mechanisms. *Eur. J. Neurosci.* 46, 2662–2673. doi: 10.1111/ejn.13726

Paradiso, G., Saint-Cyr, J. A., Lozano, A. M., Lang, A. E., and Chen, R. (2003). Involvement of the human subthalamic nucleus in movement preparation. *Neurology* 61, 1538–1545. doi: 10.1212/01.WNL.0000096021.28967.57

Sáenz-Farret, M., Loh, A., Boutet, A., Germann, J., Elias, G. J. B., Kalia, S. K., et al. (2021). Theta burst deep brain stimulation in movement disorders. *Movement Disord. Clin. Prac.* 8, 282–285. doi: 10.1002/mdc3.13130

Samii, A., Kelly, V. E., Slimp, J. C., Shumway-Cook, A., and Goodkin, R. (2007). Staged unilateral versus bilateral subthalamic nucleus stimulator implantation in Parkinson disease. *Mov. Disord.* 22, 1476–1481. doi: 10.1002/mds.21554

Schuepbach, W. M., Rau, J., Knudsen, K., Volkmann, J., Krack, P., Timmermann, L., et al. (2013). Neurostimulation for Parkinson's disease with early motor complications. *N. Engl. J. Med.* 368, 610–622. doi: 10.1056/NEJMoa1205158

Shi, L. H., Luo, F., Woodward, D. J., and Chang, J. Y. (2006). Basal ganglia neural responses during behaviorally effective deep brain stimulation of the subthalamic nucleus in rats performing a treadmill locomotion test. *Synapse* 59, 445–457. doi: 10.1002/syn.20261

Slowinski, J. L., Putzke, J. D., Uitti, R. J., Lucas, J. A., Turk, M. F., Kall, B. A., et al. (2007). Unilateral deep brain stimulation of the subthalamic nucleus for Parkinson disease. *J. Neurosurg.* 106, 626–632. doi: 10.3171/jns.2007.106.4.626

Suppa, A., Huang, Y. Z., Funke, K., Ridding, M. C., Cheeran, B., Di Lazzaro, V., et al. (2016). Ten years of Theta burst stimulation in humans: established knowledge, unknowns and prospects. *Brain Stimul* 9, 323–335. doi: 10.1016/j.brs.2016.01.006

Sweet, J. A., Eakin, K. C., Munyon, C. N., and Miller, J. P. (2014). Improved learning and memory with theta-burst stimulation of the fornix in rat model of traumatic brain injury. *Hippocampus* 24, 1592–1600. doi: 10.1002/hipo.22338

Walker, H. C., Watts, R. L., Guthrie, S., Wang, D., and Guthrie, B. L. (2009). Bilateral effects of unilateral subthalamic deep brain stimulation on Parkinson's disease at 1 year. *Neurosurgery* 65, 302–310. doi: 10.1227/01.NEU.0000349764.34211.74

Wilson, C. J. (1986). Postsynaptic potentials evoked in spiny neostriatal projection neurons by stimulation of ipsilateral and contralateral neocortex. *Brain Res.* 367, 201–213. doi: 10.1016/0006-8993(86)91593-3

frontiers | Frontiers in Human Neuroscience

TYPE Case Report
PUBLISHED 22 February 2024
DOI 10.3389/fnhum.2024.1297683

OPEN ACCESS

EDITED BY
Peter A. Tass,
Stanford University, United States

REVIEWED BY
Nada Yousif,
University of Hertfordshire, United Kingdom
Mojtaba Madadi Asl,
Institute for Research in Fundamental Sciences (IPM), Iran

*CORRESPONDENCE
Satoko Koganemaru
✉ kogane@kuhp.kyoto-u.ac.jp

RECEIVED 20 September 2023
ACCEPTED 31 January 2024
PUBLISHED 22 February 2024

CITATION
Omae E, Shima A, Tanaka K, Yamada M, Cao Y, Nakamura T, Hoshiai H, Chiba Y, Irisawa H, Mizushima T, Mima T and Koganemaru S (2024) Case report: An N-of-1 study using amplitude modulated transcranial alternating current stimulation between Broca's area and the right homotopic area to improve post-stroke aphasia with increased inter-regional synchrony.
Front. Hum. Neurosci. 18:1297683.
doi: 10.3389/fnhum.2024.1297683

Case report: An N-of-1 study using amplitude modulated transcranial alternating current stimulation between Broca's area and the right homotopic area to improve post-stroke aphasia with increased inter-regional synchrony

Erika Omae[1,2], Atsushi Shima[1], Kazuki Tanaka[1], Masako Yamada[1], Yedi Cao[1], Tomoyuki Nakamura[3], Hajime Hoshiai[3], Yumi Chiba[3], Hiroshi Irisawa[3], Takashi Mizushima[3], Tatsuya Mima[4] and Satoko Koganemaru[1,5]*

[1]Department of Regenerative Systems Neuroscience, Human Brain Research Center, Graduate School of Medicine, Kyoto University, Kyoto, Japan, [2]Department of Neurobiology and Physiology, Graduate School of Medicine, Kyoto University, Kyoto, Japan, [3]Department of Rehabilitation Medicine, Dokkyo Medical University, Tochigi, Japan, [4]The Graduate School of Core Ethics and Frontier Sciences, Ritsumeikan University, Kyoto, Japan, [5]Department of Rehabilitation Medicine, Hokkaido University Hospital, Sapporo, Japan

Over one-third of stroke survivors develop aphasia, and language dysfunction persists for the remainder of their lives. Brain language network changes in patients with aphasia. Recently, it has been reported that phase synchrony within a low beta-band (14–19 Hz) frequency between Broca's area and the homotopic region of the right hemisphere is positively correlated with language function in patients with subacute post-stroke aphasia, suggesting that synchrony is important for language recovery. Here, we employed amplitude-modulated transcranial alternating current stimulation (AM-tACS) to enhance synchrony within the low beta band frequency between Broca's area and the right homotopic area, and to improve language function in a case of chronic post-stroke aphasia. According to an N-of-1 study design, the patient underwent short-term intervention with a one-time intervention of 15 Hz-AM-tACS with Broca's and the right homotopic areas (real condition), sham stimulation (sham condition), and 15 Hz-AM-tACS with Broca's and the left parietal areas (control condition) and long-term intervention with sham and real conditions (10 sessions in total, each). In the short-term intervention, the reaction time and accuracy rate of the naming task improved after real condition, not after sham and control conditions. The synchrony between the stimulated areas evaluated by coherence largely increased after the real condition. In the long-term intervention, naming ability, verbal fluency and overall language function improved, with the increase in the synchrony, and those improvements were sustained for more than a month

after real condition. This suggests that AM-tACS on Broca's area and the right homotopic areas may be a promising therapeutic approach for patients with poststroke aphasia.

KEYWORDS

transcranial alternating current stimulation, amplitude modulation, aphasia, stroke, coherence

1 Introduction

More than one-third of stroke survivors experience aphasia with a poor prognosis. Furthermore, 30%−43% of them show persistent severe symptoms for more than 1 year after stroke onset (Bakheit et al., 2007). Their impairments include comprehension and expression of speech, reading, and writing (Brady et al., 2016), which can decrease social activities and cause them to become isolated and depressed, reducing their quality of life (Doogan et al., 2018). Speech and language therapy (SLT) has been widely implemented and recommended for treating aphasia for over half a century (Chapey, 2008). However, SLT shows moderate effects, even when administered at high intensity, depending on individual symptoms (Brady et al., 2016; Breitenstein et al., 2017). A novel strategy has been sought to achieve a greater therapeutic effect in aphasia.

Previous neuroimaging studies have shown that the right hemisphere facilitates language recovery, possibly by releasing interhemispheric inhibition from the damaged left hemisphere during recovery from post-stroke aphasia (Hamilton et al., 2011). Recently, it was reported that phase synchrony within the low beta-band (14–19 Hz) frequency between Broca's area and the homotopic region of the right hemisphere is positively correlated with language function in subacute post-stroke aphasia (Kawano et al., 2021). We hypothesized that enhancing synchrony within the low beta-band frequency between Broca's area and the homotopic region of the right hemisphere could improve the language neural network and language function in post-stroke aphasia. Transcranial alternating current stimulation (tACS) is a noninvasive brain stimulation (NIBS) method that uses sinusoidal alternating electric currents to affect cortical oscillatory neuronal activity. tACS synchronizes brain oscillations, induces long-term synaptic plasticity, and promotes functional recovery in patients with neurological diseases (Fröhlich and McCormick, 2010; Ozen et al., 2010; Reato et al., 2010; Ali et al., 2013; Koganemaru et al., 2018, 2019, 2020; Negahbani et al., 2018; Nojima et al., 2023; Shima et al., 2023a,b).

Recently, amplitude-modulated tACS (AM-tACS) was developed (Witkowski et al., 2016; Negahbani et al., 2018). It has two components of stimulation waveforms: high-frequency (>100 Hz) sinusoidal carrier frequency and low-frequency (e.g., 10–15 Hz) amplitude modulation as the envelope. Low-frequency amplitude modulation has been reported to modulate neuronal oscillations as well as low-frequency tACS (Chander et al., 2016; Witkowski et al., 2016; Minami and Amano, 2017; Esmaeilpour et al., 2021). Furthermore, the amplitude modulation phase almost coincides between the two stimulated regions when using the two electrodes, suggesting that it would help enhance inter-regional brain synchrony. While the use of beta band tACS has been limited due to phosphene induction, AM-tACS does not induce phosphenes, according to previous reports (Chander et al., 2016; Minami and Amano, 2017). Therefore, we used AM-tACS to enhance the synchrony between Broca's area and the homotopic region of the right hemisphere. We systematically compared the short- and long-term effects in a patient with chronic post-stroke aphasia according to an N-of-1 study design.

TABLE 1 Clinical course of the case.

Months	Clinical findings
0	Admission to the hospital for acute onset of difficulty in walking followed by aphasia and right hemiparesis • Magnetic resonance imaging (MRI) revealed acute cerebral infarction at the territory of the left middle cerebral artery
1.5	Transferred to the rehabilitation hospital
3	Discharged from the hospital • Aphasia remained • Right hemiparesis recovered
87	Participated in the study

2 Case description

2.1 Patient characteristics

A 76-year-old man with nonfluent aphasia due to left cerebral infarction was referred to Kyoto University Hospital. At the age of 69 years, he was admitted to the hospital with acute onset of nonfluent aphasia with right mild hemiparesis. Head magnetic resonance imaging (MRI) revealed left cerebral infarction in the territory of left middle cerebral artery, including the left operculum (Table 1). His medical history included myocardial infarction and diabetes mellitus.

2.2 Therapeutic intervention

We conducted three types of interventions to examine the effect of AM-tACS according to an N-of-1 study design: (1) AM-tACS with 120 Hz frequency of sinusoidal carrier waves with 15 Hz of sinusoidal amplitude modulation, a peak-to-peak amplitude of 3 mA (−1.5–1.5 mA) and trough amplitudes of ± 0.3 mA (Figure 1A) on the Broca's area [centering the 5×5 cm^2 electrode on F7 according to the international 10–20 electroencephalography (EEG) system] and on the homotopic

region of the right hemisphere (centering the 5×5 cm^2 electrode on F8; real condition), (2) sham AM-tACS with only 10 cycles of 15 Hz amplitude modulation of AM-tACS given on the same regions with the real condition (sham condition), and (3) AM-tACS with the Broca's area and the left parietal area using the same stimulation parameter with the real condition (control condition) by using Nurostym tES (Neuro Device Group S.A., Warsaw, Poland; Figure 1B). The stimulation sites were confirmed using a neuronavigation system with the patient's head MRI (Brainsight Brainbox Ltd., Cardiff, UK). For the short-term intervention, one-time sessions of sham, real, and control conditions were performed. Each stimulation was applied for 20 min and combined with a 20-min language training session including a naming task, different from that used in the evaluation. The interval between sessions was over 1 h, and the control condition was performed 1 day after the real and sham conditions because of patient fatigue (Figure 1C). For the long-term intervention, we performed 10 sessions of sham and real conditions (one session per day, 2 days per week for 5 weeks) with the interval of 1 month (Figure 1D).

3 Assessments

3.1 Clinical measurements

During the short-term intervention, clinical evaluations were performed before and immediately after one session of each condition (pre- and post-intervention, respectively). During the long-term intervention, they were performed before, within 1 week after, and 1 month after the total 10 sessions of each condition (pre, post0, and post1, respectively). The assessment of language function included the reaction time and accuracy rate of a naming task in a short-term intervention. The patient was asked to name as immediately the 12 line drawings extracted from the Snodgrass and Nishimoto pictures (Snodgrass and Vanderwart, 1980; Nishimoto et al., 2005) shown on a 27-inch monitor in front of him as possible. The sets of line drawings were different in each condition to prevent learning effects, while they were selected with almost the same degree of familiarity and number of morae. In the long-term intervention, we evaluated the reaction time and accuracy rate of the naming task, verbal fluency, aphasia quotient of the Western Aphasia Battery (WAB) (Kertesz, 1982). The aphasia quotient is a composite score indicated by the percentile, which provides an overall measure of aphasia severity, in which lower scores denote more severe aphasia (the maximal score is 100) and visual analog scale (VAS) for the patient's subjective assessment of the general language function (score was determined by the distance on the 10 cm line; "0" indicated the worst condition and "10" indicated the best condition). The naming task comprised 24 line drawings extracted from Snodgrass and Nishimoto's pictures. The reaction time was measured by the time interval from the onset time of the drawing on the monitor to the time for him to name it by using the video-recording (60 fps). In the verbal fluency task, the patient was asked to name as many items that begin with a certain letter of the Japanese syllabary characters, "Hiragana" [the sound of "Ka (kʌ)" and "A (ʌ)" in the sham and real conditions, respectively] and as various items of a given semantic category ("vegetables" and "vehicles" in the sham and real conditions, respectively) as possible. The number of named items was scored for each character and category. All the clinical evaluations were double-blinded.

3.2 Electroencephalography recording

We recorded EEG signals and measured the coherence within the stimulated areas to evaluate interhemispheric synchrony in the language network. The patients were seated comfortably in an armchair. The EEG signals were recorded using 64 electrodes by eegoTM sports (ANT Neuro, Hengelo, Netherlands) during 3-min resting with eyes open. EEG signals were amplified using an Eego sports amplifier. Electrodes M1 and M2 were selected as references (Kawano et al., 2021). The impedance of all the electrodes was <15 $k\Omega$. The data were recorded and saved at a sampling rate of 2 kHz.

3.3 Data analysis

3.3.1 Preprocessing

We removed artifacts of the blink, electrooculographic activities, and muscle activities from the EEG signals using independent component analysis (ICA) (Hyvärinen and Oja, 2000) with the EEGLAB MATLAB toolbox including the artifact subspace reconstruction method, which detects the time windows of signals with significant artifacts (Pedroni et al., 2019), and "ICLabel," which automatically distinguishes independent components (ICs) as brain or non-brain sources according to a large number of crowd-sourced IC labels (Pion-Tonachini et al., 2019).

3.3.2 Coherence between Broca's area and the right homotopic area

We then calculated the power spectral density of the EEG using a fast Fourier transform (FFT). We applied the FFT to 1,000 ms segments with a 50 ms time shift. The evaluated frequency range was 5–40 Hz. For the coherence analysis, using FFT, we computed the cross- and auto-spectra in the frequency domain of the EEG signals within a frequency range of 14–16 Hz in Broca's area (F7) and the right homotopic area, including AF8, F6, FC6, F8, and FT8, which were stimulated by AM-tACS. Coherence is defined as cross-spectra normalized by auto-spectra. It is expressed by the following equation (1), where $f_{xx}(j)$, $f_{yy}(j)$, and $|f_{xy}(j)|$ denote the auto-spectra and cross-spectra at frequency j (Mima et al., 2001).

$$|R_{xy}(j)|^2 = \frac{|f_{xy}(j)|^2}{f_{xx}(j)f_{yy}(j)} \quad (1)$$

To stabilize the variance, we applied an arc hyperbolic tangent transformation to the coherence according to the following equation (2):

$$\tanh^{-1}|R_{xy}(j)| = \frac{1}{2}\ln\left(\frac{1+|R_{xy}(j)|}{1-|R_{xy}(j)|}\right) \quad (2)$$

The average of the arc hyperbolic tangents transforming the coherences of F7 with AF8, F6, FC6, F8, and FT8 was calculated as an index of synchrony.

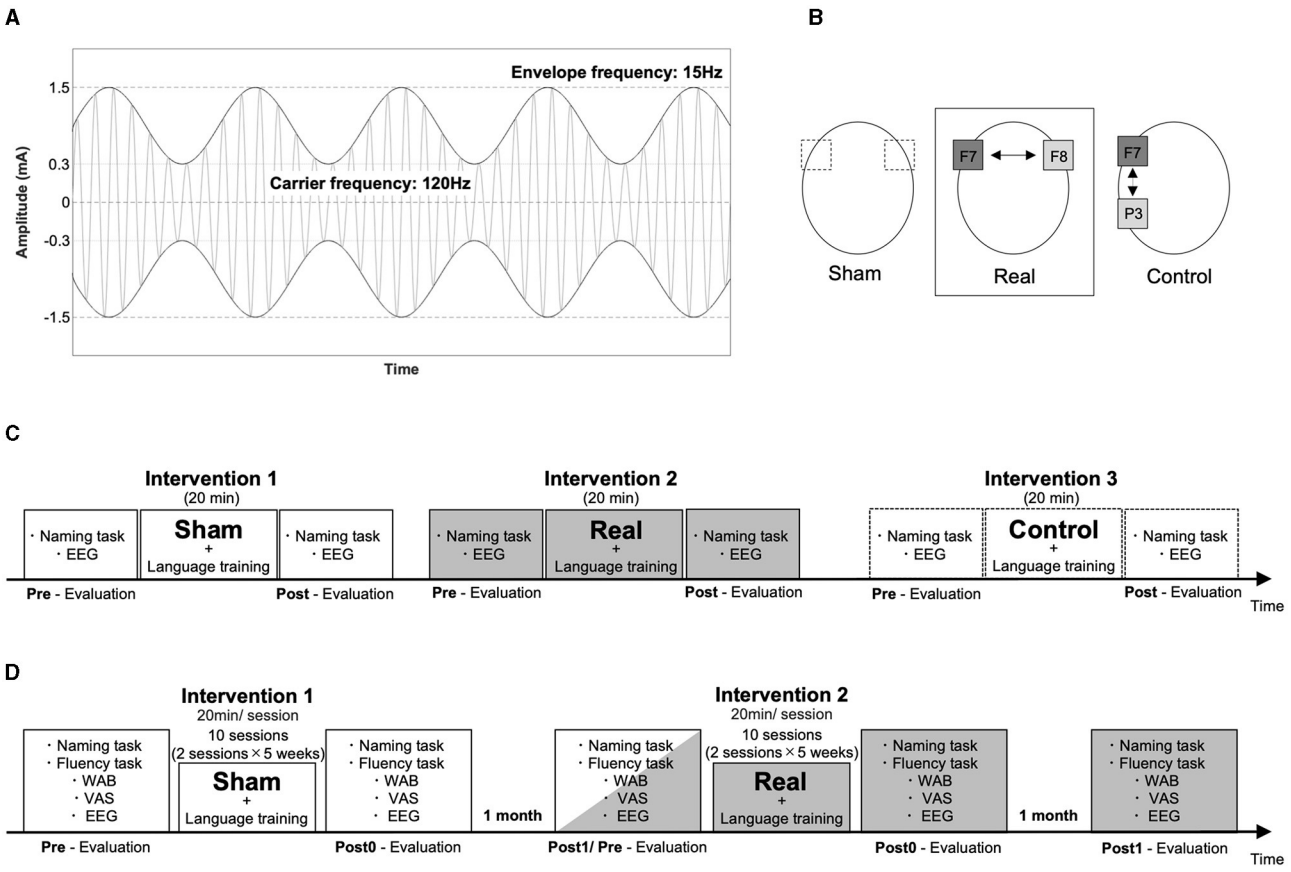

FIGURE 1
Experimental setup. The stimulator output signal during AM-tACS is illustrated with amplitude of a carrier signal (120 Hz) modulated at 15 Hz of a signal envelope **(A)**. The electrodes (5 × 5 cm) were placed on F7 and F8 in the sham and real conditions, and on F7 and P5 in the control condition **(B)**. The order of the interventions is illustrated in the short-term and long-term interventions **(C, D)**.

4 Results

No adverse or unanticipated events developed during the short- or long-term interventions. The patient did not experience sensations like phosphenes, cutaneous irritation, or pain.

4.1 Short-term intervention

For the naming task, the reaction time was shortened (Figure 2A), and the accuracy rate improved after the real condition (Figure 2B). The recorded EEG signals in each condition were shown in the Figure 2C. The synchrony between Broca's area and the right homotopic area largely increased after the real but not after the sham and control conditions (Figures 2D, E).

4.2 Long-term intervention

We found improvements in language functions evaluated using naming (Figure 3A), verbal fluency tasks (Figures 3B, C), and the aphasia quotient of the WAB (Figure 3D) after the real condition, but not after the sham condition. The VAS scores also improved after real condition (Figure 3E). The recorded EEG signals in each condition were shown in the Figure 3F. All clinical improvements were sustained for a month after the real condition. In addition, we found that synchrony increased and sustained for a month after the real condition (Figures 3G, H).

5 Discussion

The present case demonstrates the potential therapeutic effect of 15 Hz AM-tACS on Broca's area and the homotopic region of the right hemisphere combined with SLT. The short-term evaluation showed that it was effective in improving naming ability along with enhancing synchrony between the stimulated areas. In contrast, sham- or AM-tACS on Broca's area and the left parietal area did not improve them. The long-term intervention showed sustained improvements in general language function evaluated using WAB, naming ability, verbal fluency, and subjective assessment of language function, along with increased synchrony between Broca's area and the homotopic region of the right hemisphere.

Although right hemisphere recruitment may be insufficient for overall language recovery, it may facilitate recovery by releasing

10.3389/fnhum.2024.1297683

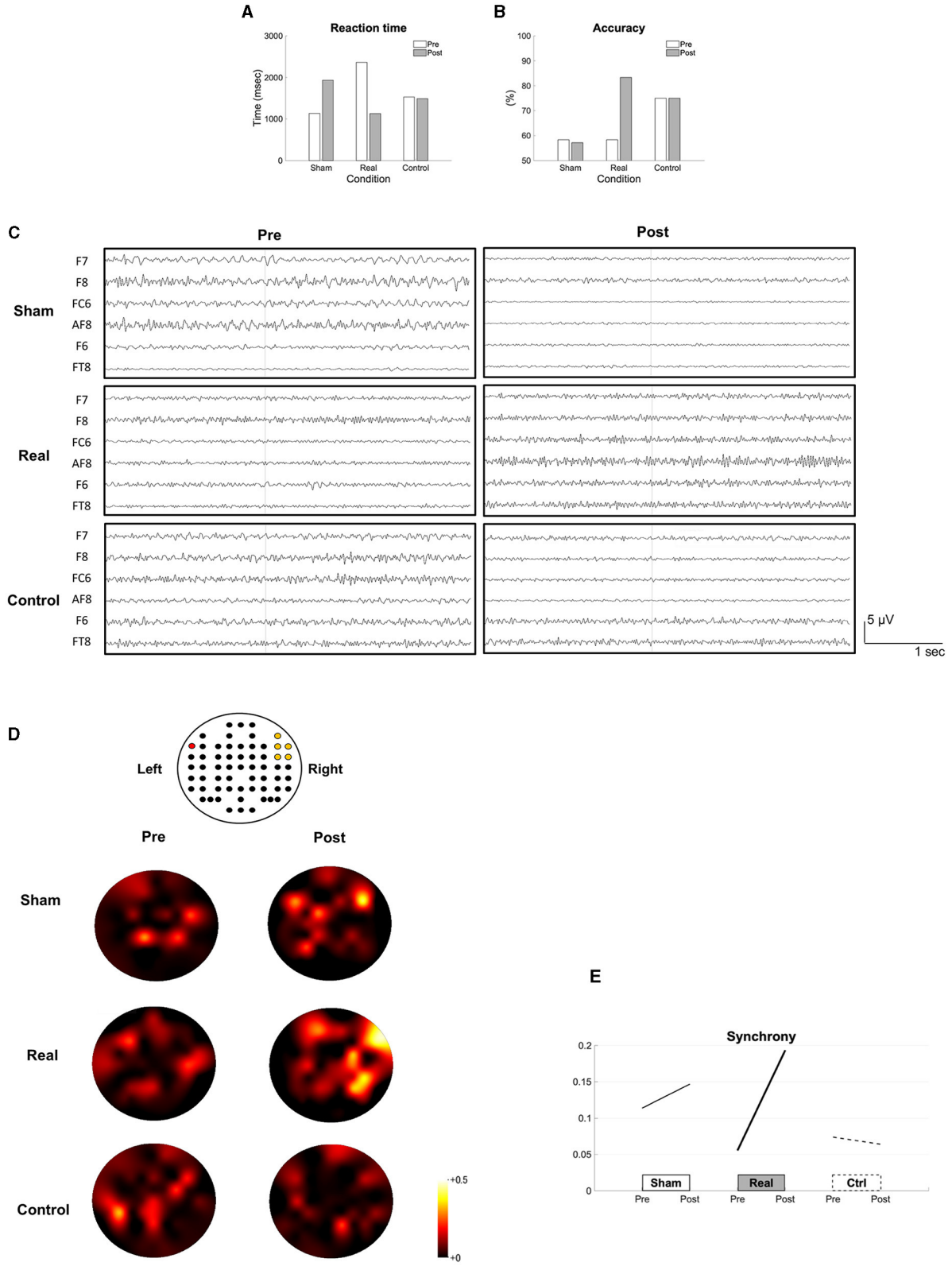

FIGURE 2
Results of the short-term intervention. The reaction time **(A)**, the accuracy rate **(B)** in the naming task, the recorded EEG data **(C)**, the topomaps of the arc hyperboric tangent of the coherence **(D)** and the synchrony **(E)** are shown before (pre) and after each intervention (post). The EEG channel location (62 channels excluding M1 and M2) is illustrated above the topomaps. The red colored channel is F7 and the yellow colored channels are AF8, F6, F8, FC6, and FT8 from top to bottom, and left to right **(D)**. The synchrony between the Broca's and the right homotopic areas is indicated by the average of the arc hyperbolic tangents transformation applied to the coherences between F7 and AF8, F7-F6, F7-FC6, F7-F8, and F7-FT8 **(E)**.

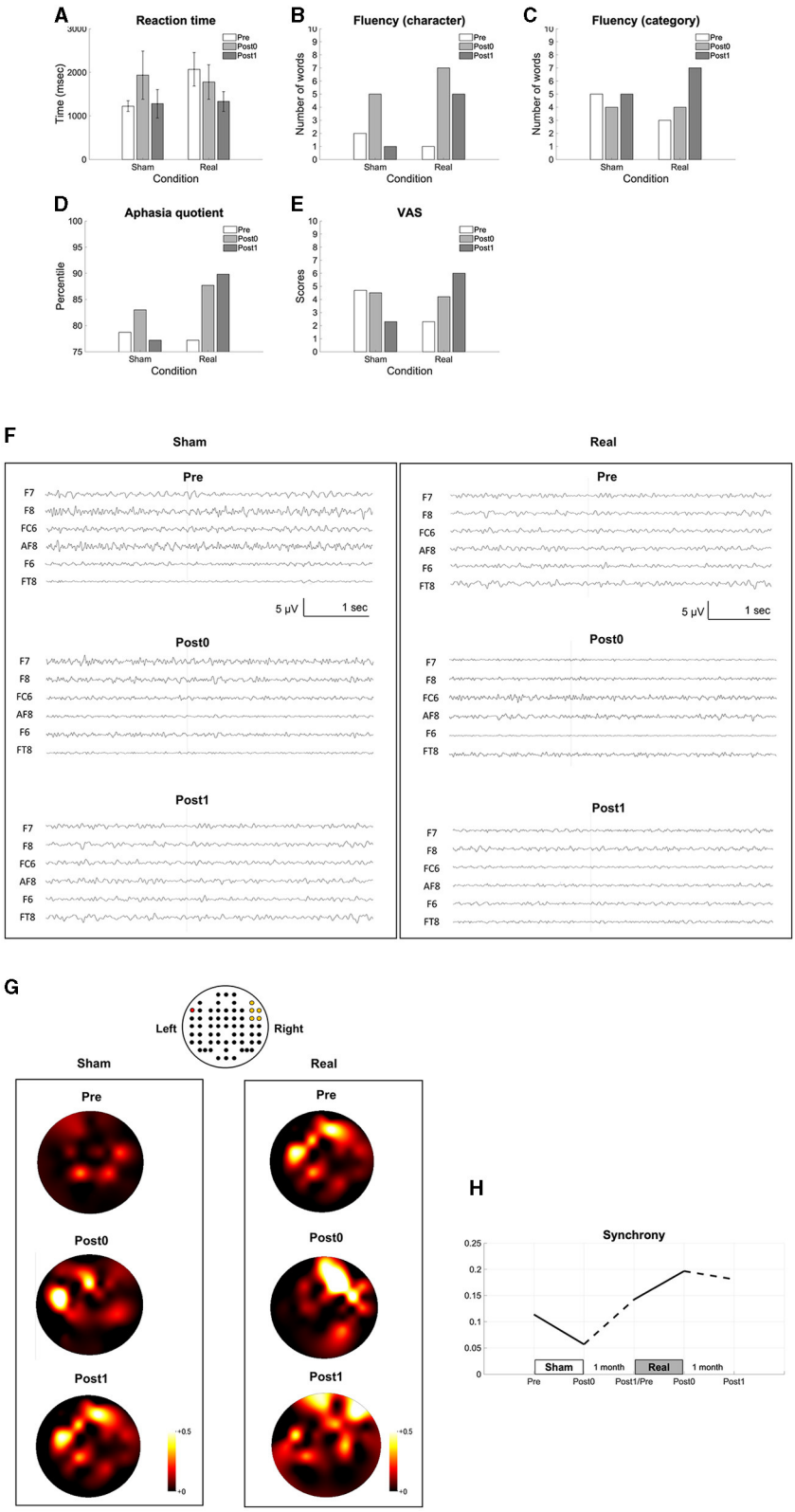

FIGURE 3
Results of the long-term intervention. The reaction time in the naming task **(A)**, the number of words in the verbal fluency task **(B, C)**, the aphasia quotient **(D)**, VAS **(E)**, the recorded EEG data **(F)**, the topomaps of the arc hyperboric tangent of the coherence **(G)** and the synchrony between the Broca's and the right homotopic areas indicated by the averaged arc hyperbolic tangents transformation applied to the coherences between F7 and AF8, F7-F6, F7-FC6, F7–F8, and F7–FT8 **(H)** are shown before (pre), within a week after (post0), and 1 month after the intervention (post1). The EEG channel location is illustrated above the topomaps in the same way as in Figure 2 **(G)**.

interhemispheric inhibition from the damaged left hemisphere (Hamilton et al., 2011). As for oscillatory brain activity, the overall connectivity of Broca's area at beta oscillation frequencies correlates with future clinical improvement in patients with aphasia (Nicolo et al., 2015). During a sentence completion task, increased power in the right hemisphere was observed within a low beta-band frequency compared with that in the left hemisphere in patients with chronic post-stroke aphasia (Lima et al., 2023). Synchrony within a low beta-band frequency between Broca's area and the homotopic region of the right hemisphere was decreased compared with that in healthy controls. It was positively correlated with language function in patients with subacute post-stroke aphasia (Kawano et al., 2021). These studies suggest that language function migrates to the non-language-dominant hemisphere in the recovery of language function and that the functional migration associated with language ability may be indicated, especially by low-beta interhemispheric oscillatory synchronization. Therefore, 15 Hz AM-tACS enabling phase-synchronized stimulation on the two given regions enhanced the synchrony within a low beta-band frequency between Broca's area and the homotopic region of the right hemisphere, suggesting that increased interhemispheric connectivity led to improved language function in this case. Further, 15 Hz AM-tACS on Broca's area and the left parietal area did not induce these effects, suggesting that enhancement of synchrony between Broca's area and the right homotopic region is important for language recovery.

Interhemispheric homotopic functional connectivity significantly decreases after stroke, and this decrease is strongly associated with behavioral impairment in post-stroke patients, including aphasia (Siegel et al., 2016). Furthermore, the longitudinal normalization of decreased interhemispheric functional connectivity is associated with clinical recovery (Carrera and Tononi, 2014). Therefore, enhanced interhemispheric synchrony associated with specific functions may be a potential therapeutic target for AM-tACS.

Our findings suggest that the combination of AM-tACS and SLT is appropriate. Combined with repetitive rehabilitation programs, NIBS can enhance functional recovery by inducing associative plasticity (Koganemaru et al., 2015). Although some studies on tDCS combined with SLT have shown language recovery in aphasia (Kang et al., 2011; You et al., 2011), the effects have been inconsistent. Thus, NIBS that targets specific functional networks would be more appropriate for inducing therapeutic effects.

In this case, the long-term intervention of repetitive sessions of SLT alone (sham condition) induced a partial improvement in language function within a week after the end of the intervention along with decreased inter-hemispheric synchrony. Further, these clinical improvements were not sustained for more than a month. This finding coincides with a previous report showing a limited effect of intensive SLT on chronic post-stroke aphasia (Breitenstein et al., 2017). In contrast, combining AM-tACS with SLT induced sustained improvement in language function for more than a month after the end of the intervention with increased inter-hemispheric synchrony. Thus, combining AM-tACS with SLT may induce long-lasting associative plasticity in the functional network required for sustained language recovery.

This case report provides a novel finding that a low-beta band frequency AM-tACS on Broca's area and the right homotopic area to enhance interhemispheric synchrony may be a promising rehabilitative approach to induce long-lasting improvement in language function in post-stroke aphasia. A further study with a larger number of patients would be necessary.

6 Patient perspective

The patient stated that he felt the improvement in fluency of words during daily conversation with others after the long-term intervention with real condition and hoped that the present findings may contribute to the development of new strategies for the treatment of aphasia.

Data availability statement

The raw data supporting the conclusions of this article will be made available by the authors, without undue reservation.

Ethics statement

The studies involving humans were approved by the Hokkaido University Certified Review Board. The studies were conducted in accordance with the local legislation and institutional requirements. The patient provided his written informed consent to participate in this study. Written informed consent was obtained from the patient for the publication of any data included in this article.

Author contributions

EO: Data curation, Investigation, Visualization, Writing—original draft. AS: Data curation, Investigation, Writing—review & editing. KT: Investigation, Writing—review & editing. MY: Data curation, Investigation, Writing—review & editing. YCa: Data curation, Investigation, Writing—review & editing. TN: Data curation, Investigation, Writing—review & editing. HH: Data curation, Investigation, Writing—review & editing. YCh: Data curation, Investigation, Writing—review & editing. HI: Investigation, Supervision, Writing—review & editing. TMiz: Project administration, Supervision, Writing—review & editing. TMim: Funding acquisition, Methodology, Validation, Writing—review & editing. SK: Conceptualization, Data curation, Formal analysis, Funding acquisition, Investigation, Methodology, Project administration, Validation, Writing—review & editing.

Funding

The author(s) declare financial support was received for the research, authorship, and/or publication of this article. This work was supported by Grants-in-Aid for Pioneering Research Initiated by the Next Generation (JST-SPRING) (JPMJSP2110) (EO), Scientific Research (B) (21H03308), Core Research for Evolutionary Science and Technology (JST-CREST) (23829912) (SK), Scientific Research (A) (19H01091, 23H00459), Challenging

Research (Exploratory) (23K18440), and Scientific Research on Innovative Areas (22H04788) (TMim).

Acknowledgments

The authors would like to thank Y. Abe, T. Takahashi, and M. Matsuhashi for the assistance with the experimental settings, clinical evaluation and rehabilitation, and analyzing data.

Conflict of interest

The authors declare that the research was conducted in the absence of any commercial or financial relationships that could be construed as a potential conflict of interest.

Publisher's note

Supplementary material

The Supplementary Material for this article can be found online at: https://www.frontiersin.org/articles/10.3389/fnhum.2024.1297683/full#supplementary-material

References

Ali, M. M., Sellers, K. K., and Fröhlich, F. (2013). Transcranial alternating current stimulation modulates large-scale cortical network activity by network resonance. *J. Neurosci.* 33, 11262–11275. doi: 10.1523/JNEUROSCI.5867-12.2013

Bakheit, A. M. O., Shaw, S., Barrett, L., Wood, J., Carrington, S., Griffiths, S., et al. (2007). A prospective, randomized, parallel group, controlled study of the effect of intensity of speech and language therapy on early recovery from poststroke aphasia. *Clin. Rehabil.* 21, 885–894. doi: 10.1177/0269215507078486

Brady, M. C., Kelly, H., Godwin, J., Enderby, P., and Campbell, P. (2016). Speech and language therapy for aphasia following stroke. *Cochrane Database Syst. Rev.* 2016:CD000425. doi: 10.1002/14651858.CD000425.pub4

Breitenstein, C., Grewe, T., Flöel, A., Ziegler, W., Springer, L., Martus, P., et al. (2017). Intensive speech and language therapy in patients with chronic aphasia after stroke: a randomised, open-label, blinded-endpoint, controlled trial in a health-care setting. *Lancet* 389, 1528–1538. doi: 10.1016/S0140-6736(17)30067-3

Carrera, E., and Tononi, G. (2014). Diaschisis: past, present, future. *Brain* 137, 2408–2422. doi: 10.1093/brain/awu101

Chander, B. S., Witkowski, M., Braun, C., Robinson, S. E., Born, J., Cohen, L. G., et al. (2016). tACS phase locking of frontal midline theta oscillations disrupts working memory performance. *Front. Cell. Neurosci.* 10:120. doi: 10.3389/fncel.2016.00120

Chapey, R. (2008). *Language Intervention Strategies in Aphasia and Related Neurogenic Communication Disorders*, 5th ed. Philadelphia, PA: Wolters Kluwer Health/Lippincott Williams and Wilkins.

Doogan, C., Dignam, J., Copland, D., and Leff, A. (2018). Aphasia recovery: when, how and who to treat? *Curr. Neurol. Neurosci. Rep.* 18:90. doi: 10.1007/s11910-018-0891-x

Esmaeilpour, Z., Kronberg, G., Reato, D., Parra, L. C., and Bikson, M. (2021). Temporal interference stimulation targets deep brain regions by modulating neural oscillations. *Brain Stimul.* 14, 55–65. doi: 10.1016/j.brs.2020.11.007

Fröhlich, F., and McCormick, D. A. (2010). Endogenous electric fields may guide neocortical network activity. *Neuron* 67, 129–143. doi: 10.1016/j.neuron.2010.06.005

Hamilton, R. H., Chrysikou, E. G., and Coslett, B. (2011). Mechanisms of aphasia recovery after stroke and the role of noninvasive brain stimulation. *Brain Lang.* 118, 40–50. doi: 10.1016/j.bandl.2011.02.005

Hyvärinen, A., and Oja, E. (2000). Independent component analysis: algorithms and applications. *Neural Netw.* 13, 411–430. doi: 10.1016/S0893-6080(00)00026-5

Kang, E., Kim, Y., Sohn, H., Cohen, L., and Paik, N. (2011). Improved picture naming in aphasia patients treated with cathodal tDCS to inhibit the right Broca's homologue area. *Restor. Neurol. Neurosci.* 29, 141–152. doi: 10.3233/RNN-2011-0587

Kawano, T., Hattori, N., Uno, Y., Hatakenaka, M., Yagura, H., Fujimoto, H., et al. (2021). Association between aphasia severity and brain network alterations after stroke assessed using the electroencephalographic phase synchrony index. *Sci. Rep.* 11:12469. doi: 10.1038/s41598-021-91978-7

Kertesz, A. (1982). *The Western Aphasia Battery*. New York, NY: Grune and Stratton.

Koganemaru, S., Fukuyama, H., and Mima, T. (2015). Two is more than one: how to combine brain stimulation rehabilitative training for functional recovery? *Front. Syst. Neurosci.* 9:154. doi: 10.3389/fnsys.2015.00154

Koganemaru, S., Kitatani, R., Fukushima-Maeda, A., Mikami, Y., Okita, Y., Matsuhashi, M., et al. (2019). Gait-synchronized rhythmic brain stimulation improves poststroke gait disturbance: a pilot study. *Stroke* 50, 3205–3212. doi: 10.1161/STROKEAHA.119.025354

Koganemaru, S., Mikami, Y., Maezawa, H., Matsuhashi, M., Ikeda, S., Ikoma, K., et al. (2018). Anodal transcranial patterned stimulation of the motor cortex during gait can induce activity-dependent corticospinal plasticity to alter human gait. *PLoS ONE* 13:e0208691. doi: 10.1371/journal.pone.0208691

Koganemaru, S., Mikami, Y., Matsuhashi, M., Truong, D. Q., Bikson, M., Kansaku, K., et al. (2020). Cerebellar transcranial alternating current stimulation modulates human gait rhythm. *Neurosci. Res.* 156, 265–270. doi: 10.1016/j.neures.2019.12.003

Lima, C., Lopes, J. A., Souza, V., Barros, S., Winkler, I., and Senna, V. (2023). Analysis of brain activation and wave frequencies during a sentence completion task: a paradigm used with EEG in aphasic participants. *PeerJ* 11:e15518. doi: 10.7717/peerj.15518

Mima, T., Oluwatimilehin, T., Hiraoka, T., and Hallett, M. (2001). Transient interhemispheric neuronal synchrony correlates with object recognition. *J. Neurosci.* 21, 3942–3948. doi: 10.1523/JNEUROSCI.21-11-03942.2001

Minami, S., and Amano, K. (2017). Illusory jitter perceived at the frequency of alpha oscillations. *Curr. Biol.* 27, 2344–2351.e4. doi: 10.1016/j.cub.2017.06.033

Negahbani, E., Kasten, F. H., Herrmann, C. S., and Fröhlich, F. (2018). Targeting alpha-band oscillations in a cortical model with amplitude-modulated high-frequency transcranial electric stimulation. *Neuroimage* 173, 3–12. doi: 10.1016/j.neuroimage.2018.02.005

Nicolo, P., Rizk, S., Magnin, C., Pietro M, Schnider, A., and Guggisberg, A. (2015). Coherent neural oscillations predict future motor and language improvement after stroke. *Brain* 138, 3048–3060. doi: 10.1093/brain/awv200

Nishimoto, T., Miyawaki, K., Ueda, T., Une, Y., and Takahashi, M. (2005). Japanese normative set of 359 pictures. *Behav. Res. Methods* 37, 398–416. doi: 10.3758/BF03192709

Nojima, I., Horiba, M., Sahashi, K., Koganemaru, S., Murakami, S., Aoyama, K., et al. (2023). Gait-combined closed-loop brain stimulation can improve walking dynamics in Parkinsonian gait disturbances: a randomised-control trial. *J. Neurol. Neurosurg. Psychiatry*. 94, 938–944. doi: 10.1136/jnnp-2022-329966

Ozen, S., Sirota, A., Belluscio, M. A., Anastassiou, C. A., Stark, E., Koch, C., et al. (2010). Transcranial electric stimulation entrains cortical neuronal populations in rats. *J. Neurosci.* 30, 11476–11485. doi: 10.1523/JNEUROSCI.5252-09.2010

Pedroni, A., Bahreini, A., and Langer, N. (2019). Automagic: standardized preprocessing of big EEG data. *Neuroimage* 200, 460–473. doi: 10.1016/j.neuroimage.2019.06.046

Pion-Tonachini, L., Kreutz-Delgado, K., and Makeig, S. (2019). ICLabel: an automated electroencephalographic independent component classifier, dataset, and website. *Neuroimage* 198, 181–197. doi: 10.1016/j.neuroimage.2019.05.026

Reato, D., Rahman, A., Bikson, M., and Parra, L. C. (2010). Low-intensity electrical stimulation affects network dynamics by modulating population rate and spike timing. *J. Neurosci.* 30, 15067–15079. doi: 10.1523/JNEUROSCI.2059-10.2010

Shima, A., Miyake, T., Tanaka, K., Ogawa, A., Omae, E., Nagamori, Y., et al. (2023a). Case report: A novel approach of closed-loop brain stimulation combined with robot gait training in post-stroke gait disturbance. *Front. Hum. Neurosci.* 17:1082556. doi: 10.3389/fnhum.2023.1082556

Shima, A., Tanaka, K., Ogawa, A., Omae, E., Miyake, T., Nagamori, Y., et al. (2023b). Case report: Backward gait training combined with gait-synchronized cerebellar transcranial alternating current stimulation in progressive supranuclear palsy. *Front. Hum. Neurosci.* 17:1082555. doi: 10.3389/fnhum.2023.1082555

Siegel, J. S., Ramsey, L. E., Snyder, A. Z., Metcalf, N. V., Chacko, R. V., Weinberger, K., et al. (2016). Disruptions of network connectivity predict impairment in multiple behavioral domains after stroke. *Proc. Natl. Acad. Sci. USA.* 113, E4367–E4376. doi: 10.1073/pnas.1521083113

Snodgrass, J. G., and Vanderwart, M. (1980). A standardized set of 260 pictures: norms for name agreement, image agreement, familiarity, and visual complexity. *J. Exp. Psychol.* 6, 174–215. doi: 10.1037/0278-7393.6.2.174

Witkowski, M., Garcia-Cossio, E., Chander, B. S., Braun, C., Birbaumer, N., Robinson, S. E., et al. (2016). Mapping entrained brain oscillations during transcranial alternating current stimulation (tACS). *Neuroimage* 140, 89–98. doi: 10.1016/j.neuroimage.2015.10.024

You, D., Kim, D., Chun, M., Jung, S., and Park, S. (2011). Cathodal transcranial direct current stimulation of the right Wernicke's area improves comprehension in subacute stroke patients. *Brain Lang.* 119:1–5. doi: 10.1016/j.bandl.2011.05.002

Frontiers in Neuroinformatics

Leading journal supporting neuroscience in the information age

Part of the most cited neuroscience journal series, developing computational models and analytical tools used to share, integrate and analyze experimental data about the nervous system functions.

Discover the latest Research Topics

See more →

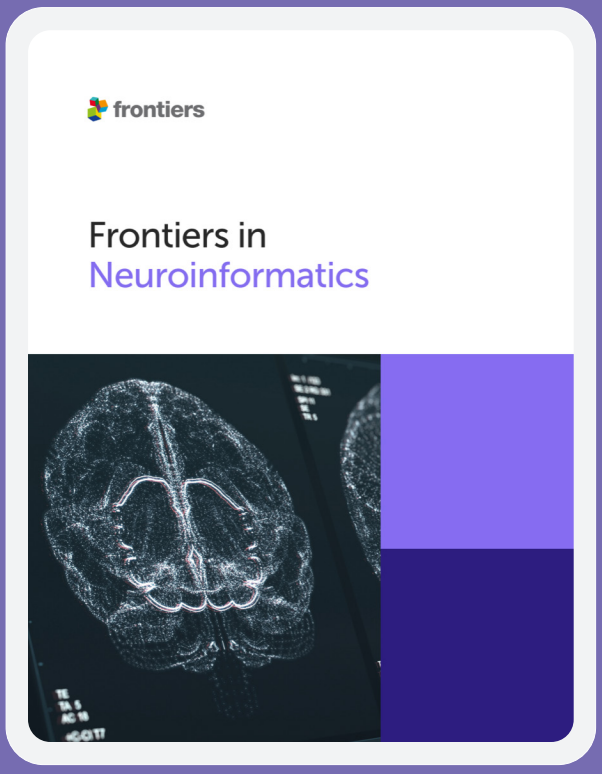

Frontiers

Avenue du Tribunal-Fédéral 34
1005 Lausanne, Switzerland
frontiersin.org

Contact us

+41 (0)21 510 17 00
frontiersin.org/about/contact